T-78325
N69-18586

NASA CR-72384

GESP-129

CASE FILE
COPY

CAVITY REACTOR CRITICAL EXPERIMENT

VOLUME III

by

G. D. Pincock and J. F. Kunze

November 15, 1968

Prepared for

NATIONAL AERONAUTICS AND SPACE ADMINISTRATION

Contract C-67747-A

MAR 1969
RECEIVED
NASA STI FACILITY
INPUT BRANCH

GENERAL ELECTRIC COMPANY

Nuclear Systems Programs

Idaho Falls, Idaho

LEGAL NOTICE

This report was prepared as an account of Government sponsored work. Neither the United States, nor the Commission, nor any person acting on behalf of the Commission:

A. Makes any warranty or representation, expressed or implied with respect to the accuracy, completeness, or usefulness of the information contained in this report, or that the use of any information, apparatus, material, method, or process disclosed in this report may not infringe privately owned rights; or

B. Assumes any liabilities with respect to the use of, or for damages resulting from the use of any information, apparatus, material, method, or process disclosed in this report.

As used in the above, "person acting on behalf of the Commission" includes any employee or contractor of the Commission, or employee of such contractor, to the extent that such employee or contractor of the Commission, or employee of such contractor prepares, disseminates, or provides access to, any information pursuant to his employment or contract with the Commission or his employment with such contractor.

CAVITY REACTOR CRITICAL EXPERIMENT

VOLUME III

by

G. D. Pincock and J. F. Kunze

November 15, 1968

Prepared for

NATIONAL AERONAUTICS AND SPACE ADMINISTRATION

Contract C-67747-A

Technical Management

NASA-Lewis Research Center

Cleveland, Ohio

Nuclear Systems Division

Robert E. Hyland, Project Manager

Advanced Systems Division

John C. Liwosz

ABSTRACT

This report is volume three of a set covering critical experiments performed on a large cavity reactor system at the National Reactor Testing Station. This volume describes experiments designed to investigate the effects of specific engineering design factors needed for an operating power reactor, and how these factors influence the ultimate critical mass of the system. Included are effects of a liner material to protect the cavity wall from thermal and pressure effects , the hydrogen propellant gas that will occupy the space between this liner and the core, and the appropriate placement of fuel in the reflector in order to reduce the required critical mass in the core.

ACKNOWLEDGEMENTS

This report is only the final product of five months of experiments. The authors wish to acknowledge the fine contributions of

C. G. Cooper
R. R. Jones
D. H. Suckling

in the reactor operations area and of J. W. Morfitt, R. E. Wood, and R. E. Hyland (NASA) for program consultation and advice. In addition, the efforts of A. B. Walker in editing and proof reading the final copy, of Mrs. P. L. Chase in data tabulation and illustration preparation, and Mrs. R. M. Creasey for typing are appreciated.

TABLE OF CONTENTS

TABLE OF CONTENTS

(Continued)

TABLE OF CONTENTS

(Continued)

FIGURES

TABLE OF CONTENTS

(Continued)

Page

FIGURES

(Cont'd)

TABLE OF CONTENTS

(Continued)

TABLE OF CONTENTS

(Continued)

Page

FIGURES

(Cont'd)

TABLE OF CONTENTS

(Continued)

Page

FIGURES

(Cont'd)

TABLE OF CONTENTS

(Continued)

Page

FIGURES

(Cont'd)

TABLE OF CONTENTS

(Continued)

Page

FIGURES

(Cont'd)

TABLE OF CONTENTS

(Continued)

Page

FIGURES

(Cont'd)

TABLE OF CONTENTS

(Continued)

TABLE OF CONTENTS

(Continued)

TABLE OF CONTENTS

(Continued)

Page

TABLES

(Cont'd)

TABLE OF CONTENTS

(Continued)

Page

TABLES

(Cont'd)

TABLE OF CONTENTS

(Continued)

Page

TABLES

(Cont'd)

1.0 INTRODUCTION

The General Electric Company has performed a number of Cavity Reactor Critical Experiments for the National Aeronautics and Space Administration, Lewis Research Center (1) (2). These previous experiments have been designed as basic reactor physics measurements, and have not included a full mockup of structural material on the cavity wall or a complete simulation of the coolant passing between the core and the reflector. This report contains data obtained from critical experiments with an aim at evaluating engineering design considerations. These include the effect of a stainless steel liner on the cavity wall, the filling of the void region between the active core and cavity with hydrogen (simulated with polyethylene (CH_2), and the insertion of fuel in the D_2O reflector in order to reduce the required fuel in the core. The initial coolant simulation work was done with a uniform hydrogen density of 2×10^{21} atoms/cc hydrogen in the void. This was followed with a variable hydrogen experiment where the hydrogen densities varied radially and axially through the void region and through the outer portion of the active core. Hydrogen was simulated with both polyethylene and polystyrene (CH) in these experiments.

In addition to the hydrogen simulation experiments, two major configurations were tested where uranium, in the form of MTR type fuel plates, was placed in the radial reflector. These experiments were performed to determine the savings that could be achieved in total critical mass and the resulting fraction of core power generated in the fuel annulus. A reduction in critical mass would result in a reduced internal pressure requirement in the power reactor core. But, fuel in the reflector must be limited by the allowable fraction of power that can be tolerated in the reflector. For a hydrogen-cooled system in which inlet and exit core temperatures of nominally 1000°F and 10,000°F, respectively, are considered and with the hydrogen initially cooling the reflector, about 15% of the total reactor power may be generated in the reflector without imposing unusual structural material requirements.

All of the experiments discussed in this volume were performed on a large system, 305 cm (10 ft) long by 366 cm (12 ft) diameter outer dimensions with a cavity that was 121.9 cm (4 ft) long by 182.9 cm (6 ft) diameter. The core size was nominally a cylinder 117 cm long by 124 cm diameter, equivalent to a fuel to cavity radius ratio of 0.68.

This was same basic reactor configuration as described in Reference 2. The cavity region wall (182.9 cm in diameter by 121.9 cm long) inner dimensions, was aluminum, type 6061, 1.27 cm (1.2 inch) thick on the ends and 0.95 cm (3/8 in.) thick on the cylindrical sides and was surrounded by D_2O, 90.2 cm (35-1/2 in.) thick on the ends and 91.5 cm (35-5/8 in.) thick on the radius. The outer dimensions of the reactor assembly were usually taken as those of the D_2O, though the walls containing this water were 1/2 in. thick 6061 aluminum.

A simulated heat shield in the form of beryllium, 10.16 cm thick (4 in.), was placed in the radial reflector at an average distance of 6.5 cm from the wet surface of the cavity wall on the hydrogen simulation experiments. The beryllium was removed when fuel was placed in the reflector.

Various measurements were performed on each configuration including initial critical loading, rod worths, material worths, power mapping with catcher foils and flux mapping with gold foils. In one case, the hydrogeneous material (polyethylene) was heated to about 74°C to measure the temperature coefficient of reactivity.

2.0 DESCRIPTION OF TEST ASSEMBLY AND TEST PROCEDURES

2.1 Reactor Description

The cavity reactor consisted of a split tank assembly as shown in Figure 2.1. The main tank was stationary and contained the cavity region. The other tank was mounted on a 4-wheel dolly which carried one of the end reflectors. The cavity region was constructed to be 182.9 cm in diameter by 121.9 cm long, but in practice a 1.27 cm (1/2 inch) gap was allowed to remain between the two parts of the reflector, adding this additional length to the cavity. All of the radial walls of the cavity and two tanks were 0.9525 cm (3/8 in.) thick Al and the ends of the cavity and tanks were 1.270 cm (1/2 inch) thick Al. Extra Al support structure, including support rails for the beryllium, but not including cavity walls or end plates was located within the tanks. This support material weighed 221 kg. The two tanks contained heavy water (D_2O) 89 cm thick, which served as both a reflector and a moderator.

The end reflector of the main tank contained 36 holes 2.093 cm in diameter into which control rods could be inserted for reactor control. These holes represented 1% of the end reflector volume. The control rods were actuator driven and were made of boron-carbide clad with stainless steel. Each actuator could handle as many as three rods and had both shim and safety or scram functions. The location of the rods and actuators is shown in Figure 2.2.

The D_2O contained 0.22 mole percent H_2O. An argon atmosphere was maintained over the top of the tanks at all times to prevent contamination by atmospheric moisture. A separate storage tank was provided in the test cell so that all of the D_2O in the main reactor tank could be transferred from the reactor when it was necessary to install or remove materials, such as beryllium, in the reflector region.

Each of the hydrogen simulation configurations included in this report had a ring of beryllium in the radial reflector as shown in Figure 2.3. This beryllium consisted of several rectangular blocks 106.7 cm long, 10.16 cm thick and of varying widths. The average distance between the beryllium surface closest to the cavity and the wet surface of the cavity wall was 6.5 cm. The triangular D_2O regions found along the edges of the beryllium slabs where adjacent pieces butt together represent about 4% of the volume in the beryllium annulus.

The reactor was fueled with highly enriched (93.2% U^{235}) solid sheet uranium. The sheets were nominally 0.00254 cm (0.001 in.) thick by 7.303 cm square. Some larger rectangular sheets which were the same height but 1.5 times the length of the square sheets were also used. The square sheets will be referred to as size 1.0 and the rectangular sheets as size 1.5 sheets. There were 2.62 ± 0.01* gm and 3.878 ± 0.01* gm of uranium in the size 1.0 and size 1.5 sheets, respectively.

* These uncertainties represent a standard deviation on the average weight of a sheet of material. The statistical variation among the various sheet gave a standard deviation of 0.10 gm.

The cavity region contained a fuel support structure consisting of several large cells into which fuel elements could be inserted as shown in Figure 2.4. Type 1100 aluminum was used in the cell dividers; however, the support ring to which the sheet material was welded and which was bolted to the end reflector was type 6061 aluminum. This entire structure contained 15.15 kg of type 6061 Al and 38.60 kg of type 1100 Al.

The sheets of fuel were placed into fuel elements as shown in Figure 2.5. These fuel elements were 7.47 cm square by 116.8 cm long and were made of type 1100 aluminum. A total compliment of these fuel elements (208) weighed 106.3 kg. Type 1100 Al lids were used on each element. The weight of all the lids totaled to 6.16 kg. The fuel was loaded and spaced within the fuel element as shown in the above figure. The staggered orientation was used to prevent low absorption paths through the active core. The spacer rings were type 1100 Al and weighed on the average of 3.46 gm each.

It will be noted from Figure 2.5 that there were three fuel orientations when loading the fuel elements with size 1.0 fuel sheets. These orientations were numbered as follows:

Orientation Number	Description
1	The fuel sheets are parallel to the bottom of the element
2	The fuel sheets are normal to the bottom and parallel to the ends of the element
3	The fuel sheets are normal to the bottom and parallel to the sides of the element

The fuel elements were classified according to the type of loading orientation on the first stage facing the separation plane of the reactor. Three additional types of fuel elements were, therefore, obtained by simply turning the fuel elements around so that the opposite end faced the separation plane. The fuel elements were thus typed 1, 2, 3, 1A, 2A, and 3A where the A types were the types 1, 2, and 3 turned end for end.

When loading the fuel elements with the size 1.5 sheets of fuel, only four types of elements were possible, types 1, 3, 1A and 3A. The type 2 fuel orientation was used as dividers between type 1 and type 3 stages.

The exact fuel loading for each of the configurations will be discussed in subsequent sections.

In order to specify fuel element positions within the active core region, a numbering system was used which consisted of a main cell and a fuel element number. This designation is demonstrated in Figure 2.6.

Further description of the reactor can be found in References 1 and 2. The description of the hydrogen simulation structures and fuel annulus will be given in subsequent sections.

The stainless steel liner consisted of 0.0965 cm thick 304 stainless steel. The liner was placed against the cavity wall such that there were 48.5 kg on the radial wall, 19.1 kg at the separation plane fastened to the movable tank and 15.5 kg on the back end of the cavity. (The area of the supporting yoke was not covered with stainless steel).

Because of the air flow plates which had to be placed at the separation plane when heating the polyethylene on the uniform hydrogen experiment, it was necessary to offset the fuel elements 2.54 cm (1.0 in.) towards the end of the core containing the control rods. The cavity was 121.9 cm long and the fuel elements were 116.8 cm long so that when centered in the cavity there would normally be a gap of 2.54 cm on each end of the core. However, the fuel elements were pushed as far as they would go towards the back end of the cavity for these experiments. This was the position of the fuel for all of the experiments covered by this report.

2.2 Experimental Procedures

Control rods were remotely operated from the control room as was the movable table. Their positions were monitored on a digital voltmeter-ratiometer. Rod worth curves were not normally measured for each configuration, however, a curve was generated for a single actuator or rods on the configuration with the stainless steel liner in the cavity. This curve and on all rod (normally 6 to 7 actuators and 17 to 20 rods) curves were used to reduce the data for this report. These curves were reduced to tabular form and are presented in Tables 2.1 and 2.2. The normal "rods in" position was 118 digits on the ratiometer and in the withdrawn position the reading was generally 9766. There were 112.3 digits per cm of rod travel. The "rod bump" technique was used to calibrate the rods. This was accomplished by pulling the rods a small increment and measuring the resulting period. The fraction of the total rod worth was determined from the rod worth curve the critical position and the period measurement position of the rods. The reactivity worth of the period divided by the fractional rod worth was the total reactivity worth of the rod or rods.

The period measurements were reduced to reactivity by using the usual inhour equation. The effective delayed neutron parameters used in the equation are given in Table 2.3. The value of a dollar was 0.00765 using the usual six delayed fission groups plus nine (α, n) groups, with an estimated uncertainty of +0.0002. The assumed neutron lifetime was 4.0 milliseconds. The ratio of β/β eff for fission neutrons was assumed to be essentially 1.0 (the calculated value was 0.964). Most of the neutron leakage occurred at low (thermal) energies. Although the ratio of β/β eff is slightly less than 1.0, this discrepancy is masked by the uncertainty in gamma-neutron production.

Power mapping was done with catcher foils. A catcher foil is a thin disc of aluminum which is exposed in the reactor against a clean, bare disc of enriched uranium. Fission products from the outer surface of the uranium embed themselves in the aluminum and the resulting radioactivity of these fission products was counted on a beta oscintillation foil counting system. The activity is proportional to power and by using known calibration factors, absolute power can be deduced. The foils were normally 1.429 cm (9/16 inch) in diameter. Both bare and cadmium covered foils were used within the cavity region. Cadmium covers were nominally 0.0508 cm thick.

Neutron flux measurements were obtained primarily with bare and cadmium covered gold foils. However, other resonance detectors such as In and Mn were also exposed in some of the configurations. The foils were usually thin and, in the case of indium, relatively dilute. However, in most cases, the foil activities were corrected to infinitely dilute activities by using the equations in Section 4.4.2 of Reference 1. These foils were exposed in both the cavity and reflector regions and they were counted on the 256-channel gamma-ray analyzer to obtain absolute activity. All resonance detector foil data were decay corrected to shutdown time.

2.3 Data Reporting Units and Conventions

Throughout the report consistent data reporting schemes have been utilized, but an explanation of these would appear to be appropriate.

1. Fuel Mass

   All fuel masses are quoted as that of "Oralloy" metal, with a composition of 93.18 atom percent U^{235}.

0.98	U^{234}
0.52	U^{236}
5.32	U^{238}

   The fuel contained a few percent of impurities (oxygen, teflon, etc.) but only the actual uranium mass, accurate to less than ±1/2% is reported.

2. Effective Multiplication Factor and Table Gap

   Throughout the report, the effective multiplication factor, as measured, is reported. Exceptions to this rule will be noted. No correction was made for the table gap or the end plug. If the gap (necessary for safety considerations) were eliminated (but the aluminum faces still remained), the reactivity would increase 0.55%Δk. If the 30.5 cm (1 foot) diameter end plug hole, simulating an exhaust nozzle, were plugged with D_2O, 0.70% reactivity would be gained.

3. Power Distribution

   Reported power distributions are usually normalized to 1.0 at the axial and radial center of the reactor. Powers are

reported as relative specific powers, i.e., power per unit fuel mass. Because of the nature of the catcher foil process, surface activity is principally recorded, and resonance self-shielding is not involved because the combination of the fission product range (0.0005 cm), the foil thickness (0.0025 cm), and the beta particle range that is generally greater than the foil thickness. Thermal flux perturbation of an isolated uranium foil 0.0025 cm thick in heavy water is about 12%. Self-shielding was about half of this. However, this effect is only of concern near the edge of the core where the uranium is in "essential" contact with heavy water. Measurement of the fission rate on the moderator side of the uranium foil will measure the peak value.

4. Reactor Locations

In referring to specific locations in the reactor, all radial dimensions are from the centerline. All axial dimensions are referenced from the beginning of the D_2O reflector at the end of the fixed table. This point is thus 0 cm, the cavity begins at 91.5 cm, and ends at 212.8 cm, which is also the separation plane location. The movable table reflector ends at 304.3 cm. No consideration for the table gap is included in these location dimensions, i.e, the gap is assumed to not exist.

5. Gold Measurements

Most gold foil measurements were made using foils of thickness between 0.0005 cm and 0.0013 cm. The use of thin foils virtually eliminates the need for any thermal flux perturbation corrections. However, for such thin foils the response to the resonance neutron flux greatly exceeds the thermal response. A great deal of flux data was obtained with bare foils alone (no accompanying cadmium covered data). This data must be correlated by using appropriate resonance self-shielding factors with multigroup computer calculations if misleading results are to be avoided. Unless otherwise noted, the bare gold data was obtained with 0.0005 cm thick foils.

TABLE 2.1

Tabular Rod Worth Curve Actuator No. 6

Ratiometer Reading — Percent of Rod Worth Inserted

	0	100	200	300	400	500	600	700	800	900
0	100.00	100.00	97.15	94.30	91.45	88.63	85.80	82.98	80.16	77.38
1000	74.65	71.97	69.36	66.80	64.32	61.91	59.55	57.26	55.05	52.88
2000	50.76	48.71	46.72	44.79	42.92	41.11	39.36	37.66	36.02	34.43
3000	32.89	31.41	29.97	28.58	27.25	25.97	24.73	23.54	22.40	21.29
4000	20.23	19.22	18.24	17.31	16.41	15.56	14.74	13.96	13.21	12.51
5000	11.83	11.18	10.57	9.99	9.42	8.89	8.39	7.90	7.45	7.02
6000	6.62	6.24	5.87	5.52	5.19	4.88	4.58	4.29	4.03	3.78
7000	3.54	3.31	3.09	2.89	2.70	2.51	2.33	2.16	2.00	1.84
8000	1.69	1.55	1.42	1.29	1.17	1.05	.94	.83	.74	.64
9000	.56	.48	.40	.33	.26	.20	.14	.09	.04	0

Difference Table

Ratiometer Reading

	0	100	200	300	400	500	600	700	800	900
0	0	0	2.85	2.85	2.84	2.83	2.83	2.82	2.82	2.78
1000	2.73	2.68	2.61	2.56	2.48	2.41	2.36	2.29	2.21	2.17
2000	2.12	2.05	1.99	1.93	1.87	1.81	1.75	1.70	1.64	1.59
3000	1.54	1.48	1.44	1.39	1.33	1.28	1.24	1.19	1.14	1.11
4000	1.06	1.01	.98	.93	.90	.85	.82	.78	.75	.70
5000	.68	.65	.61	.58	.57	.53	.50	.49	.45	.43
6000	.40	.38	.37	.35	.33	.31	.30	.29	.26	.25
7000	.23	.23	.22	.20	.19	.19	.18	.17	.16	.16
8000	.15	.14	.13	.13	.12	.12	.11	.11	.09	.10
9000	.08	.08	.08	.07	.07	.06	.06	.05	.05	.04

TABLE 2.2

Tabular Rod Worth Curve All Rods - Subcritical Measurements

Ratiometer Reading	Percent of rod worth inserted									
	0	100	200	300	400	500	600	700	800	900
0	100.00	100.00	96.54	93.16	89.86	86.64	83.50	80.43	77.74	74.52
1000	71.68	68.92	66.23	63.62	61.08	58.61	56.22	53.90	51.64	49.45
2000	47.34	45.29	43.30	41.38	39.52	37.72	35.99	34.32	32.71	31.16
3000	29.66	28.21	26.82	25.48	24.19	22.95	21.77	20.63	19.53	18.48
4000	17.48	16.52	15.60	14.72	13.88	13.08	12.32	11.59	10.89	10.23
5000	9.59	8.99	8.42	7.87	7.34	6.85	6.38	5.93	5.50	5.10
6000	4.72	4.35	4.01	3.68	3.38	3.08	2.81	2.55	2.30	2.08
7000	1.86	1.66	1.47	1.30	1.14	.99	.85	.73	.62	.52
8000	.43	.35	.28	.22	.18	.14	.11	.09	.08	.08

DIFFERENCE TABLE

	0	100	200	300	400	500	600	700	800	900
0	0	0	3.46	3.38	3.30	3.22	3.14	3.07	2.99	2.92
1000	2.84	2.76	2.69	2.61	2.54	2.47	2.39	2.32	2.26	2.19
2000	2.11	2.05	1.99	1.92	1.86	1.80	1.73	1.67	1.61	1.55
3000	1.50	1.45	1.39	1.34	1.27	1.24	1.18	1.14	1.10	1.05
4000	1.00	.96	.92	.88	.84	.80	.76	.73	.70	.66
5000	.64	.60	.57	.55	.53	.49	.47	.45	.43	.40
6000	.38	.37	.34	.33	.30	.30	.27	.26	.25	.22
7000	.22	.20	.19	.17	.16	.15	.14	.12	.11	.10
8000	.09	.08	.07	.06	.04	.04	.03	.02	.01	.00

TABLE 2.3

Effective Delayed Neutron Parameters

Group	β_i	λ_i
1	0.000210	0.012400
2	0.001410	0.030500
3	0.00127	0.111000
4	0.002550	0.301000
5	0.000740	1.100000
6	0.000270	3.000000
7	0.000780	0.277000
8	0.000240	0.016900
9	0.000084	0.004810
10	0.000040	0.001500
11	0.000025	0.000428
12	0.000028	0.000117
13	0.000004	0.000044
14	0.000001	0.000004
	0.007652	

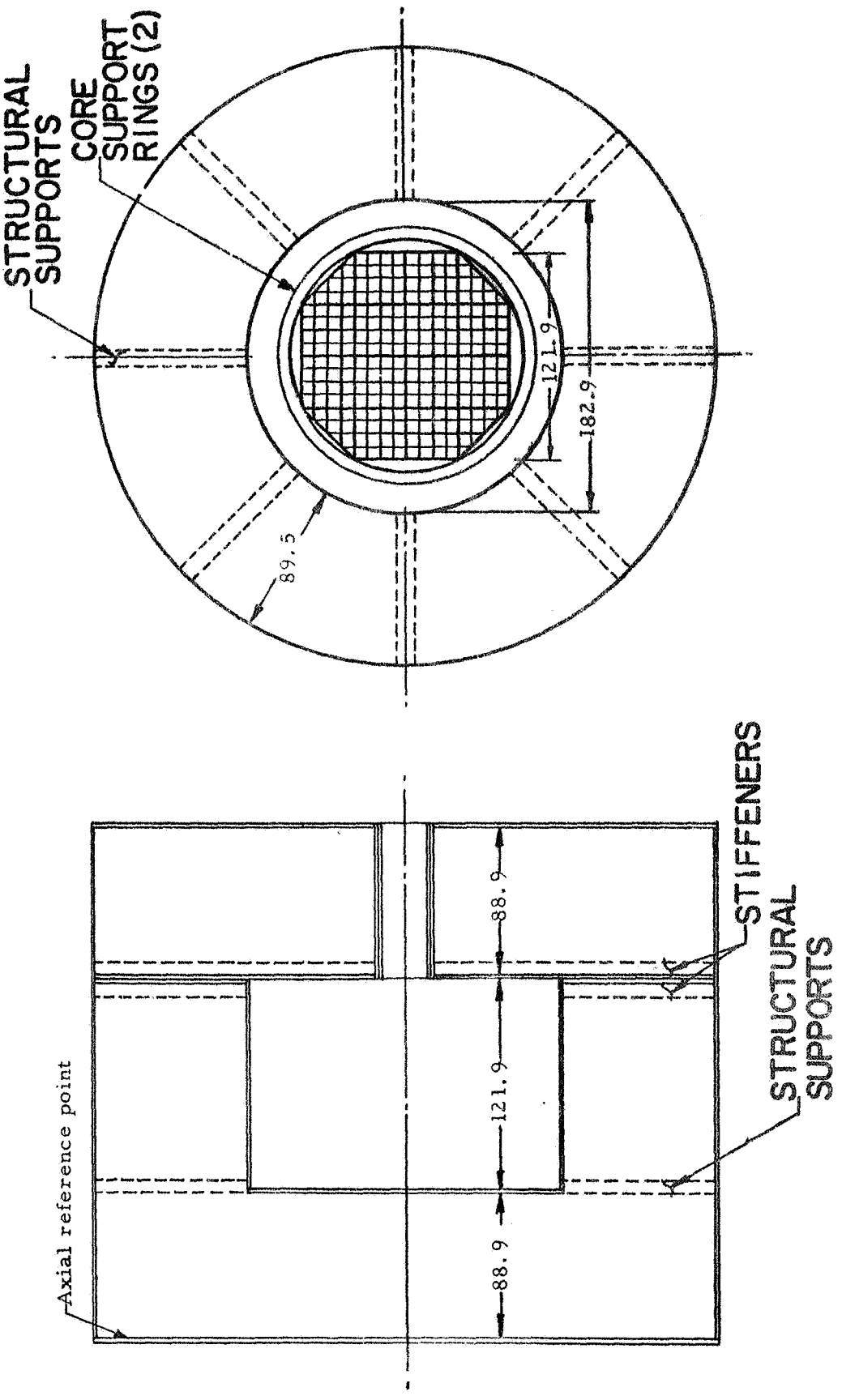

Fig. 2.1 Cavity reactor, orthographic views

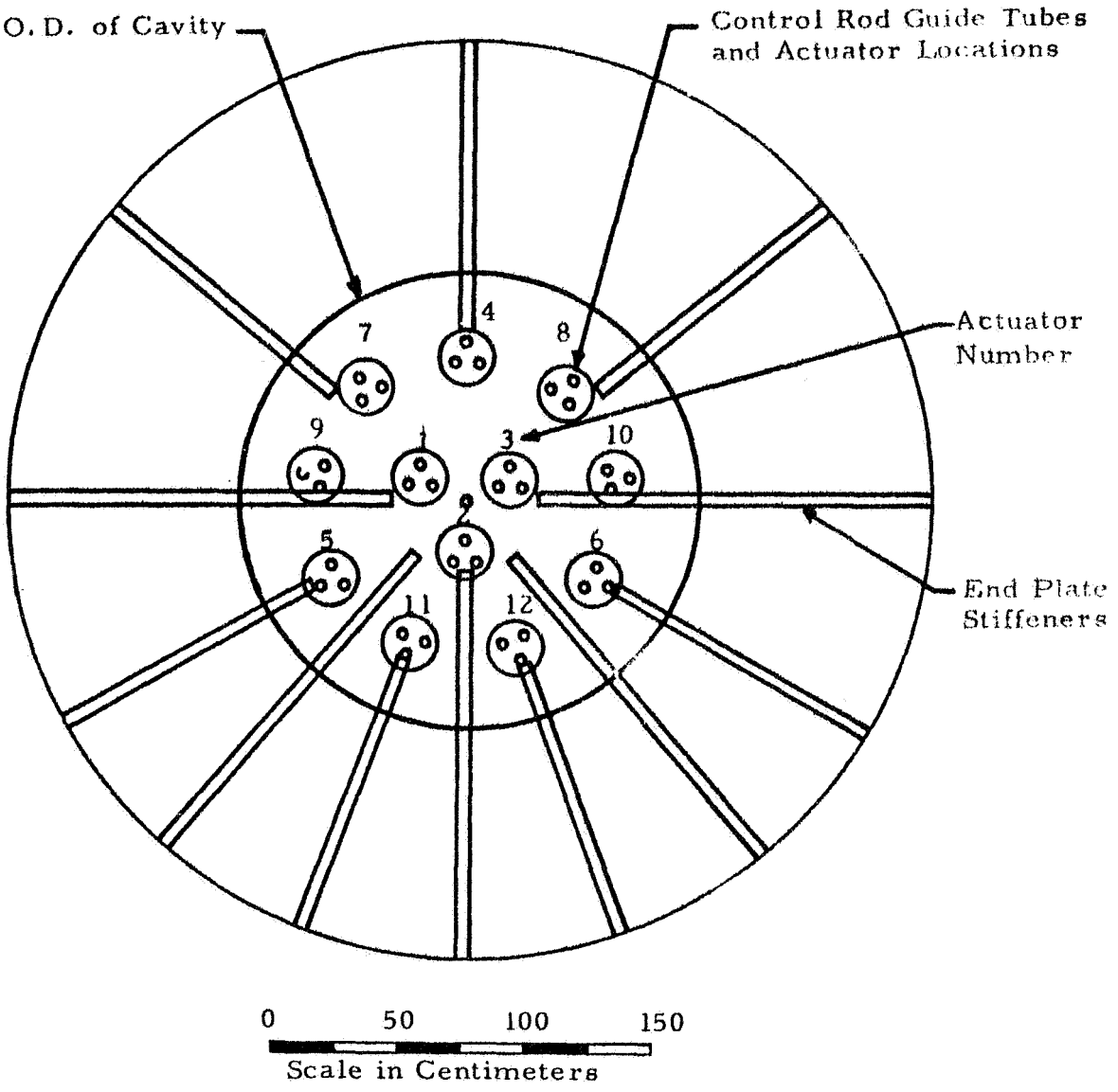

Fig. 2.2 Cavity reactor control rod and actuator layout in fixed table

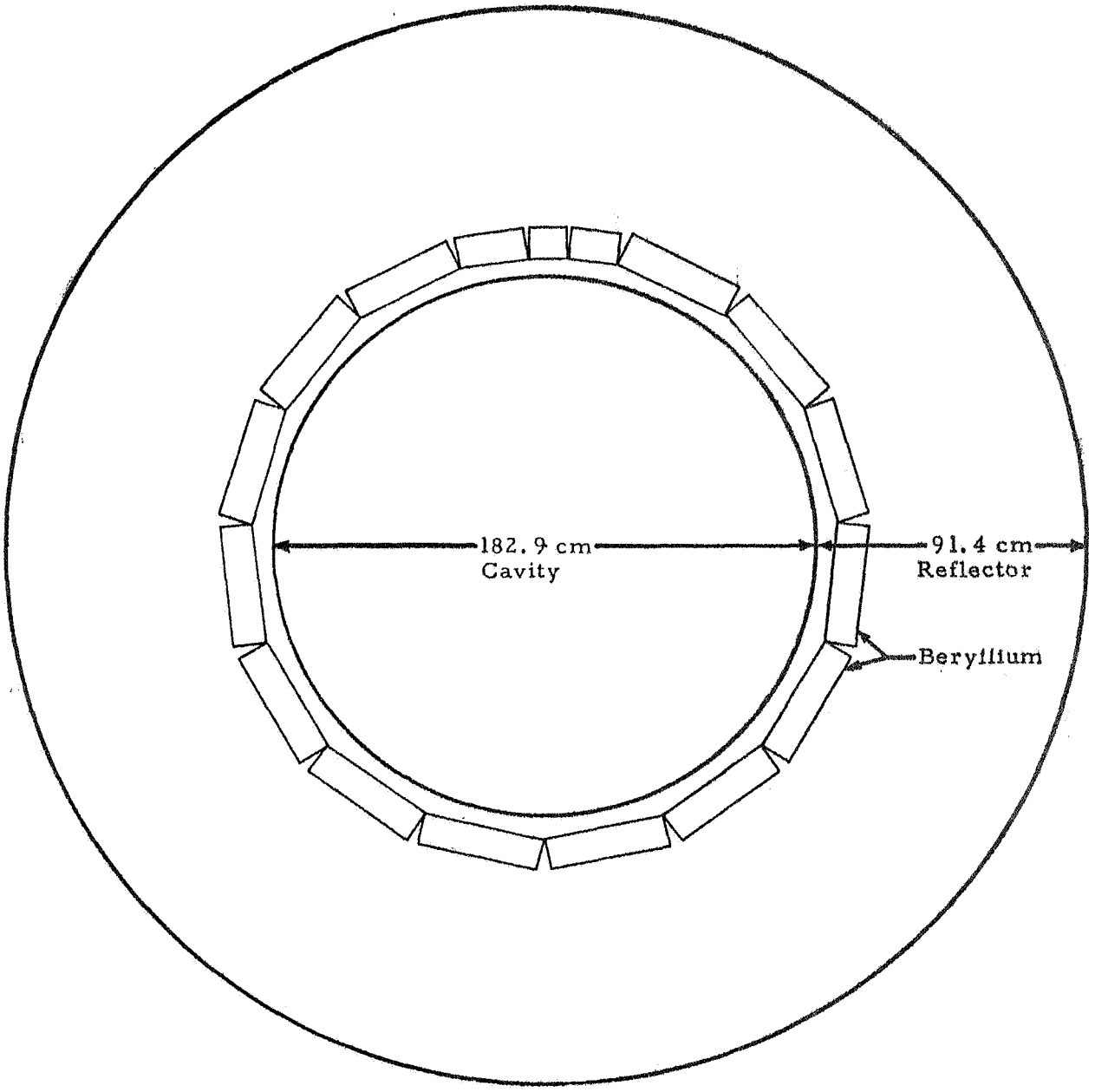

Fig. 2.3 Beryllium ring in radial reflector, simulated hydrogen configuration

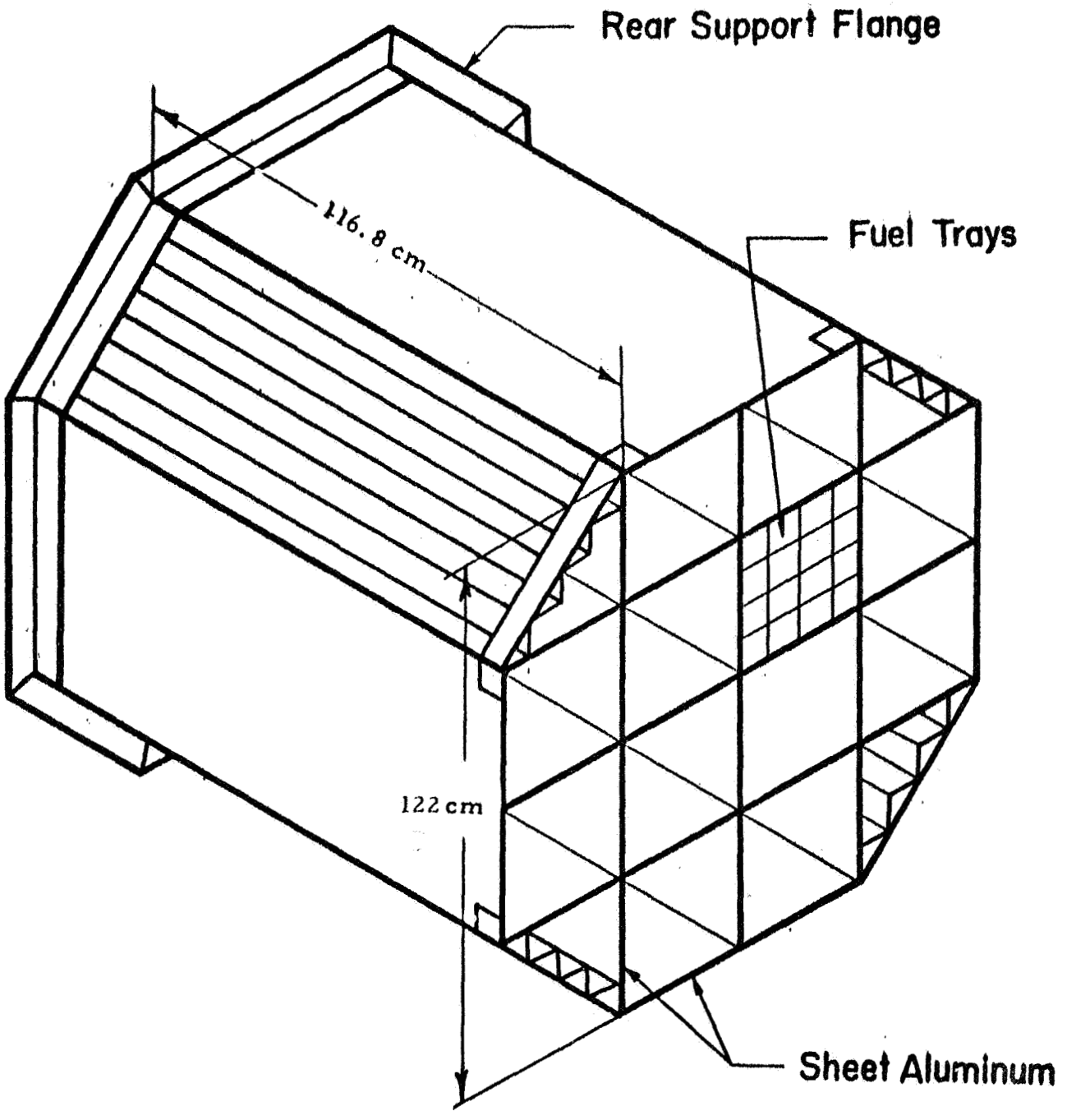

Fig. 2.4 Core support structure

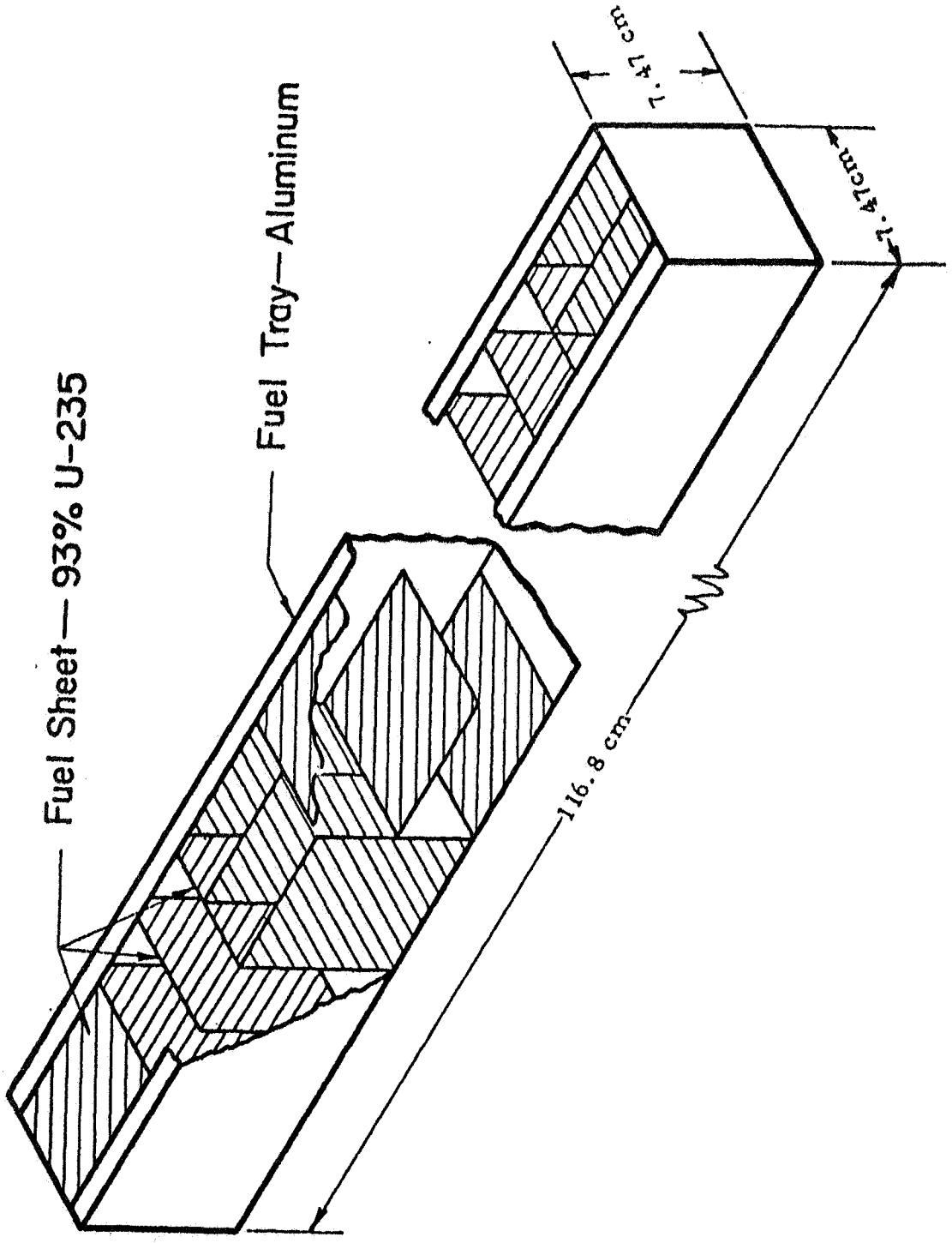

Fig. 2.5 Fuel tray and fuel sheet orientation

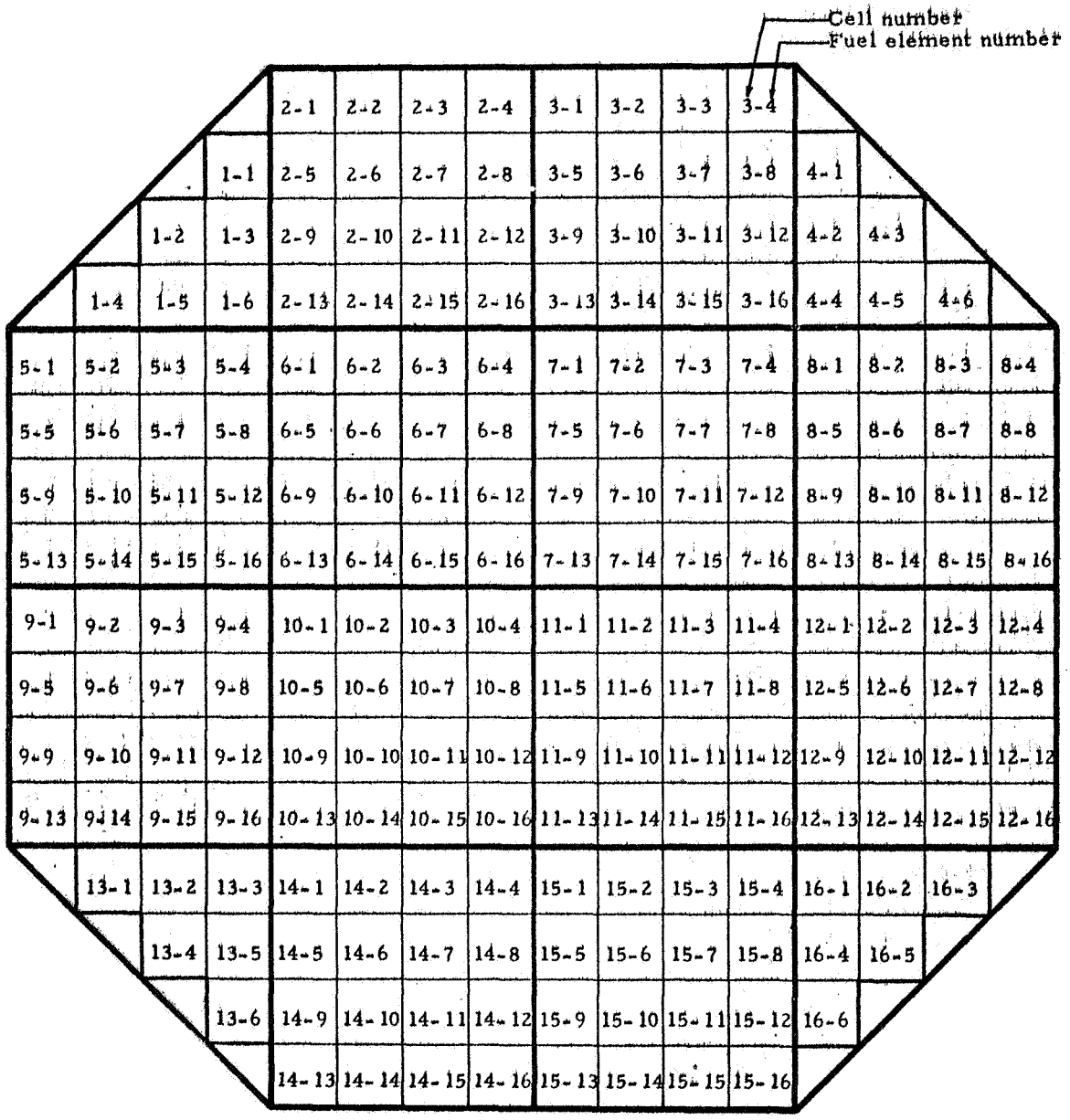

End view facing the fixed table

Fig. 2.6 Fuel element numbering system within active core

3.0 SUMMARY AND CONCLUSIONS

This report covers seven major configurations of the cavity reactor. All had a fuel radius ratio with respect to the cavity radius of nominally 2/3 (actually 0.68) and are therefore comparable to experiments 3 to 6, and 8 to 10 in Reference 1. Table 3.1 lists these major configurations and the significant measured parameters for each, including critical mass and fuel worth. All of the cores were uniformly fueled, and the fuel was distributed with a uniform density in a volume equivalent to that of a cylinder 124.3 cm in diameter and 117 cm long. This fuel was off center in the 183 cm diameter by 122 cm long cavity by 2.54 cm, being shifted towards the end of the core containing the control rods.

This set of configurations was constructed in order to evaluate the full scale effects of materials that would enter into the considerations for a power cavity reactor experiment. These are principally the effects of 1) structural, high temperature-capability liner on the cavity wall, in this case 0.095 cm of stainless steel, 2) the propellant that will flow between the wall of the cavity and the core, and 3) any fuel installed in the reflector region in order to enchance the capabilities of the cavity reactor concept by reducing the mass of uranium required in the core to attain criticality.

3.1 Critical Mass Comparisons

Figure 3.1 represents these configurations. Since most of the configurations described in Reference 1 were simpler in detail, "cleaner" from reactor physics considerations and had similar core dimensions, it is of interest to make critical mass comparisons with these, as is shown in Figure 3.2. The logrithmic ordinate scale of this figure makes it possible to extrapolate to other unmeasured configurations by utilizing slopes of measured effects. This prescription is by no means rigorously valid, but is useful as an approximate technique to evaluate the critical mass of various design iterations. Note that data on critical mass reported throughout this report refers to the experimentally measured values. No correction has been made for the apparent bias between the fuel sheet experiments and the equivalent gas core experiments (see Reference 2). This bias is nominally 4% for the experiments reports in this volume. For further discussion, see Section 3.6.

3.2 Fuel Worth Comparisons

The fuel worth varies principally with the amount of fuel present in the reactor cavity. The configuration of the fuel and the presence of various "structural" components has a significant but lesser effect on the fuel worth. Table 3.2 is an expansion of a similar table (3.6 in Reference 2) to which has been added the results obtained from the configurations reported in this volume. Figure 3.3 is a graph to show the trend of decreasing fuel worth vs. increasing critical mass. Note that sub-curves can be identified on this plot for various configuration sets with similar characteristics (such as a different curve for the mockups than for the gas experiments of Reference 2), but in general the fuel worth function is rather well defined. The higher loadings, above 30 kg, impose a significant

penalty in being able to compensate with fuel for reactivity effects imposed by other reactor material changes. The amount of fuel required for compensation becomes huge. This reason, as well as the practical reason that with loadings exceeding 30 kg, excessive operating pressures in a power cavity reactor dictate a limitation on the critical loading to the order of 30 kg.

3.3 Effects of Fuel in Reflector

Placing fuel in the D_2O reflector is an effective method of reducing the critical mass required in the core. A companion consideration, however, is the power producing effect of this fuel. Since the reactivity effect is a function of both the direct flux and its adjoint (importance) while the power is a function of the direct flux alone, an optimum location is available which gives the maximum reactivity benefit for the minimum power production. For a single pass series flow of the coolant, in which first the reflector is cooled and then the heat removed from the core, power production in the reflector needs to be limited to about 15% of the total reactor power (certainly no more than 20%) if unreasonable material requirements are not to be imposed. This fraction should include the neutron and gamma heat from the core neutrons. A two pass, parallel flow system in which only part of the coolant passes through the core would allow greater power fractions for the reflector and consequently lower critical mass for the core, but of course, would result in lower average exhaust temperatures.

For the configurations measured, one kilogram of fuel optimally placed in the reflector was found to produce close to 20% of the total power for core loadings in the 20 to 30 kg range and to require approximately 30% less fuel in the core. Furthermore, this small mass of fuel in the reflector was found to be such a dilute concentration that it was essentially a first order perturbation effect with regard to the thermal flux. Essentially no advantage could be gained by attempts to self-shield the fuel from the direct flux but not from its adjoint. Figure 3.4 shows the effect of fuel placement on reactivity and power production in the radial reflector. The maxima and minima of these two curves nearly coincide, and indicate the optimum radial location for fuel in the reflector. Moving off this optimum point results in a greater fractional loss in reactivity than loss in fractional reflector power, i.e., the reactivity vs distance curve has a steeper slope than the reflector specific power curve. Thus, the optimum radial location of the fuel is at about 15 cm from the cavity wall in the D_2O.

The question of fuel effectiveness in the end reflector or the corner reflector is less easily determined as a complete mockup because of the difficult access to these areas. Therefore, only probe-type measurements of reactivity worth and specific power were made in these other reflector regions. The results should be valid to a full ring or plate of fuel of a mass of 1 kg or less since it has been shown that this small concentration of fuel gives only a first order perturbation. Figure 3.5 shows the approximate iso-reactivity and specific power lines within the reflector region. It is apparent that the end reflector appears to be the best location, giving the greatest reactivity gain for the least power production.

3.4 Material Worth Measurements

In addition to fuel worths (Section 3.2), a number of other material reactivity coefficients were measured a specific location in the reactor. These measurements are summarized in Table 3.3.

1. Aluminum Worth in Core

The structure to support the fuel sheets was type 1100 aluminum, and its worth is of interest because aluminum structure would not be present inside a gaseous core. As shown in Table 3.3, the worth of aluminum decreases with core loading, both in terms of absolute worth and with respect to the equivalent amount of uranium.

2. Magnesium vs Aluminum

Because of the parasitic effect of the aluminum structure it absorbs approximately 20% of the neutrons. The use of magnesium which has about 1/4 of the atomic absorption cross section of aluminum was considered. Comparing the two materials on a unit mass basis, which is nominally the same as equivalent strength basis can be done by referring to Table 3.3. Magnesium offers better than a factor of two advantage within the reflector, but its advantage becomes less and less toward the cavity wall and into the void. At the outer boundary of the core the two materials are virtually equivalent. Evidently, the high scattering cross section of magnesium compared to aluminum is a disadvantage in the void region, where a good scatterer tends to scatter more neutrons away from the core than are scattered into it. Furthermore, the low absorptivity of these materials is insignificant compared to a high absorber in the same vicinity.

3. Teflon (CF_2), carbon, and fluorine

Because of the interest in fluorine worth in connection with the UF_6 experiment (Reference 2), fluorine worth in the core was evaluated for both a light and heavily loaded core. In the heavily loaded core (86 kg U), carbon, fluorine, and teflon are all positive, except perhaps at the very edge of the core. In the lightly loaded core (23 kg), all are negative, except for carbon near the center of the core (see Table 3.3). All of these materials do some moderating, and are thus positive reactivity effects in the heavily loaded core interiors which are well shielded from thermal neutrons. But in the lightly loaded cores, the moderating effects are not as effective but the absorption cross section, though quite small in both C and F, become important because the fuel is so dilute.

4. Hydrogen Worth in the Cavity as Determined with Polyethylene (CH_2) and Polystyrene (CH)

Hydrogen worth as deduced from the measured worth of carbon and polyethylene or polystyrene is not a true indication of the worth of gaseous hydrogen. The carbon contribution to the worth of the plastic material is usually only about 10% of the total. But part of the effect of the plastic worth is apparently a result of its reflecting properties, since the worth (negative in all cases) more than doubles from the cavity wall to the inner edge of the core. It would be expected that significant differences in binding energies of the CH, CH_2, and H_2 molecules could noticeable influence the worth of these materials. Of course, the absorption characteristics as they effect the worth can easily be scaled from one material to the other. The difference in molecular binding effects is, in part, believed to be the cause of the difference in worth between hydrogen in CH and hydrogen in CH_2, the former appearing to be worth about 35% more.

In the core, a hydrogeneous moderator has a relatively large positive reactivity effect averaged throughout the core. This is particularly true in the heavily loaded cores, where H = 0.7%Δk/kg averaged throughout the 86 kg core. However, the effect near the outer edge of the core is negative, as it is in the void between core and reflector. For instance, in the entire mixing region of fuel and hydrogen simulated in the variable H experiment, the worth of hydrogen was a negative 0.2%Δk/kg. Thus, these results indicate that normal slight mixing of hydrogen into the fuel region is not likely to cause serious reactivity perturbations. It is only in the case of complete collapse of the fuel-hydrogen separation so that both mix completely throughout the cavity that a catastrophic positive reactivity addition is expected. Hydrogen mixing throughout the core is positive and fuel expansion into the full cavity is highly positive (Reference 1 page 50). Thus, one can conclude that a loss of hydrogen flow or a decrease in flow sufficient to wash out the boundary between core and hydrogen would be a serious reactivity perturbation.

5. Support Structure for Beryllium

The variation in worth of the beryllium slabs, 10 cm thick, placed in the D_2O reflector was reported in Reference 1, page 365. The experimental results did not agree well with any of the calculations, principally because the worth of the support structure (aluminum, steel, and teflon) holding the beryllium was not separated from the beryllium effect. The worth of this support structure at the 5.8 cm position was measured in both a heavily loaded and a lightly loaded configuration. The results were -2.3%Δk and -2.7%Δk, respectively, for structure that supported all of the beryllium blocks in the reflector at the 5.8 cm location. If the worth of this structure is assumed to vary in a similar manner to the worth of aluminum in the reflector (Reference 1)

page 162), then the corrected values for beryllium worth alone are:

Be reflector 0.8 cm from cavity wall	=	-5.5%Δk
at 5.8 cm	=	-2.4%Δk
at 10.8 cm	=	-2.2%Δk

3.5 Hydrogen Temperature Coefficient of Reactivity

The heating of the polyethylene structure between the core and reflector resulted in a positive change in reactivity, 0.8%Δk from 20 to 77°C. This measurement was made on a heavily loaded core, 90 kg U, in which the power ratio from the outside corner to the center was a factor of 18. Thus, the core was quite gray, even black to thermal neutrons. The heating of the polyethylene hardened the overall reactor spectrum slightly, resulting in somewhat less absorption in the reflector and the polyethylene but little effect on absorption in the core because it was already nearly black. Though the experiment did not perfectly insulate the core and reflector, the reflector temperature change and the core expansion effects were negligible effects on reactivity compared to the measured total temperature coefficient.

3.6 Design and Structural Perturbations and Considerations

A cavity reactor experiment involves two nuclear effects which are particularly important to simulate in order to obtain good correlation with reactor physics computer calculations. First, the thermal neutron lifetime and migration distance in the reflector are quite large. Absorption by structural material is, therefore, an important consideration. In Section 3.4 the advantage of magnesium vs aluminum was given. Placement of the structure within the reflector is also a critical consideration, and additional data on this effect is given in Reference 1, p. 163. Severe structural perturbations in the reflector, such as the gap between tables, required for safety considerations are to be avoided if possible. This gap was measured on a lightly loaded core and reported in Reference 1 as being worth approximately 0.55%Δk per cm. This effect was remeasured on the heavily loaded variable CH_2 configuration (86 kg U) and the identical result was obtained.

For the core of the critical experiments described in this volume, the sheet fuel arrangement was intended to simulate a gaseous core. The simulation had some shortcomings, one being the large quantity of aluminum oriented as sheets parallel to the three principal cartesian axes. The fuel, furthermore, was of sheets oriented in these same principal directions. This identical core arrangement was used in the lightly loaded (20 to 30 kg U), UF_6 mockup experiments (Reference 2) and it was found that the critical mass of the mockup reactors was about 4% greater than that of the equivalent UF_6 gas-core reactor. It is not known if this 4% correction applies to the more heavily loaded configurations. It is assumed that the relative spread in path lengths about the average path length is nominally the same in both cases. If this spread (variance) is small and there are essentially no streaming

paths, then the bias between a sheet fuel core and a gaseous core would in these heavily loaded configurations be no worse than the previously measured 4% on the lightly loaded configurations.

A heavier core might be expected to suffer more severly from streaming effects down the aluminum structure. Both reactivity and flux measurements were made to check the effect of the structure, but it was found to not create streaming. The flux was not higher along the aluminum and the reactivity worth of fuel did not appear to depend on its orientation at any given location nor on its proximity to aluminum sheets. Further details of these measurements can be found in Section 9.

At the outer edge of the core, a perfect cylindrical boundary did not exist. In fact, the unevenness of the outer boundary was a fortuitious simulation of the diffuse core boundary that would actually occur in the flowing gas reactor. This unusual boundary, however, is not conducive to simplification of reactor physics computer calculations. As discussed in more detail in Reference 2, p. 202, the core can be defined, for computer calculations, as a cylinder with 124.4 cm outer diameter, but with only 25% of the normal fuel density in the annulus from 121.9 cm diameter to 124.4 cm diameter.

3.7 Flux and Power Distribution Comparisons

3.7.1 Power Distribution

Both bare and cadmium catcher foils have been exposed in the cavity region of most of the cavity critical experiments. These configurations subsequently produced significant differences in the materials in the region between the core and reflector and the reflector itself. However, the core fuel loading had a major effect on power distribution, therefore, some of the data were assembled from References 1 and 2, as well as the data from this report, to show the change in the ratio of the power at the outer edge of the fuel to the core center as well as the U^{235} cadmium ratios (infinitely dilute) at the outer edge of the fuel and core center. These data are shown in Table 3.4 and Figure 3.6. The ratio of the bare catcher foil activity (total fission rate) on the axial midplane from the outer edge of the fuel to the core center follows closely a linearly increasing function while the cadmium ratios are approximately exponential decreasing functions of the core loading. The core loading is, of course, not the only effect on these data as there were major changes in the materials outside the active core. Nevertheless, the trends in the data for the most part are representative of the effects of variations in fuel loading in the core, since the incident thermal flux originating from the reflector varied little from one configuration to the other.

3.7.2 Thermal Neutron Flux

Where both bare and cadmium covered gold foil data have been obtained on each configuration, infinitely dilute cadmium ratios and thermal neutron fluxes have been calculated. These values have been tabulated for a number of experiments in Table 3.5. The flux in the core is a very strong function of core loading. The flux at the outside and at the center of the core

are plotted against core loading in Figure 3.7 to show this relationship. These curves look much like the catcher foil cadmium ratio curves, as would be expected.

The reflector regions do not show appreciable changes due to core loading variations but apparently respond more to the materials placed in the region between the active core and cavity wall and in the reflector.

TABLE 3.1

Summary of Configurations

(No correction has been applied for the worth of the table gap)

Code Identification	Configuration (1) Description	Loading (kg Oralloy) and Measured k-excess	Radial Power Ratio (2) Surface/Center	Core Average to Core-Center Power Ratio	Core Average Fuel Worth %Δk/kg	Critical [k = 1.0[4]] Mass
SS	Only the 0.095 cm thick ss liner Be reflector slabs	36.8 kg at 1.31%	2.7	1.88	0.468	31.5 kg Oralloy
18 CH_2	18.1 kg CH_2 in cavity[3] (0.95×10^{21} H/cc) Be reflector slabs	57.4 kg at 0.70%	---	---	0.204	54.1
38 CH_2	38.3 kg CH_2 in cavity[3] (2×10^{21} H/cc) Be reflector slabs	89.6 kg at 0.41%	5.1	3.88	0.116	86.0
Hot CH_2	36.5 kg CH_2 heated to 78°C extra support structure Be reflector slabs	89.6 kg at 1.20%	3.7	---	---	82.6
Var CH_2	20 kg CH_2 in non-uniform distribution in cavity Be reflector slabs	86.2 kg at 2.23%	4.4	3.50	---	72.0
3 in. fuel	739 gm U^{235} in reflector at 7.6 cm from inner wall	23.25 kg at 1.25%	2.0	1.63	---	21.7[5]
7-1/2 in.	823 gm U^{235} in reflector at 19 cm from inner wall	23.25 kg at 3.54 %	---	---	---	18.7

TABLE 3.1

(Continued)

(1) All configurations contained the 0.095 cm thick stainless steel liner.

(2) This is a longitudinal average along the core.

(3) In discussion of hydrogen density the "cavity" refers to the annulus between the core and reflector and equal to the core length.

(4) This is the experimental value, extrapolated from measurements. Note that if the table gap and end exhaust nozzle are to be deleted from the configuration, then the effective multiplication factor would be 1.0125.

(5) This value would read 21.3 if corrected for Al in fuel annulus.

TABLE 3.2

Summary of Fuel Worth

Configuration	Core Loading (kg U)	Uranium Worth (%Δk/kg U)	$\frac{\Delta k/k}{\Delta m/m}$
1	10.6	3.017 ± 0.275	0.349 ± 0.030
2B	19.7	0.902 ± 0.560	0.184 ± 0.114
3A	14.0	1.760 ± 0.296	0.255 ± 0.043
3B	14.5	1.681 ± 0.168	0.252 ± 0.025
4	20.8	0.837 ± 0.055	0.180 ± 0.012
5A	20.8	1.010 ± 0.106	0.217 ± 0.023
5B	19.4	0.826 ± 0.031	0.165 ± 0.006
6	19.1	1.074 ± 0.113	0.212 ± 0.022
7B	20.2	0.831 ± 0.055	0.174 ± 0.011
Mockup No. 1 - Be	27.8	0.644 ± 0.055	0.185 ± 0.016
Mockup No. 2 - Be	27.2	0.703 ± 0.034	0.187 ± 0.009
Mockup No. 2 - No Be	20.8	1.105 ± 0.055	0.222 ± 0.011
UF_6 - Be	23.4	0.766 ± 0.054	0.179 ± 0.013
UF_6 - Be	24.2	0.627 ± 0.015	0.152 ± 0.004
UF_6 - Be	24.9	0.598 ± 0.007	0.149 ± 0.002
UF_6 - Be	25.3	0.612 ± 0.035	0.155 ± 0.009
UF_6 - Be	26.0	0.588 ± 0.043	0.152 ± 0.011
UF_6 - No Be	17.7	1.060 ± 0.020	0.188 ± 0.004
SS liner in cavity	36.6	0.468 ± 0.023	0.172 ± 0.008
SS liner and polyethylene in cavity	57.3	0.208 ± 0.010	0.116 ± 0.006
SS liner andpolyethylene in cavity	89.6	0.116 ± 0.006	0.104 ± 0.005
7.6 cm fuel annulus	23.3	0.770 ± 0.015	0.180 ± 0.004

NOTE: For description of configurations refer to References 1 and 2

TABLE 3.3

Material Worth Measurements

Material	Configuration	Core Loading	Location of Measurement	Worth %Δk/kg	Comments
Aluminum (1100)	SS	36 kg	Core average	-0.0137	34.2 kg Al/kg U
	18 kg CH_2	58	Core average	-0.0114	17.9 gk Al/kg U
	38 kg CH_2	90	Core average	-0.0075	15.4 kg Al/kg U
	(Mockup UF_6) (1)	(21)	(Core average)	(-0.021)	(50 kg Al/kg U)
Aluminum (6061)	Var. CH_2	86	Cavity wall	-0.0180	
Mg			wet surface	-0.0075	
Aluminum (6061)	Var. CH_2	86	Reflector, 7.6 cm	-0.0402	
Mg			from wall	-0.0292	
Aluminum (6061)	7.6 cm fuel ring	23	Core edge	-0.0267	
Mg				-0.0251	
Aluminum (1100)				-0.0255	
Teflon (CF_2)	Var. CH_2	86	Core average	+0.0028	
C			Mid core radius	+0.0023	
F			Core average	+0.0030	CH_2 - C
Teflon (CF_2)	7.6 cm fuel ring	23	Core average	-0.00126	
C			Core center	+0.00018	
C			Mid core radius	-0.00037	
F			Core average	-0.00154	CH_2 - C
CH_2	38 kg CH_2	90	Core edge	-0.46	
			mid void	-0.17	
			Cavity wall	-0.17	
	Var. CH_2	86	Core average	+0.12	
			Outer 7 cm core	-0.38	
			Mid core radius	+0.24	
Structure to Support Be	Var. CH_2	86	5.8 cm in	-2.3	
	7.6 cm fuel	23	Be reflector	-2.7	

(1) Page 42 of Reference 2

TABLE 3.4

Summary of Power Distribution Trends

Configuration	Core Loading (kg U)	Power Ratio Core edge/Core center	Cadmium Ratio Core edge	Cadmium Ratio Core Center
3A - all D_2O (1)	14.5	1.93	27.8	15.2
3B - all D_2O, end nozzle (1)	15.0	1.83	--	--
4 - Be at 0.8 cm (1)	21.5	2.27	--	--
5A - Be at 5.8 cm (1)	21.5	2.13	--	--
6 - Be at 10.8 cm (1)	19.7	2.10	--	--
Mockup No. 1 with Be (2)	28.3	2.86	15.2	6.6
Mockup No. 2, all D_2O (2)	20.8	2.15	17.4	8.2
Mockup No. 2 with Be (2)	27.2	2.81	14.7	6.4
UF_6, all D_2O (2)	17.3	2.0	--	--
UF_6 with Be (2)	23.6	2.47	15.1	6.9
SS liner alone	36.8	3.49	--	--
36.5 kg CH_2	89.6	8.80	11.4	1.8
Variable CH_2	86.2	8.50	9.9	1.7
7.6 cm Fuel annulus	23.2	2.51	17.4	7.8

NOTE: The core edge is the outer edge of the active core at the axial midplane.

(1) Reference 1
(2) Reference 2

TABLE 3.5

Summary of Gold Foil Cadmium Ratios and Thermal Neutron Flux

Configuration	Core Loading (kg U)	Thermal Neutron Flux - $n/cm^2/sec/watt \times 10^{-6}$				Gold Infinitely Dilute Cadmium Ratio	
		Core Center	Outer edge of Fuel	108 cm Radial Reflector	75 cm End Reflector	108 cm Radial Reflector	75 cm End Reflector
3A	14.5	1.11	2.14	4.90	5.60	4.51	3.63
4	21.5	0.80	1.67	4.84	5.75	4.43	3.29
5A	21.5	0.73	1.70	4.40	4.53	4.66	3.39
6	19.7	0.94	1.65	3.91	5.58	3.32	3.33
Mockup No. 1 with Be	28.3	0.44	1.54	4.05	5.14	3.70	3.40
Mockup No. 2 with Be	20.8	0.52	1.57	4.73	5.82	4.35	3.15
Mockup No. 2	27.2	0.78	1.75	5.98	6.02	3.87	3.01
UF_6 with Be	23.6	0.65	1.55	4.59	6.13	3.89	3.38
SS + 36.5 kg CH_2	89.6	0.006	0.75	3.75	4.74	4.5	3.2
SS + variable CH_2	86.2	0.065	0.94	4.19	4.51	4.5	3.0
SS + fuel annulus, 7.6 cm	23.2	0.78	1.83	6.21	6.25	3.6	3.1

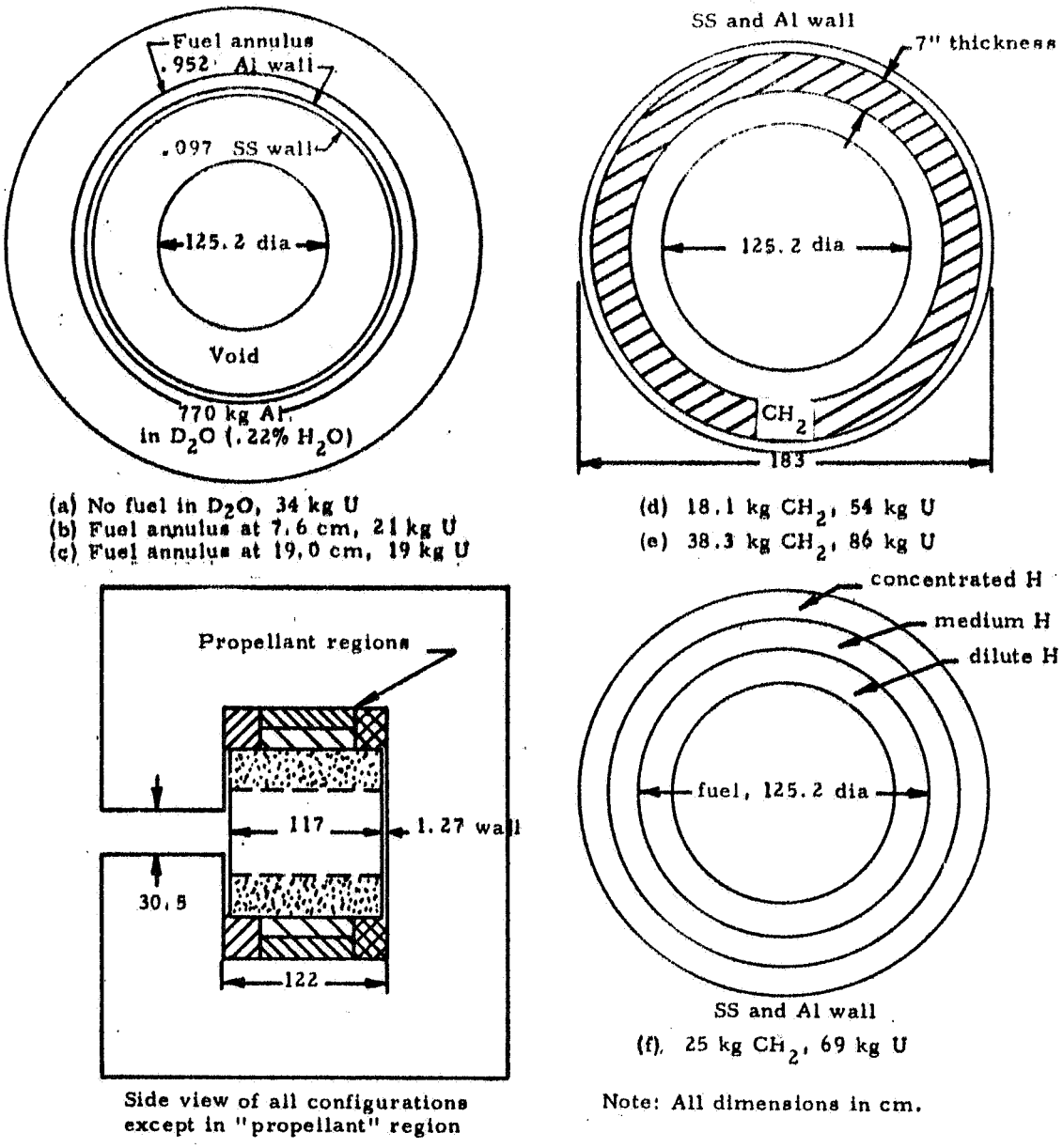

Fig. 3.1 Reactor configurations and their critical masses (D_2O thickness is 88.9 cm)

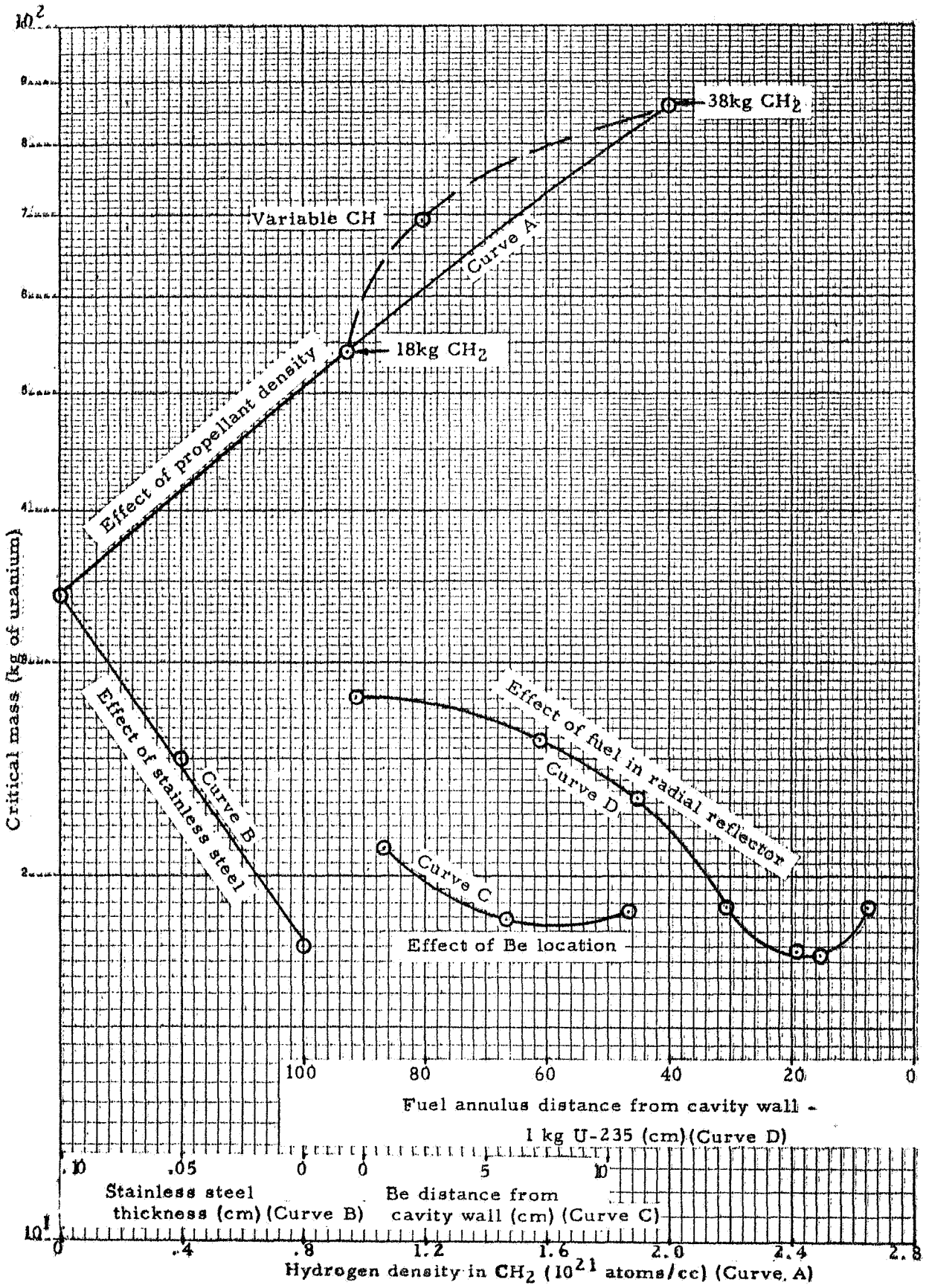

Fig. 3.2 Critical mass comparisons of various reactor configurations

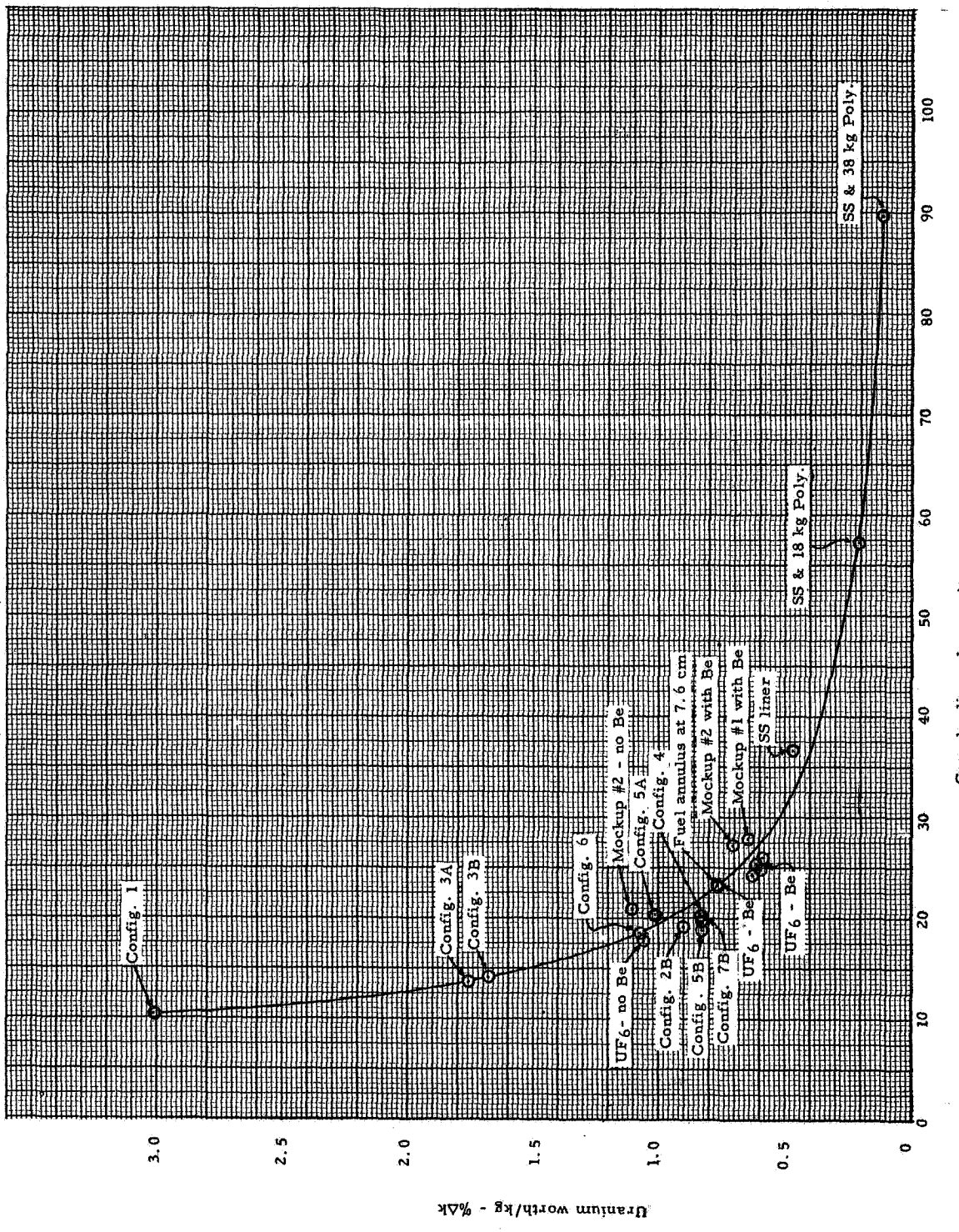

Fig. 3.3 The effect of core loading on fuel worth

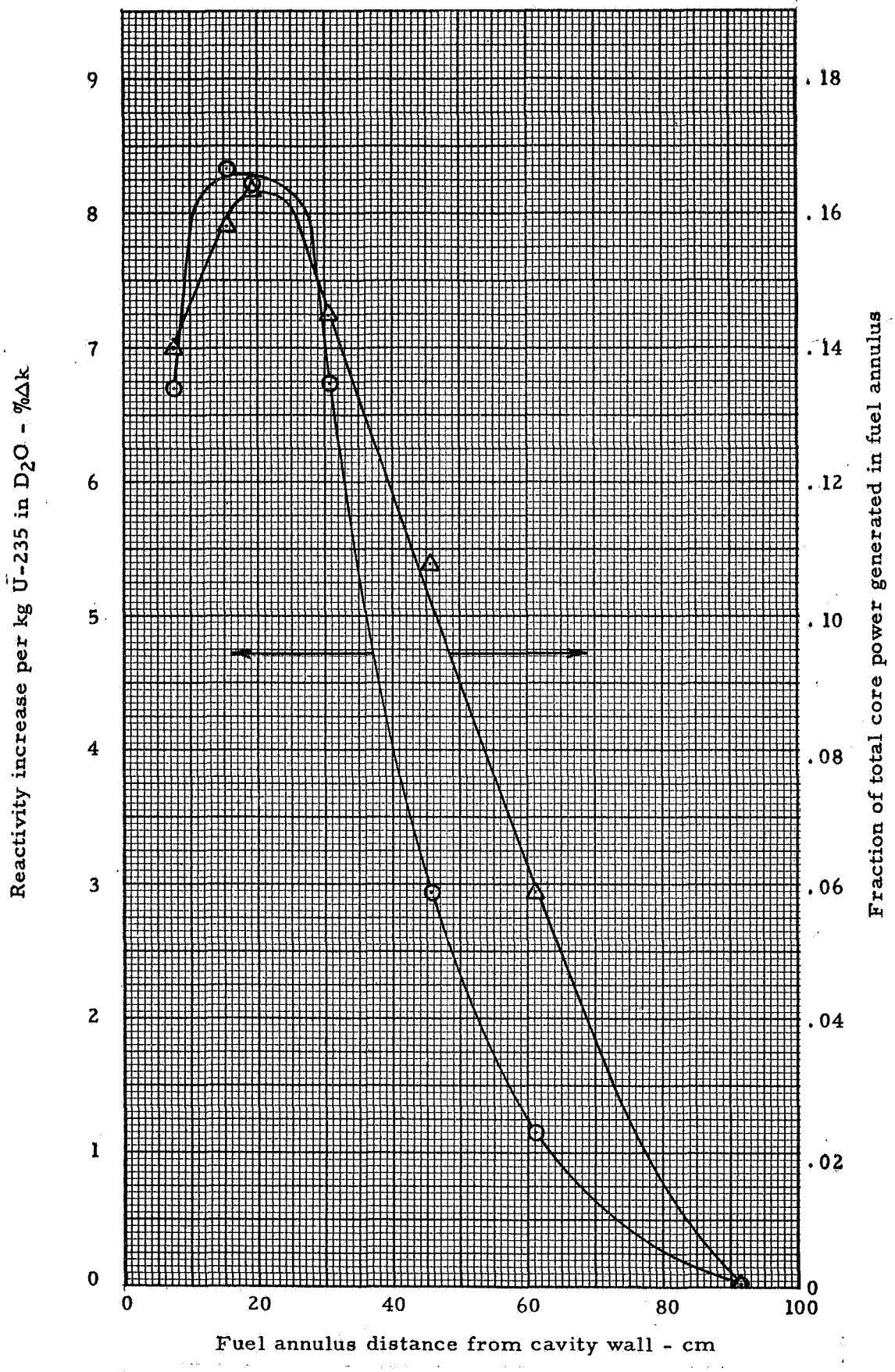

Fig. 3.4 Power production effects of fuel in the radial reflector

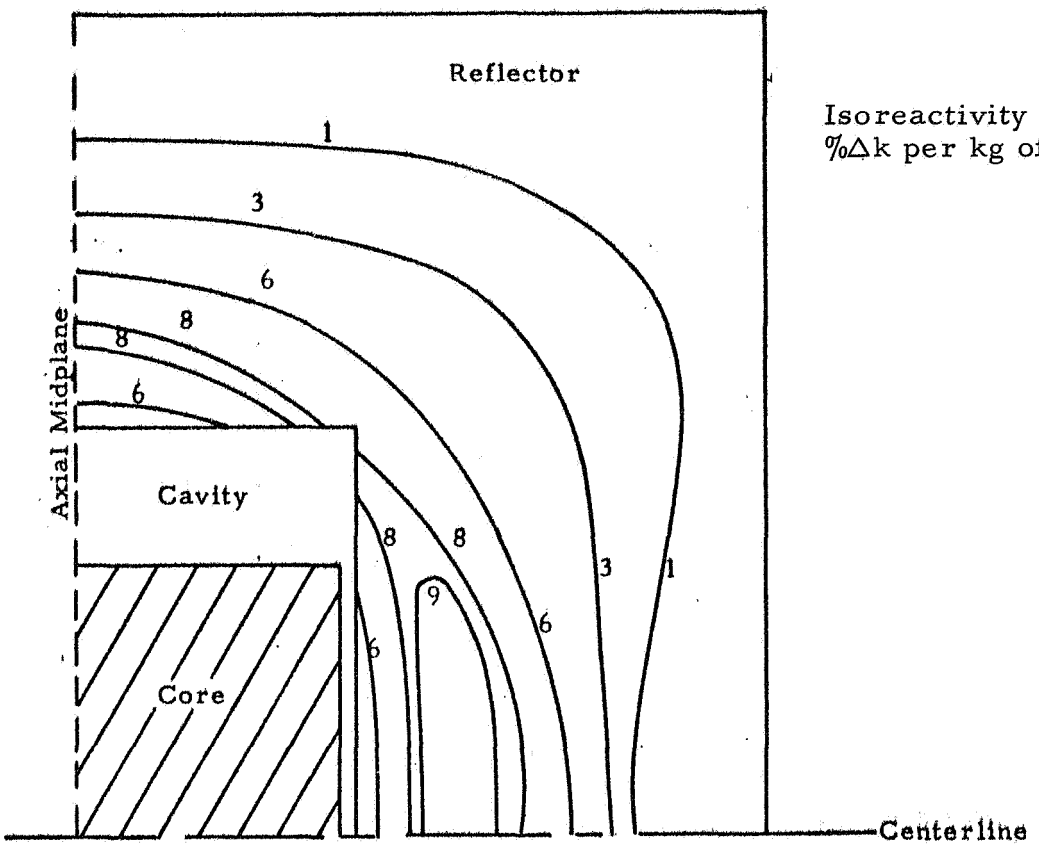

Isoreactivity by lines - %Δk per kg of U-235

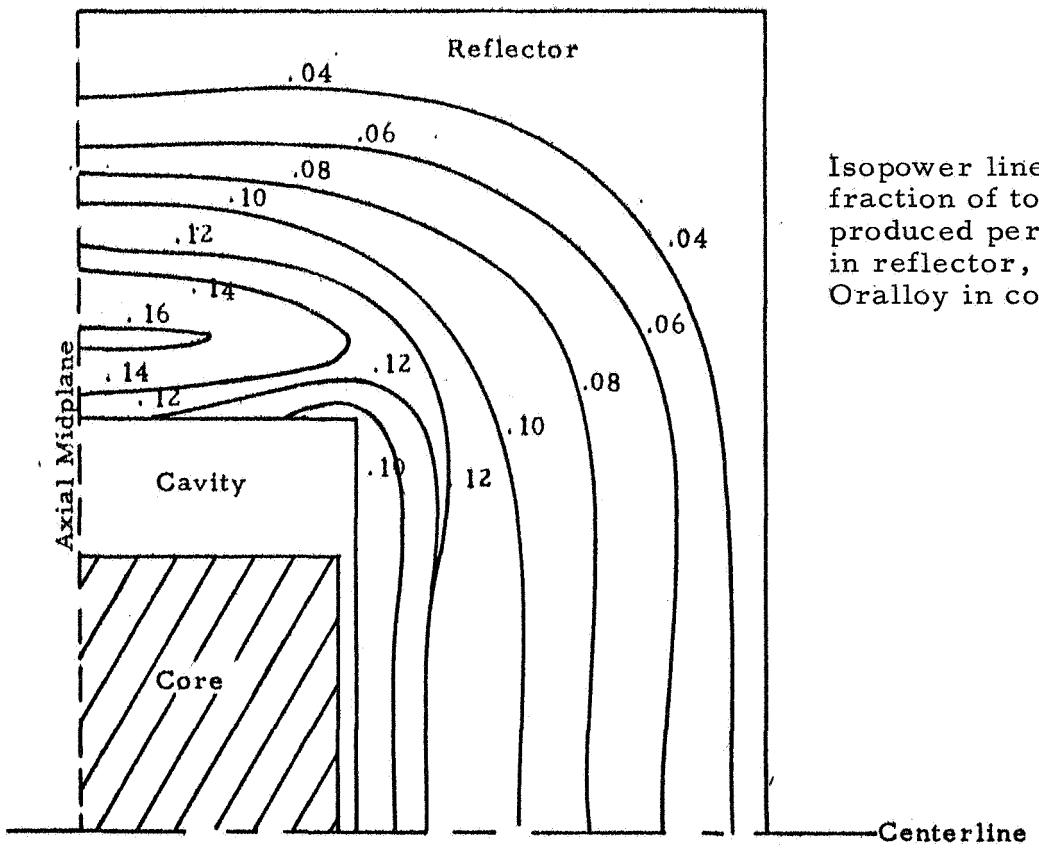

Isopower lines - fraction of total power produced per kg of U-235 in reflector, with 23.25 kg Oralloy in core

Fig. 3.5 Effectiveness of fuel in the reflector

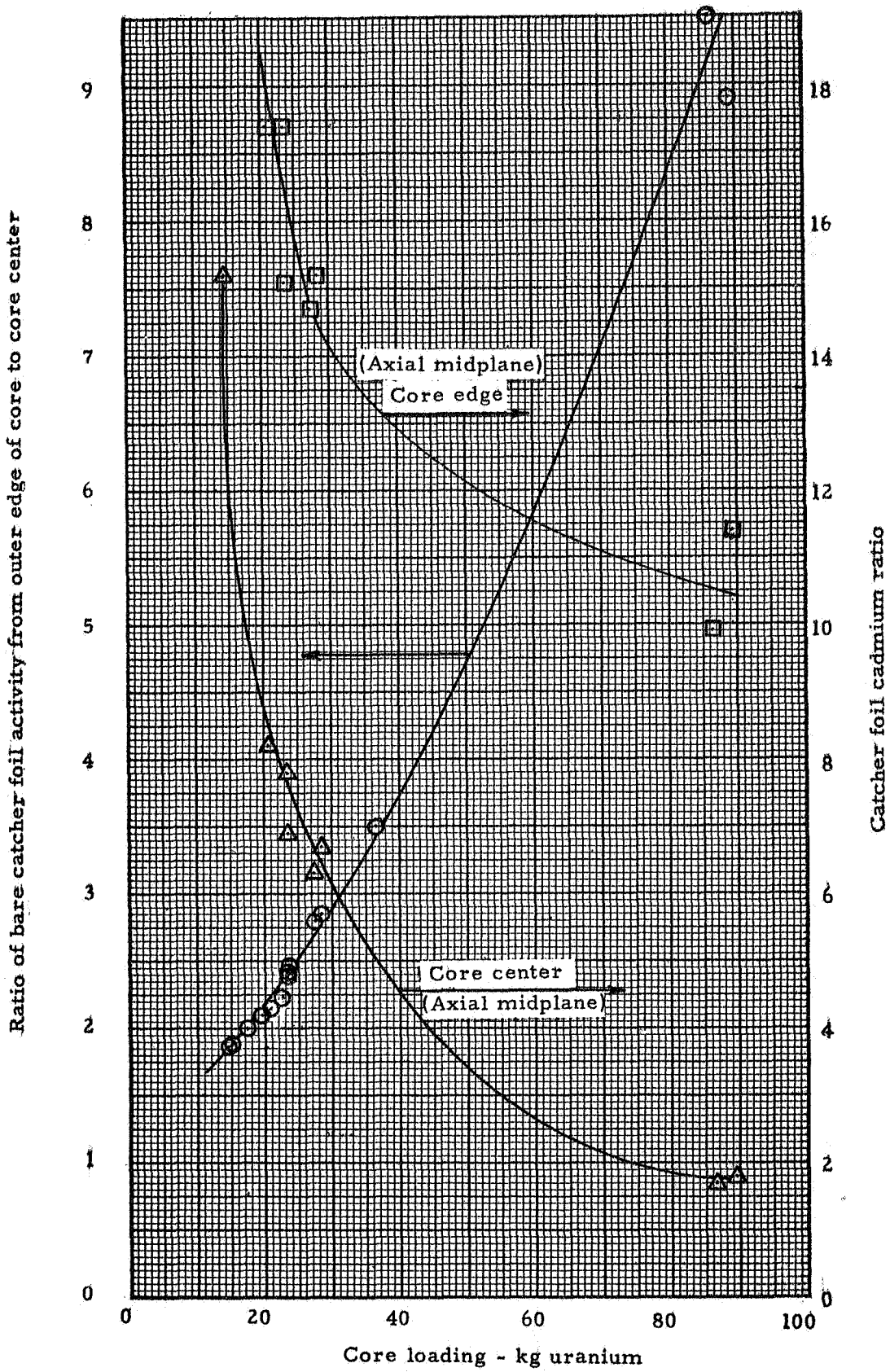

Fig. 3.6 Power distribution curves, bare and cadmium foil ratios as a function of core loading

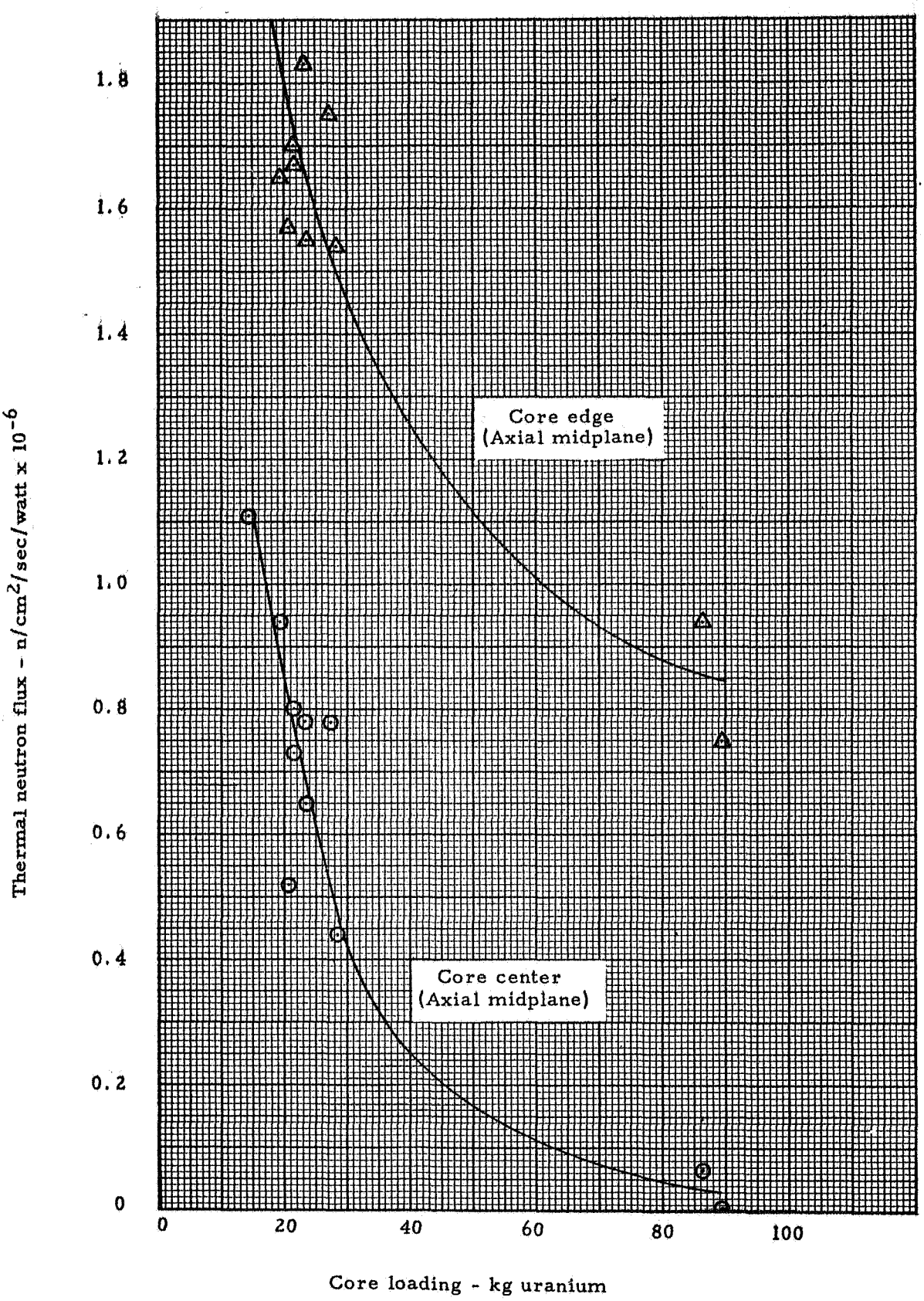

Fig. 3.7 Thermal neutron flux as a function of core loading

4.0 STAINLESS LINER

4.1 Initial Loading

Initial loading of this reactor began December 8, 1967. A conservative estimate of the critical loading was made from the results of the previous UF_6 mockup experiments (Reference 2). It was estimated that it would require in the order of 70 kg of fuel to make a critical assembly with 83.1 kg of stainless steel lining the cavity wall. Therefore, the fuel elements were loaded with 60 size 1.5 sheets of fuel, 6 per stage over 10 stages, and 35 size 1.0 sheets of fuel. There was a single size 1.0 sheet at each end of the element, three between each stage containing size 1.5 sheets and a size 1.0 fuel sheet stage at the end of the element containing an additional 6 sheets for a total of 35 size 1.0 sheets of fuel. A full loading of this prescription with 208 fuel elements would have been 68 kg.

A normal incremental loading procedure was followed. Three counting channels were used to monitor multiplication. After 7 increments and a total of 113 fuel elements had been placed in the reactor, it was critical and k-excess was 0.118%Δk. The data obtained from the counting channels over this loading process are given in Table 4.1 and the inverse multiplication is shown in Figure 4.1. The total fuel loading was 36.7 kg and the location of each fuel element in the reactor at this point is given in Figure 4.2, along with incremental order of loading.

It was obvious at this point that the fuel density would have to be reduced significantly in order to achieve a uniformly loaded core. Prior to doing this, 14 fuel elements were removed from the reactor and the remaining were uniformally distributed throughout the active core as shown in Figure 4.3. Empty fuel elements were placed in the reactor where needed to support the elements containing fuel. The multiplication data obtained for this arrangement are also given in Table 4.1.

The plan at this point was to reduce the loading of the fuel elements to 88 equivalent size 1.0 sheets by removing 10 size 1.5 sheets and 22 size 1.0 sheets of fuel. There would be 104 of these fuel elements and an additional 104 fuel elements were assembled each containing a total of 48 size 1.0 sheets. The lighter loaded fuel elements were loaded with 16 stages of fuel, each stage containing three size 1.0 sheets of fuel. The changeover was accomplished in fairly large steps while holding the total core loading essentially constant, as will be observed from Table 4.1, until there were 104 88-sheet elements and 87 48-sheet elements in the reactor (35.0 kg). With this loading the reactor was critical and k-excess was 0.459%Δk.

The final loading of 104 88-sheet elements and 104 48-sheet elements had a k-excess of 1.305±0.021%Δk and there were 36.8 kg of uranium in the core. The D_2O temperature was 21°C at this point. There were 5616 aluminum fuel spacers in the fuel elements. These weighed 19.43 kg and are in addition to the aluminum weights given in Section 2.1 of this report. The layout of the types of fuel elements and their location within the reactor is presented in Figure 4.4.

4.2 Reactivity Measurements

4.2.1 Rod Worths

Several rod worth measurements were performed after the reactor was a critical assembly and the results are presented in Table 4.2. The average for Actuators 3 and 6 was -1.553 ± 0.025%Δk for three separate measurements. The value obtained on Run 300 was not used in the average as it appears that this measurement was not valid, for the result is far outside the normal error for the other rod worth measurements. The average worth of all six actuators (17 rods) was -4.082 ± 0.071%Δk.

The worth of Actuator 6 was obtained by incrementally pulling the rods from all the way inserted to the withdrawn position. The purpose of the measurement was twofold, to measure the worth of the actuator of rods and to generate a rod worth curve. The measured results, are given in Table 4.3. The total rod worth was -0.6568%Δk and reduces to the rod worth curve shown in Figure 4.5. Included in the figure is a previously measured curve from Actuators 3 and 6 and it will be observed that there was excellent agreement between the two curves. This new curve was reduced to tabular form and the data are given in Table 2.1. When using all rods as a unit the tabular rod worth curve in Table 2.2 was used to evaluate total rod worth and k-excess, otherwise the curve for the single actuator was used.

4.2.2 Material Worths

The worth of uranium was measured by interchanging 48-sheet with 32-sheet fuel elements at several radial locations within the active core. In addition, a couple of measurements were obtained by interchanging 88 with 120 sheet fuel elements. Three fuel elements were exchanged when measuring the difference between the light loaded fuel elements and two were used for the heavy loaded fuel elements. The results are shown in Table 4.4 and Figure 4.6. The volume weighted core average was 0.468%Δk/kg. The difference in the points at the core boundary was to be expected since the lighter loaded fuel elements would have less self-shielding to thermal neutrons than the heavier loaded fuel elements and would thus give a higher fuel worth. As the data indicates, this difference would be reduced to essentially zero near the core center because of the harder spectrum.

The core average worth of type 1100 aluminum was measured to be $-(1.367 \pm 0.064) \times 10^{-2}$%Δk/kg. With reference to the worth of uranium, it takes 1 kg of uranium to compensate for 34.2 kg of aluminum averaged over the active core.

4.3 Power Distribution Measurements - Bare Catcher Foils

Bare catcher foils were exposed in the cavity region of the reactor containing the stainless steel liner only. The data are given in Table 4.5. The axial power distributor was measured at several radial positions as shown in Figure 4.7. Each of the axial profiles was averaged giving the radial power profile shown in Figure 4.8. The volume weighted average over the active core was 1.882 with respect to the point at the core center.

A number of catcher foils were also placed at the separation plane to measure the power distribution across the face of the core, as shown in Figure 4.9. The 30.5 cm diameter hole in the end reflector, which simulates the exhaust nozzle, caused a significant increase in power over the nozzle region as seen from this figure. There is no obvious reason for the slightly skewed distribution, except for slight uncertainties in location of the foils.

The foil exposures were made with all rods equally withdrawn to about 3000 on the ratiometer or 25.7 cm, and the D_2O temperature was 21°C. There were six actuators and 17 rods attached to these actuators.

4.4 Resonance Detector Data - Bare Gold Foils

Only bare gold foils 0.0013 cm thick were exposed in the reflector regions and outer surface of the cavity of this configuration. The tabulated data are given in Table 4.6 and these are shown graphically in Figures 4.10 and 4.11. Beyond 34 cm from the cavity wall the fixed end reflector gold foil activities fall below the radial reflector. This was due to the position of the control rods in the end reflector.

The gold foil activities on the surface of the cavity wall on the cavity side of the stainless steel liner show a very flat distribution, Figure 4.11.

TABLE 4.1

Inverse Multiplication

Initial Loading-Stainless Steel on Cavity Wall

Increment	Total Number Elements	Channel No. 1 CPM	Channel No. 1 CPMo/CPM	Channel No. 2 CPM	Channel No. 2 CPMo/CPM	Channel No. 3 CPM	Channel No. 3 CPMo/CPM	Rod Positions
0	B kg	1109	1.000	1145	1.000	863	1.000	In
0	B kg	1235	1.000	1296	1.000	965	1.000	Out
1	31	3970	0.279	4162	0.275	3021	0.286	In
1	31	4894	0.252	5223	0.248	3738	0.258	Out
2	37	4596	0.241	5014	0.228	3572	0.242	In
2	37	5960	0.207	6382	0.203	4574	0.211	Out
3	55	7384	0.150	7945	0.144	5865	0.147	In
3	55	10442	0.118	11253	0.115	8096	0.117	Out
4	65	9550	0.118	10194	0.112	7434	0.116	In
4	65	14383	0.0859	15511	0.0836	11118	0.0868	Out
5	84	15638	0.0709	16426	0.0697	11896	0.0725	In
5	84	29677	0.0416	31378	0.0413	22797	0.0423	Out
6	99	24014	0.0462	25072	0.0457	18332	0.0471	In
6	99	73754	0.0167	75850	0.0171	54348	0.0178	Out
7	113	39422	0.0281	41714	0.0274	30160	0.0286	In
7	113	Critical with a k-excexx of 0.1178%Δk.						
		Rearranged Fuel Elements as per Figure 4.3						
	99	32256	0.0344	29689	0.0386	22131	0.0390	In
	99	151010	0.0082	136846	0.0095	97444	0.0089	Out
		Rearranged Fuel Elements						
Number of Fuel Sheets		67 125-sheet elements 37 88-sheet elements 15 48-sheet elements 12351 sheets						
12351		29720	0.0373	30037	0.0381	21630	0.0399	In
12351		144296	0.0086	141701	0.0092	97041	0.0099	Out
		104 88-sheet elements, 67 48-sheet elements						
12368		30617	0.0362	31611	0.0362	22956	0.0376	In
12368		190349	0.0065	188969	0.0069	130110	0.0074	Out
		104 88-sheet elements, 87 48-sheet elements						
13040		37460	0.0396	39264	0.0292	27912	0.0294	In
13040		Critical with k-excess of 0.459%Δk						

TABLE 4.2

Control Rod Worth Measurements

Stainless Steel on Cavity Wall

Run Number	Actuator Combinations	Reactivity worth of rods - %Δk
300	3 and 6 (6 rods)	-1.154
302	3 and 6 (6 rods)	-1.537
303	3 and 6 (6 rods)	-1.582
304	3 and 6 (6 rods)	-1.541
301	1 to 6 (17 rods)	-4.132
305	1 to 6 (17 rods)=	-4.032
306 to 313	6 (3 rods)	-0.6568

TABLE 4.3

Rod Worth Curve Measurement

Actuator 6

Run Number	Actuators 1 to 5	Actuator 6 position	Reactivity Worth of Increment -%Δk
306	1, 2, 3, 4 out 5 at 200	in (099) to 1000	0.1699
307	Same as run 306	in to 600	0.0949
308	1, 2, 3, out, 5 in 4 at 2999	1000 to 2200	0,1871
309	1, 2, 3 out, 5 in 4 at 1209	2200 to 4101	0.1805
310	2, 3, out, 4, 5, in 1 at 6103	4101 to out (9817)	0.1193
311	1, 2, 3 out, 5 in 4 at 323	3501 to out	0.1660
312	1, 2, 3 out, 5 in 4 at 312	3501 to 7500	0.1570
313	1, 2, 3, out, 5 in 4 at 312	3501 to 6001	0.1311

NOTE: Rod positions are ratiometer readings

TABLE 4.4

Fuel Worth Measurements

Stainless Steel on Cavity Wall

Run No.	Radial Distance (cm)	U weight difference (gm) (1)	Reactivity change (%Δk) (2)	Uranium Worth (%6k/
		Interchange of 32 and 48 sheet fuel elements		
314	7.6	154.46	0.0439	0.284
315	26.9	153.81	0.0448	0.291
316	59.2	154.02	0.1279	0.830
318	59.2	154.02	0.1280	0.831
319	43.5	153.81	0.0650	0.423
		Interchange of 88 with 120 sheet fuel elements		
324	5.4	146.36	0.0427	0.292
325	60.2	146.36	0.1031	0.704

(1) Fuel weights are accurate to ±1.0%.
(2) Estimated error in reactivity change is 0.005%Δk or less.

TABLE 4.5

Bare Catcher Foil Data

Stainless Steel Liner on Cavity Wall

Foil No.	Location Radial (cm)	Location Axial (cm)	Normalized Counts	Ratio of Local to Core Center (Foil No. X)
Run No. 1084				
1	0	206.9	74327	2.970
2	0	189.2	36015	1.439
3	0	173.9	24775	0.990
4	0	158.7	23679	0.946
5	0	148.5	25022	1.0 (X)
6	0	138.4	23742	0.949
7	0	123.1	24328	0.972
8	0	107.9	30592	1.223
9	0	90.8	59261	2.368
10	61.0	206.9	96861	3.871
11	61.0	189.2	92294	3.688
12	61.0	173.9	81871	3.272
13	61.0	158.7	81697	3.265
14	61.0	148.5	87306	3.489
15	61.0	138.4	86377	3.452
16	61.0	123.1	83117	3.322
17	61.0	107.9	91663	3.663
18	61.0	90.8	105103	4.200
Run No. 1085				
1	0	206.9	70490	2.794
2	0	189.2	35286	1.399
3	0	173.9	24915	0.988
4	0	158.7	22911	0.908
5	0	148.5	25227	1.000 (X)
6	0	138.4	23920	0.948
7	0	123.1	25251	1.001
8	0	107.9	30953	1.227
9	0	90.8	60458	2.397
10	19.1	206.9	63611	2.522
11	19.1	189.2	30250	1.199
12	19.1	173.9	27570	1.093
13	19.1	158.7	24775	0.982
14	19.1	148.5	25327	1.004
15	19.1	138.4	25151	0.997
16	19.1	123.1	24301	0.963
17	19.1	107.9	32000	1.268
18	19.1	90.8	55266	2.191
19	34.3	206.9	71437	2.832

TABLE 4.5

(Continued)

Foil No.	Location Radial (cm)	Location Axial (cm)	Normalized Counts	Ratio of Local to Core Center (Foil No. X)
Run No. 1085 (Cont'd)				
20	34.3	189.2	41746	1.655
21	34.3	173.9	33824	1.341
22	34.3	158.7	31157	1.235
23	34.3	148.5	32692	1.296
24	34.3	138.4	27818	1.103
25	34.3	123.1	38124	1.511
26	34.3	107.9	38834	1.539
27	34.3	90.8	59612	2.363
28	41.9	206.9	76476	3.032
29	41.9	189.2	43308	1.717
30	41.9	173.9	40502	1.605
31	41.9	158.7	31206	1.237
32	41.9	148.5	37874	1.501
33	41.9	138.4	36648	1.453
34	41.9	123.1	36630	1.452
35	41.9	107.9	45657	1.810
36	41.9	90.8	67925	2.693
37	49.5	206.9	83864	3.285
38	49.5	189.2	55220	2.189
39	49.5	173.9	46237	1.833
40	49.5	158.7	47690	1.890
41	49.5	148.5	46587	1.847
42	49.5	138.4	48379	1.914
43	49.5	123.1	48088	1.906
44	49.5	107.9	49277	1.953
45	49.5	90.8	70883	2.810
46	57.2	206.9	86415	3.425
47	57.2	189.2	66045	2.618
48	57.2	173.9	70592	2.798
49	57.2	158.7	60411	2.395
50	57.2	148.5	62787	2.489
51	57.2	138.4	65482	2.596
52	57.2	123.1	62161	2.464
53	57.2	107.9	69158	2.741
54	57.2	90.8	94822	3.759
55	61.0	206.9	94121	3.731
56	53.4	206.9	84883	3.365
57	45.8	206.9	76916	3.049
58	38.1	206.9	75394	2.989
59	30.5	206.9	68347	2.709
60	22.9	206.9	67333	2.669
61	15.3	206.9	68578	2.711
62	7.7	206.9	76288	3.024
63	0	206.9	79964	3.170

TABLE 4.5

(Continued)

Foil No.	Location Radial (cm)	Location Axial (cm)	Normalized Counts	Ratio of Local to Core Center (Foil No. X)
Run No. 1085 (Cont'd)				
64	7.7	206.9	82949	3.288
65	15.3	206.9	75817	3.005
66	22.9	206.9	68912	2.732
67	30.5	206.9	66223	2.625
68	38.1	206.9	74368	2.948
69	45.8	206.9	83666	3.317
70	53.4	206.9	89974	3.567
71	61.0	206.9	109175	4.328

TABLE 4.6

Gold Foil Data (0.0013 cm thick)

Stainless Steel Liner on Cavity Wall

Foil No.	Foil Type	Location Radial (cm)	Location Axial (cm)	Foil Weight (gm)	Specific Activity d/m/gm x 10^{-6}
Run 1084					
1	Bare	0	87.6	0.0364	3.634
2	Bare	0	82.5	0.04255	5.874
3	Bare	0	74.9	0.0409	7.042
4	Bare	0	67.2	0.0483	6.372
5	Bare	0	59.6	0.0302	5.089
6	Bare	0	44.4	0.0328	2.581
7	Bare	0	29.1	0.0298	1.249
8	Bare	0	13.9	0.0323	0.523
9	Bare	95.0	151.1	0.0408	4.964
10	Bare	100.1	151.1	0.0410	6.209
11	Bare	107.7	151.1	0.0369	6.182
12	Bare	115.4	151.1	0.0418	5.435
13	Bare	123.0	151.1	0.0397	4.625
14	Bare	138.2	151.1	0.0390	3.129
15	Bare	153.5	151.1	0.0392	1.989
16	Bare	168.7	151.1	0.0385	1.072
17	Bare	0	215.5	0.0388	3.372
18	Bare	0	220.6	0.03745	3.623
19	Bare	0	228.2	0.03524	4.234
20	Bare	0	235.8	0.0370	4.414
21	Bare	0	243.5	0.0333	4.208
22	Bare	0	258.7	0.0385	3.462
23	Bare	0	273.9	0.0302	2.671
24	Bare	0	289.2	0.0399	1.667
25	Bare	91.4	206.9	0.0385	3.429
26	Bare	91.4	189.2	0.0273	3.918
27	Bare	91.4	173.9	0.0312	3.770
28	Bare	91.4	158.7	0.0308	3.618
29	Bare	91.4	148.5	0.0363	3.600
30	Bare	91.4	138.4	0.0410	3.571
31	Bare	91.4	123.1	0.0322	3.712
32	Bare	91.4	107.9	0.0389	3.637
33	Bare	91.4	91.8	0.0402	3.652

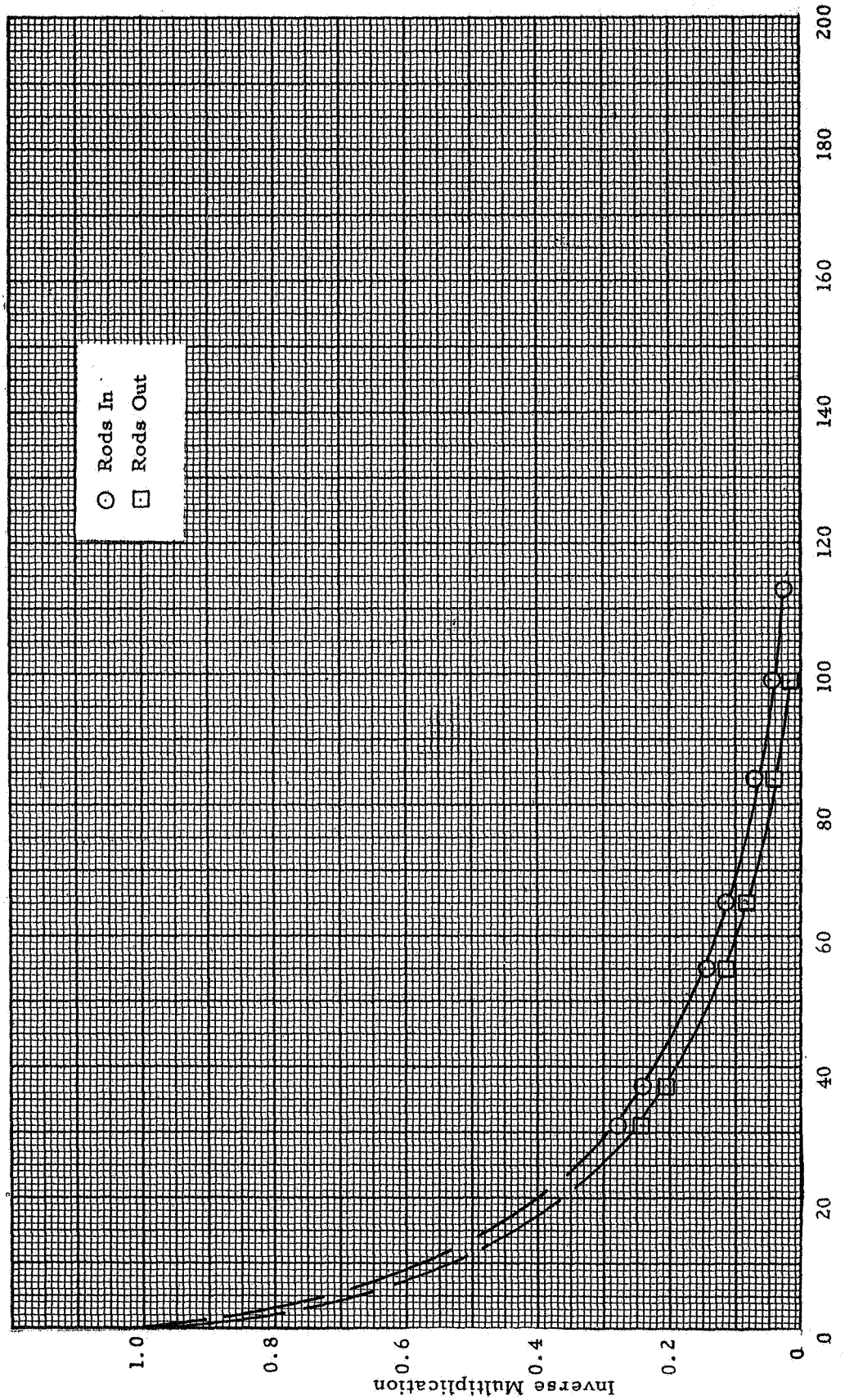

Fig. 4.1 Inverse multiplication curves, stainless steel liner

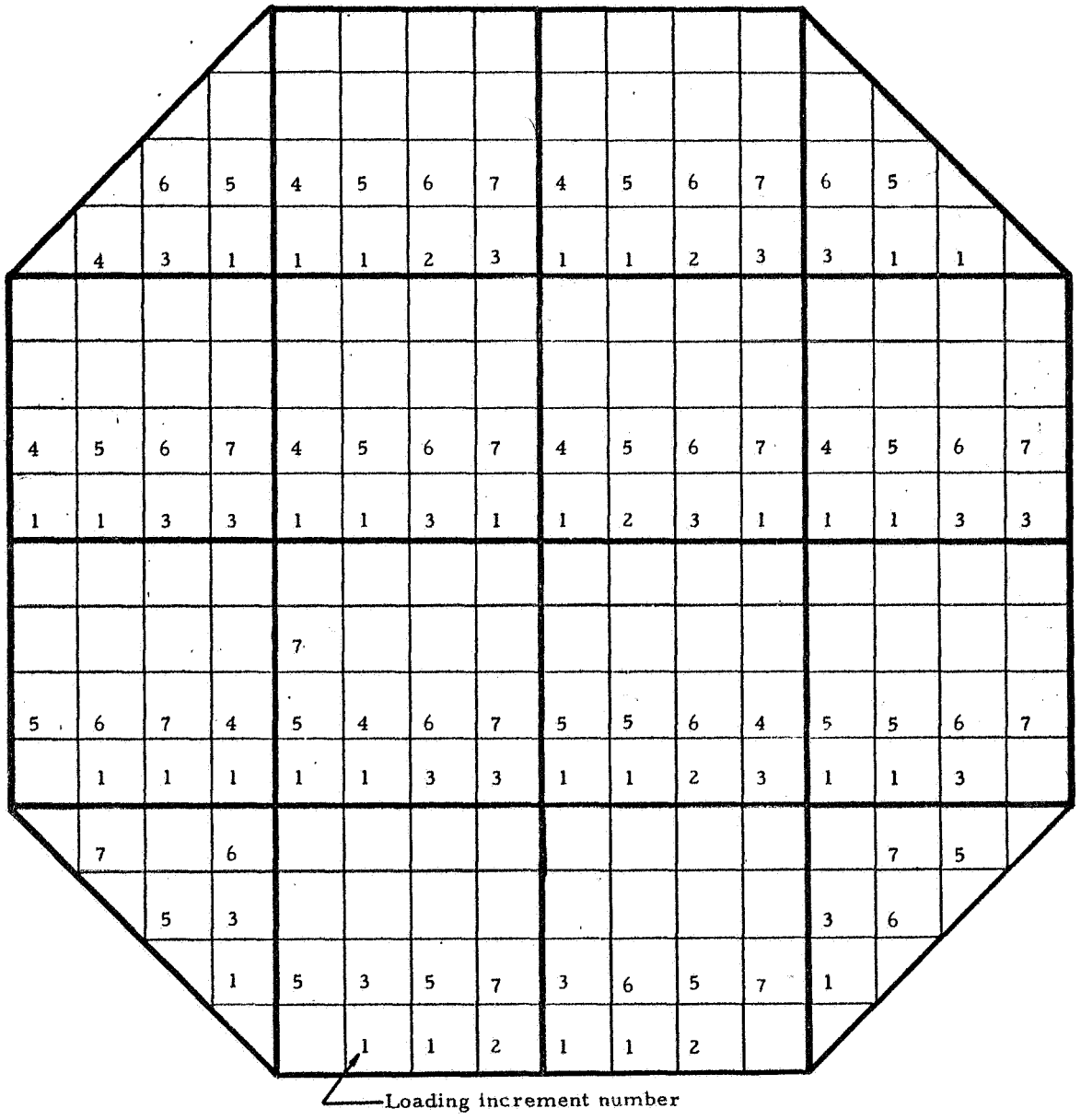

Fig. 4.2 Fuel element location at initial incremental loading, stainless steel liner

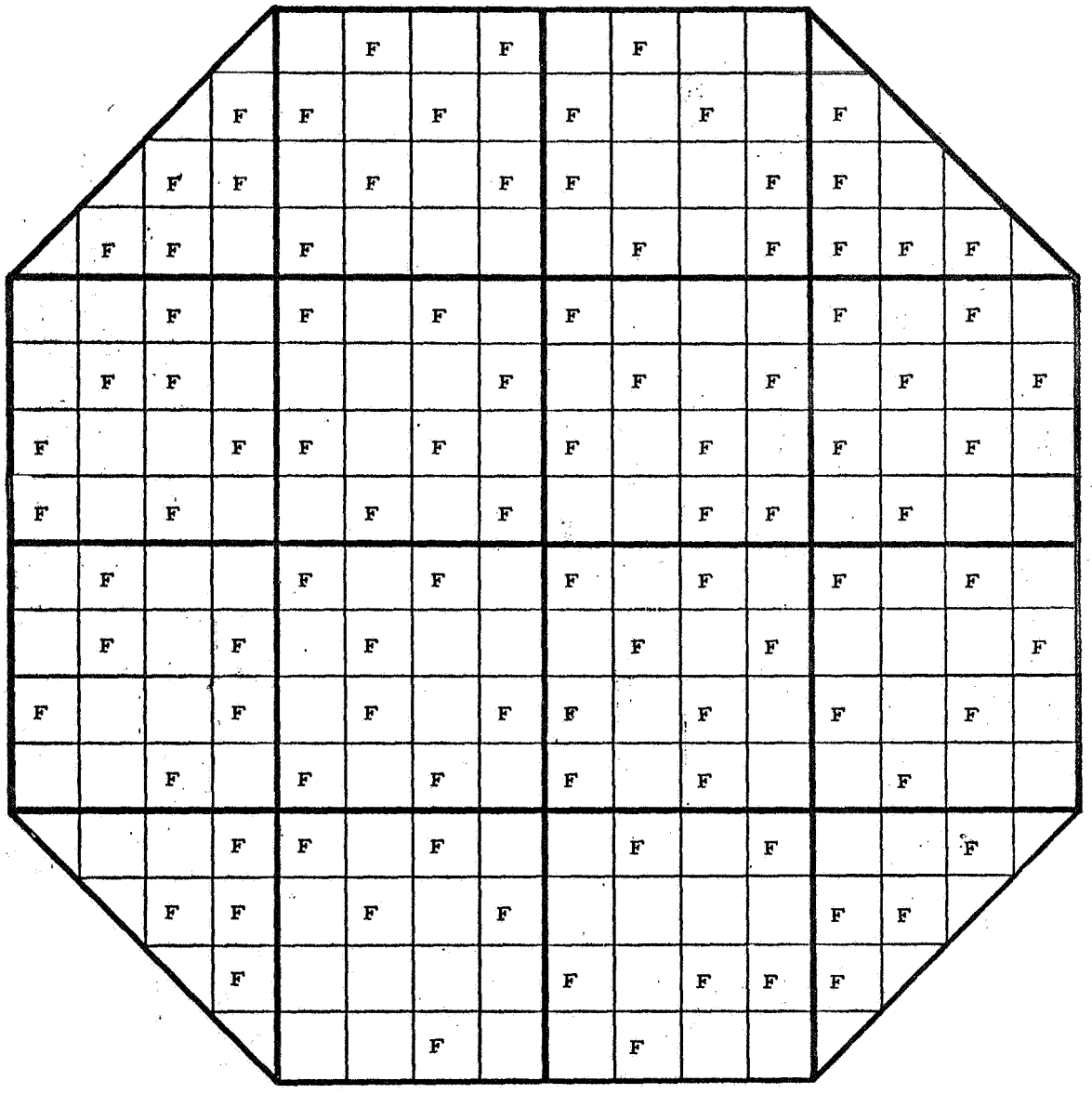

Fig. 4.3 Fuel element location after uniform distribution, stainless steel liner

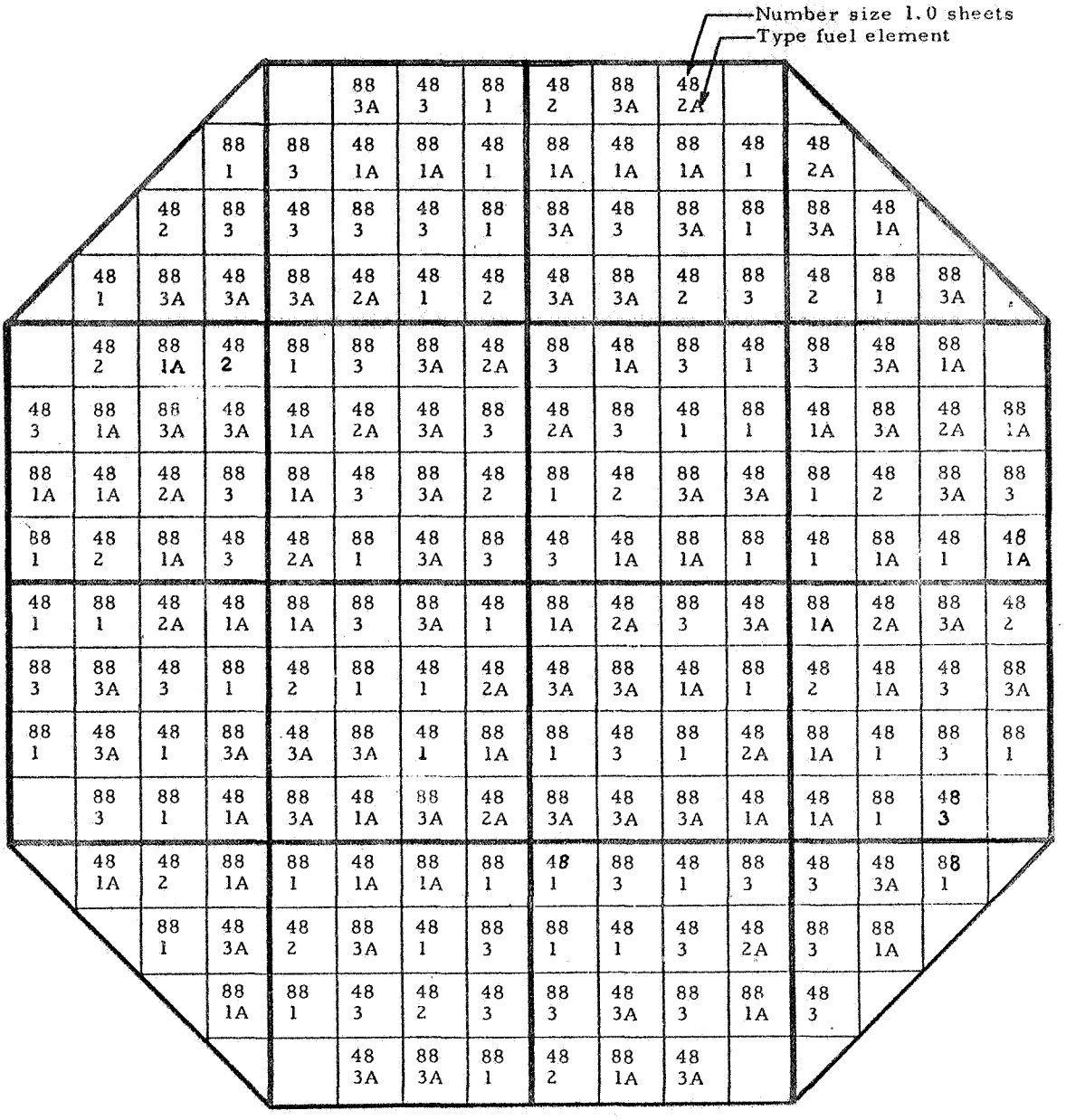

				88 3A	48 3	88 1	48 2	88 3A	48 2A						
			88 1	88 3	48 1A	88 1A	48 1	88 1A	48 1A	88 1A	48 1	48 2A			
		48 2	88 3	48 3	88 3	48 3	88 1	88 3A	48 3	88 3A	88 1	88 3A	48 1A		
	48 1	88 3A	48 3A	88 3A	48 2A	48 1	48 2	48 3A	88 3A	48 2	88 3	48 2	88 1	88 3A	
	48 2	88 1A	48 2	88 1	88 3	88 3A	48 2A	88 3	48 1A	88 3	48 1	88 3	48 3A	88 1A	
48 3	88 1A	88 3A	48 3A	48 1A	48 2A	48 3A	88 3	48 2A	88 3	48 1	88 1	48 1A	88 3A	48 2A	88 1A
88 1A	48 1A	48 2A	88 3	88 1A	48 3	88 3A	48 2	88 1	48 2	88 3A	48 3A	88 1	48 2	88 3A	88 3
88 1	48 2	88 1A	48 3	48 2A	88 1	48 3A	88 3	48 3	48 1A	88 1A	88 1	48 1	88 1A	48 1	48 1A
48 1	88 1	48 2A	48 1A	88 1A	88 3	88 3A	48 1	88 1A	48 2A	88 3	48 3A	88 1A	48 2A	88 3A	48 2
88 3	88 3A	48 3	88 1	48 2	88 1	48 1	48 2A	48 3A	88 3A	48 1A	88 1	48 2	48 1A	48 3	88 3A
88 1	48 3A	48 1	88 3A	48 3A	88 3A	48 1	88 1A	88 1	48 3	88 1	48 2A	88 1A	48 1	88 3	88 1
	88 3	88 1	48 1A	88 3A	48 1A	88 3A	48 2A	88 3A	48 3A	88 3A	48 1A	48 1A	88 1	48 3	
	48 1A	48 2	88 1A	88 1	48 1A	88 1A	88 1	48 1	88 3	48 1	88 3	48 3	48 3A	88 1	
		88 1	48 3A	48 2	88 3A	48 1	88 3	88 1	48 1	48 3	48 2A	88 3	88 1A		
			88 1A	88 1	48 3	48 2	48 3	88 3	48 3A	88 3	88 1A	48 3			
					48 3A	88 3A	88 1	48 2	88 1A	48 3A					

Fig. 4.4 Fuel element final loading distribution, stainless steel liner

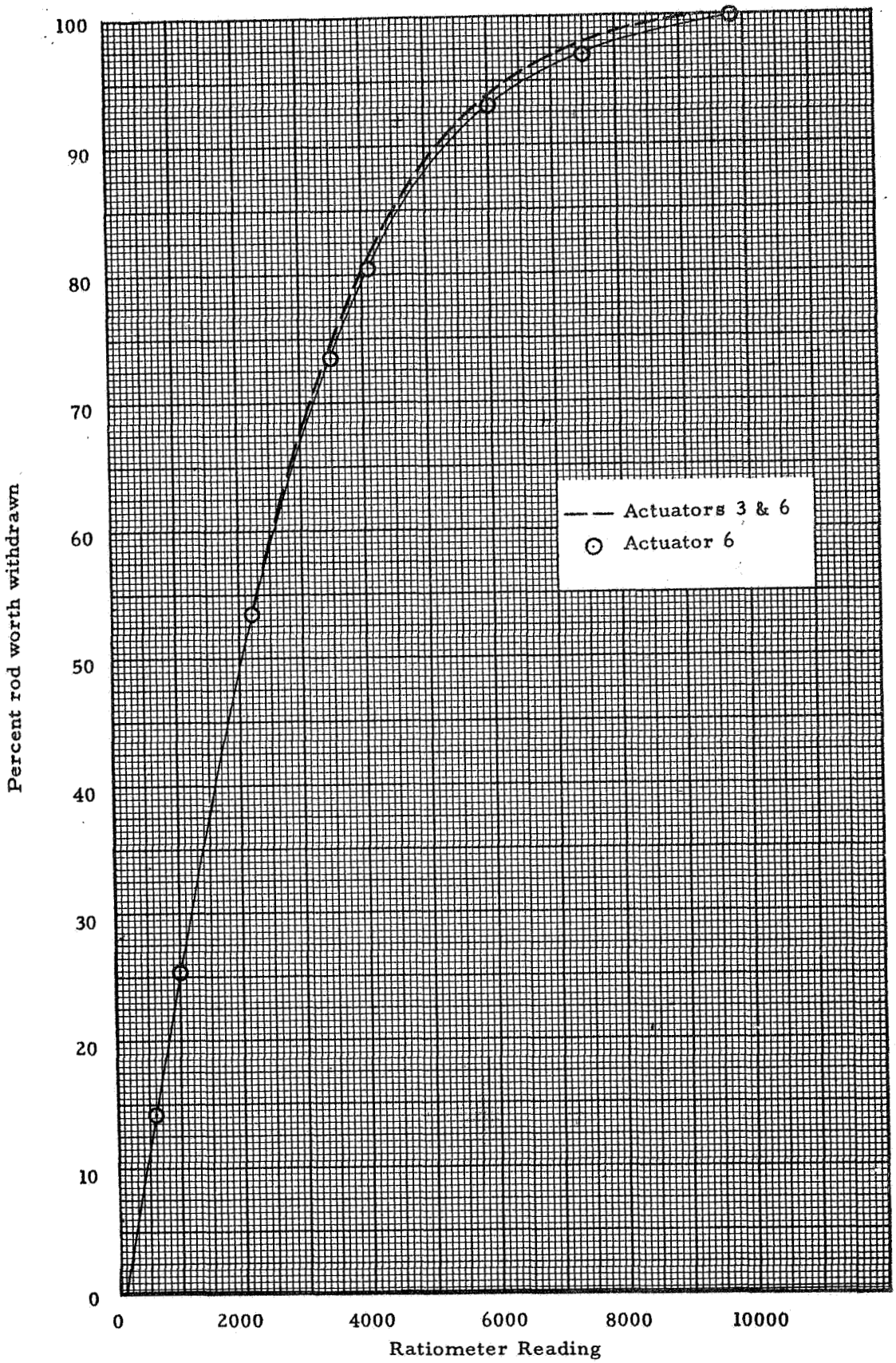

Fig. 4.5 Rod worth curve for Actuator 6 and Actuators 3 and 6 together

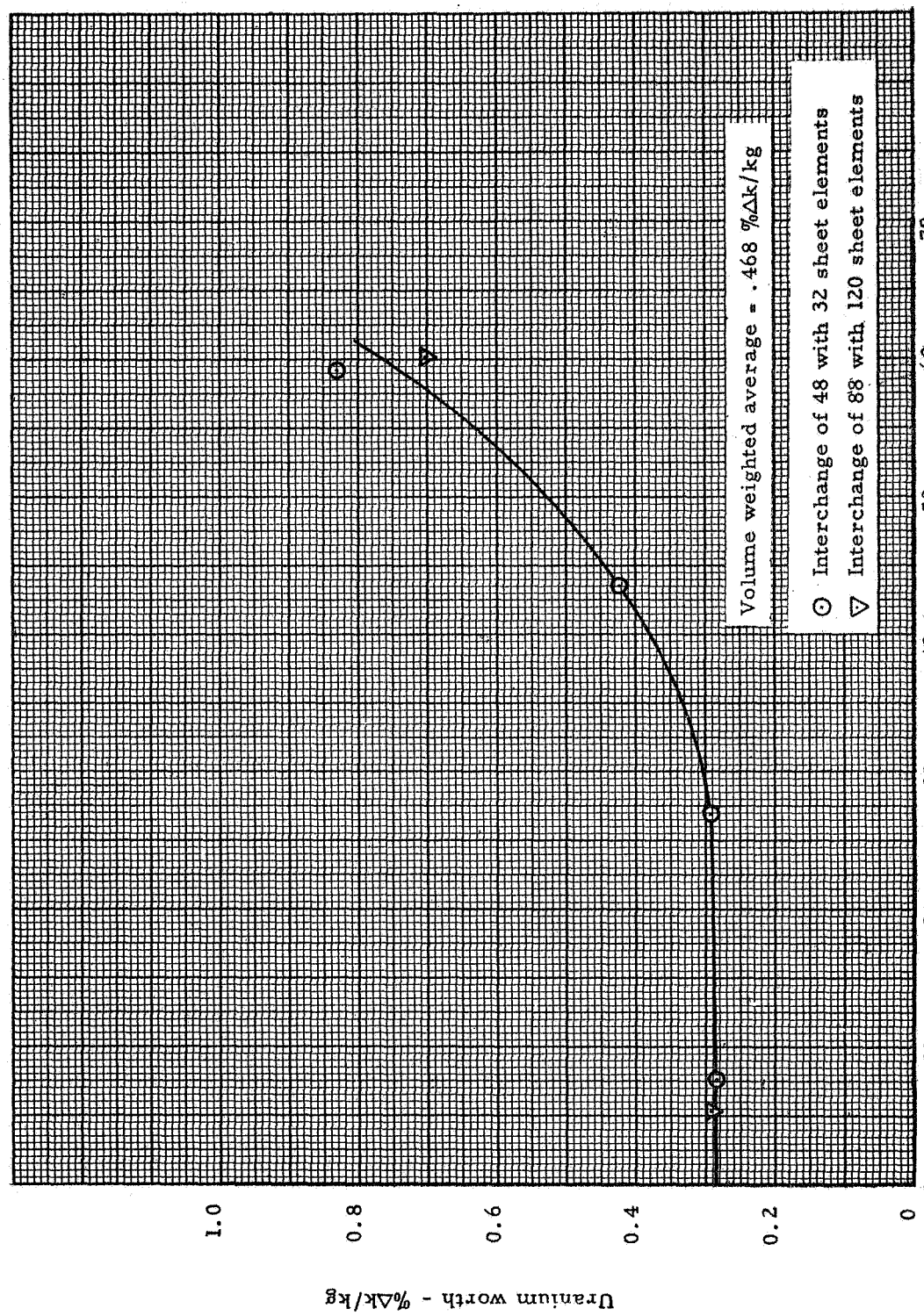

Fig. 4.6 Uranium worth curve with interchanged fuel elements

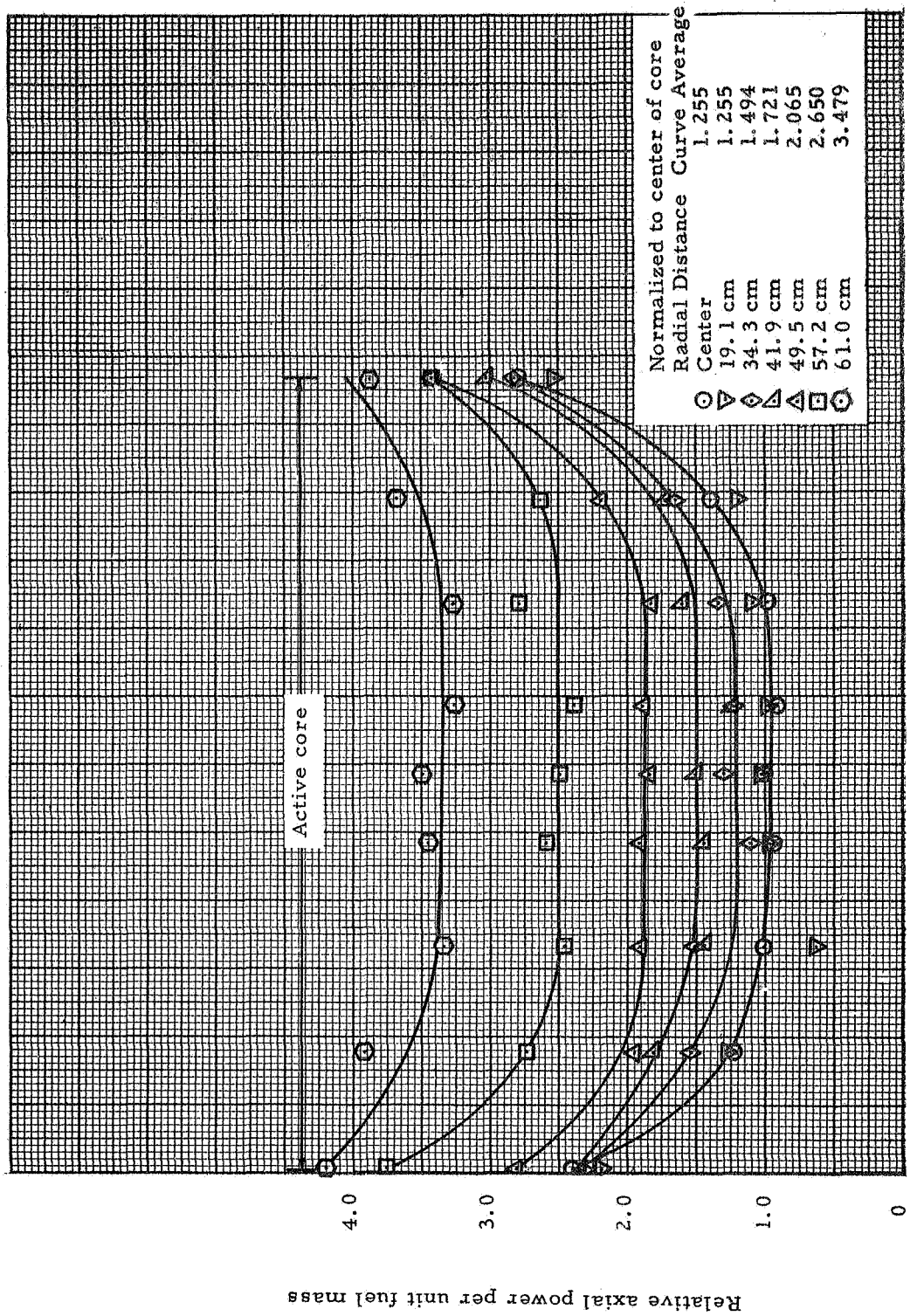

Fig. 4.7 Axial power distribution within the active core region - stainless steel liner

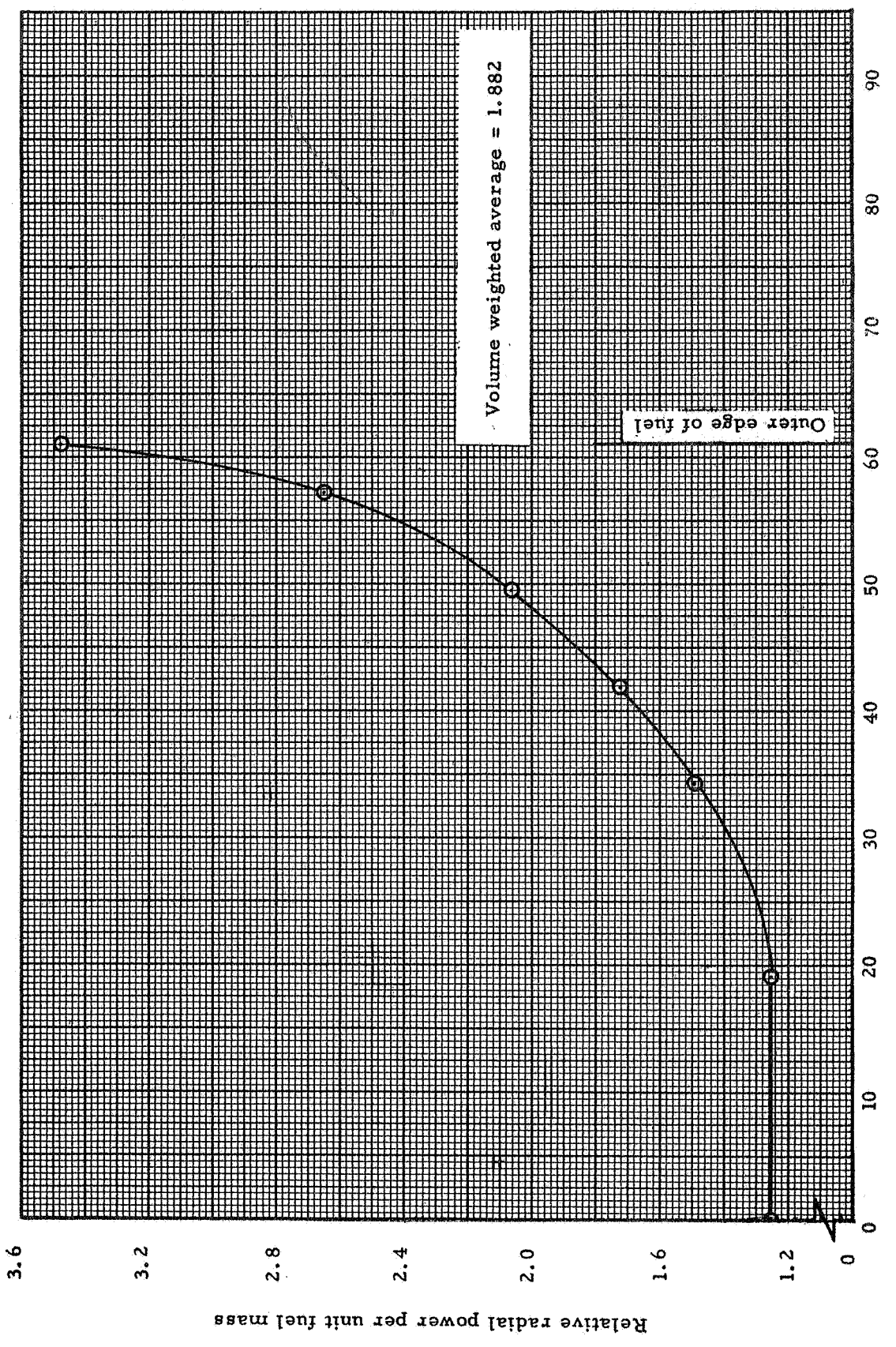

Fig. 4.8 Radial power distribution at the center of the active core - stainless steel liner

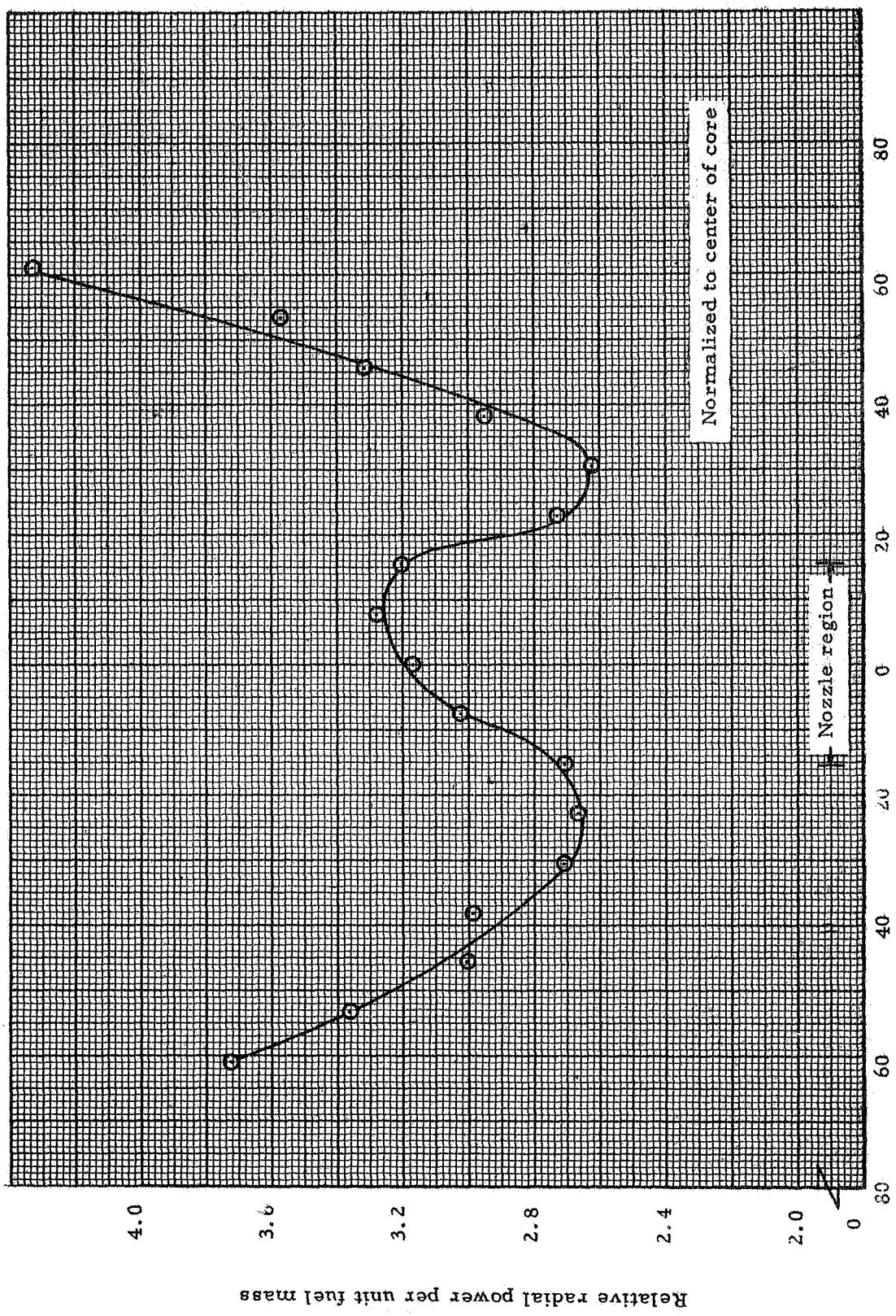

Fig. 4.9 Power distribution curve across core face, separation end, stainless steel liner

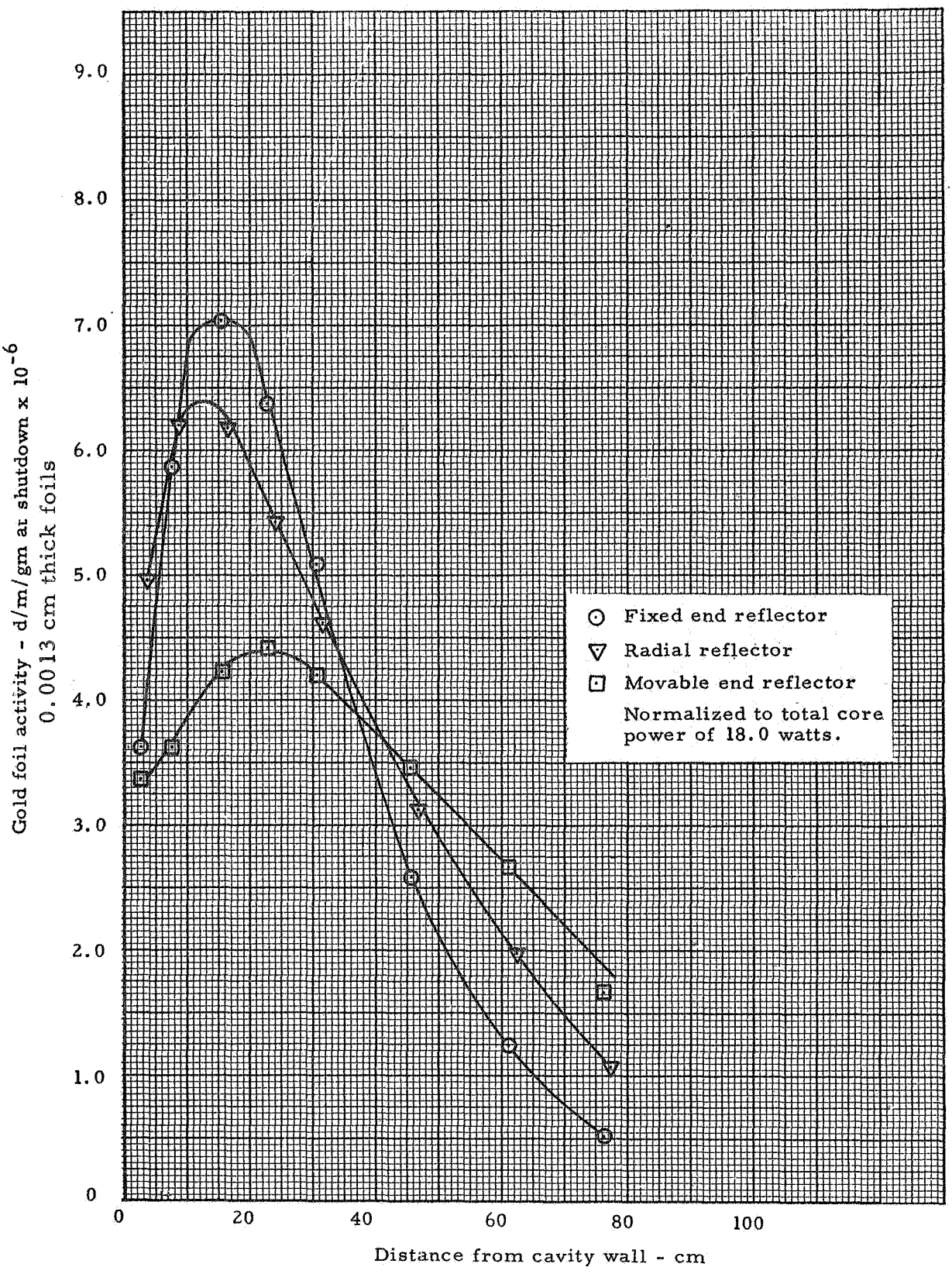

Fig. 4.10 Relative neutron flux distribution in reflector region - bare gold foil detectors - stainless steel liner

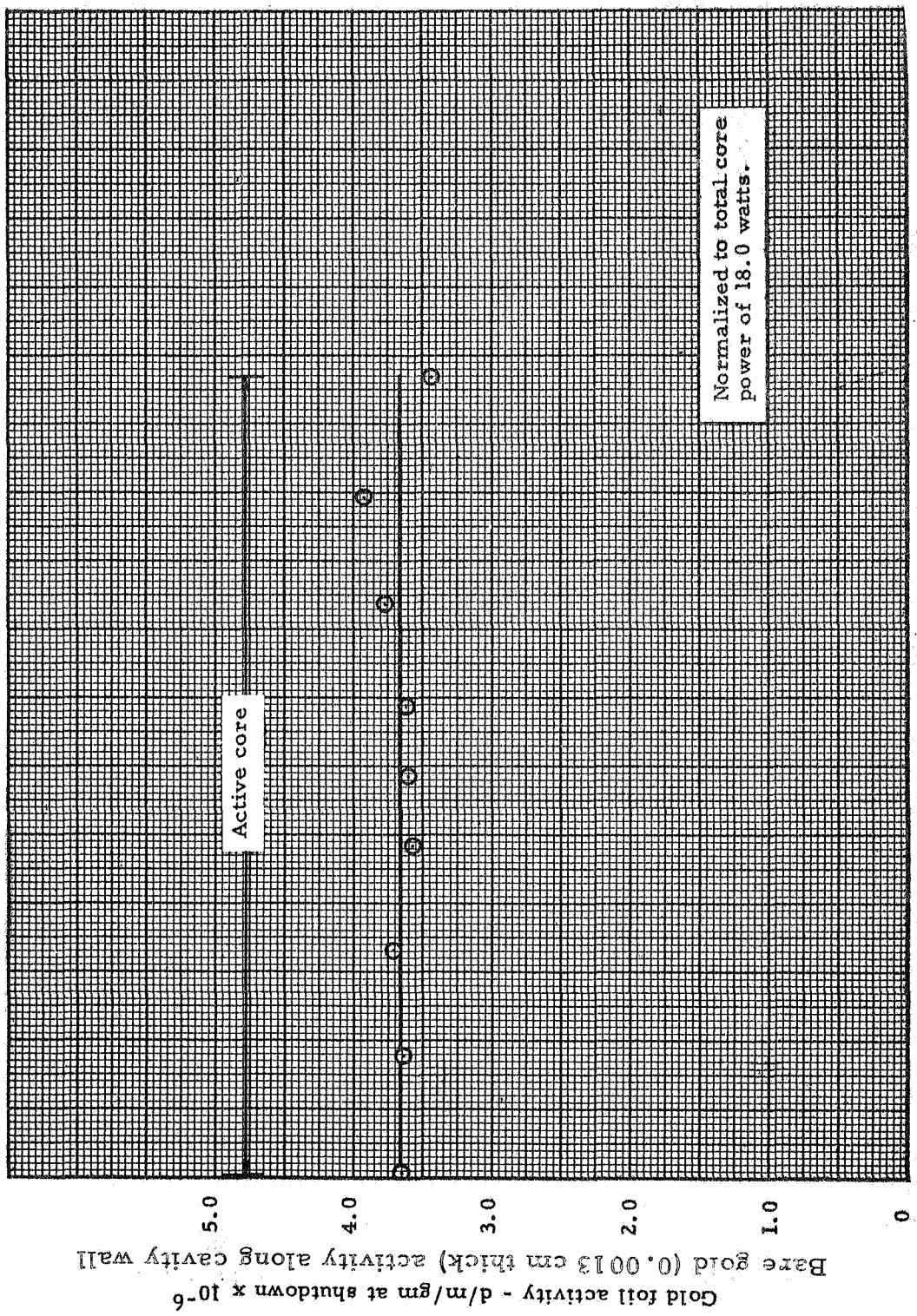

Fig. 4.11 Relative neutron flux distribution along cavity wall - bare gold foil detectors - stainless steel liner

5.0 18.1 kg of POLYETHYLENE PLUS STAINLESS STEEL LINER IN CAVITY

A special polyethylene (CH_2) structure shown in Figure 5.1 was built for this portion of the experiment. The polyethylene fit around the active core and could be heated from room temperature to about 80°C. Ultimately, the void region between the active core and cavity wall was filled with sufficient polyethylene to provide a density of 2.0×10^{21} atoms/cc of hydrogen over the annulus between the core and the radial cavity wall. The main support structure weighed 18.1 kg and thus provided a hydrogen density of 0.95×10^{21} atoms/cc. The remaining material, which was to be added later, was in the form of tubes which could be inserted into the main structure.

It should be noted that the complete volume between the active core and cavity wall was not entirely occupied by the polyethylene. The stated hydrogen densities were provided over that portion of the void between the radial core boundary and cavity wall over a length of 113 cm, the length of the polyethylene structure. The active core length was 117 cm and the cavity 122 cm, but these additional regions were void of polyethylene.

The polyethylene was heated by forcing hot air through the polyethylene structure as illustrated in Figure 5.2. Thermocouples were placed at several locations within the polyethylene so that temperature could be monitored in the control room during reactor operations (see Section 7.0).

Besides the polyethylene, there were other components which were used within the cavity region to support the plastic and to direct the air flow. These are itemized as follows:

		Weights
1.	Support ring for polyethylene (6061 Al)	10.5 kg
2.	Air ducting cover plates (6061 Al)	26.8 kg
3.	Saddle for polyethylene (6061 Al)	6.7 kg
4.	Air ducting in end reflector (6061 Al)	4.0 kg
	Total	48.0 kg

The above support materials were not placed in the reactor until the entire 38.3 kg of polyethylene had been installed in the reactor. The effect on reactivity will be discussed in the subsequent section.

There were no power or flux mapping measurements obtained with this configuration. There were, however, several reactivity and material worth measurements made which will be discussed in subsequent sections.

5.1 Initial Loading

Prior to placing any polyethylene in the reactor, the existing configuration was that at the conclusion of the stainless steel liner configuration described in Section 4.1. There were 104 88-sheet and 104 48-sheet fuel elements in the reactor for a total of 36.8 kg of uranium, plus a stainless steel liner on the cavity wall which weighed 83.1 kg. The addition of 18.1 kg of polyethylene caused the reactor to be subcritical thus requiring a significant increase in fuel loading. Only the 48-sheet fuel elements were modified to increase the fuel loading. These fuel elements were completely reloaded so that they contained 60 size 1.5 and 35 size 1.0 sheets of fuel. There were 6 size 1.5 sheets per stage over 10 stages and 3 size 1.0 sheets between each of these 10 stages. In addition there was a single size 1.0 sheet on each end of the element and one stage of 1.0 sheets at one end of the element containing 6 fuel sheets. The elements will be referred to as 125-sheet elements.

The fuel was added in 6 increments as shown in Table 5.1 and Figure 5.3. The amount of fuel in the reactor was recorded and plotted in terms of equivalent size 1.0 fuel sheets during this loading process. The base loading before any fuel elements were modified contained 14144 equivalent size 1.0 fuel sheets and the final loading was 21459 equivalent size 1.0 fuel sheets with an excess reactivity of $0.382 \pm 0.005\% \Delta k$. At this point there were 104 88-sheet 95 125-sheet and 9 48-sheet fuel elements in the reactor. In order to produce a more uniform loading, the remaining 9 48-sheet elements were changed to 125-sheet elements, thus making 104 each of the two major types of fuel elements remaining in the core, as shown in Figure 5.4. The core loading at this point was 57.4 kg of uranium and k-excess was $0.699 \pm 0.019\% \Delta k$. The D_2O temperature was $21.7^{\circ}C$.

5.2 Reactivity Measurements -

5.2.1 Rod Worth Measurements

A listing of the rod worth measurements obtained on the previous core configuration and this assembly is given in Table 5.2. The averages given here along with the data in Tables 2.1 and 2.2 were used to determine k-excess. The standard errors on these averages are all less than 3% which is considered normal for this type of measurement. The reason for including the results from the previous configuration was that the change in core constituents did not appear to effect the rod worths and the additional measurements were used to give better overall averages.

5.2.2 Material Worths

The core average fuel worth was obtained by interchanging the core fuel elements with both heavy and light-loaded fuel elements. This was done at several radial positions in the reactor as shown in Table 5.3 and Figure 5.5. The data fit a smooth curve very well and give a core average fuel worth of $0.204\% \Delta k/kg$.

The core average type 1100 aluminum worth was $-(1.140 \pm 0.059) \times 10^{-2}\% \Delta k/kg$. With reference to the worth of uranium, one kg of uranium will compensate for 17.9 kg of aluminum.

The average worth of polyethylene within the polyethylene structure around the core was measured by adding 514.9 gm. This caused k-excess to decrease 0.1205 ± 0.005%Δk which gives a worth of -0.234 ± 0.010%Δk/kg of CH_2.

Carbon strips 5.08 cm wide by 117 cm long by 1.27 cm thick were placed in the empty fuel element positions and measured to be worth -(2.611 ± 0.032) x 10^{-2}%Δk/kg of carbon. If this value is used to determine the critical mass of the reactor for pure hydrogen in the reactor, the following corrections are needed:

1. Carbon worth = $0.856 \times 19.1 \times (-2.611 \pm 0.032 \times 10^{-2})$

$= -0.405 \pm 0.005\%\Delta k$

2. Excess reactivity = $\dfrac{-0.699 \pm 0.019\%\Delta k}{1.104 + 0.020\%\Delta k}$

The reactor contained 57.4 kg of fuel and the fuel worth was 0.204%Δk/kg of uranium. Interpolating between this fuel worth and the worth of fuel with only stainless steel in the reactor and a core loading of 36.8 kg of uranium, the 1.104%Δk correction would be worth 4.9 kg of uranium. This gives a critical mass of 52.5 kg of uranium with 2.61 kg of hydrogen only or 54.1 kg with 18.1 kg of CH_2. The materials within the reactor were the same as given in Section 2.1 of this report except for the stainless steel liner which weighed 83.1 kg, the 18.1 kg polyethylene (or the equivalent hydrogen), the beryllium ring in the radial reflector 6.5 cm from the cavity wall, and 15.83 kg of type 1100 aluminum in the fuel spacer rings.

TABLE 5.1

Inverse Multiplication

Stainless Steel Liner

Addition of 18.1 kg Polyethylene

Increment	Total No. Fuel Sheets	Channel No. 1 CPM	Channel No. 1 CPMo/CPM	Channel No. 2 CPM	Channel No. 2 CPMo/CPM	Channel No. 3 CPM	Channel No. 3 CPMo/CPM	Avg.	Rod Positions
18.1 kg polyethylene in cavity									
Decay corrected CPMo		1014		1047		789			In
		1129		1185		882			Out
0	14144	14788	0.0686	14256	0.0734	10426	0.0757	0.0726	In
0	14144	28974	0.0390	28266	0.0419	20325	0.0434	0.0414	Out
1	14452	14958	0.0678	14610	0.0717	10570	0.0746	0.0714	In
1	14452	30619	0.0369	29589	0.0400	21204	0.0416	0.0395	Out
2	14760	15187	0.0668	15103	0.0693	10930	0.0722	0.0694	In
2	14760	31779	0.0355	31406	0.0377	22566	0.0391	0.0374	Out
3	16531	18838	0.0538	18827	0.0556	13600	0.0580	0.0558	In
3	16531	42457	0.0266	48740	0.0243	35142	0.0251	0.0253	Out
4	18302	23932	0.0424	24250	0.0432	17524	0.0450	0.0435	In
4	18302	95038	0.0119	93790	0.0126	65748	0.0134	0.0126	Out
Decay corrected CPMo		987		1019		768			
		1099		1153		859			
5	20073	30082	0.0328	30914	0.0330	21810	0.0352	0.0337	In
5	20073	326883	0.00336	310464	0.00371	210537	0.00408	0.00372	Out
6	21459	37469	0.0263	38448	0.0265	27462	0.0280	0.0269	In
6	21459	Critical with k-excess of 0.388%Δk							

TABLE 5.2

Control Rod Worth Measurements

Stainless Steel Liner on Cavity Wall

18.1 kg Polyethylene in Cavity

Run No.	Actuator Combinations and Reactivity Worth (%Δk)		
	Actuators 3 and 6	Actuator 6	All Rods (20 rods)
300	-1.154		-4.132
301			
302	-1.537		
303	-1.582		
304	-1.541		
305			-4.032
306		-0.6568	
327		-0.6684	
328		-0.6511	
329	-1.483		
332			-4.017
Averages	-1.536±0.041	-0.6588±0.0088	-4.060±0.063

TABLE 5.3

Fuel Worth Measurements - Polyethylene and Stainless Steel in Cavity

Radial	Reactivity Difference (%Δk)	Fuel Mass Difference (gm)	Fuel Worth per gram (%Δk) x 10^3
Interchange of 88 sheet elements with 120 sheet elements			
5.4	0.0177	140.84	0.126
26.9	0.0197	140.84	0.140
43.5	0.0242	140.84	0.172
60.2	0.0550	140.84	0.391
50.8	0.0298	140.84	0.212
Interchange of 125 sheet elements for 80 sheet elements			
60.2	0.1142	284.10	0.402
59.2	0.1035	284.10	0.364

NOTE: The fuel weights are accurate to ±1.0% and the estimated error on the reactivity difference is ±0.005%Δk or less.

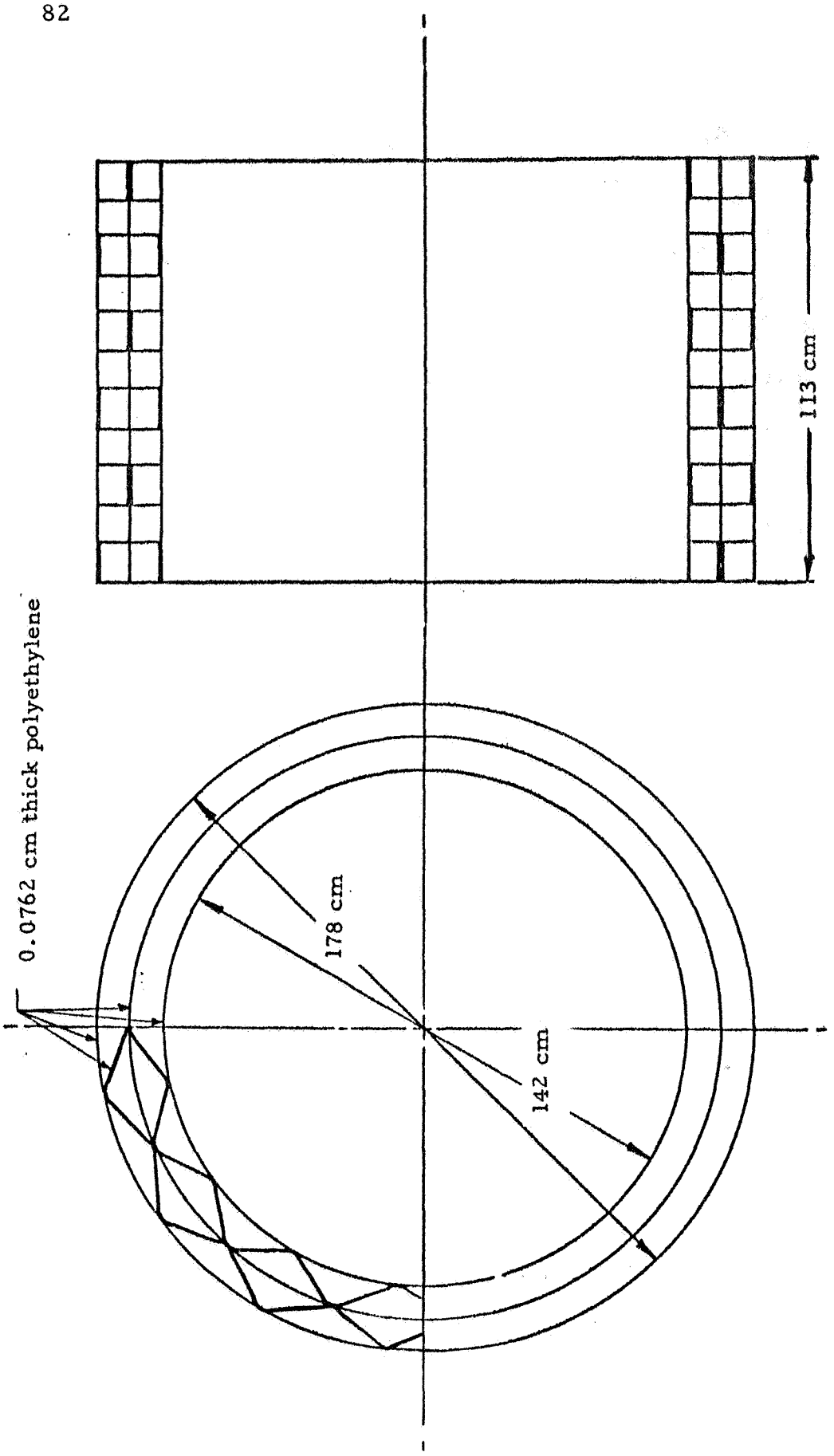

Fig. 5.1 Polyethylene configuration - uniform hydrogen mockup, 18.1 kg CH_2 plus stainless steel liner

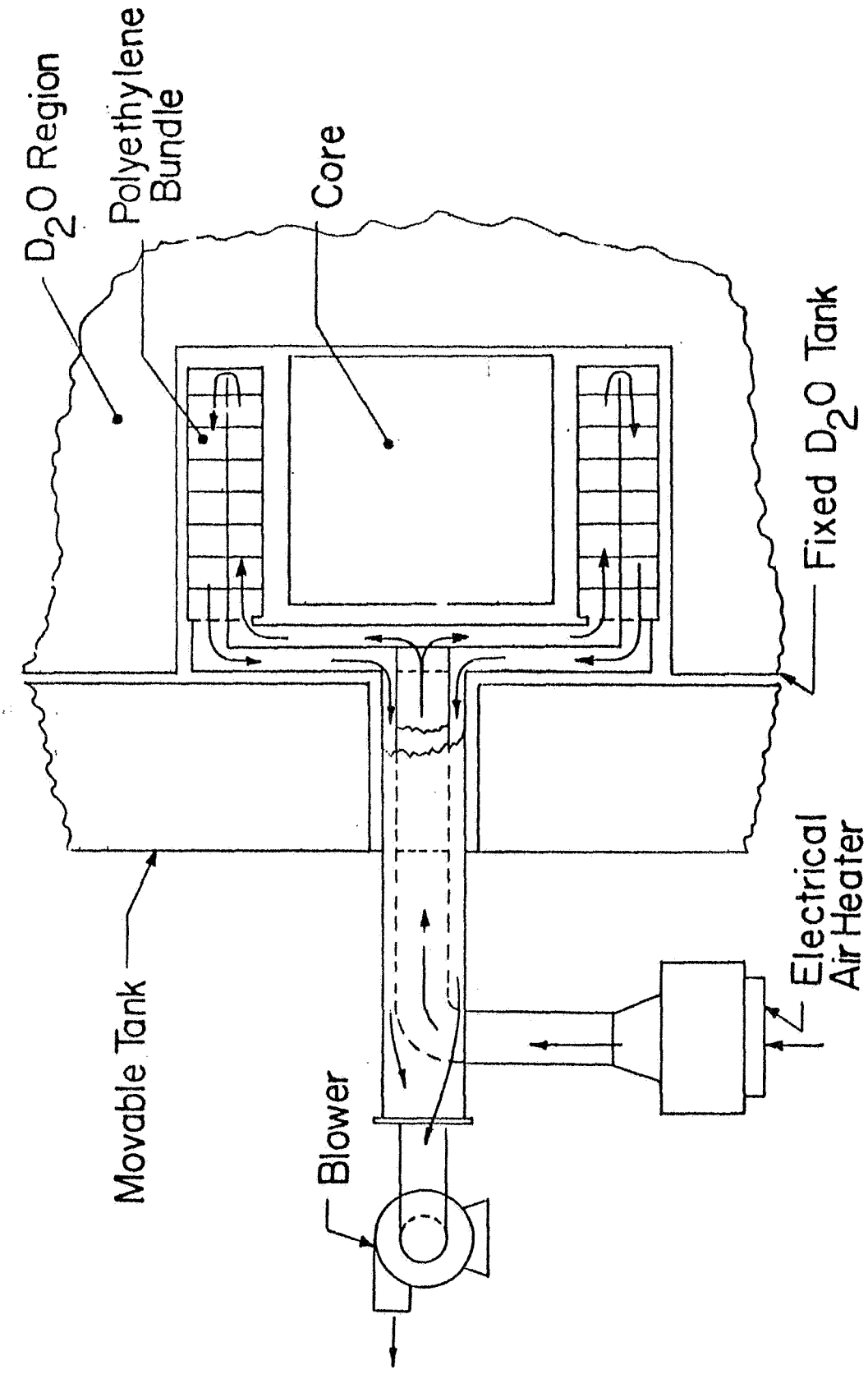

Fig. 5.2 Schematic of polyethylene heating system

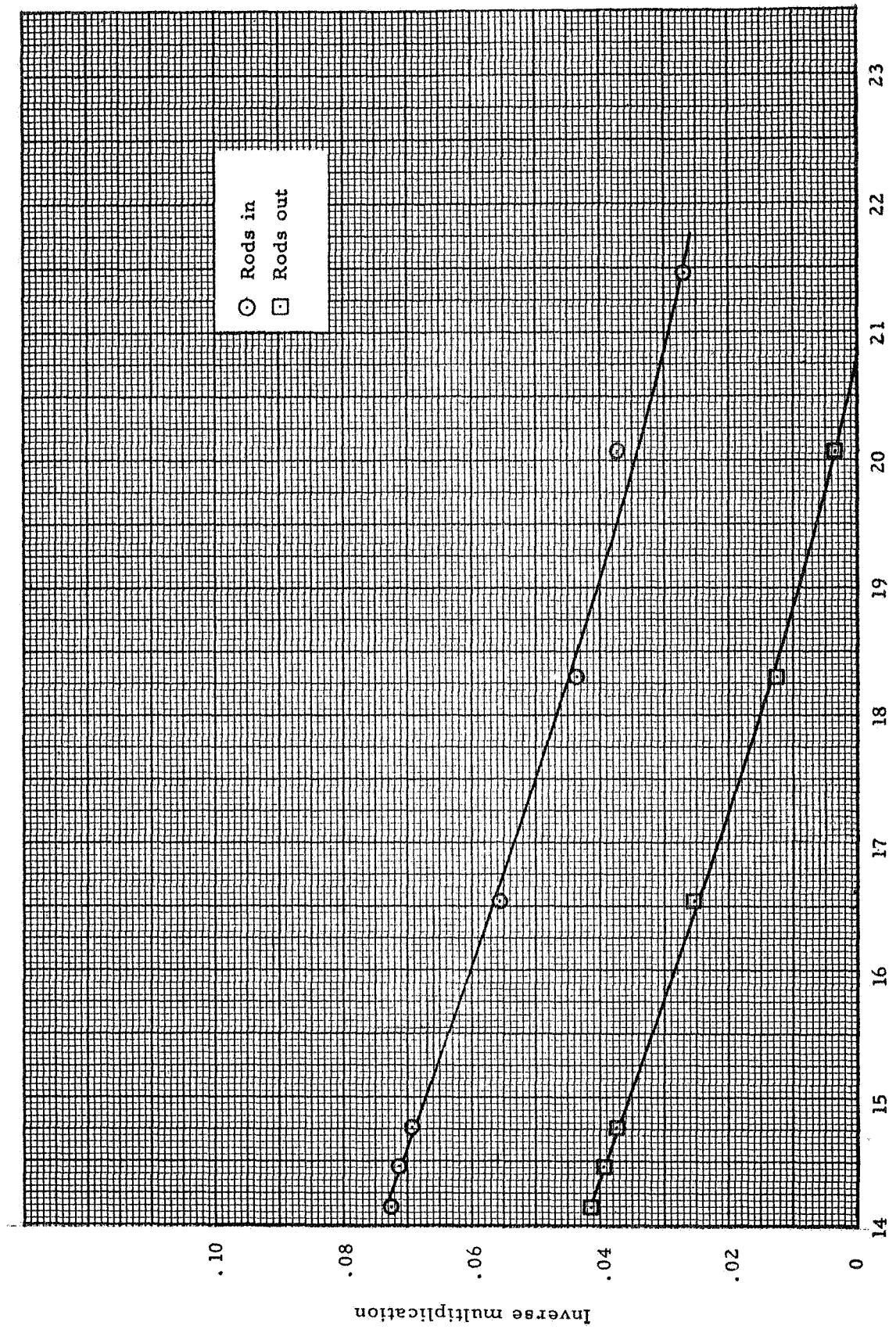

Fig. 5.3 Inverse multiplication curves - 18.1 kg CH_2 plus stainless steel liner

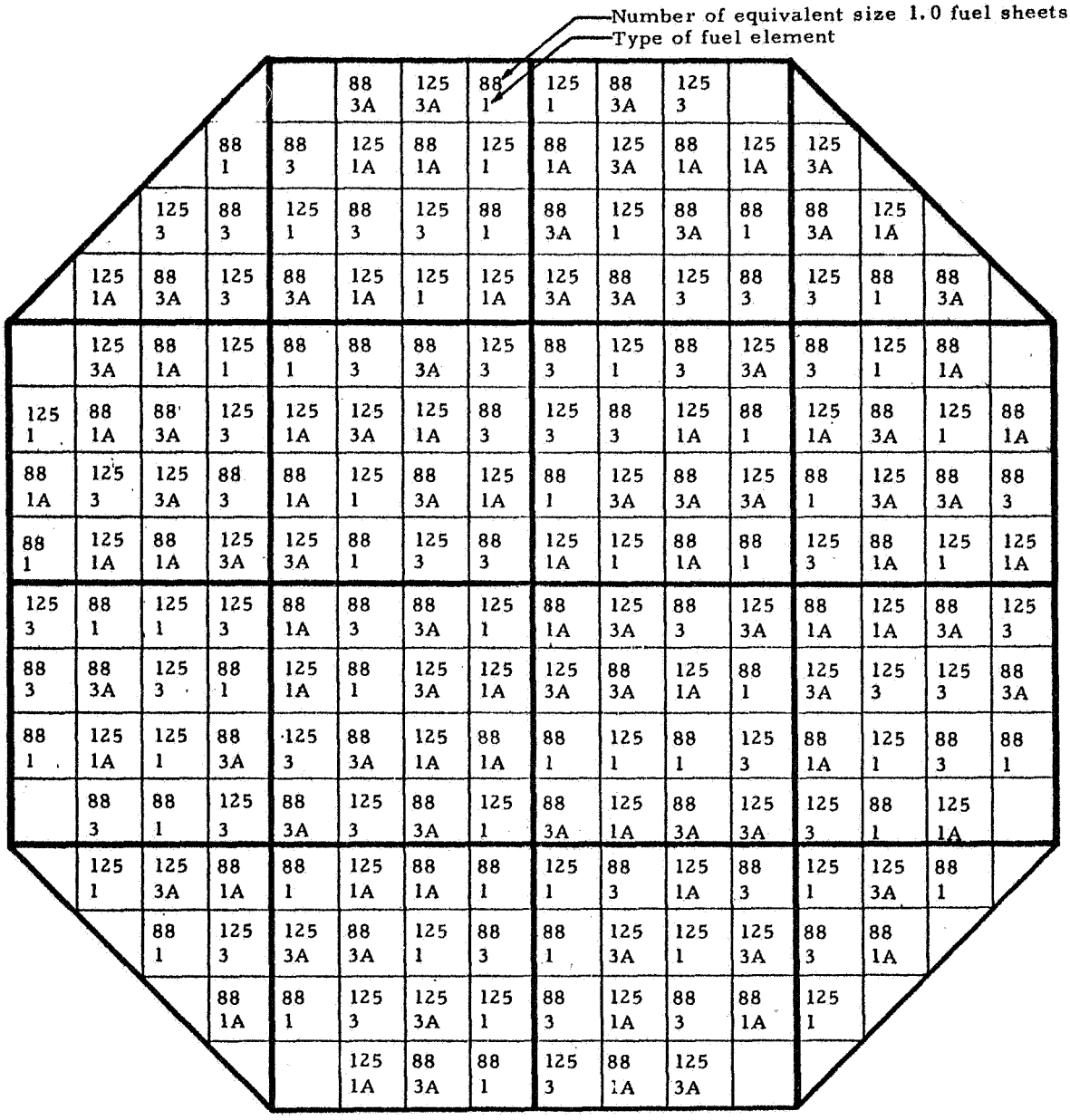

				88 3A	125 3A	88 1	125 1	88 3A	125 3					
		88 1	88 3	125 1A	88 1A	125 1	88 1A	125 3A	88 1A	125 1A	125 3A			
	125 3	88 3	125 1	88 3	125 3	88 1	88 3A	125 1	88 3A	88 1	88 3A	125 1A		
125 1A	88 3A	125 3	88 3A	125 1A	125 1	125 1A	125 3A	88 3A	125 3	88 3	125 3	88 1	88 3A	
125 3A	88 1A	125 1	88 1	88 3	88 3A	125 3	88 3	125 1	88 3	125 3A	88 3	125 1	88 1A	
125 1	88 1A	88 3A	125 3	125 1A	125 3A	125 1A	88 3	125 3	88 3	125 1A	88 1	125 1A	88 3A	125 1	88 1A
88 1A	125 3	125 3A	88 3	88 1A	125 1	88 3A	125 1A	88 1	125 3A	88 3A	125 3A	88 1	125 3A	88 3A	88 3
88 1	125 1A	88 1A	125 3A	125 3A	88 1	125 3	88 3	125 1A	125 1	88 1A	88 1	125 3	88 1A	125 1	125 1A
125 3	88 1	125 1	125 3	88 1A	88 3	88 3A	125 1	88 1A	125 3A	88 3	125 3A	88 1A	125 1A	88 3A	125 3
88 3	88 3A	125 3	88 1	125 1A	88 1	125 3A	125 1A	125 3A	88 3A	125 1A	88 1	125 3A	125 3	125 3	88 3A
88 1	125 1A	125 1	88 3A	125 3	88 3A	125 1A	88 1A	88 1	125 1	88 1	125 3	88 1A	125 1	88 3	88 1
	88 3	88 1	125 3	88 3A	125 3	88 3A	125 1	88 3A	125 1A	88 3A	125 3A	125 3	88 1	125 1A	
	125 1	125 3A	88 1A	88 1	125 1A	88 1A	88 1	125 1	88 3	125 1A	88 3	125 1	125 3A	88 1	
		88 1	125 3	125 3A	88 3A	125 1	88 3	88 1	125 3A	125 1	125 3A	88 3	88 1A		
			88 1A	88 1	125 3	125 3A	125 1	88 3	125 1A	88 3	88 1A	125 1			
					125 1A	88 3A	88 1	125 3	88 1A	125 3A					

Fig. 5.4 Final fuel element loading distribution, 18.1 kg CH_2 plus stainless steel liner

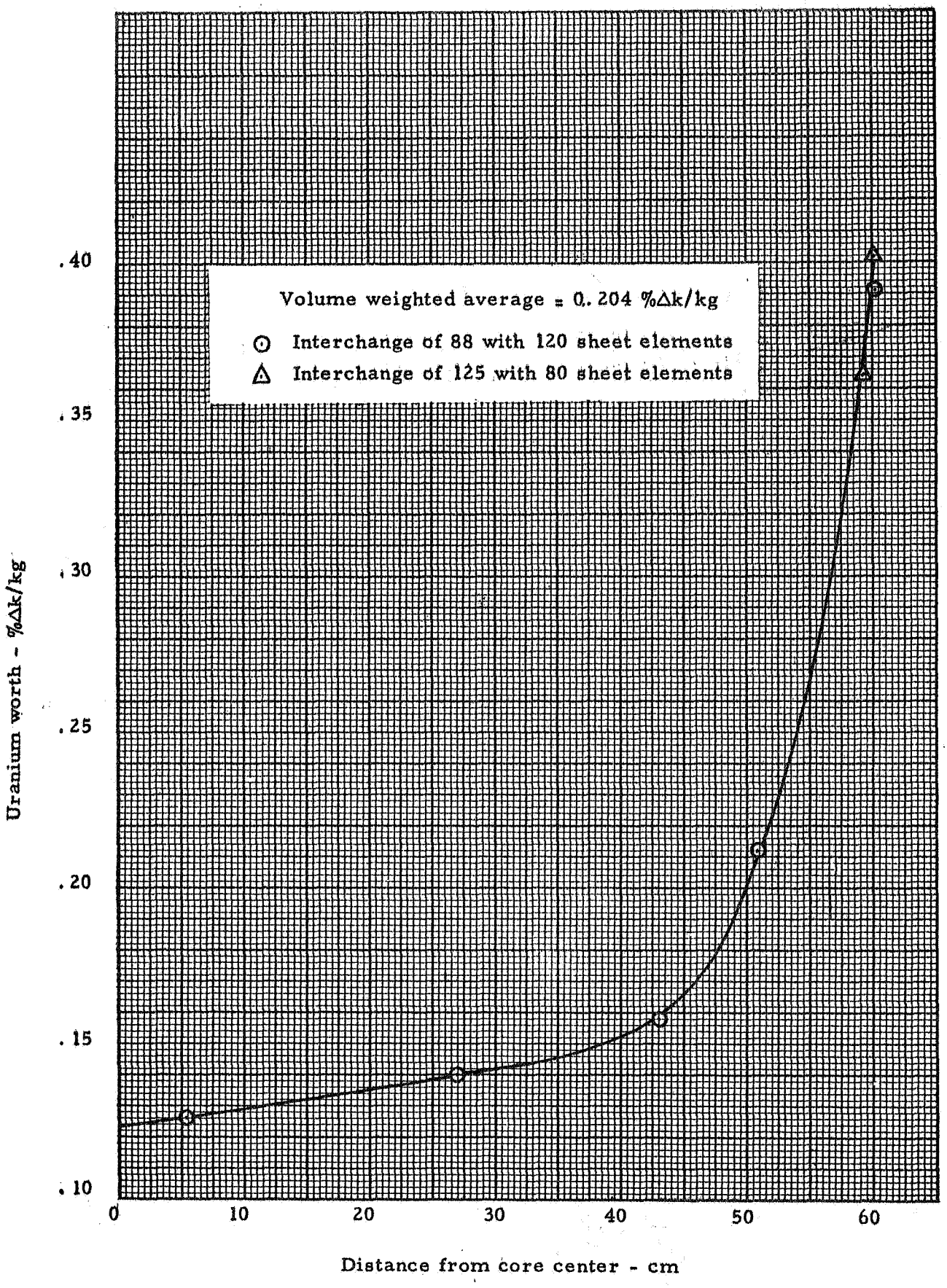

Fig. 5.5 Fuel worth as a function of core radius, 18.1 kg of CH_2 plus stainless steel liner

6.0 STAINLESS STEEL LINER PLUS 38.3 kg OF POLYETHYLENE IN CAVITY - ROOM TEMPERATURE

The only change made to the reactor over the configuration with 18.1 kg of polyethylene in the region between the active core and cavity wall was the addition of polyethylene tubes to the main plastic structure which increased the total polyethylene to 38.3 kg. The additional polyethylene did, of course, cause a significant decrease in reactivity which necessitated an increase in fuel loading.

6.1 Initial Loading

The base loading was 22152 equivalent size 1.0 fuel sheets which were contained in 104 88-sheet and 104 125-sheet fuel elements. It was anticipated that it would require in the order of 90 kg to make the reactor critical. Therefore, a fuel loading of 166* equivalent size 1.0 fuel sheets per fuel element was chosen for the first attempt to go critical. The fuel was loaded in eight increments, as will be noted from Table 6.1 and Figure 6.1. As with the previous configuration, the total loading and the inverse multiplication was recorded vs number of equivalent size 1.0 fuel sheets in the reactor. After the first increment had been placed in the core, the polyethylene tubes were rearranged to some extent within the annulus. There were two sizes of tubes used and when placing the material inside the structure, the tubes were doubled up with one small tube inside of the larger tube. It was decided at this point that the basic structure was arranged so that enough spaces could be found to insert each individual tube into the structure at unique locations rather than doubling them up. This gave a more uniform polyethylene density over the polyethylene annulus. The data clearly show a negative effect caused by the rearrangement.

The reactor first went critical with 33175 equivalent size 1.0 sheets or 86.1 kg of uranium in the reactor and k-excess was 0.0684%Δk. The fuel loading was further increased to 89.6 kg so that each fuel element contained 166 equivalent size 1.0 fuel sheets as shown in Figure 6.2, and k-excess was 0.414 + 0.013%Δk. The D_2O temperature was 21°C.

6.2 Reactivity Measurements

6.2.1 Rod Worths

The worth of all six actuators as a bank was measured once with this configuration and the value was -3.925%Δk. Three separate measurements of Actuator 6 gave an average of -0.5976 ± 0.0283%Δk and two sets of data for Actuator 5 averaged -0.5264 ± 0.0155%Δk. There appears to have been a slight reduction in rod worth at this higher loading polyethylene and fuel. The six actuators as a bank decreased 3.3% and the worth of Actuator 6 went down 9.3%.

---

* Ten stages of eight 1.5 size sheets, between each stage were four 1.0 size sheets, one 1.0 size sheet at each end, and the eleventh stage had eight 1.0 size sheets.

6.2.2 Material Worths

The reactivity worth of uranium was measured much the same way as with the previous configurations. The 166-sheet fuel elements were interchanged with 120-sheet elements at several radial positions as shown in Table 6.2 and Figure 6.3. The core average was 0.1158%Δk/kg.

The worth of polyethylene was measured several times with the primary purpose of comparing its worth with polystyrene (CH). There were three CH_2 measurements at essentially the same location, items 1, 4, and 8 as given in Table 6.3, which gave an average of -0.456 ± 0.061 %Δk/kg. Polystyrene of the type eventually used in the variable hydrogen experiment was worth -0.451%Δk/kg. Carbon was worth -0.0418%Δk/kg at the outer edge of the core where the above polyethylene and polystyrene measurements were obtained. From these values one can extract the worth of hydrogen in the two plastic materials as follows:

1. "Polyethylene hydrogen" $= \frac{-[0.456 - (0.856 \times 0.0418)]}{0.144} =$

$-2.92\%\Delta k/kg$

2. "Polystyrene hydrogen" $\frac{-[0.451 - (0.923 \times 0.0418)]}{0.077} =$

$-5.35\%\Delta k/kg$

A set of measurements were also made on the inner surface of the polyethylene annulus for the same purpose of comparing polyethylene and polystyrene. These data are also shown in Table 6.3. The following hydrogen worths were deduced from these results:

1. "Polyethylene hydrogen" $= \frac{-[0.439 - (0.856 \times 0.0294)]}{0.144} =$

$-2.88\%\Delta k/kg$

2. "Polystyrene hydrogen" $= \frac{-[0.321 - (0.923 \times 0.0294)]}{0.077} =$

$-3.82\%\Delta k/kg$

This second set of measurements is considered to be more accurate because the specific location of the three materials was more exact. These results show the hydrogen in the polystyrene to be worth 1.34 times that in polyethylene.

It was determined from direct conversation with the manufacturer of polystyrene that the material is expanded with methyl chloride (CH_3Cl) gas and some of this gas was believed to be captured in some of the air pockets. The relatively high (33 barn) cross section for chlorine was considered to be the reason for the more negative reactivity worth of the hydrogen in polystyrene compared to the hydrogen in polyethylene. A

chemical analysis* showed, however, less than 5 ppm of chlorine, by weight. Therefore, it appears that the difference in worth between these two materials is not the result of absorption cross section differences, but may be due to differences in molecular binding and the resulting scattering effects.

A core average aluminum worth was also measured. Placing 8.528 kg of type 1100 Al dispersed over the active core cause k-excess to decrease 0.0641%Δk. This gives a worth of -0.00752%Δk/kg. In terms of uranium worth, one kg of uranium will compensate for 15.4 kg of type 1100 aluminum in the active core at this loading.

The reactivity worth of five MTR type fuel plates was measured at four locations in the radial reflector. A sector of the beryllium reflector was removed from the reactor and an aluminum tray was placed in the D_2O into which five fuel plates containing 42 grams of U^{235} were placed. The results of these measurements are given in Table 6.4. The aluminum corrections were based on the data given on page 162 of Reference 1. The base point was with the aluminum tray, which weighed 6.08 kg, at 30.5 cm from the cavity wall; therefore, no correction was required at this location. The fuel plates were 50.8 cm long by 6.2 cm wide and were clamped onto an Al backup plate which was 56.4 cm long by 7.0 cm wide and each of these plates contained 8.4 grams of U^{235}. The aluminum tray was 117 cm long and the plates were located on this tray as shown in Figure 6.4.

6.2.3 Corrections to Critical Mass

The critical mass correction for this configuration containing 83.1 kg of stainless steel on the cavity walls, 5.5 kg of hydrogen between the active core and the cavity wall, and the beryllium ring in the radial reflector at 6.5 cm from the cavity wall was as follows:

1.	k-excess	= -0.414 ± 0.013%Δk
2.	Carbon worth	= 0.856 x 38.2 x (-0.0195 ± 0.0003)
		= -0.638 ± 0.010%Δk
	Total correction	= -1.052 ± 0.016%Δk

Based on the core average fuel worths between this configuration and the one containing 18.11 kg of polyethylene, the above correction amounts to 8.8 kg of uranium. This gives a critical mass of 80.8 kg with only hydrogen (5.5 kg) as coolant between the core and reflector. Correcting for k-excess only gives a critical mass of 86.0 kg with 38.3 kg of CH_2 simulated coolant. Other core constituents are the same as given in Sections 2.1 and 5.2.2 of this report.

---

* Private communication from Idaho Chemical Processing Plant, Analytical Section.

6.3 Power Distribution Measurements

Prior to doing any power mapping, all of the hardware was placed on the face of the polyethylene structure so that it was ready for the heating experiment. A total of 43.9 kg of aluminum was added at the separation plane which included an end support ring attached directly to the polyethylene, the two air flow plates and a support plate between the polyethylene and the core support structure to better support the polyethylene during heating. Because of the resulting decrease in reactivity it was necessary to decrease the polyethylene loading by 1825 grams. The amount was removed in the form of tubes and the resulting k-excess with 36.5 kg of polyethylene was 0.38%Δk. *

Foil exposure runs were made with all rods with drawn except Actuator 5 which was withdrawn about 13 cm. The D_2O temperature was held at about 22°C.

6.3.1 Bare Catcher Foils

Both bare and cadmium covered catcher foil were exposed within the cavity to measure fission power distribution and the foil actuators are given in Table 6.5. All of the bare foil data were normalized to the foil at the center of the core and the relative axial distribution at each radial location is presented in Figure 6.5. It will be noted that the points near the outer edge of the cavity show unusual fluctuations. The radial position of 71.1 cm was on the inner surface of the polyethylene structure directly opposite core position 8.16. The 81.5 cm position was at the center of the polyethylene and the 88.9 cm location was between the outer surface of the polyethylene and the inner surface of the stainless steel liner. Part of the variation could be caused by the physical structure of the basic polyethylene assembly which had strips of polyethylene running between the outer, center and inner rings of polyethylene as shown in Figure 5.1. This caused double thickness of polyethylene where these strips were attached to the outer ring of polyethylene. The repeat measurement, however, did not show the same peaks or valleys but when averaged with the first set of data points yields a fairly normal distribution. Part of the uncertainty appears to be position errors and part due to normal catcher foil statistics.

Each of the axial profiles given in Figure 6.5 was averaged and these averages were plotted to give the radial power distribution as shown in Figure 6.6. The volume weighted average over the active core was 3.88 with respect to the point at the core center.

6.3.2 Cadmium Ratios

The cadmium ratios obtained from the bare and cadmium covered catcher foils are given in Table 6.6 and Figures 6.7 and 6.8. The axial profiles appears to be perfectly normal. However, it is suspected that on the radial profile (Figure 6.8) at the 148.5 cm position, the point at the outer edge of the fuel may be high. It will be noted that the bare foil activity at 148.5 cm on the axial curve 61.0 cm from the core center in Figure 6.5 is above a smooth curve by 9%. If this were corrected accordingly, the

---

* 36.5 kg of CH_2 was maintained throughout the remainder of the uniform hydrogen mockup portion of the experiment.

cadmium ratio would be 10.3 at the outer edge of the fuel. The point at cavity wall (88.9 cm from the core center) is based on an average of the two bare foil values, as discussed in the previous section.

6.4 Resonance Detector Data

6.4.1 Gold Foil Data

Both bare and cadmium covered gold foils were exposed in the cavity and reflector region of this reactor. Most of the foils within the cavity region were concentrated in the polyethylene region as this was the area where changes due to heating were expected to be most noticeable. These data are given in Table 6.7 and include both bare and cadmium covered foils.

The power normalization factors obtained from each of the foil exposure runs with reference to Run 1084 are given in Table 6.8. Included here are all the foil runs for the cold and heated polyethylene. It will be noted that the calibration factor between the normal counting system and the PC_3 (2π counter) system changed slightly. This was due to an adjustment in the counting heads of the normal counting system. There was a scram during Run 1089 so the normalization factor was determined by comparing the foil data with previous results and may have a larger than usual uncertainty.

The bare gold data within the cavity were normalized to the foil nearest the center of the core and the axial distribution plotted and averaged as shown in Figure 6.9. The averages were then plotted to show the radial distribution as seen in Figure 6.10. Also given in Figures 6.10 are the individual points obtained along the axial centerline of the reactor. The two sets of data show very good agreement and the separation between the two curves is consistent with the data given in Figure 6.9.

It will be noted from Figure 6.9 that there is considerable data scatter near the outer edges of the polyethylene. Part of this appears to be due to the way the polyethylene assembly was built. The strips of polyethylene which were in the form of waves between the cylinders caused heavy concentrations of polyethylene and thus significant flux perturbations where the waves and cylinders joined..

The gold foil activity within the reflector regions are given in Figures 6.11 and 6.12. Both bare and cadmium foil data are plotted in these figures for comparison. Some bad data were obtained in the end reflector on Run 1089 and these were repeated on Run 1098. The second set of data are much more in line with expected results although both sets of data are given in the figure.

It will be noted from Figure 6.11 that there was an additional traverse obtained in the end reflector. The foils were placed in an unoccupied rod guide tube which was 56.8 cm from the center of the core. The foil activities are consistently below the values at the center of the core except at the core reflector interface where the opposite is true. This comparison is nearly identical to that calculated with a two-

dimensional diffusion code. However, it should be pointed out that there were minor configuration differences for Runs 1098, 1099, and 1100 in which the measurements were taken in the 56.8 cm tube. Just prior to Run 1098, the worth of fuel in the radial reflector was measured, and it was necessary to remove a sector of the beryllium (a 20 degree segment). This was inadvertently left out of the reactor for the above mentioned foil exposure runs. Furthermore, k-excess was slightly higher which required Actuator 6 to be withdrawn about 8 cm instead of 13 cm. However, Actuator No. 6 was far removed from the guide tube in which the measurements were made, and the change in rod position should have had little or no effect on the measured flux distribution in the end reflector. Furthermore, it is not likely that the removal of the small sector of beryllium in the side reflector had much effect on the end reflector. Therefore, these configuration differences are considered trivial, and the comparison in Figure 6.11 is considered to be correct.

Both bare and cadmium covered gold foils were also exposed at the separation plane and along the gap between the two tables. These data were obtained with the above mentioned beryllium sector removed. The resulting distribution is given in Figure 6.13.

6.4.2 Indium Data

Both bare and cadmium covered indium data were also exposed in the cavity and reflector regions after the 20^{o} beryllium sector was removed. These data are given in Table 6.9. The distribution at the separation plane is shown in Figure 6.14. These data will be compared to other types of foils in a subsequent section.

6.4.3 Manganese Data

A few manganese foils were also exposed in the cavity and at separation plane. The foil data are given in Table 6.10 and the foil activity distribution at the separation plane can be seen in Figure 6.15.

6.4.4 Cadmium Ratios

The gold cadmium ratios throughout the reactor are given in Table 6.11. The cadmium ratios were obtained after calculating the infinitely dilute foil activities according to the procedures given in Section 2.2 of this report. Within the cavity region the cadmium ratio distributions are shown in Figure 6.16 and 6.17. These data are generally consistent except for the points on the two outer axial traverses (Figure 6.16) at an axial position of 118 cm which appear to be high. The cadmium ratios in the reflector regions are presented in Figure 6.18. Also included here are the data at 56.8 cm in the end reflector. The two positions in the end reflector show excellent agreement except at 30.5 cm. There appears to be a high point around the 46 cm and this shows up in both the end and radial reflectors. There is no apparent reason for this and data on previous configurations have not shown any peak in this region.

The cadmium ratios across the separation plane are shown in Figure 6.19. The increase near the center of the core is real and caused by the 30.5 cm hole in the end reflector which simulates the exhaust nozzle.

Cadmium ratios were also obtained for indium and manganese at the separation plane and at a few points within other portions of the cavity. These data are given in Tables 6.12 and 6.13. The distributions across the separation plane are presented in Figure 6.20 and 6.21 for In and Mn, respectively. Table 6.17 lists, for comparison purposes, the infinitely dilute cadmium ratios for these three different detector materials.

The comparison of the gold, indium, and manganese cadmium ratios can be used to infer the shape of the slowing down spectrum. If the spectrum was 1/E, then the ratio of sub-cadmium to epi-cadmium activation (the cadmium ratio minus 1.0) should be equal to the ratio of thermal cross section to the resonance integral times a constant factor. If this factor is not constant, i.e., differs between the three different detectors, then the flux as determined by the principal resonances of the three detectors is not 1/E. These principal resonances are at 1.44, 4.96, and 337 ev for In, Au, and Mn, respectively, and thus span a considerable range of the slowing down spectrum.

Listed below are the thermal and resonance integral cross sections and their ratios for the three detectors.

	In*	Au	Mn
2200 m/sec σ	162	98	13.4
R.I ∞	2500	1555	15 (Ref. 4)
Ratio	0.065	0.063	0.89

* This is for the 54-minute activity only, Reference 3

Indium and gold, fortuitously, have the identical ratio of thermal to resonance integral cross sections, except for differences in effective thermal cross section and effective cadmium cut-off energy (References 5 and 6). These latter differences are only of the order of 10%, however. Examination of Table 6.17 shows that the measured cadmium ratios of these two detectors are nominally the same in the reflector about 20 to 40 cm from the cavity wall. In the core the cadmium ratios differ, though much of this may be because of experimental uncertainties since the ratio is so close to 1.0, and near the cavity wall and deep within the reflector the cadmium ratios are significantly different. Thus, only in the 20 to 40 cm range in the reflector is the flux spectrum between 1.4 and 5 ev nominally 1/E. Multigroup computer calculations confirm this result*. With reference to the manganese cadmium ratio there is an indication of constant 1/E spectrum between 337 ev and 1.44 ev in a few locations, particularly near the cavity wall. But inside the reflector the manganese result does not indicate a 1/E flux spectrum. Note, however, that manganese comparisons are only qualitative and not conclusively indicative of the flux at the 337 ev resonance, for the 1/v contribution to the 14 barn resonance integral is 6 barns.

---

* Reference is made on page 356, Section 18.8 of Reference 1 where it was stated that a 1/E flux spectrum was more generally applicable over the entire reactor. This is not true, and the erroneous conclusion was caused by measurements which unfortunately were limited to the region where the 1/E spectrum exists.

6.4.5 Thermal Neutron Flux

The thermal neutron flux is readily calculated from the bare and cadmium covered foil results and the procedures used to make these calculations are given in Section 4.4.2 of Reference 1. Tables 6.14, 6.15, and 6.16 contain the flux values from gold, indium, and manganese, respectively. The axial distributions within the cavity region are shown in Figure 6.22 for the gold data results. It will be noted that two sets of data are given for the axial traverse at 88.9 cm. There were two sets of cadmium covered foils but only one set of bare foil data used in these calculations. On the average the second set of data give a higher flux by 2.7%; however, the standard error on the five points was ±5.3%. This higher value could actually be real since a sector of the beryllium was removed when obtaining the second set of cadmium covered foil.

The complete radial and axial flux profiles through the axial and radial centers of the reactor are shown in Figures 6.23 and 6.24 as obtained from the gold foils. The data appear to consistent and follow closely a smooth curve.

There were several regions in the reactor where thermal flux values were obtained for the three different types of resonance detectors. These data are compared in Table 6.17. It should be pointed out that all of these results were obtained with the sector of beryllium removed from the reflector. On the average, the indium showed higher thermal neutron flux than gold by about 11%, being about 10% higher in the reflector and 16% higher in the core regions while manganese results gave lower values than gold by 2.2% on the average, though at several points the discrepancy was substantially larger. The thermal flux from the three resonance detectors at the separation plane are plotted in Figure 6.25. This comparison clearly shows the differences and particularly the higher values for the indium data.

The calculation of "thermal" flux from indium activation data is difficult because of the low lying (1.44 ev) broad resonance, which significantly influences the effective thermal cross section (Reference 5) or the effective cadmium cutoff energy (Reference 6). The 10 to 15% difference observed experimentally is fully to be expected unless corrections for the non-1/v shape of the indium cross section are applied. Existing experimental data is insufficient to deduce these corrections, though they can be obtained from multigroup computer calculations.

TABLE 6.1

Inverse Multiplication

Stainless Steel Liner and 38.3 kg of Polyethylene in the Cavity

Increment	Fuel Loading Equivalent Size 1.0 sheets	Channel No. 1 CR	Channel No. 1 CRo/CR	Channel No. 2 CR	Channel No. 2 CRo/CR	Channel No. 3 CR	Channel No. 3 CRo/CR	Average CRo/CR	Rod Positions
Decay corrected CPMo		940		971		732			In
		1047		1099		818			Out
0	22152	18356	.0512	16293	.0596	11936	.0613	.0514	In
0	22152	44956	.0233	40000	.0275	28790	.0284	.0264	Out
1	23088	19682	.0478	17489	.0555	12883	.0568	.0534	In
1	23088	52111	.0201	46799	.0235	33826	.0242	.0226	Out
Rearranged polyethylene tubes									
2	24024	17303	.0543	16150	.0601	11710	.0625	.0590	In
2	24024	41875	.0250	39162	.0281	27853	.0294	.0275	Out
3	24960	18332	.0513	17307	.0561	31934	.0581	.0552	In
3	24960	47927	.0218	44447	.0247	32337	.0243	.0243	Out
4	26208	19603	.0480	18573	.0523	13835	.0529	.0511	In
4	26208	56255	.0186	53213	.0207	38369	.0213	.0202	Out
5	29640	24908	.0377	24259	.0400	17721	.0413	.0397	In
5	29640	127052	.0082	118527	.0093	84800	.0096	.0090	Out
6	31699	29723	.0316	28984	.0335	21341	.0343	.0331	In
6	31699	358561	.0029	327606	.0034	228627	.0036	.0033	Out
7	33175	32682	.0288	32605	.0298	24240	.0302	.0296	In
7	33175	Critical	0.0684%Δk excess reactivity						Out
8	34528	41096	.0229	36264	.0268	26887	.0272	.0255	In
8	34528	Critical	0.4 %Δk excess reactivity						Out

TABLE 6.2

Fuel Worth Measurement

Stainless Steel Liner and 38.3 kg Polyethylene in Reactor

Radius	Reactivity Difference (%Δk)	Fuel Mass Difference (gm U)	Fuel Worth (%Δk/kg)
5.4	0.0200 ± 0.0021	253.8	0.0788 ± 0.0083
26.9	0.0215 ± 0.0021	263.9	0.0815 ± 0.0080
43.5	0.0248 ± 0.0021	260.2	0.0953 ± 0.0081
50.8	0.0284 ± 0.0021	252.4	0.1125 ± 0.0083
60.2	0.0554 ± 0.0021	249.8	0.2218 ± 0.0084

TABLE 6.3

Material Worth Measurements Stainless Steel Liner and 38.3 kg of Polyethylene in the Cavity

Material	Location	Mass (gm)	Reactivity Change (%Δk) (1)	Material Worth (%Δk/kg)
Polyethylene	Positions 5-1, 12-16	330.8	-0.1574	-0.476
Polyethylene	76.0 cm from core center (center of polyethylene annulus)	330.8	-0.0559	-0.169
Polyethylene	Cavity wall	357.6	-0.0625	-0.175
Polyethylene	Positions 5-1, 12-16	330.8	-0.1281	-0.387
Polystyrene (CH)	Positions 2-1, 5-1, 8-4, 14-13, 15-16	318.9	-0.1312	-0.411
Polystyrene	Positions 2-1, 3-4, 5-1, 8-4, 9-13, 12-16, 14-13	443.0	-0.1660	-0.375
Polyethylene	Same as item 6	299.8	-0.1514	-0.505
Carbon	Same as item 6	9094.8	-0.3800	-0.0418
Polystyrene	Positions 2-1, 3-4, 5-1, 8-4, 9-13, 12-16, 14-13	343.0	-0.1546	-0.451
Polystyrene	Inner surface of polyethylene structure	214.0	-0.0687	-0.321
Polyethylene	Same as item 11	112.0	-0.0492	-0.439
Carbon	Same as item 11	2592	-0.0763	-0.0294
Carbon	Across polyethylene annulus	15470	-0.3019	-0.0195
Aluminum	Core average	8528	-0.0641	-0.00752

NOTE: The polystyrene used in items 5 and 6 was a different type of material than used for items 10 and 11. The latter was actually used in the variable hydrogen experiment.

(1) Normal standard error on these changes is 0.005%Δk or less

TABLE 6.4

MTR Type Fuel Plate Worth in Radial Reflector

Distance From Cavity Wall (cm)	Mass U^{235} (gm)	Total Reactivity Change (%Δk)	Aluminum Correction	Uranium Worth (%Δk/kg)
0	42	0.1512	0.057	4.96
7.6	42	0.1695	0.091	6.20
15.2	42	0.1747	0.071	5.85
30.5	42	0.1287	0.00	3.064

TABLE 6.5

Catcher Foil Data

Stainless Steel Liner and 36.5 kg of Polyethylene in Cavity Room Temperature (21°C)

Run 1086		Location			
Foil No.	Type	Radial	Axial	Normalized Counts	Local to Foil (X)
1	Bare	15.2	90.8	40298	6.628
2	Bare	15.2	102.8	14183	2.333
3	Bare	15.2	118.0	8356	1.374
4	Bare	15.2	133.3	6761	1.112
5	Bare	15.2	148.5	6080	1.000 (X)
6	Bare	15.2	179.0	6494	1.068
7	Bare	15.2	179.0	8526	1.402
8	Bare	15.2	194.2	13699	2.253
9	Bare	15.2	206.9	46002	7.566
10	Bare	61.0	90.8	84637	13.92
11	Bare	61.0	102.8	73799	12.14
12	Bare	61.0	118.0	63199	10.39
13	Bare	61.0	133.3	57056	9.384
14	Bare	61.0	148.5	59454	9.778
15	Bare	61.0	163.8	56209	9.245
16	Bare	61.0	179.0	56596	9.300
17	Bare	61.0	194.2	69016	11.35
18	Bare	61.0	206.9	86729	14.26
19	Bare	45.7	90.8	52443	8.625
20	Bare	45.7	118.0	16993	2.795
21	Bare	45.7	148.5	12690	2.087
22	Bare	45.7	179.0	18092	2.976
23	Bare	45.7	206.9	49906	8.208
24	Bare	30.5	90.8	47122	7.750
25	Bare	30.5	118.0	9800	1.612
26	Bare	30.5	148.5	9148	1.505
27	Bare	30.5	179.0	10571	1.739
28	Bare	30.5	206.9	47446	7.803
29	Bare	71.1	90.8	104812	17.24
30	Bare	71.1	102.8	82456	13.56
31	Bare	71.1	118.0	74783	12.30
32	Bare	71.1	133.3	65505	10.77
33	Bare	71.1	148.5	61209	10.07
34	Bare	71.1	163.8	65454	10.77
35	Bare	71.1	179.0	64379	10.59
36	Bare	71.1	194.2	77968	12.82
37	Bare	71.1	206.9	83496	13.73
38	Bare	81.3	90.8	134532	22.13
39	Bare	81.3	102.8	122885	20.21
40	Bare	81.3	118.0	128145	21.08
41	Bare	81.3	148.5	112141	18.44

TABLE 6.5
(Continued)

Run 1086 (Cont'd)		Location		Normalized	Local to
Foil No.	Type	Radial	Axial	Counts	Foil (X)
42	Bare	81.3	148.5	112141	18.44
43	Bare	81.3	163.8	116068	19.09
44	Bare	81.3	179.0	120945	19.89
45	Bare	81.3	194.2	122255	20.11
46	Bare	81.3	206.9	127456	20.96
47	Bare	88.9	90.8	147577	24.27
48	Bare	88.9	102.8	137849	22.67
49	Bare	88.9	118.0	148838	24.48
50	Bare	88.9	133.3	138450	22.77
51	Bare	88.9	148.5	120687	19.85
52	Bare	88.9	163.8	144217	23.72
53	Bare	88.9	179.0	144675	23.79
54	Bare	88.9	194.2	129114	21.24
55	Bare	88.9	206.9	123258	20.27
Run 1087					
1	Cd	15.2	90.8	4655	
2	Cd	15.2	206.9	4577	
3	Cd	45.7	148.5	4159	
4	Cd	61.0	90.8	5558	
5	Cd	61.0	118.0	5321	
6	Cd	61.0	206.9	5405	
7	Cd	81.3	148.5	6354	
Run 1090					
1	Cd	15.2	118.0	3816	
2	Cd	15.2	179.0	3370	
3	Cd	88.9	148.5	6374	
Run 1091					
1	Cd	45.7	90.8	5300	
2	Cd	71.1	148.5	5654	
3	Cd	45.7	206.9	5125	
Run 1092					
1	Cd	15.2	148.5	3444	
2	Cd	45.7	118.0	3898	
3	Cd	45.7	179.0	3853	
4	Cd	81.3	148.5	5947	

TABLE 6.5
(Continued)

Foil No.	Type	Location		Normalized Counts	Local to Foil (X)
		Radial	Axial		
Run 1098					
1	Cd	61.0	148.5	5232	--
2	Cd	61.0	179.0	5104	--
3	Bare	88.9	90.8	150331	24.72
4	Bare	88.9	102.8	144492	23.76
5	Bare	88.9	118.0	137262	22.58
6	Bare	88.9	133.3	142046	23.36
7	Bare	88.9	148.5	145284	23.89
8	Bare	88.9	163.8	147718	24.30
9	Bare	88.9	179.0	136243	22.41
10	Bare	88.9	194.2	130589	21.48
11	Bare	88.9	206.9	139986	23.02

TABLE 6.6

Catcher Foil Cadmium Ratios

Stainless Steel Liner and 36.5 kg of Polyethylene in Cavity - Room Temperature

Location		Foil Activity		Cadmium
Radial (cm)	Axial (cm)	Cadmium	Bare	Ratio
15.2	90.8	4655	40298	8.66
15.2	118.0	3816	8356	2.19
15.2	148.5	3444	6080	1.77
15.2	179.0	3370	8526	2.53
15.2	206.9	4577	46002	10.05
45.7	148.5	4159	12690	3.05
71.1	148.5	5654	61209	10.83
81.3	148.5	5947	112141	18.86
88.9	148.5	6374	139645	21.91
45.7	90.9	5300	52443	9.89
45.7	118.0	3898	16993	4.36
45.7	148.5	4159	12690	3.05
45.7	179.0	3853	18092	4.70
45.7	206.9	5125	49906	9.74
61.0	90.8	5558	84637	15.23
61.0	118.0	5321	63199	11.88
61.0	148.5	5232	59454	11.36
61.0	179.0	5104	56596	11.09
61.0	206.9	5405	86729	16.05

TABLE 6.7

Gold Foil Data

Stainless Steel Liner and 36.5 kg of Polyethylene in Cavity - Cold Polyethylene

Foil No.	Foil Type	Location Radial (cm)	Location Axial (cm)	Foil Weight (gm)	Specific Activity d/m/gm x 10^{-6}	Local to Foil (X)
Run 1086						
1	Bare	0	89.4	0.0343	2.468	2.353
2	Bare	0	74.9	0.0335	7.737	7.376
3	Bare	0	59.6	0.0341	6.784	6.467
4	Bare	0	44.4	0.0384	4.699	4.479
5	Bare	0	29.1	0.0338	2.953	2.815
6	Bare	0	13.9	0.0376	1.474	1.405
7	Bare	0	0	0.0354	0.211	0.201
8	Bare	93.2	151.1	0.0358	4.845	4.619
9	Bare	107.7	151.1	0.0384	5.704	5.438
10	Bare	123.0	151.1	0.0417	4.272	4.072
11	Bare	138.2	151.1	0.0414	2.958	2.820
12	Bare	153.5	151.1	0.03657	1.859	1.772
13	Bare	168.7	151.1	0.0400	0.983	0.937
14	Bare	183.9	151.1	0.03217	0.272	0.259
Run 1087						
1	Cd	0	59.6	0.0335	0.384	
2	Cd	0	29.1	0.0330	0.011	
3	Cd	123.0	151.1	0.0415	0.128	
4	Cd	153.5	151.1	0.0354	0.0045	
5	Cd	15.2	148.5	0.0408	1.050	
Run 1088						
1	Bare	15.2	90.8	0.0364	1.824	1.739
2	Bare	15.2	102.8	0.04255	1.161	1.107
3	Bare	15.2	118.0	0.0409	1.033	0.985
4	Bare	15.2	133.3	0.0483	0.926	0.883
5	Bare	15.2	148.4	0.0302	1.049	1.000 (X)
6	Bare	15.2	163.8	0.0328	1.043	0.994
7	Bare	15.2	179.0	0.0298	1.117	1.065
8	Bare	15.2	194.2	0.0338	1.203	1.147
9	Bare	15.2	206.9	0.0282	1.967	1.875
10	Bare	61.0	206.9	0.0357	2.740	2.612
11	Bare	71.1	206.9	0.04166	2.854	2.721
12	Bare	81.3	194.2	0.0381	3.723	3.549
13	Bare	81.3	206.9	0.04325	3.467	3.305
14	Bare	88.9	90.8	0.0339	4.361	4.157
15	Bare	88.9	118.0	0.0348	4.350	4.147

TABLE 6.7
(Continued)

Foil No.	Foil Type	Location Radial (cm)	Location Axial (cm)	Foil Weight (gm)	Specific Activity d/m/gm x 10^{-6}	Local to Foil (X)
Run 1088 (Cont'd)						
16	Bare	88.9	179.0	0.0416	4.153	3.959
17	Bare	88.9	194.2	0.0337	4.032	3.844
18	Bare	88.9	206.9	0.0350	3.806	3.628
19	Cd	0	74.9	0.0335	1.273	
20	Cd	0	44.4	0.0421	0.0453	
21	Cd	107.7	151.1	0.0318	0.635	
22	Cd	138.2	151.1	0.03385	0.0138	
23	Cd	61.0	148.5	0.0307	1.373	
24	Cd	61.0	179.0	0.0475	1.141	
25	Cd	71.1	90.8			
26	Cd	71.1	118.0	0.0319	1.416	
27	Cd	88.9	148.5	0.0325	1.676	
Run 1089						
1	Bare	0	82.5	0.0323	2.489	2.373
2	Bare	0	67.2	0.0408	6.906	6.583
3	Bare	0	52.0	0.410	6.858	6.538
4	Bare	100.1	151.1	0.0369	6,138	5.851
5	Bare	115.4	151.1	0.0418	5.203	4.960
6	Bare	130.6	151.1	0.0397	3.668	3.497
7	Bare	30.5	148.5	0.0390	1.110	1.058
8	Bare	45.7	148.5	0.0392	1.238	1.180
9	Bare	61.0	148.5	0.0385	2.772	2.166
10	Bare	71.1	148.5	0.0388	2.613	2.491
11	Bare	81.3	148.5	0.03745	3.679	3.507
12	Bare	88.9	102.8	0.03524	4.284	4.084
13	Bare	88.9	133.3	0.0373	4.373	4.169
14	Bare	88.9	148.5	0.333	4.305	4.104
15	Bare	88.9	163.8	0,0385	4.232	4.034
16	Cd	15.2	90.8	0.0302	1.279	
17	Cd	15.2	206.9	0.0399	1.066	
18	Cd	71.1	179.0	0.0385	1.310	
19	Cd	71.1	206.9	0.0273	1.450	
20	Cd	81.3	90.8	0.0312	1.497	
21	Cd	81.3	118.0	0.03077	1.531	
22	Cd	88.9	206.9	0.0363	1.318	

TABLE 6.7
(Continued)

Foil No.	Foil Type	Location Radial (cm)	Location Axial (cm)	Foil Weight (gm)	Specific Activity d/m/gm x 10^{-6}	Local to Foil (X)
Run 1090						
1	Bare	61.0	90.8	0.0420	2.887	2.752
2	Bare	61.0	102.8	0.0380	2.576	2.456
3	Bare	61.0	118.0	0.04177	2.427	2.314
4	Bare	61.0	133.3	0.0356	2.416	2.303
5	Bare	61.0	163.8	0.0361	2.358	2.248
6	Bare	61.0	179.0	0.0376	2.369	2.258
7	Bare	61.0	194.2	0.0367	2.546	2.427
8	Bare	71.1	90.8	0.0390	3.284	3.131
9	Bare	71.1	102.8	0.0368	3.011	2.870
10	Bare	71.1	118.0	0.0414	2.747	2.619
11	Bare	71.1	133.3	0.0392	2.703	2.577
12	Bare	71.1	163.8	0.0399	2.552	2.433
13	Bare	71.1	179.0	0.0404	2.624	2.501
14	Bare	71.1	194.2	0.0413	2.742	2.614
15	Cd	45.7	148.5	0.0360	1.136	
16	Cd	81.3	148.5	0.0379	1.633	
17	Cd	81.3	206.9	0.0411	1.264	
18	Cd	88.9	90.8	0.0357	1.385	
19	Cd	88.9	118.0	0.0402	1.237	
20	Cd	88.9	179.0	0.0386	1.595	
Run 1091						
1	Cd	0	89.4	0.0402	1.084	
2	Cd	93.2	151.1	0.0402	1.609	
3	Cd	15.2	118.0	0.0389	0.955	
4	Cd	15.2	179.0	0.0322	0.958	
5	Cd	30.5	148.5	0.0410	0.938	
6	Cd	81.3	163.8	0.0379	1.518	
7	Cd	81.3	179.0	0.0380	1.493	
8	Bare	81.3	90.8	0.0280	4.109	3.917
9	Bare	81.3	102.8	0.0381	3.784	3.607
10	Bare	81.3	118.0	0.0354	3.956	3.771
11	Bare	81.3	133.3	0.0391	3.717	3.543
12	Cd	71.1	90.8	0.0345	1.343	
Run 1092						
1	Bare	88.9	102.8	0.0209	4.728	4.507
2	Bare	88.9	133.3	0.0168	4.858	4.631
3	Bare	88.9	163.8	0.0177	4.761	4.539
4	Bare	81.3	179.0	0.0148	4.310	4.109

TABLE 6.7
(Continued)

Foil No.	Foil Type	Location Radial (cm)	Location Axial (cm)	Foil Weight (gm)	Specific Activity d/m/gm x 10^{-6}	Local to Foil (X)
Run 1092 (Cont'd)						
5	Cd	61.0	90.8	0.0183	1.682	
6	Cd	61.0	118.0	0.0191	1.602	
7	Cd	71.1	148.5	0.0208	1.681	
8	Cd	61.0	206.9	0.0200	1.554	
Run 1098 (Be sector removed)						
1	Bare	56.8	89.4	0.0147	3.346	
2	Bare	56.8	74.9	0.01735	6.790	
3	Bare	56.8	59.6	0.0162	5.681	
4	Bare	56.8	44.4	0.0198	4.054	
5	Bare	56.8	29.1	0.0194	2.587	
6	Bare	56.8	13.9	0.0206	1.302	
7	Bare	56.8	0	0.0161	0.183	
8	Bare	0	82.5	0.0156	5.810	
9	Bare	0	67.2	0.0141	6.933	
10	Bare	0	52.0	0.0165	5.361	
11	Bare	93.2	151.1	0.01965	5.188	
12	Bare	100.1	151.1	0.0175	6.369	
13	Bare	107.7	151.1	0.0146	5.722	
14	Bare	115.4	151.1	0.0163	5.247	
15	Bare	123.0	151.1	0.0147	4.301	
16	Bare	15.2	212.0	0.0156	2.256	
17	Bare	30.5	212.0	0.0154	2.367	
18	Bare	45.7	212.0	0.0161	2.622	
19	Bare	61.0	212.0	0.0194	2.996	
20	Bare	76.2	212.0	0.0203	3.605	
21	Bare	91.4	212.0	0.0164	3.873	
22	Bare	106.6	212.0	0.0184	3.136	
23	Bare	121.9	212.0	0.0163	2.158	
24	Bare	137.1	212.0	0.0184	1.339	
25	Bare	152.4	212.0	0.0192	0.759	
26	Bare	167.6	212.0	0.0174	0.357	
27	Bare	182.8	212.0	0.0166	0.068	
28	Cd	30.5	212.0	0.0179	1.455	
29	Cd	61.0	212.0	0.0184	1.636	
30	Cd	91.4	212.0	0.0178	1.360	
31	Cd	121.9	212.0	0.0168	0.224	
32	Cd	182.8	212.0	0.0166	0.024	
33	Cd	15.2	148.5	0.0155	1.955	
34	Cd	56.8	74.9	0.0153	1.431	
35	Cd	56.8	44.4	0.0178	0.048	

TABLE 6.7
(Continued)

Foil No.	Foil Type	Location Radial (cm)	Location Axial (cm)	Foil Weight (gm)	Specific Activity d/m/gm x 10^{-6}	Local to Foil (X)
Run 1099 (Be sector removed)						
1	Cd	0	44.4	0.0169	0.059	
2	Cd	56.8	89.4	0.0171	1.690	
3	Cd	56.8	59.6	0.0193	0.313	
4	Cd	88.9	90.8	0.0161	1.673	
5	Cd	88.9	118.0	0.01835	1.911	
6	Cd	88.9	148.5	0.0158	1.957	
7	Cd	88.9	179.0	0.01835	1.900	
8	Cd	88.9	206.9	0.0178	1.612	
9	Cd	138.2	151.1	0.0160	0.021	
10	Cd	15.2	212.0	0.0193	0.990	
11	Cd	45.7	212.0	0.0211	1.482	
12	Cd	76.2	212.0	0.0206	1.594	
13	Cd	106.6	212.0	0.0173	0.736	
14	Cd	137.1	212.0	0.0181	0.072	
15	Bare	71.1	140.9	0.0168	2.815	
16	Bare	88.9	140.9	0.0198	4.718	

TABLE 6.8

Power Normalization Factors

Stainless Steel Liner and 36.5 kg Polyethylene in Cavity

Run	Time	Decay Time (min)	Decay Factor	Activity (CPM)	Corrected Activity (1) (CPM)	Normal. Factor
1084	1605.00	42.28	0.826	324656	268166	
	1606.00	44.28	0.869	308162	267793	
	1607.75	46.03	0.909	297746	270651	
					268870	1.000
1085	1446.50	43.74	0.857	302020	258831	
	1448.35	45.59	0.910	288241	262299	
	1450.25	47.49	0.941	273890	257730	
					259620	1.036
1086	1153.31	55.62	1.135	109298	124053	
	1155.13	57.44	1.180	104630	123463	
	1156.83	59.14	1.223	101742	124436	
					123982	2.169
1087	1439.00	39.99	0.777	313258	243401	
	1440.61	41.60	0.811	301332	244380	
	1442.22	43.21	0.846	290727	245955	
					244579	1.099
1088	1608.15	19.60	0.396	725789	287412	
	1609.85	21.36	0.424	677753	287367	
	1611.40	22.91	0.451	639321	288334	
					287704	0.935
1089	A scram occurred during this run. A forced normalization factor was used which gave a good fit of the data compared to previous results.					0.949
1090	The time was determined from a stop watch	41.0	0.798	343750	274313	
		42.5	0.831	330521	274663	
		44.0	0.863	317979	274416	
					274464	0.980
1091	The time was determined from a stop watch	55.5	1.132	255087	288758	
		57.5	1.182	244648	289174	
		59.5	1.232	234429	288165	
					288699	0.931
1092	1602.90	27.90	0.538	531032	285695	
	1604.55	29.55	0.570	502361	286346	
	1606.20	31.20	0.600	476686	286012	
					286018	0.940

TABLE 6.8

(Continued)

Run	Time	Decay Time (min)	Decay Factor	Activity (CPM)	Corrected Activity (1) (CPM)	Normal. Factor
1093	1510.30	48.77	0.971	291727	283267	
	1512.00	50.47	1.011	280102	283183	
	1514.90	53.37	1.080	262427	283421	
					283290	0.916
	Counting system calibration correction 2.31/2.24 x 283290 = 293406					
1094	1601.80	34.41	0.663	436583	289455	
	1603.80	36.41	0.703	410782	288780	
	1605.80	38.41	0.744	388292	288889	
					289041	0.902
	Counting system calibration correction 2.31/2.24 x 289041 = 298074					
1095	1228.00	45.77	0.903	312507	282194	
	1230.00	47.77	0.948	297195	281741	
	1232.00	49.77	0.994	283544	281843	
					281926	0.925
	Counting system calibration correction 2.31/2.24 x 281926 = 290736					
1096	1422.20	46.31	0.915	309899	283558	
	1424.20	48.31	0.960	294437	282660	
	1426.20	50.31	1.007	281014	282981	
					283066	0.921
	Counting system calibration correction 2.31/2.24 x 283066 = 291912					
1097	1554.00	30.60	0.589	483541	284806	
	1556.00	32.60	0.628	453545	284826	
	1558.00	34.60	0.667	426178	284261	
					284631	0.916
	Counting system calibration correction 2.31/2.24 x 284631 = 293526					
1098	1532.80	43.88	0.861	330099	280914	
	1534.80	45.88	0.905	314029	284196	
	1536.80	47.88	0.951	298642	284009	
					283040	0.921
	Counting system calibration correction 2.31/2.24 x 283040 = 291885					
1099	1247.80	49.77	0.994	286355	284637	
	1249.80	51.77	1.041	273226	284428	
	1251.80	53.77	1.090	261118	284619	
					284561	0.916
	Counting system calibration correction 2.31/2.24 x 284561 = 293454					

TABLE 6.8

(Continued)

Run	Time	Decay Time (min)	Decay Factor	Activity (CPM)	Corrected Activity (1) (CPM)	Normal. Factor
1100	1506.70	33.00	0.635	445534	282914	
	1508.35	34.65	0.668	424874	283816	
	1509.88	36.18	0.698	406938	284043	
					283591	0.919
	Counting system calibration correction 2.31/2.24 x 283581 = 292453					

(1) Corrected to shutdown time.

TABLE 6.9

Indium Data Results

Stainless Steel Liner and 36.5 kg Polyethylene in Cavity

Foil No.	Foil Type	Location Radial	Location Axial	Foil Weight (gm)	Specific Activity d/m/gm x 10^{-8}
Run 1099					
18	Bare	71.1	148.5	0.00510	6.285
21	Cd	71.1	148.5	0.00562	3.869
15	Bare	88.9	148.5	0.00515	9.718
Run 1100					
17	Bare	56.8	59.6	0.00740	10.73
13	Cd	56.8	59.6	0.00512	0.794
620	Bare	56.8	89.4	0.00231	6.100
492	Cd	56.8	89.4	0.00222	3.138
632	Bare	15.2	118.0	0.00230	2.838
404	Cd	15.2	118.0	0.00229	2.552
812	Bare	15.2	148.5	0.00228	2.704
664	Cd	15.2	148.5	0.00228	2.395
642	Bare	30.5	212.0	0.00229	4.613
14	Cd	30.5	212.0	0.00649	3.217
829	Bare	61.0	212.0	0.00230	5.763
19	Cd	61.0	212.0	0.00679	3.423
729	Bare	91.4	212.0	0.00231	7.143
11	Cd	91.4	212.0	0.00584	2.710
763	Bare	121.9	212.0	0.00233	4.274
20	Cd	121.9	212.0	0.00519	0.300
822	Bare	152.4	212.0	0.00228	1.605
12	Cd	152.4	212.0	0.00518	0.0566

TABLE 6.10

Manganese Foil Data

Stainless Steel Liner and 36.5 kg of Polyethylene in Cavity

Foil		Location			
No.	Type	Radial (cm)	Axial (cm)	Foil Weight (gm)	Specific Activity d/m/gm x 10^{-7}
3	Cd	121.9	212.0	0.0415	0.0214
5	Cd	30.5	212.0	0.04255	0.177
10	Cd	71.1	148.5	0.04586	0.172
12	Bare	30.5	212.0	0.0415	1.145
13	Bare	91.4	212.0	0.0423	2.934
17	Bare	71.1	148.5	0.0432	1.438
18	Bare	152.4	212.0	0.04235	0.860
19	Bare	88.9	148.5	0.0434	3.070
20	Bare	121.9	212.0	0.04385	2.862
21	Bare	61.0	212.0	0.0433	1.678
23	Cd	88.9	148.5	0.0437	0.204
24	Cd	61.0	212.0	0.0407	0.179
25	Cd	91.4	212.0	0.0459	0.140
26	Cd	152.4	212.0	0.0438	0.00228

TABLE 6.11

Gold Foil Cadmium Ratios

Stainless Steel Liner and 36.5 kg of Polyethylene in Cavity - Cold Polyethylene

Location		Infinitely Dilute Foil Activity d/m/gm x 10^{-6}		
Radial (cm)	Axial (cm)	Bare Foil	Cd Foil	Cadmium Ratios
15.2	90.8	3.441	2.803	1.228
15.2	118.0	2.417	2.319	1.042
15.2	148.5	2.288	2.278	--
15.2	179.0	2.369	2.313	1.024
15.2	206.9	3.357	2.616	1.284
61.0	90.8	4.725	3.058	1.545
61.0	118.0	4.202	2.956	1.421
61.0	148.5	4.048	3.029	1.337
61.0	179.0	4.125	3.015	1.368
61.0	206.9	4.411	2.915	1.513
71.1	90.8	5.112	3.105	1.646
71.0	118.0	4.646	3.172	1.465
71.1	148.5	4.493	3.198	1.405
71.1	179.0	4.508	3.168	1.423
71.1	206.9	4.686	3.055	1.534
81.3	90.8	5.870	3.323	1.766
81.3	118.0	5.889	3.380	1.742
81.3	148.5	5.961	3.923	1.519
81.3	179.0	5.779	3.591	1.609
81.3	206.9	5.371	3.141	1.710
88.9	90.8	6.193	3.247	1.908
88.9	118.0	6.083	3.046	1.997
88.9	148.5	6.427	3.782	1.699
88.9	179.0	6.468	3.861	1.675
88.9	206.9	5.579	3.111	1.793
30.5	148.5	2.481	2.329	1.066
45.7	148.5	2.813	2.672	1.053
0	89.4	3.980	2.669	1.491
0	74.9	9.372	2.909	3.222
0	59.6	7.280	0.877	8.299
0	44.4	4.765	0.113	43.90
0	29.1	2.967	0.0250	118.8
93.2	151.1	7.119	3.962	1.797
107.7	151.1	6.536	1.421	4.602
123.0	151.1	4.464	0.319	13.98
138.2	151.1	2.977	0.0317	94.04
153.5	151.1	1.865	0.0105	177.4

TABLE 6.11
(Continued)

Location		Infinitely Dilute Foil Activity d/m/gm x 10^{-6}		
Radial (cm)	Axial (cm)	Bare Foil	Cd Foil	Cadmium Ratios
Sector of Be removed from radial reflector				
56.8	89.4	4.570	3.001	1.523
56.8	74.9	7.866	2.448	3.213
56.8	59.6	5.928	0.580	10.23
56.8	44.4	4.094	0.086	47.38
15.2	212.0	3.025	1.834	1.650
30.5	212.0	3.461	2.625	1.319
45.7	212.0	3.827	2.834	1.350
61.0	212.0	4.370	2.980	1.467
76.2	212.0	5.024	3.022	1.663
91.4	212.0	4.923	2.449	2.011
106.6	212.0	3.728	1.312	2.841
121.9	212.0	2.327	0.395	5.886
137.1	212.0	1.398	0.130	10.72
71.1	140.9	4.163	3.109 (assumed)	1.339
88.9	140.9	6.384	3.580 (assumed)	1.783

TABLE 6.12

Manganese Cadmium Ratios

Stainless Steel Liner and 36.5 kg of Polyethylene in Cavity

Location		Infinitely Dilute Foil Activity - d/m/gm x 10^{-6}		
Radial (cm)	Axial (cm)	Bare Foil	Cd Foil	Corrected Cadmium Ratio
71.1	148.5	1.447	0.181	8.010
88.9	148.5	3.080	0.214	14.38
30.5	212.0	1.154	0.186	6.208
61.0	212.0	1.687	0.188	8.976
91.4	212.0	2.941	0.147	20.01
121.9	212.0	2.863	0.0225	127.4
152.4	212.0	0.861	0.00239	359.3

TABLE 6.13

Indium Cadmium Ratios

Stainless Steel Liner and 36.5 kg of Polyethylene in Cavity

Location		Infinitely Dilute Foil Activity d/m/gm x 10^{-6}		
Radial (cm)	Axial (cm)	Bare Foil	Cd Foil	Cadmium Ratio
56.8	59.6	11.14	1.124	9.907
56.8	89.4	8.624	5.620	1.535
15.2	118.0	4.909	4.619	1.063
15.2	148.5	4.638	4.329	1.071
71.1	148.5	7.930	5.611	1.413
88.9	148.5	11.42	5.755	1.984
30.5	212.0	6.783	4.850	1.399
61.0	212.0	8.107	5.227	1.551
91.4	212.0	8.924	3.967	2.249
121.9	212.0	4.466	4.268	10.74
152.4	212.0	1.641	0.0803	20.43

TABLE 6.14

Thermal Neutron Flux - Gold Foil Data

Stainless Steel Liner and 36.5 kg of Polyethylene in Cavity

Location		Thermal Neutron Flux
Radial (cm)	Axial (cm)	$n/cm^2/sec/watt \times 10^{-6}$
0	89.4	0.961
0	74.9	4.736
0	59.6	4.692
0	44.4	3.409
0	29.1	2.156
0	13.0	1.076 (1)
0	0	0.154 (1)
93.2	151.1	2.313
107.7	151.1	3.749
123.0	151.1	3.037
138.2	151.1	2.158
153.5	151.1	1.359
168.7	151.1	0.718 (1)
183.9	151.1	0.199 (1)
15.2	90.8	0.467
15.2	118.0	0.0716
15.2	148.5	0.0058
15.2	179.0	0.0409
15.2	206.9	0.542
61.0	90.8	1.222
61.0	118.0	0.913
61.0	148.5	0.747
61.0	179.0	0.814
61.0	206.9	1.097
71.1	90.8	1.471
71.1	118.0	1.081
71.1	148.5	0.949
71.1	179.0	0.983
71.1	206.9	1.196
81.3	90.8	1.866
81.3	118.0	1.839
81.3	148.5	1.493
81.3	179.0	1.603
81.3	206.9	1.634
88.9	90.8	2.159
88.9	118.0	2.225
88.9	148.5	1.939
88.9	179.0	1.910
88.9	206.9	1.808
30.5	148.5	0.112
45.7	148.5	0.103

TABLE 6.14
(Continued)

Location		
Radial (cm)	Axial (cm)	Thermal Neutron Flux $n/cm^2/sec/watt \times 10^{-6}$
0	44.4	3.395
15.2	148.5	0.114
56.8	44.4	2.923
56.8	59.6	3.900
56.8	74.6	3.951
56.8	89.4	1.144
88.9	90.8	2.256
88.9	118.0	2.079
88.9	148.5	2.057
88.9	179.5	2.019
88.9	209.5	1.865
138.2	151.1	2.148
15.2	212.0	0.869
30.5	212.0	0.610
61.0	212.0	1.014
91.4	212.0	1.804
121.9	212.0	1.409
152.4	212.0	0.039

(1) These values are based on an extrapolation of the cadmium covered foil activity.

TABLE 6.15

Indium Thermal Flux Values

Stainless Steel Liner and 36.5 kg of Polyethylene in Cavity

Location		
Radial (cm)	Axial (cm)	Thermal Neutron Flux $n/cm^2/sec/watt \times 10^{-6}$
56.8	59.6	4.084
56.8	89.4	1.226
15.2	118.0	0.116
15.2	148.5	0.126
71.1	148.5	0.946
88.9	148.5	2.309
30.5	212.0	0.789
61.0	212.0	1.174
91.4	212.0	2.022
121.9	212.0	1.648
152.4	212.0	0.637

TABLE 6.16

Manganese Thermal Flux Values

Stainless Steel Liner and 36.5 kg of Polyethylene in Cavity

Location		
Radial (cm)	Axial (cm)	Thermal Neutron Flux $n/cm^2/sec/watt \times 10^{-6}$
71.1	148.5	0.800
88.9	148.5	1.812
30.5	212.0	0.612
61.0	212.0	0.948
91.4	212.0	1.766
121.9	212.0	1.796
152.4	212.0	0.542

TABLE 6.17

Stainless Steel Liner and 36.5 kg of Polyethylene in Cavity

Comparison of Neutron Fluxes for Gold, Indium and Manganese

Location		Thermal Neutron Flux $n/cm^2/sec/watt$					Infinitely Dilute Cadmium Ratios		
Radial (cm)	Axial (cm)	Gold	Indium	Manganese	$\frac{Au}{In}$	$\frac{Au}{Mn}$	Gold	In	Mn
56.8	59.6 (refl.)	3.900	4.084	--	0.954	--	10.3	9.9	--
56.8	89.4 (refl.)	1.144	1.226	--	0.933	--	1.52	1.54	--
15.2	118.0 (core)	0.0716 (1)	0.116	--	--	--	1.04	1.06	--
15.2	148.5 (core)	0.114	0.126	--	0.905	--	1.005	1.07	--
71.1	148.5 (CH_2)	0.949	0.946	0.800	1.003	1.186	1.40	1.41	8.0
88.9	148.5 (refl.)	1.939	2.309	1.812	0.840	1.070	1.70	1.98	14.4
30.5	212.0 (core)	0.610	0.789	0.612	0.773	0.997	1.32	1.40	6.2
61.0	212.0 (core)	1.014	1.174	0.948	0.864	1.070	1.42	1.55	9.0
91.4	212.0 (refl.)	1.804	2.022	1.766	0.892	1.022	2.01	2.25	20.0
121.9	212.0 (refl.)	1.409	1.648	1.796	0.855	0.785	5.9	10.74	127.4
152.4	212.0 (refl.)	0.039 (1)	0.637	0.542	--	--	--	20.43	359.0
				Average	.891±.067	1.022±.133			

(1) This value is low, probably in error, and has not been included in the averages.

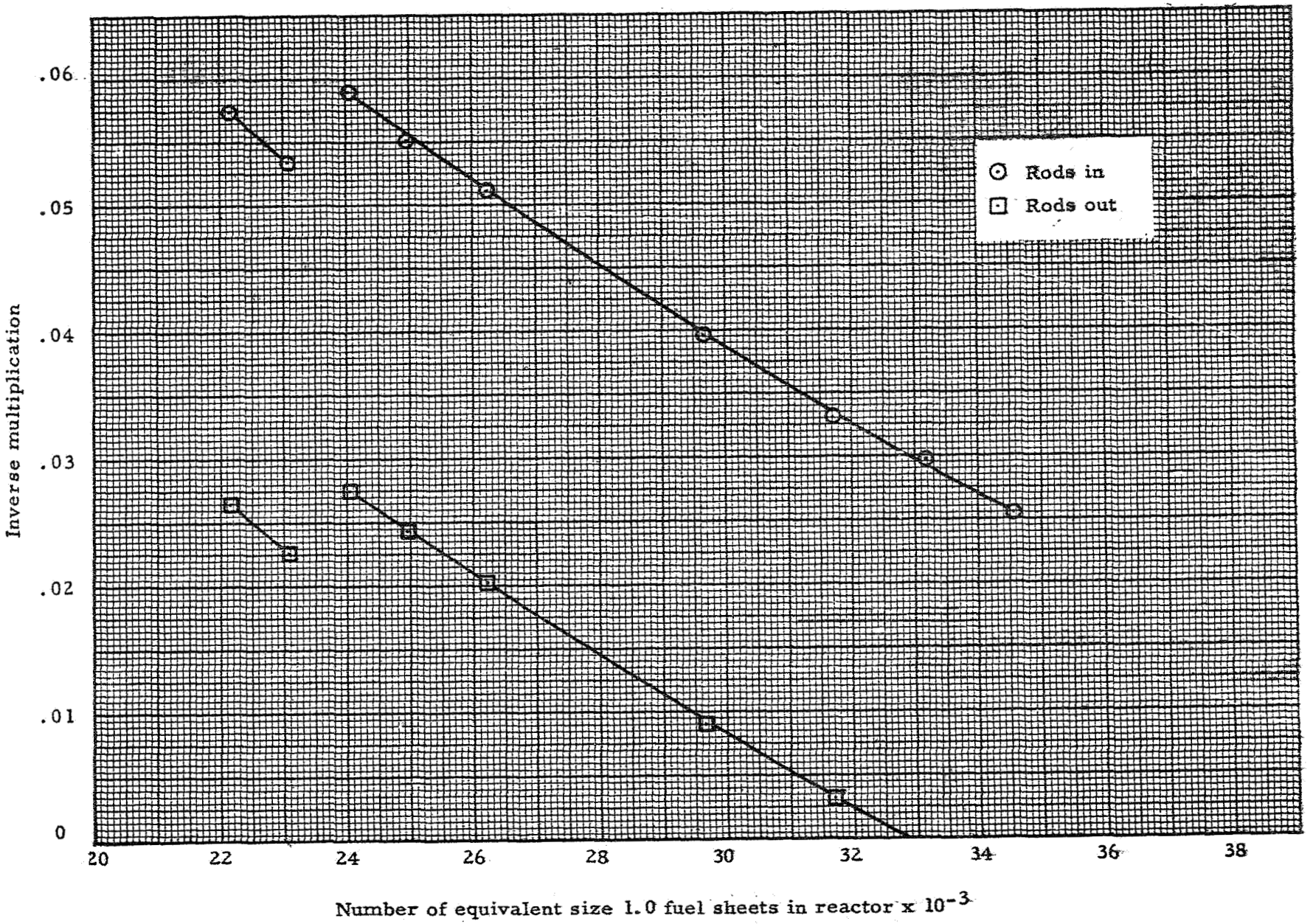

Fig. 6.1 Inverse multiplication curves, 38.3 kg CH_2 plus stainless steel liner

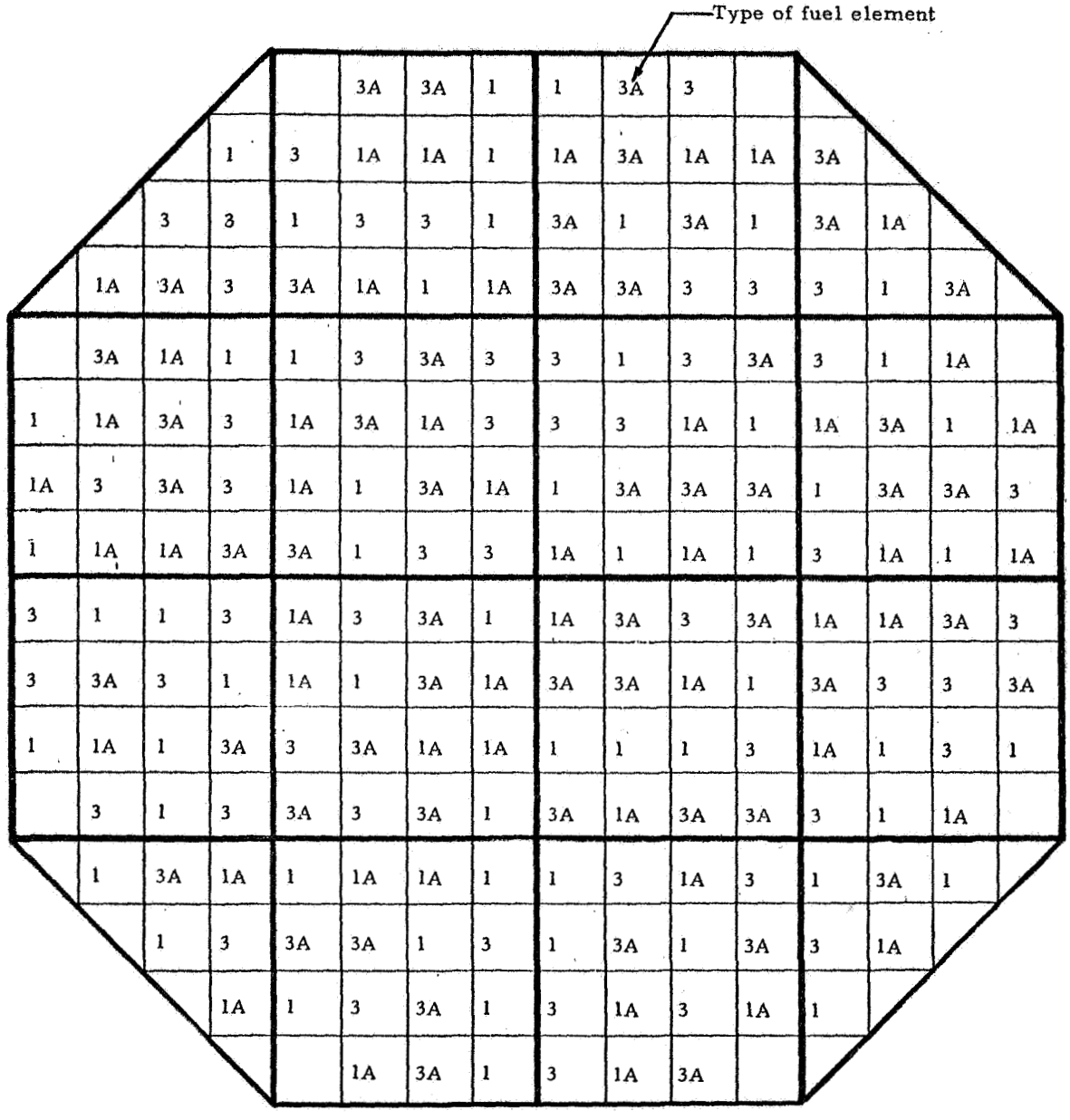

				3A	3A	1	1	3A	3						
			1	3	1A	1A	1	1A	3A	1A	1A	3A			
		3	3	1	3	3	1	3A	1	3A	1	3A	1A		
	1A	3A	3	3A	1A	1	1A	3A	3A	3	3	3	1	3A	
	3A	1A	1	1	3	3A	3	3	1	3	3A	3	1	1A	
1	1A	3A	3	1A	3A	1A	3	3	3	1A	1	1A	3A	1	1A
1A	3	3A	3	1A	1	3A	1A	1	3A	3A	3A	1	3A	3A	3
1	1A	1A	3A	3A	1	3	3	1A	1	1A	1	3	1A	1	1A
3	1	1	3	1A	3	3A	1	1A	3A	3	3A	1A	1A	3A	3
3	3A	3	1	1A	1	3A	1A	3A	3A	1A	1	3A	3	3	3A
1	1A	1	3A	3	3A	1A	1A	1	1	1	3	1A	1	3	1
	3	1	3	3A	3	3A	1	3A	1A	3A	3A	3	1	1A	
	1	3A	1A	1	1A	1A	1	1	3	1A	3	1	3A	1	
		1	3	3A	3A	1	3	1	3A	1	3A	3	1A		
			1A	1	3	3A	1	3	1A	3	1A	1			
					1A	3A	1	3	1A	3A					

Fig. 6.2 Fuel load distribution, 38.3 kg CH_2 plus stainless steel liner

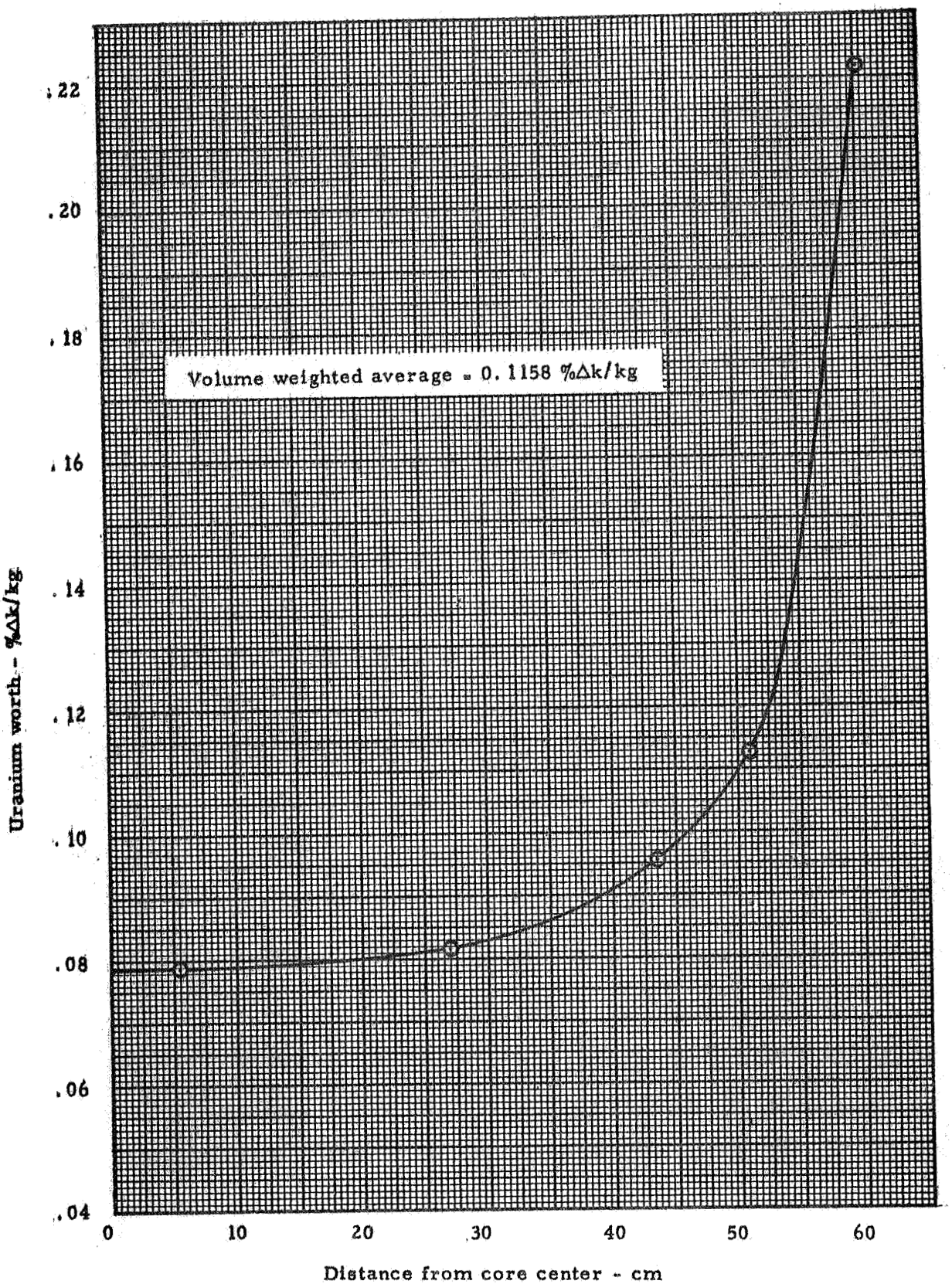

Fig. 6.3 Fuel worth as a function of core radius, 38.3 kg plus stainless steel liner

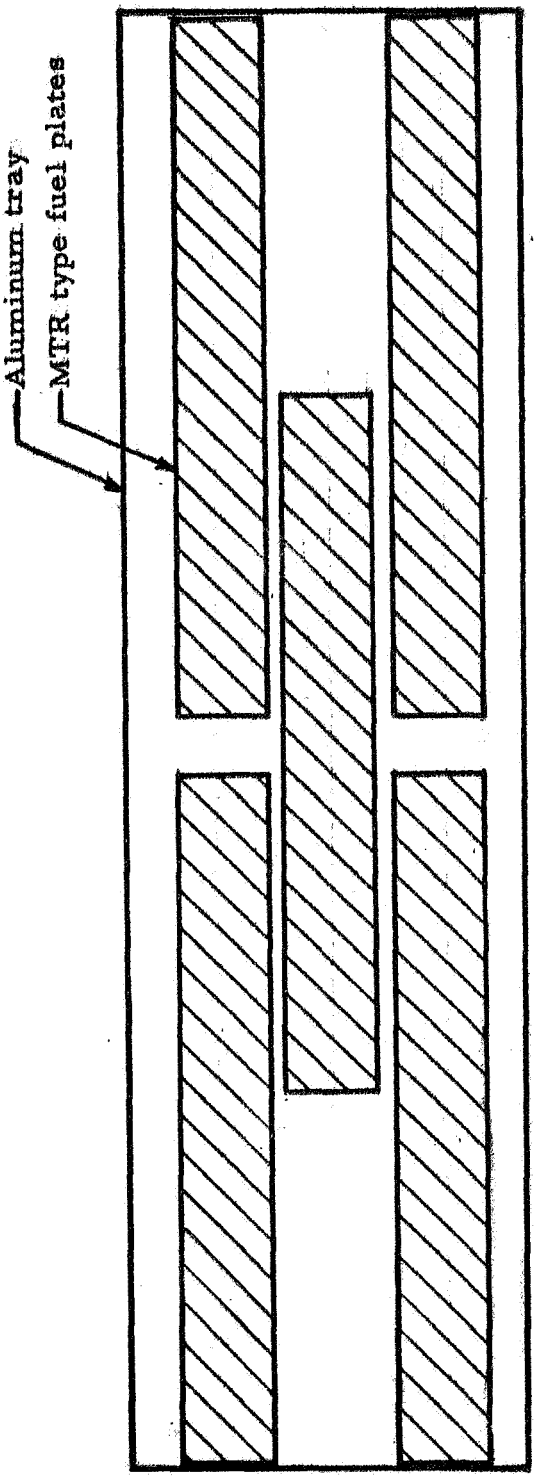

Figure 6.4 Location of MTR type fuel trays during reactivity measurements in D_2O radial reflector

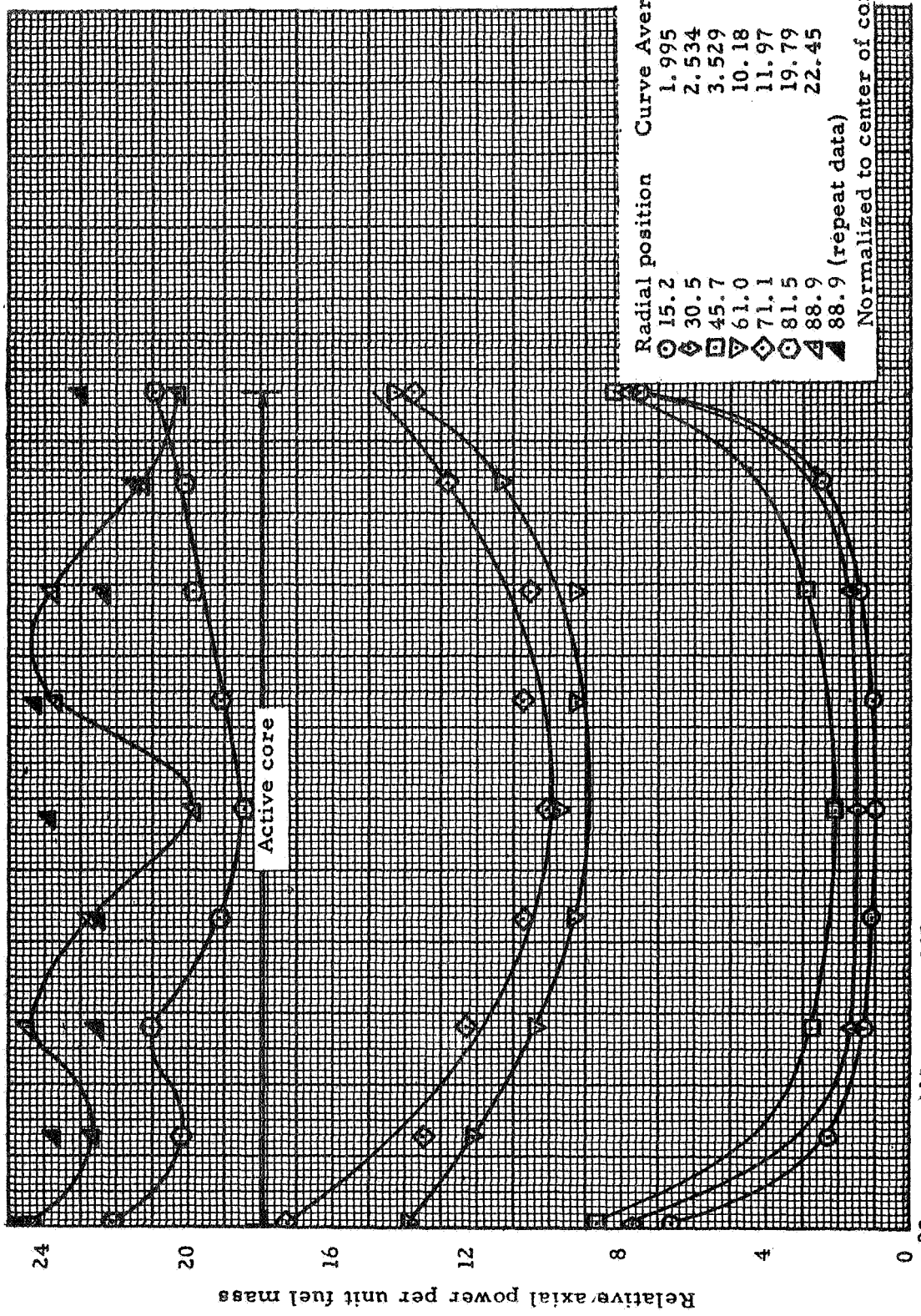

Fig. 6.5 Axial power distribution within the active core - CH_2 load decreased to 36.5 kg, stainless steel liner

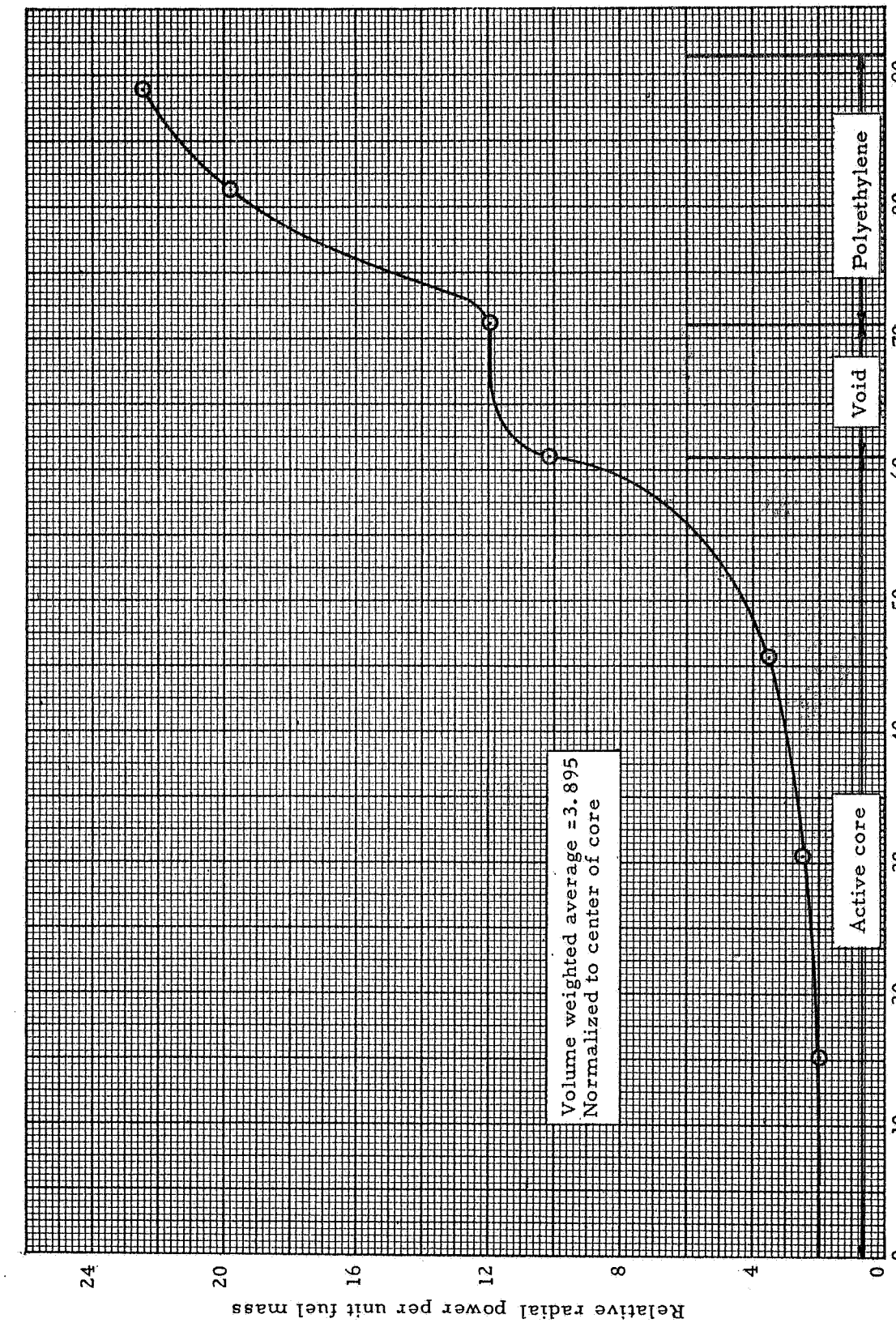

Fig. 6.6 Relative radial power distribution at axial center of core, 36.5 kg CH_2 plus stainless steel liner

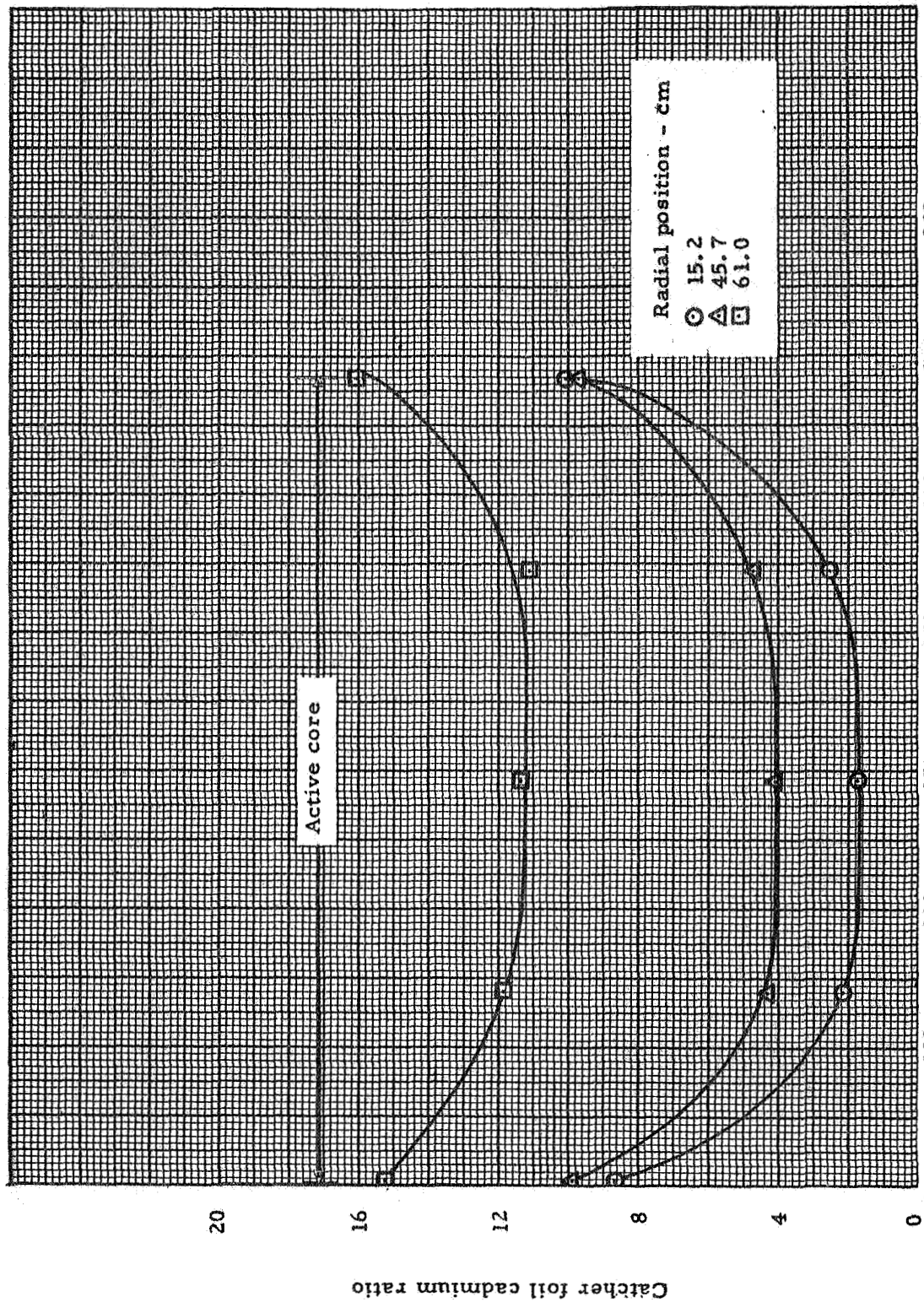

Fig. 6.7 Axial catcher foil cadmium ratio distribution within the active core - 36.5 kg CH_2 plus stainless steel liner

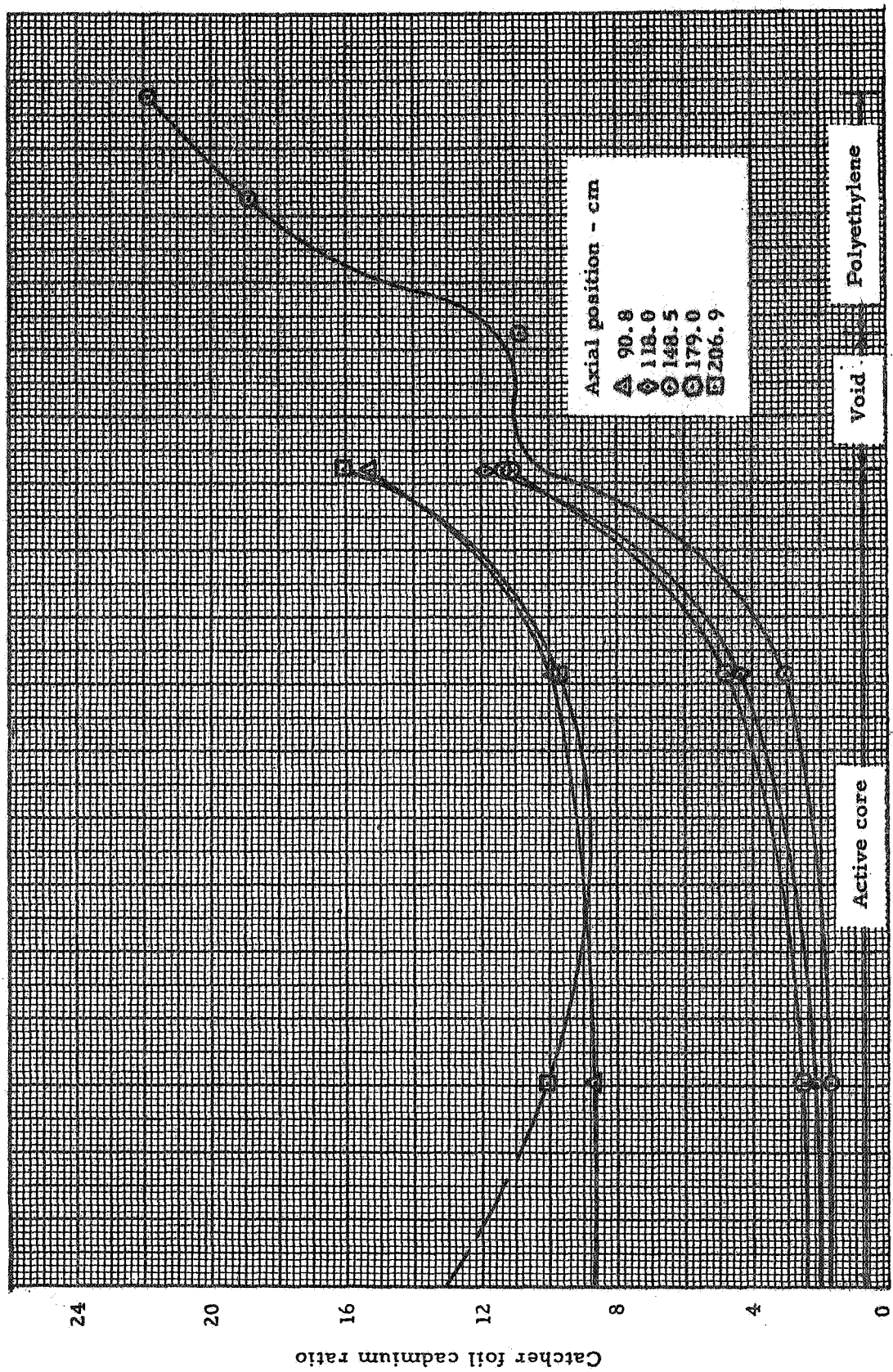

Fig. 6.8 Radial catcher foil cadmium ratio distribution for various axial positions, 36.5 kg CH_2 plus stainless steel liner

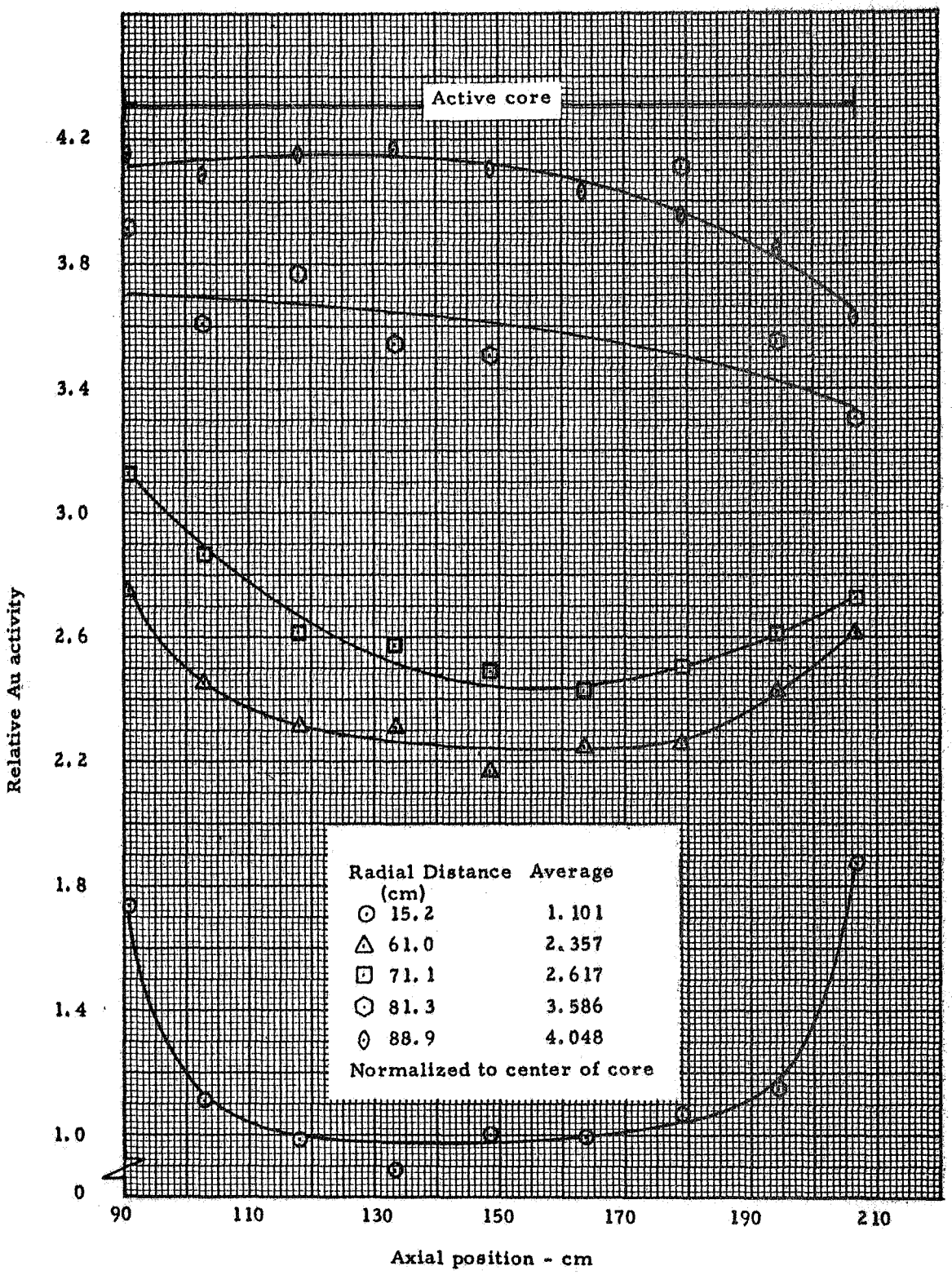

Fig. 6.9 Axial distribution, bare gold foil activity normalized to foil nearest core center

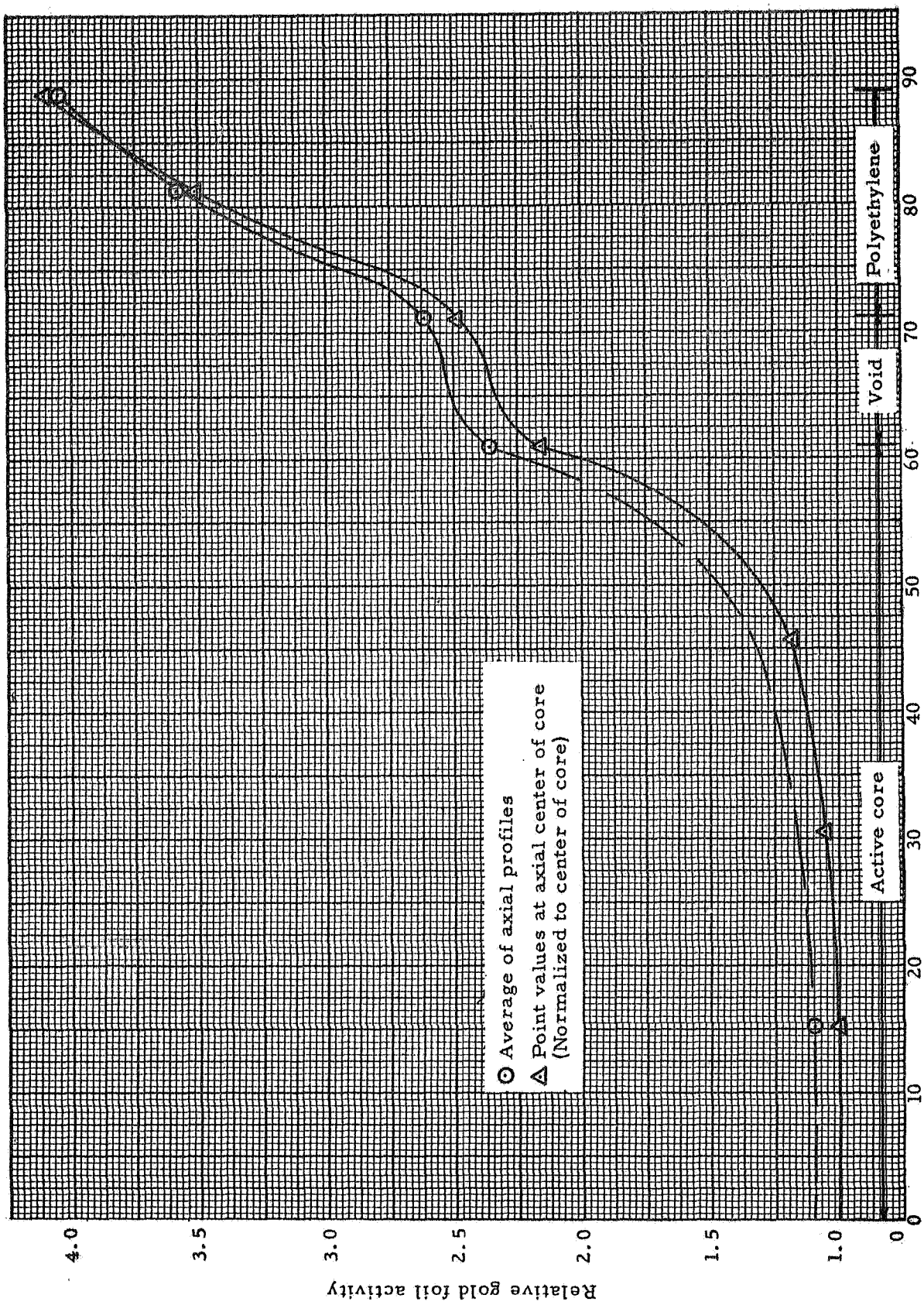

Fig. 6.10 Relative radial distribution, bare gold foil activity

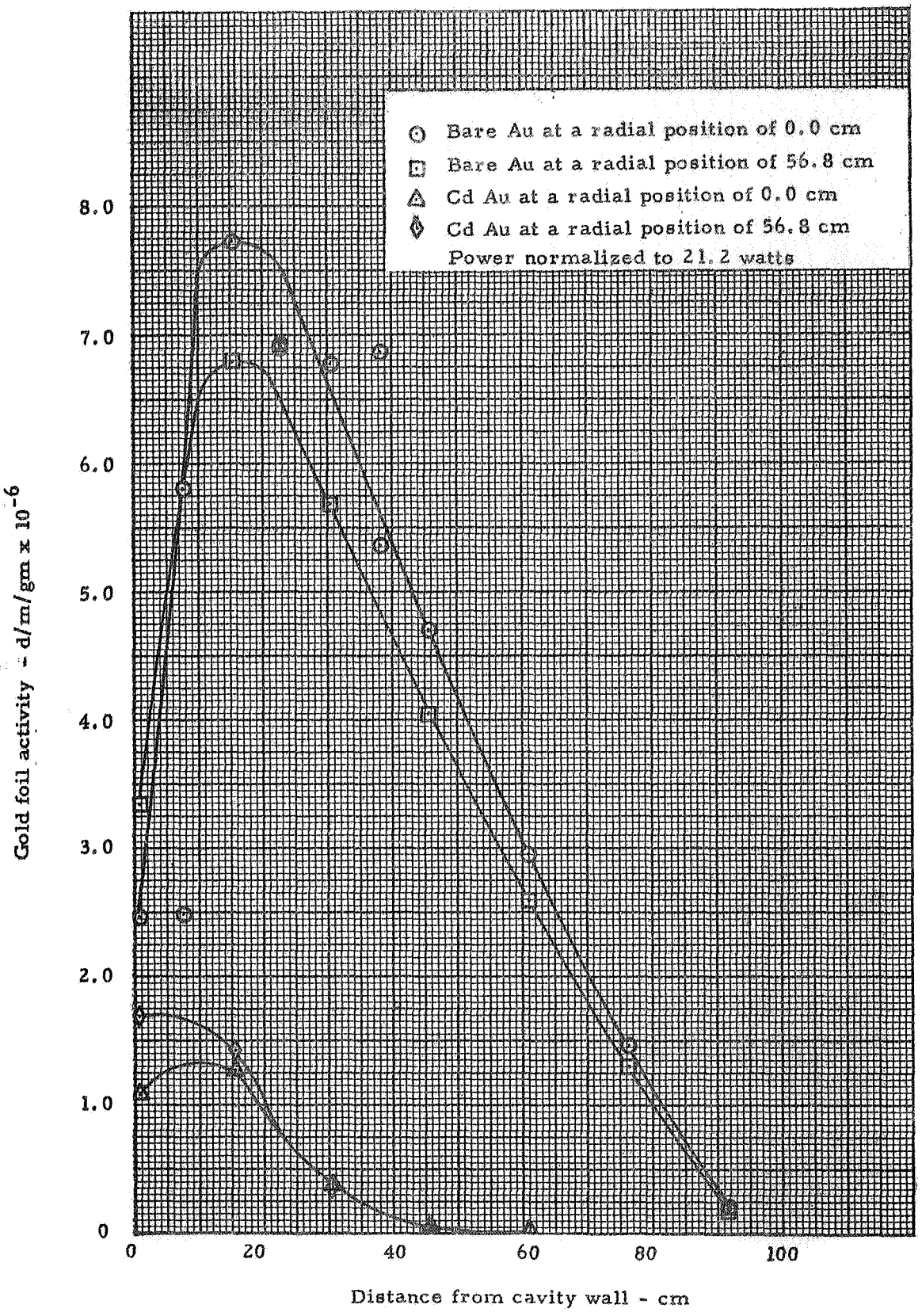

Fig. 6.11 Bare and cadmium covered gold foil activity, end reflector

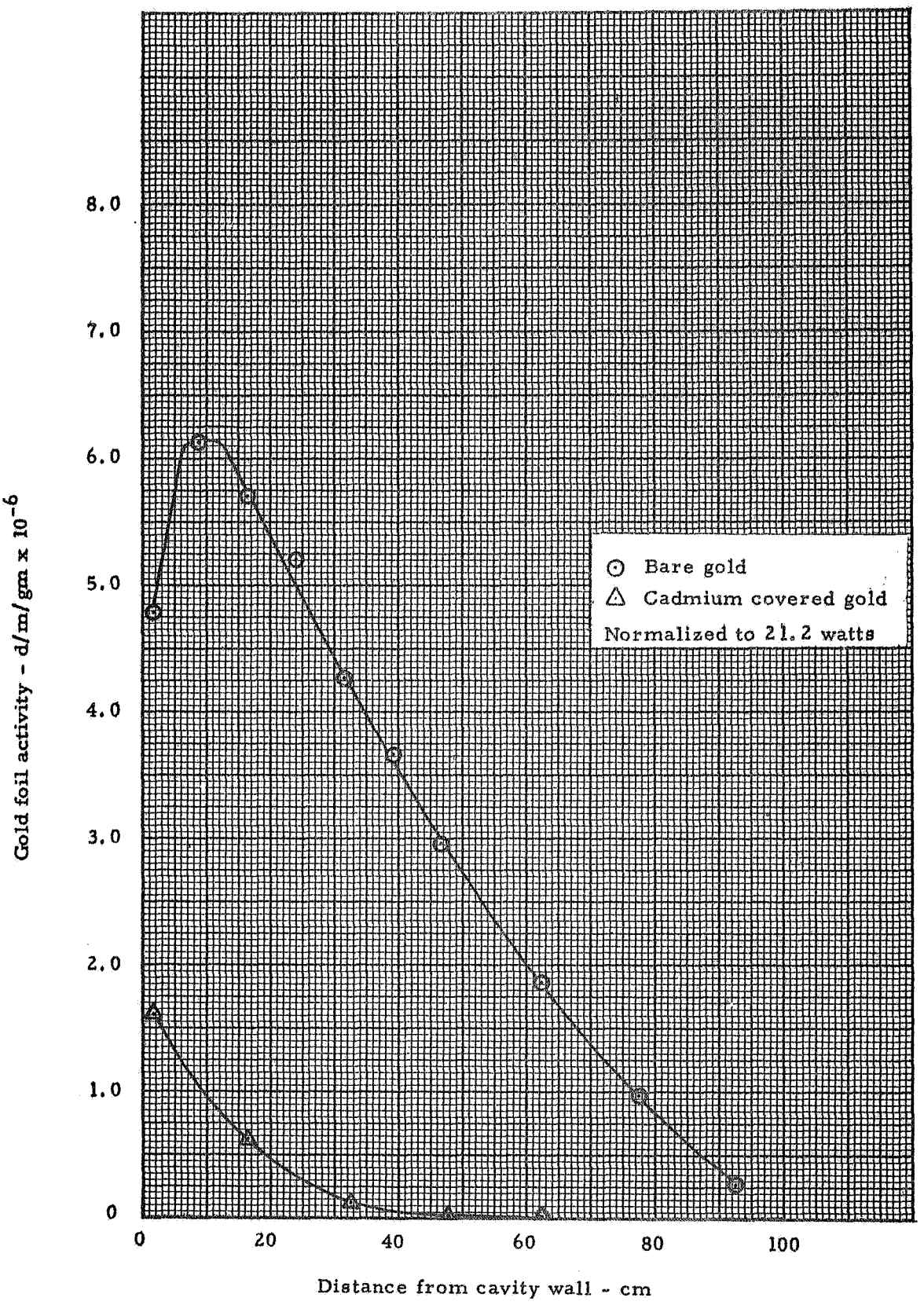

Fig. 6.12 Bare and cadmium covered gold foil activity, radial reflector

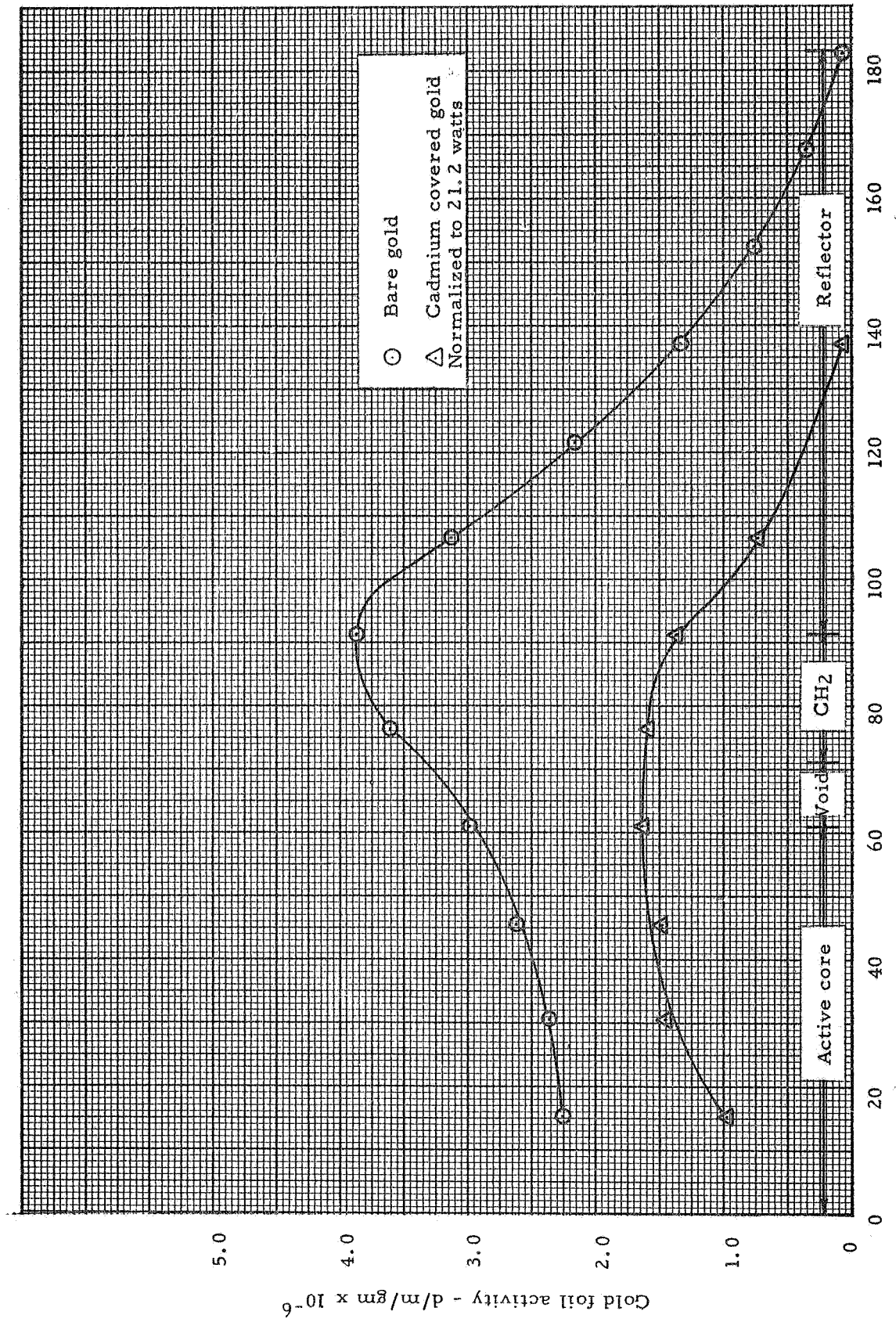

Fig. 6.13 Bare and cadmium covered gold foil activity, separation plane

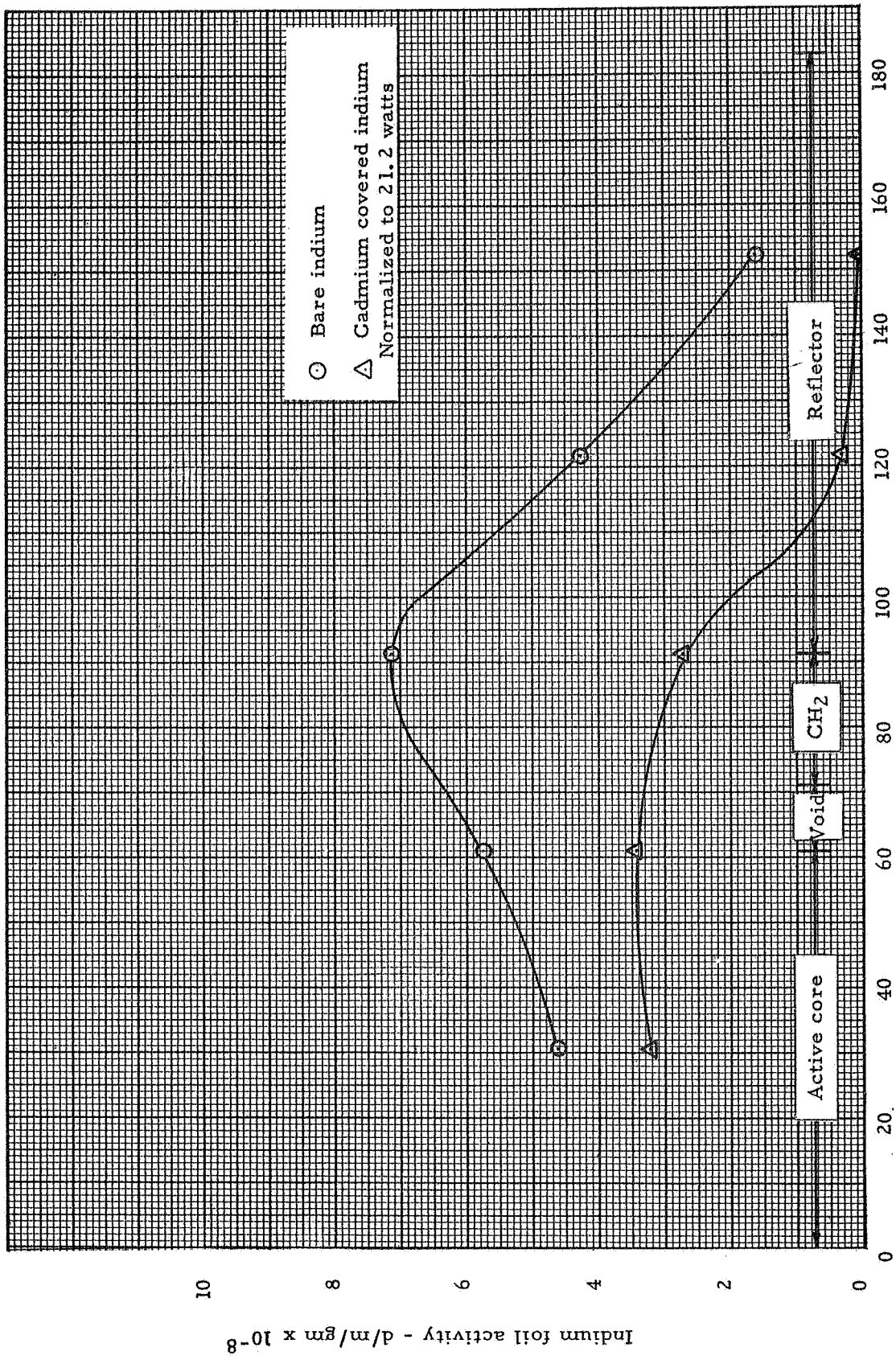

Fig. 6.14 Bare and cadmium covered indium foil activity, separation plane

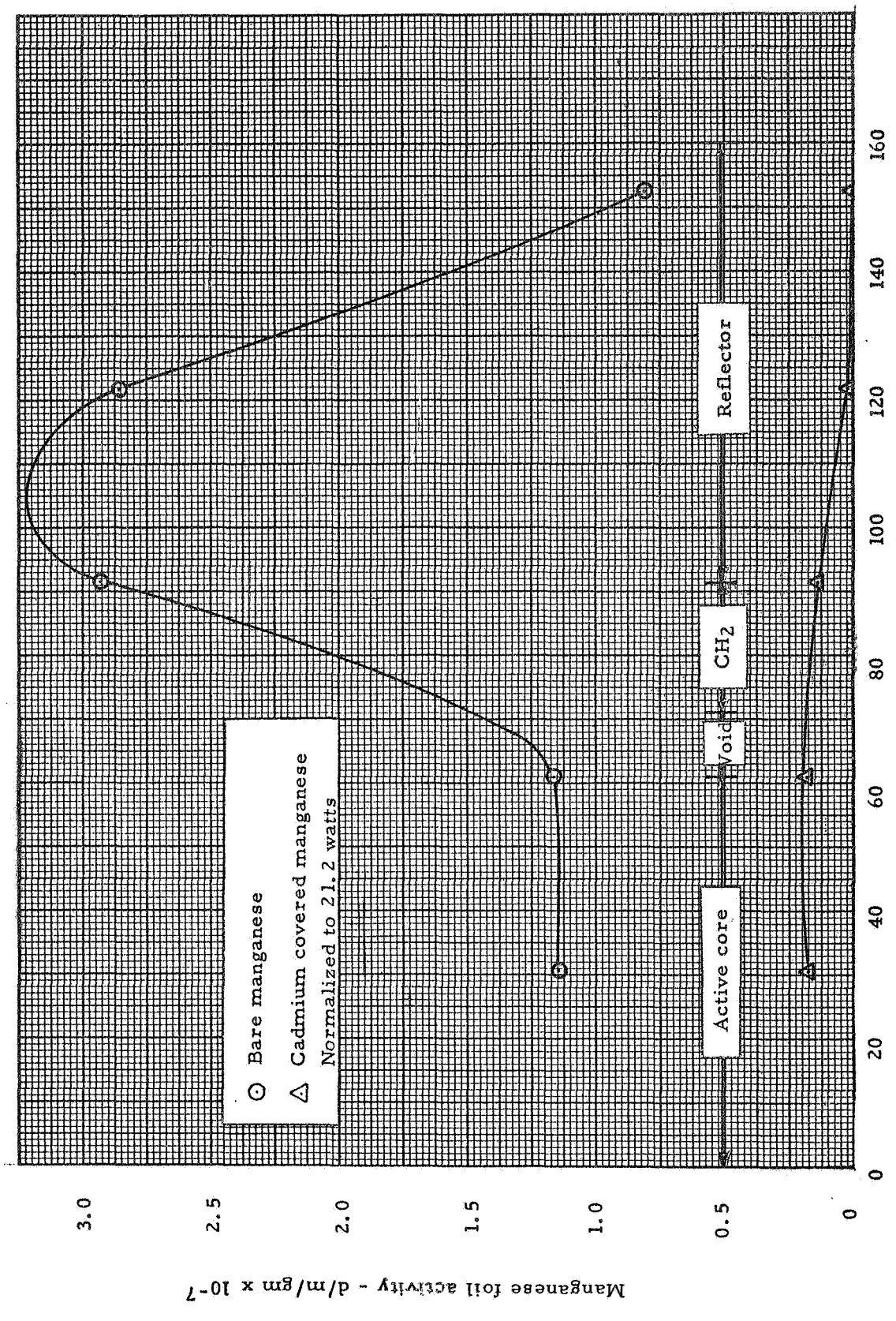

Fig. 6.15 Manganese foil activity, separation plane

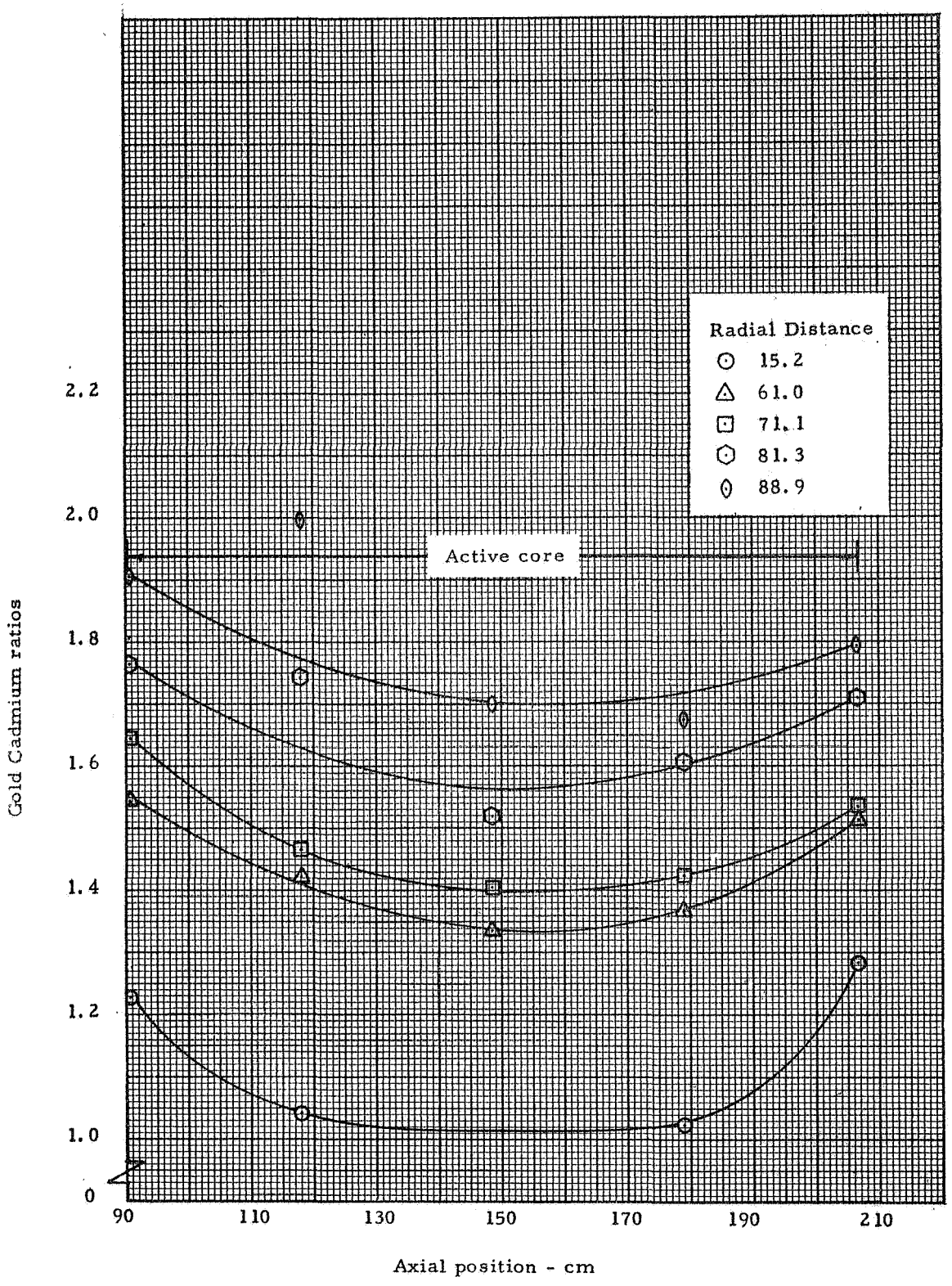

Fig. 6.16 Gold cadmium ratio distributions, axial position

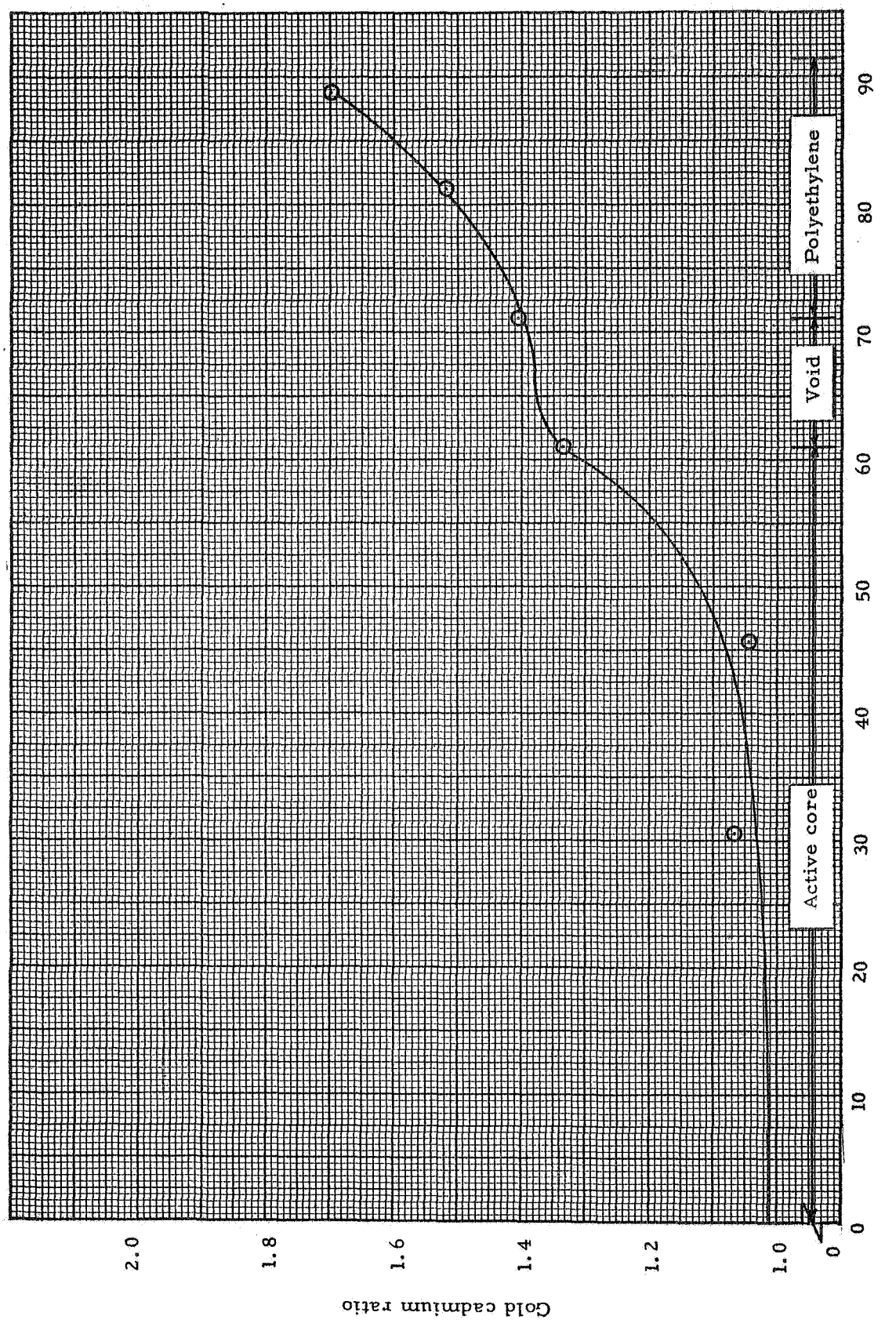

Fig. 6.17 Gold cadmium ratio distributions, radial position

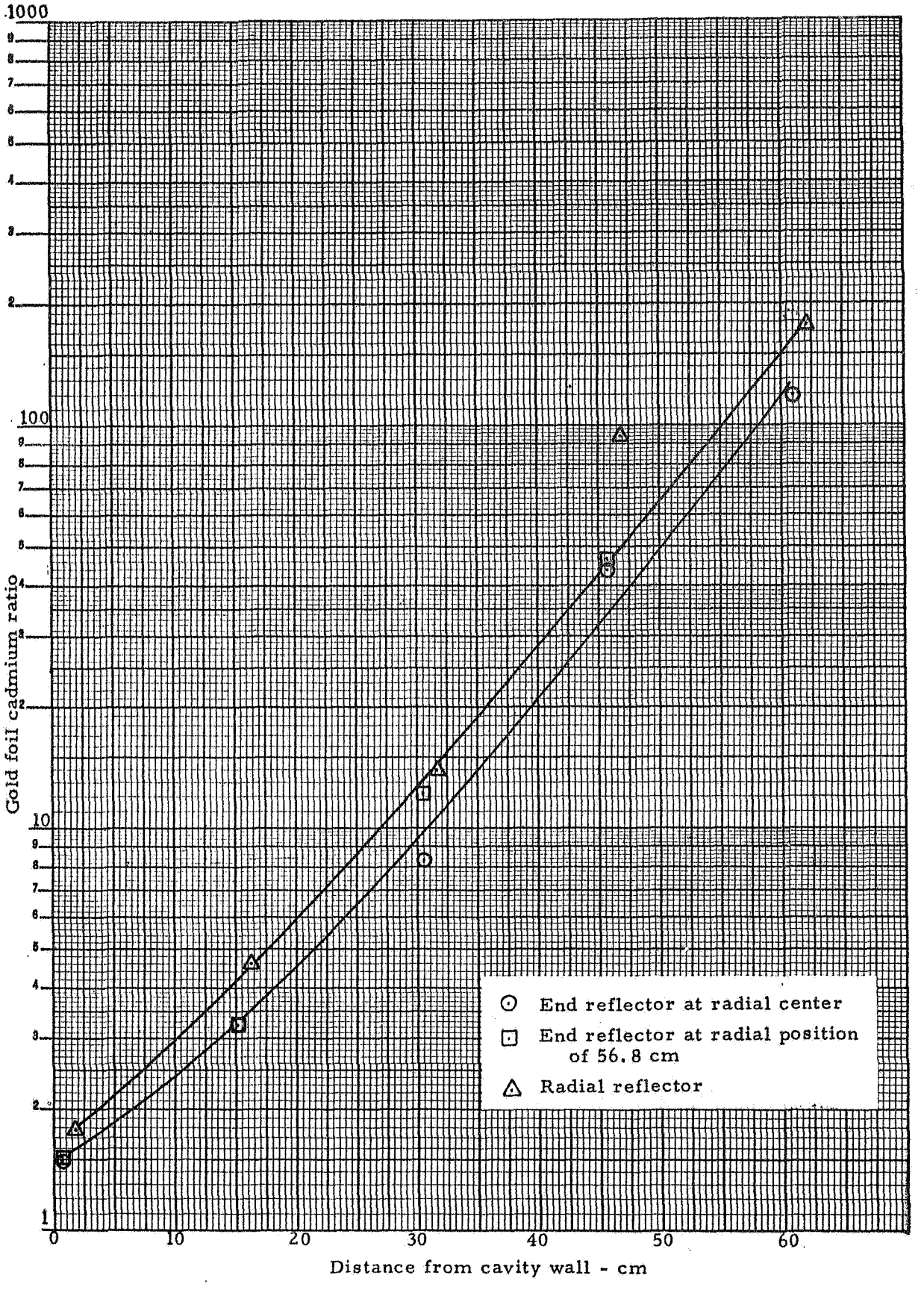

Fig. 6.18 Gold cadmium ratio distribution, reflector region

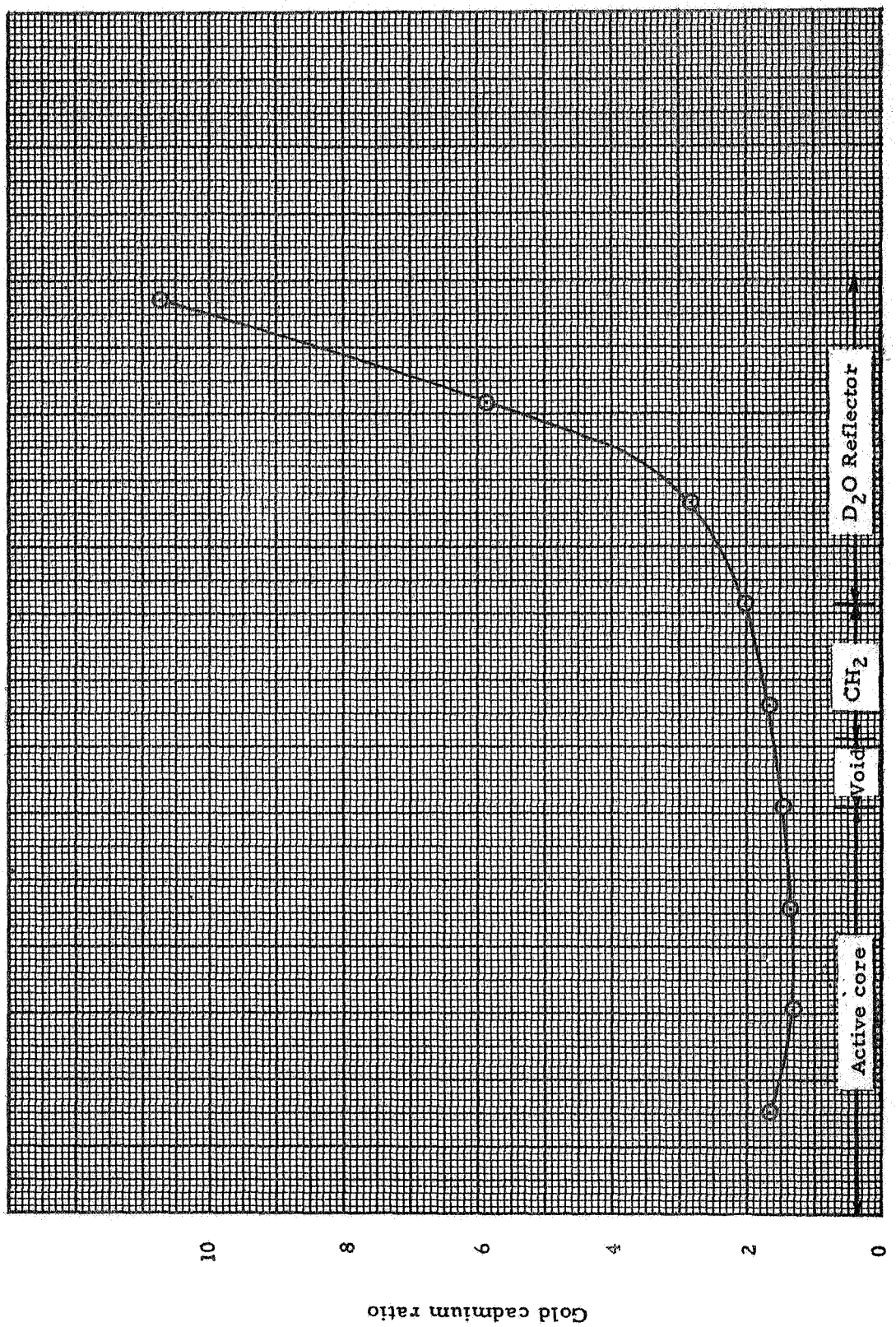

Fig. 6.19 Gold cadmium ratio distribution, separation plane

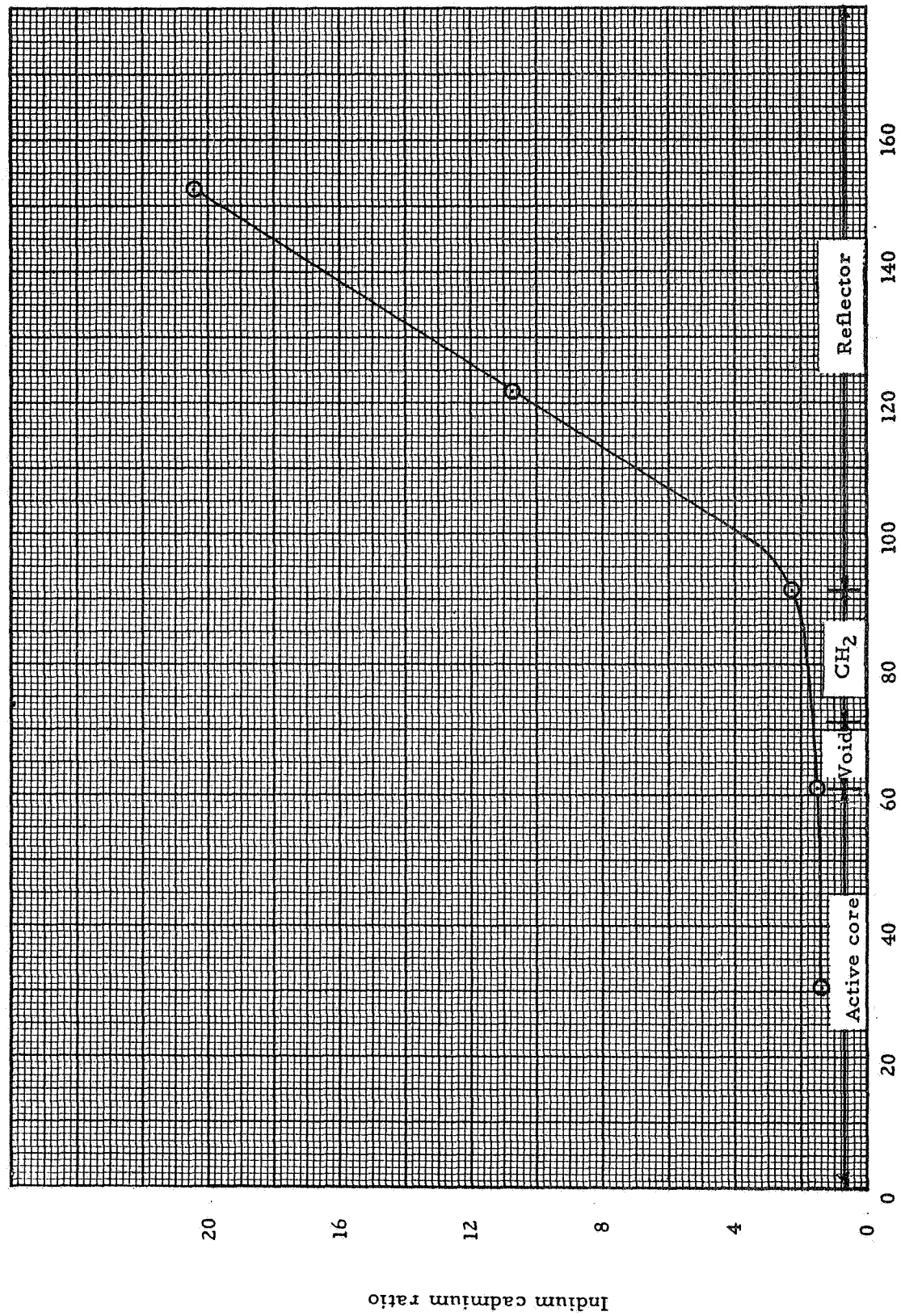

Fig. 6.20 Indium cadmium ratio distribution, separation plane

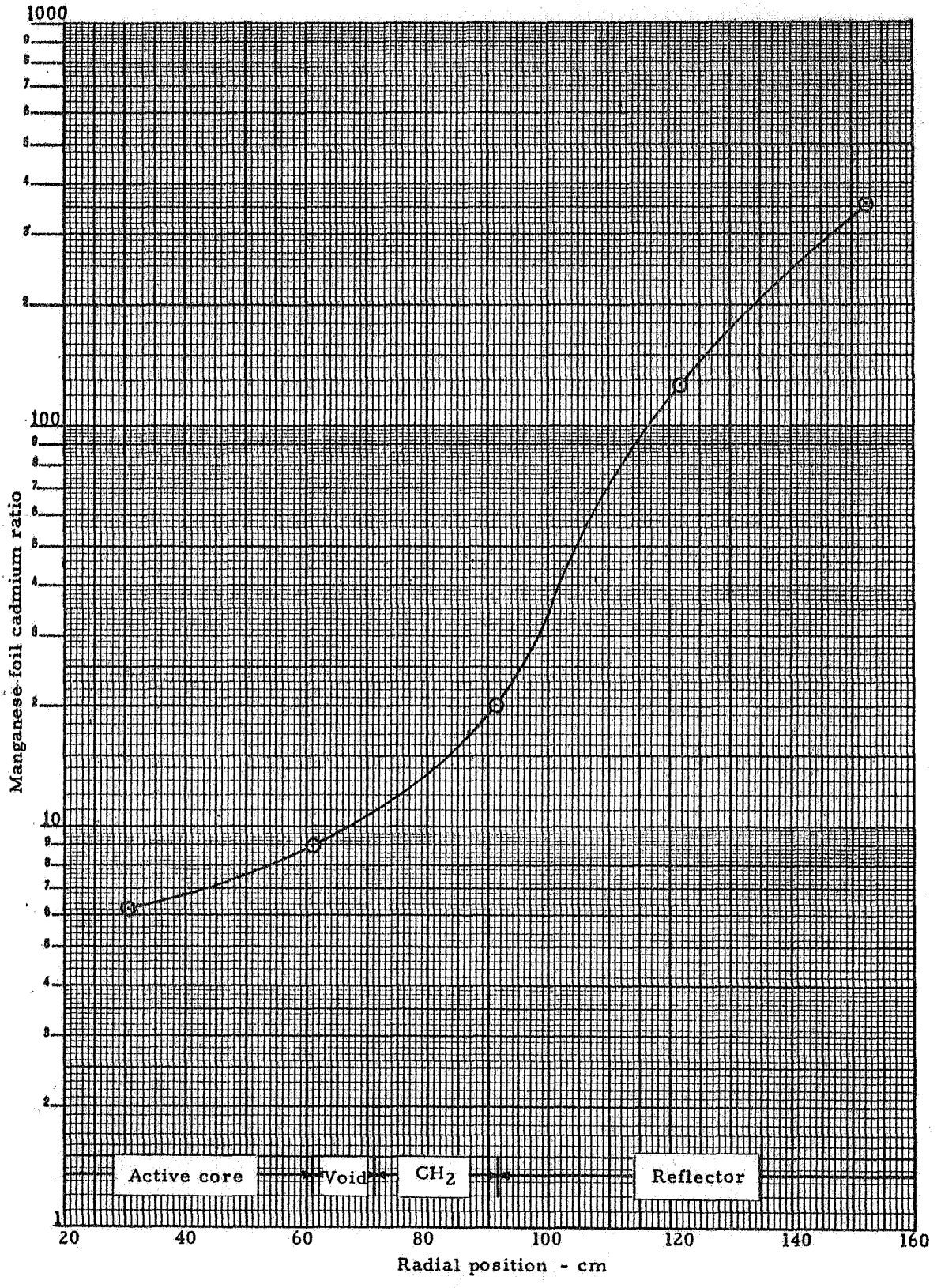

Fig. 6.21 Manganese cadmium ratio distribution, separation plane

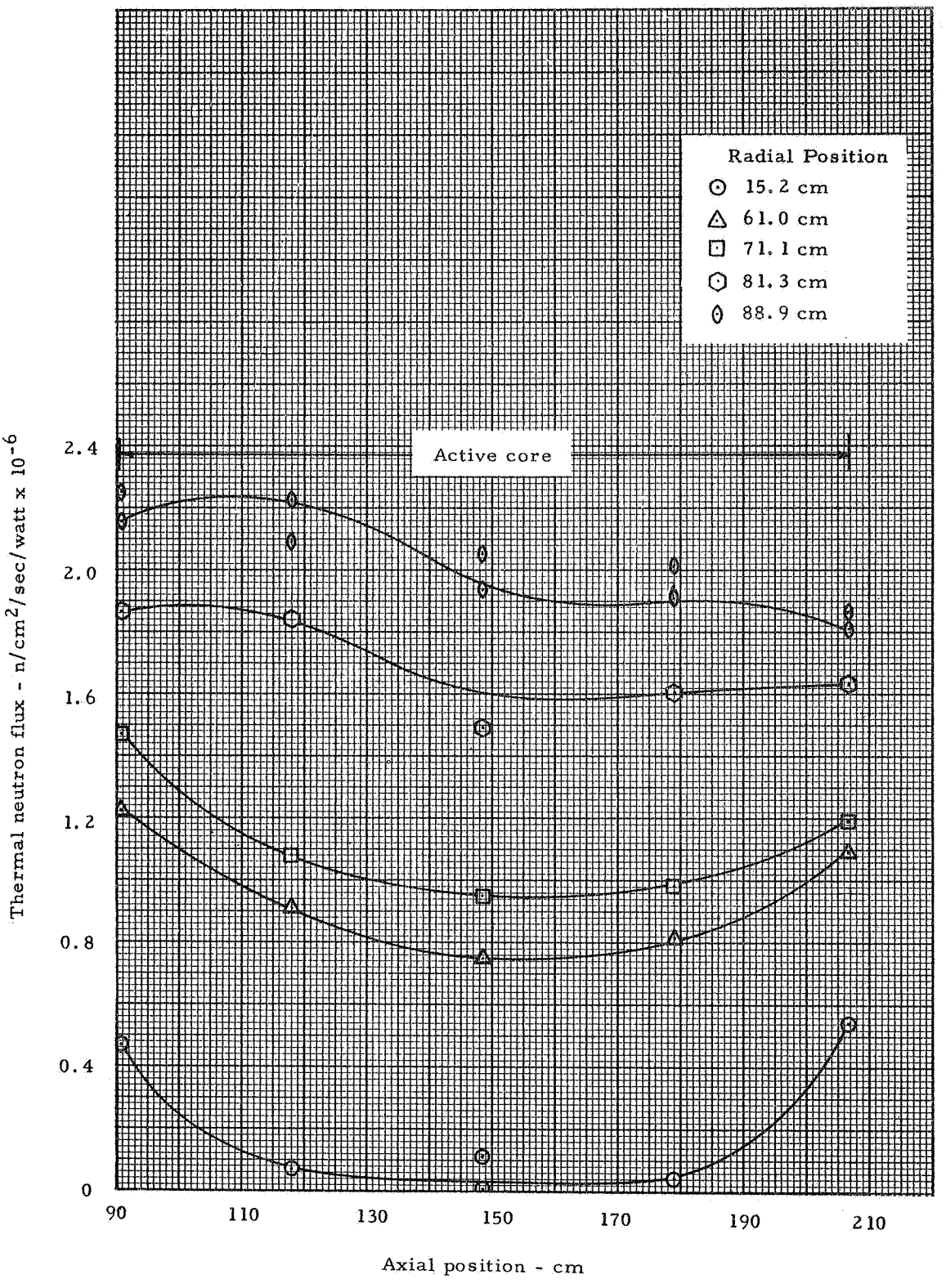

Fig. 6.22 Thermal neutron flux, axial distributions, gold detectors

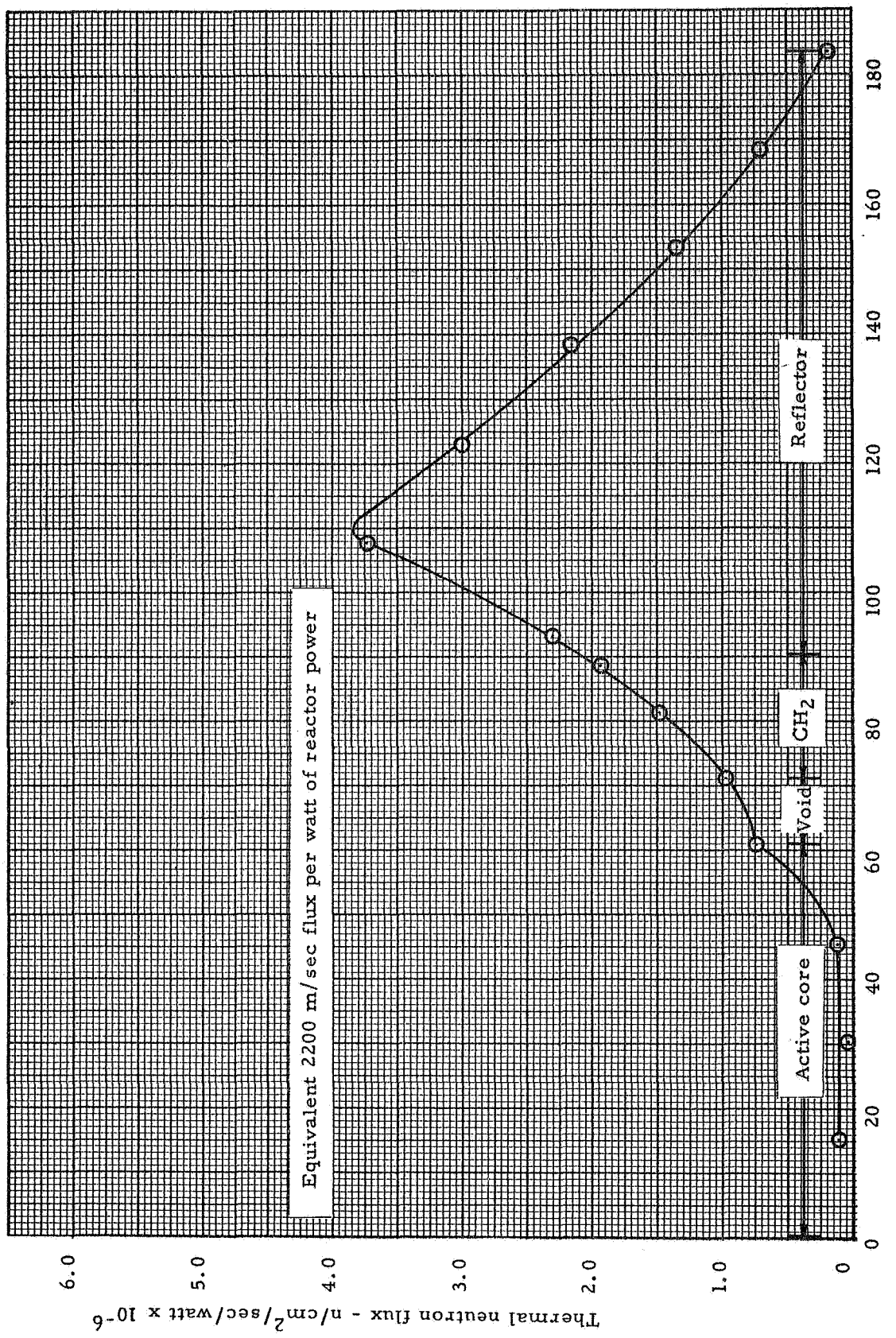

Fig. 6.23 Thermal neutron flux, radial profile, gold detectors

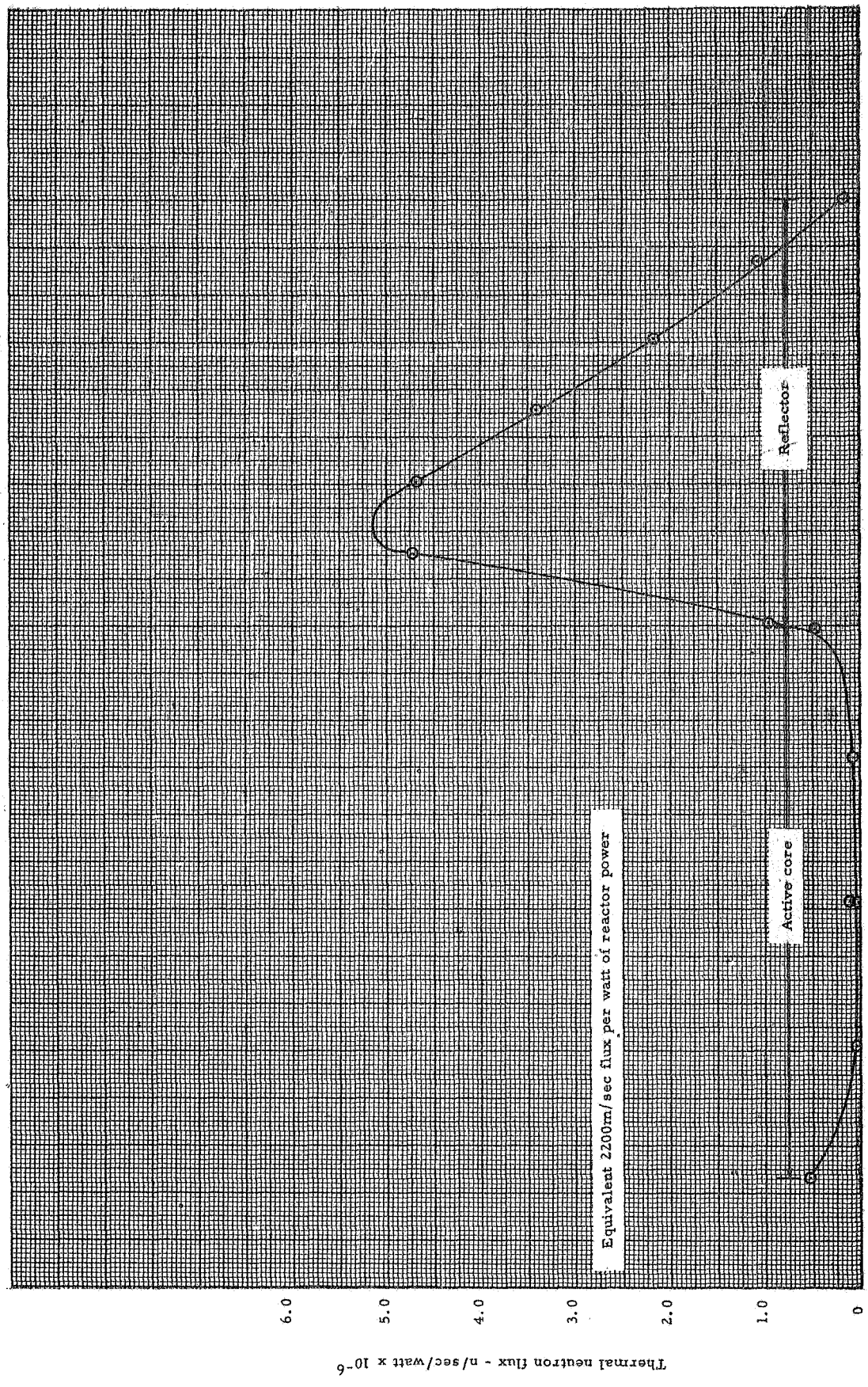

Fig. 6.24 Thermal neutron flux, axial profile, gold detectors

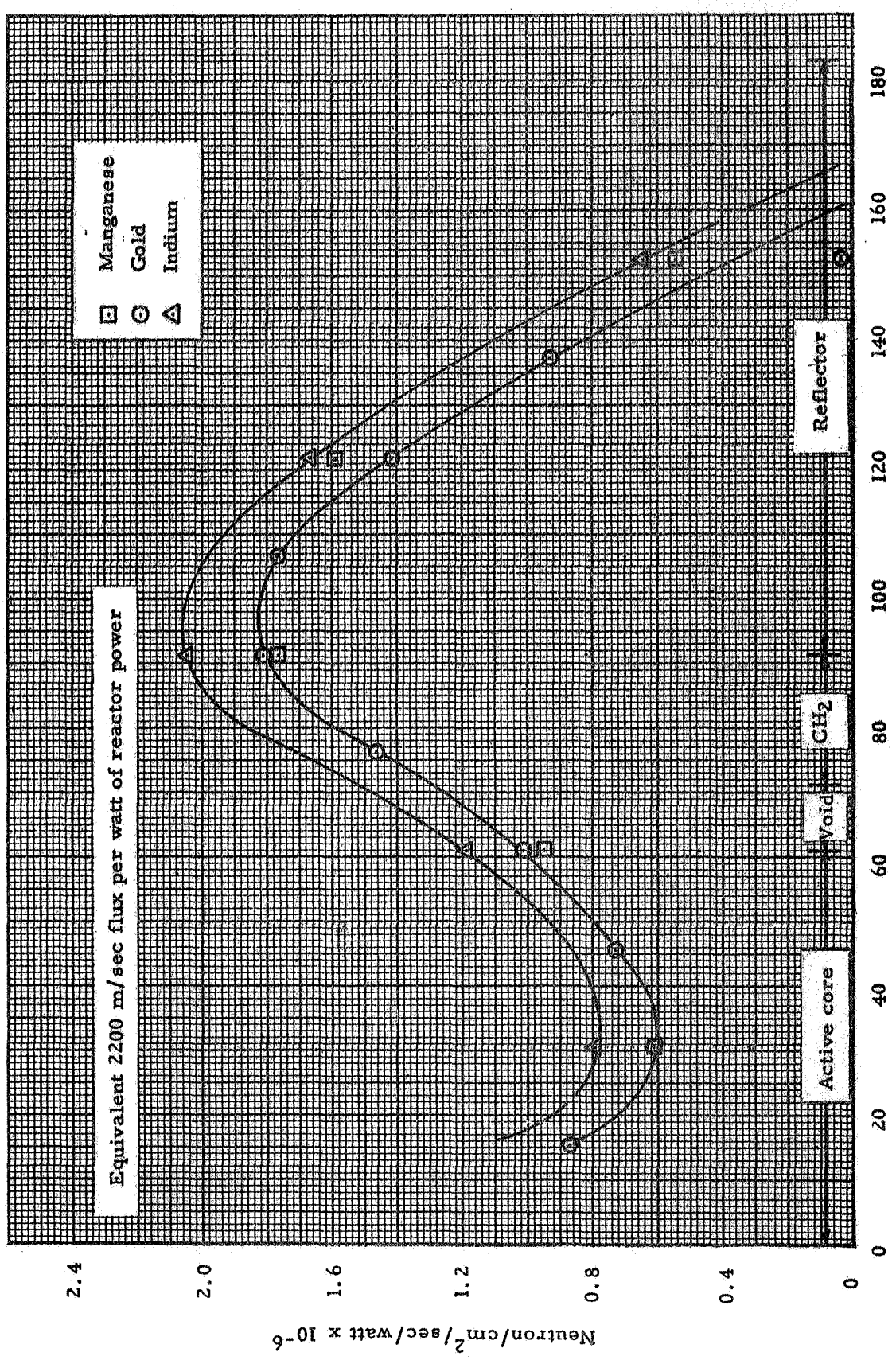

Fig. 6.25 Thermal neutron flux - separation plane - manganese, gold and indium detectors

7.0 STAINLESS STEEL LINER PLUS 36.5 kg OF POLYETHYLENE IN CAVITY - HOT POLYETHYLENE

All of the power mapping data obtained with the polyethylene at room temperature was with the heat ducting hardware in the reactor so that direct comparison could be made between the hot and cold measurements. Prior to placing this hardware in the reactor, there were 38.3 kg of polyethylene in the reactor but with the added poison in the heat ducting it was necessary to remove 1.8 kg of polyethylene thus giving a total of 36.5 kg between the active core and cavity wall.

The primary purpose of the heating phase of the experiment was to determine temperature effects on the reactivity and power and flux distribution. The polyethylene was heated by forcing hot air through the structure as shown in Figure 5.2. The temperature of the polyethylene was monitored with thermocouples.

A sector of the core was accessible without removing the air ducting from the face of the reactor so that power mapping could be performed with relative ease. This arrangement is shown in Figure 7.1. There was little or no air flow through the portion of polyethylene in this pie sector, but it lagged behind the rest of the structure by a time constant of only a few minutes.

7.1 Reactivity Measurements

The polyethylene was heated five times from room temperature to about 70°C during the course of this experiment. Thermocouples were located at six positions within the structure as follows:

Thermocouple Number	Location
1	Outlet side at back end of structure
2	Inlet side at back end of structure
3	Back of polyethylene on pie sector for access to core
4	Front of polyethylene on pie sector for access to core
5	Outlet side of front end of structure
6	Inlet side of front end of structure.

Reported polyethylene temperatures to follow will represent an average of these six thermocouples. In general, there was a ±10°C spread in the observed temperatures with the outlet side at the back of the structure being the cold spot and the inlet side at the front (separation plane) being the hot region. The circulation of hot air through the polyethylene was not ideal as there was considerable cross flow of air between the two cylindrical segments of the structure at the front or the separation plane and through holes which were made when welding the narrow polyethylene strips to the cylindrical segments of the

structure. This caused the front portion of the polyethylene to be hotter than the back end, by a difference of as much as 15°C. There was also loss of air due to leakage around the polyethylene structure and where the flow direction plates attached to the polyethylene. This caused the fueled region of the reactor to increase in temperature during the heating cycle. Although thermocouples placed in the fueled region indicated an increase of as much as 70% of the average increase in polyethylene temperature during the heating cycle. Nevertheless, the major effect on reactivity was due to the heated polyethylene, since core expansion effects for these temperature changes are negligible.* The reflector temperature was nominally 72°F and no indicated change on the reflector thermocouples occurred during the heating of the polyethylene.

The average polyethylene temperature and k-excess as a function of lapsed time since the heaters and blower were turned on for each of the heating cycles are given in Table 7.1. There was a definite increase in k-excess as the polyethylene temperature increased as will be noted from Figure 7.2. It will also be noted here that there was a gradual decrease in k-excess between cycles. Following the 4th cycle, several of the air passageways on the inlet side of the polyethylene structure were taped shut in an attempt to increase the air velocity through the open ports and thus more effectively force the air to the back portion of the structure. It was anticipated that such a modification would improve the temperature distribution in the polyethylene. However, no improvement was noted. The tape which was used to block the passageways was a poison and so the shift in the curves between the 4th and 5th cycle or measurement was larger than noted for the previous measurements.

The reason for the gradual decrease in k-excess was that the heat caused the outer portion of the polyethylene structure to distort and collapse inward somewhat. The inner surface of the structure was supported by an aluminum plate. However, the only support the outer portion of the assembly had was from the polyethylene structure itself. The hot polyethylene became more flexible and at top would sag under its own weight while around the remainder of the circumference, some inward distortion occurred as a result of repeated heating and cooling. Previous measurements had shown that polyethylene was more poisonous as it moved closer to the fueled region in the space between the cavity wall and active core. Each heating cycle caused some inward collapse of the structure and thus accounts for the data noted in Figure 7.2.

Increasing the polyethylene temperature from about 20 to 77°C caused k-excess to increase approximately 0.8%Δk. The exact mechanism behind this change in reactivity is not fully understood at this writing. However, power profiles and elementary investigations by means of computer calculations have suggested an explanation. That is, the polyethylene is sufficiently thick to create a slight change in overall neutron temperatures of neutrons returning from the reflector to enter the core. This increase in neutron temperature as the polyethylene is heated results

---

* For a 70°F temperature rise, the aluminum core structure expands about 0.013 cm over its length or diameter. Using the data in Reference 1, page 50, and the fuel worth of 0.1%Δk/kg for this configuration, the core expansion effects are less than 0.01%Δk.

in a shift to a slightly harder neutron spectrum and thus less absorptions in the polyethylene and aluminum structure. Most of the reduction in absorption occurs in the polyethylene structure because it sees a larger fraction of the neutrons leaving the inner reflector wall. The core, with its heavy loading, is approaching blackness to thermal neutrons, and hence changes in thermal neutron temperature of neutrons entering the core will have little effect on the absorption rate in the core. Finally, heating of the polyethylene and the core (by air leakage) will cause expansion of both. Polyethylene expansion is a negative reactivity effect, core expansion is positive. However, as discussed above the core expansion effect was negligible. The expansion effect of polyethylene is not known, but in any case would be such as to reduce the magnitude of the measured temperature coefficient. Thus, it is concluded that the heating of polyethylene is an overall positive effect, principally due to hardening of the spectrum and the resultant reduced absorption by the polyethylene.

7.2 Power Distribution Measurements

7.2.1 Bare Catcher Foils

Catcher foil data was minimal with the polyethylene structure heated as the gold foil data was of prime interest. A single axial profile at 15 cm from the radial center of the core and a radial profile at the axial center of the core were measured using both bare and cadmium covered catcher foils. These data are given in Table 7.2 and include both bare and cadmium covered foils as well as the cadmium ratios. The bare foil data normalized to the core center are plotted in Figure 7.3 and 7.4. Also given in these figures are the data from the cold polyethylene measurements. Within the central region of the active core there is little difference between the hot and cold polyethylene cases. There is, however, a definite decrease in the power ratio near the core boundary with respect to the core center. The average axial profile decreased 5.5% and the weighted radial was 15.3% lower than with the cold polyethylene. The flatter power profile indicates a harder spectrum incident on the core, consistent with the explanation of the positive temperature coefficient.

7.2.2 Catcher Foil Cadmium Ratios

The cadmium ratios are given in Table 7.2. These are plotted for comparison with the cold polyethylene in Figures 7.5 and 7.6. The axial profile shows a lower cadmium ratio at the ends of the core but about the same value in the main core region, again showing a harder spectrum for the hot polyethylene. The radial profile shows similar results as the axial profile at the outer edge of the core but rather inconclusive changes across the polyethylene.

7.3 Resonance Detector Data

7.3.1 Bare Gold

Resonance detectors included only gold with the polyethylene heated. Both bare and cadmium covered data were obtained and these results are given in Table 7.3. The axial and radial profiles in the cavity normalized to the center of the core are shown in Figures 7.7

and 7.8. Figure 7.8 includes the radial distribution from individual foils along the axial centerline of the core and the distribution obtained from the average axial profiles given in Figure 7.7.

In order to compare these data with the cold polyethylene data, the bare foils were first reduced to infinitely dilute activity where both bare and cadmium foil activities were available and then tabulated as shown in Table 7.4. The hot polyethylene configuration consistently exhibited a higher foil activity by 4.5 ± 2.4% in the cavity region. It was noted in the previous section that the catcher foil data showed a flatter power distribution for the hot polyethylene. If these catcher foil data are reduced to equivalent relative powers and normalized to the same power density at the core center, the relative core power was 0.886 for the hot polyethylene compared to 1.00 for the cold polyethylene experiment. This comparison is based on the curves given in Figures 7.3 and 7.4. In order to compare the gold foil data to equal reactor power levels, the gold foil data given in Table 7.4 for the hot case have been power normalized to the cold polyethylene relative power level by first normalizing to the core center power density and then by increasing the hot polyethylene data by 12.9% so that both represent the same total core power.

There may be some question at this point concerning the above power correction when the power normalization foils are exposed on each foil exposure for the express purpose of power normalization. The power normalization foils are located on the D_2O tank at the separation plane and it is assumed that for any given configuration the power distribution in the active core region remains constant. However, when changes are made which affect the power distribution within the cavity region, the power normalization foils do not necessarily see the changes, only to the extent that the reflector responds to the change.

Therefore, these normalizer foils first were compared to the core-center power density and then an additional correction was necessary in order to place the gold foil data on the same power level before comparing the results from the cold and hot polyethylene experiments.

The bare gold data in the reflector regions are shown in Figures 7.9 and 7.10. The results from both experiments are given here and infinitely dilute foil activities were used. The radial reflector shows a 10.2 ± 4.4% increase in bare foil activity for the hot over the cold polyethylene experiment. The end reflector showed less difference with the hot polyethylene bare foil activities being 4.4 ± 4.2%, on the average, higher than for the cold polyethylene experiment. The increase in the cavity region was the same small value as in the end reflector. But the radial reflector showed a definite increase (10%, or 6% higher than the other reactor regions) total activity for the hot polyethylene experiment, indicating a greater overall change in the radial reflector.

Figures 7.9 and 7.10 also contain the cadmium covered foil activities for comparison.

7.3.2 Cadmium Ratios

The cadmium covered foil data from the two experiments were reduced to infinitely dilute activities, as was done with the bare foil data, so as to compare the hot and cold polyethylene results. These data are shown in Table 7.5. Within the cavity region, there was a 4.5 ± 3.8% increase in the foil activity for the hot polyethylene.

The comparison in the reflector regions was somewhat uncertain, as will be noted from Table 7.5. If the points farthest from the cavity wall are not considered, as these positions are difficult to measure because of very low activation rates, there was an increase in the end reflector cadmium covered gold foil activity but little or no change in the radial reflector.

The cadmium ratios obtained from the gold foil data are given in Table 7.6 and Figures 7.11 and 7.12. Included in both the table and figures are the data from the cold polyethylene experiment. Within the cavity region the hot polyethylene cadmium ratios were, on the average, 1.4 ± 3.1% lower than for the cold polyethylene experiment. The difference was small and somewhat uncertain as indicated by the standard error. The reflector regions also showed an uncertain change. If the points furthest from the cavity wall are ignored, the end reflector cadmium ratios were unchanged within the experimental uncertainty. The three points in the radial reflector closest to the cavity wall showed higher cadmium ratios with the polyethylene heated but beyond about 35 cm the comparison is uncertain.

7.4 Thermal Neutron Flux

Where both bare and cadmium covered gold foils were available, thermal neutron flux was calculated. The results, including the data for both the cold and hot polyethylene, are presented in Table 7.7 and Figures 7.13 and 7.14. The thermal flux in the end reflector was unchanged but in the radial reflector, the hot polyethylene experiment flux was 15.2 ± 3.7% higher than for the cold polyethylene. Within the active core region, there was no measurable change in flux due to heating the polyethylene (for the same core power). However, on the inner surface of the polyethylene there was an indicated reduction of about 5% in thermal flux level per watt of reactor power. Moving through the polyethylene towards the cavity wall, the thermal flux level increased as a result of heating so that at the cavity wall there was 10.3 ± 3.7% more thermal flux than for the cold polyethylene experiments.

This is consistent with the radial reflector data, as noted above. This higher thermal flux implies less absorption in the cavity region, in this case in the CH_2 since the core power is constant. Thus, these thermal flux differences are compatible with the reason given for the positive temperature coefficient. It is concluded from these data that the thermal neutron flux level decreased by about 5% and the outer region of the active core but was enhanced by as much as 10% at the cavity-reflector inner face and 15% in the radial reflector because of heating the polyethylene from about 20 to 77°C. Most of the observed flux change was in the sub-cadmium range, since the slowing down flux per unit core power was not significantly affected by heating of the polyethylene.

TABLE 7.1

Heating Cycle Measurements

Stainless Steel Liner and 36.5 kg Polyethylene in Cavity

Lapsed Time (minute)	k-excess (%Δk)	Lapsed Time	Temperature °C
Cycle No. 1			
0	0.3588	15	38.3
5	0.4189	25	48.3
10	0.5370	45	58.3
14	0.6282	54	61.7
15	0.6593	65	62.2
20	0.7449	75	65.6
43	0.8960	85	66.1
50	0.9229	90	66.7
55	0.9368		
60	0.9417		
65	0.9505		
70	0.9547		
80	0.9619		
85	0.9659		
90	0.9693		
Cycle No. 2			
0	0.2073	1	17.5
5	0.2066	11	25.3
10	0.2889	21	35.4
15	0.3754	31	42.3
20	0.4668	41	46.2
25	0.5599	51	50.3
31	0.6053	61	51.8
36	0.6538	75	53.6
41	0.6849	83	54.3
46	0.7040	91	54.9
51	0.7375	101	55.9
56	0.7432	116	56.0
61	0.7586	126	56.8
66	0.7586		
71	0.7681		
76	0.7737		
81	0.7824		
86	0.7870		
91	0.7974		
96	0.7971		
101	0.7983		
106	0.8046		
111	0.8087		
116	0.8111		
121	0.8144		
126	0.8167		

TABLE 7.1

(Continued)

Lapsed Time (minute)	k-excess (%Δk)	Lapsed Time	Temperature °C
Cycle No. 3			
0	0.3184	2	27.1
5	0.3550	5	
10	0.3796	10	29.2
15	0.5109	20	41.9
20	0.5529	30	52.2
25	0.6800	50	59.2
30	0.7281	60	61.4
35	0.7958	70	
55	0.8251		
60	0.8665		
65	0.8763		
70	0.8857		
Cycle No. 4			
0	0.4037	10	29.4
5	0.3826	13	On
10	0.3500	20	33.9
15	0.3399	30	45.6
20	0.3986	40	52.2
25	0.4593	50	60.0
30	0.5576	70	66.1
35	0.6282	80	67.8
40	0.6997	90	70.0
45	0.7424	100	72.2
50	0.7742	110	73.3
55	0.8075	120	73.9
60	0.8332	130	75.0
65	0.8563	140	75.6
70	0.8702	160	76.1
75	0.8844	168	76.7
80	0.8919	230	76.7
85	0.9066	275	77.8
90	0.9137	330	77.2
95	0.9196	340	77.2
100	0.9300	345	76.7
105	0.9350	350	71.7
110	0.9404	355	67.8
115	0.9427		
120	0.9481		
125	0.9486		
130	0.9540		
135	0.9571		
140	0.9583		
145	0.9612		
150	0.9618		

TABLE 7.1

(Continued)

Lapsed Time (minute)		k-excess (%Δk)	Lapsed Time	Temperature °C
Cycle No. 4 (Cont'd)				
155		0.9658		
160		0.9661		
165		0.9681		
170		0.9700		
175		0.9715		
240	Foil	0.9149		
245	Exposure	0.9247		
250		0.9260		
255		0.9288		
325		0.9998		
330		0.9989		
335	Heaters off	0.9998		
340		0.9954		
345		0.9587		
350		0.9043		
Cycle No. 5				
15		0.2066	0	21.1
20		0.2997	10	27.8
25		0.3854	15	36.1
30		0.4657	25	45.0
35		0.5275	40	56.7
40		0.5769	50	63.3
45		0.6263	60	65.6
50		0.6831	80	70.0
55		0.7027	95	73.3
60		0.7284	105	74.4
65		0.7415	115	75.0
70		0.7598	125	75.6
75		0.7751	135	76.7
80		0.7863	145	77.2
85		0.7986	155	77.8
90		0.8117	255	78.9
95		0.8188		
100		0.8274		
105		0.8344		
110		0.8460		
115		0.8468		
120		0.8516		
125		0.8551		
130		0.8611		
135		0.8640		
140		0.8709		

TABLE 7.1

(Continued)

Lapsed Time (minute)	k-excess (%Δk)	Lapsed Time	Temperature °C
Cycle No. 5 (Cont'd)			
145	0.9819		
150	0.8766		
155	0.8782		

Prior to this run 6 of every 7 holes in the inlet plenum to the polyethylene were taped to prevent air flow through these holes. This was done to try and improve temperature distribution in polyethylene assembly.

TABLE 7.2

Catcher Foil Data

Hot Polyethylene

Foil No.	Foil Type	Location Radial (cm)	Location Axial (cm)	Normalized Counts	Local to Foil (X)
Run 1096					
1	Bare	15.2	90.8	36820	5.471
2	Bare	15.2	102.8	14513	2.156
3	Bare	15.2	118.0	8849	1.315
4	Bare	15.2	133.3	7171	1.065
5	Bare	15.2	148.5	6730	1.000 (X)
6	Bare	15.2	163.8	7282	1.082
7	Bare	15.2	179.0	8297	1.233
8	Bare	15.2	194.2	14670	2.180
9	Bare	15.2	206.9	43177	6.415
10	Bare	30.5	148.5	8903	1.323
11	Bare	45.7	148.5	12768	1.897
12	Bare	61.0	148.5	47824	7.106
13	Bare	71.1	148.5	63843	9.486
14	Bare	81.3	148.5	105720	15.708
15	Bare	88.9	148.5	142673	21.198
Run 1097					Cd Ratios
1	Cd	15.2	90.8	5010	7.35
2	Cd	15.2	118.0	3606	2.45
3	Cd	15.2	148.5	3222	2.09
4	Cd	15.2	179.0	3487	2.39
5	Cd	15.2	206.9	4559	9.47
6	Cd	45.7	148.5	4202	3.04
7	Cd	61.0	148.5	5263	9.09
8	Cd	71.1	148.5	5592	11.42
9	Cd	83.3	148.5	5772	18.32
10	Cd	88.9	148.5	6432	22.18

TABLE 7.3

Gold Foil Data with Stainless Steel Liner and 36.5 kg Polyethylene in Reactor

Hot Polyethylene

Foil No.	Foil Type	Location Radial (cm)	Location Axial (cm)	Weight (gm)	Specific Activity d/m/gm x 10^{-6}	Local to Foil (X)
Run 1093						
1	Bare	15.2	90.8	0.0159	1.998	1.701
2	Bare	15.2	102.8	0.0151	1.407	1.205
3	Bare	15.2	118.0	0.0186	1.253	1.073
4	Bare	15.2	133.3	0.0145	1.216	1.041
5	Bare	15.2	148.5	0.0171	1.168	1.000 (X)
6	Bare	15.2	163.8	0.0160	1.196	1.024
7	Bare	15.2	179.0	0.0182	1.232	1.055
8	Bare	15.2	194.2	0.0176	1.342	1.149
9	Bare	15.2	206.9	0.0161	2.043	1.749
10	Bare	61.0	206.9	0.0170	2.963	2.537
11	Bare	71.1	206.9	0.0163	3.103	2.657
12	Bare	81.3	194.2	0.0182	3.911	3.348
13	Bare	81.3	206.9	0.0154	3.833	3.282
14	Bare	88.9	90.8	0.0211	4.521	3.871
15	Bare	88.9	118.0	0.0193	4.319	3.698
16	Bare	88.9	179.0	0.0171	4.475	3.831
17	Bare	88.9	194.2	0.0163	4.084	3.497
18	Bare	88.9	206.9	0.0177	3.888	3.329
19	Cd	0	74.9	0.0200	1.513	1.300
20	Cd	0	44.4	0.0134	0.067	0.057
21	Cd	107.7	151.1	0.0183	0.695	0.595
22	Cd	138.2	151.1	0.0171	0.023	0.020
23	Cd	61.0	148.5	0.0143	1.696	1.452
24	Cd	61.0	179.0	0.0155	1.592	1.363
25	Cd	71.1	90.8	0.0158	1.705	1.460
26	Cd	71.1	118.0	0.0142	1.810	1.550
27	Cd	88.9	148.5	0.0153	1.966	1.683
Run 1094						
1	Cd	0	89.4	0.0183	1.491	
2	Cd	0	59.6	0.0198	0.358	
3	Cd	15.2	206.9	0.0182	1.335	
4	Cd	15.2	148.5	0.0173	1.169	
5	Cd	15.2	90.8	0.0173	1.430	
6	Cd	30.5	148.5	0.0190	1.157	
7	Cd	61.0	118.0	0.0156	1.548	
8	Cd	61.0	90.8	0.0178	1.604	

TABLE 7.3
(Continued)

Foil No.	Foil Type	Location Radial (cm)	Location Axial (cm)	Weight (gm)	Specific Activity d/m/gm x 10^{-6}	Local to Foil (X)
Run 1094 (Cont'd)						
9	Cd	71.1	90.8	0.0173	1.693	
10	Cd	71.1	118.0	0.0167	1.686	
11	Cd	71.1	148.5	0.0161	1.737	
12	Cd	81.3	148.5	0.0160	1.930	
13	Cd	93.2	151.1	0.0164	2.032	
14	Cd	123.0	151.1	0.0184	0.125	
15	Bare	81.3	179.0	0.0193	3.909	3.347
16	Bare	81.3	118.0	0.0199	4.034	3.454
17	Bare	81.3	90.8	0.0159	4.191	3.588
Run 1095						
1	Bare	0	89.4	0.0145	2.740	2.346
2	Bare	0	74.9	0.0202	6.988	5.983
3	Bare	0	59.6	0.01935	6.111	5.232
4	Bare	0	44.4	0.0187	4.379	3.749
5	Bare	0	29.1	0.0175	2.609	2.234
6	Bare	0	13.9	0.0166	1.424	1.219
7	Bare	0	0	0.0160	0.202	0.173
8	Bare	30.5	148.5	0.0169	1.333	1.141
9	Bare	45.7	148.5	0.0170	1.509	1.292
10	Bare	61.0	90.8	0.0178	3.006	2.574
11	Bare	61.0	118.0	0.0148	2.641	2.261
12	Bare	61.0	148.5	0.0216	2.414	2.067
13	Bare	61.0	179.0	0.0200	2.447	2.095
14	Bare	71.1	90.8	0.0197	3.308	2.832
15	Bare	71.1	118.0	0.0161	2.906	2.488
16	Bare	71.1	148.5	0.020	2.699	2.311
17	Bare	71.1	179.0	0.0163	2.809	2.405
18	Bare	81.3	148.5	0.0170	3.930	3.365
19	Bare	88.9	148.5	0.0147	4.562	3.906
20	Bare	93.2	151.1	0.0177	5.376	4.603
21	Bare	107.7	151.1	0.0202	5.799	4.965
22	Bare	123.0	151.1	0.0143	4.386	3.755
23	Bare	138.2	151.1	0.0162	2.958	2.533
24	Bare	153.5	151.1	0.0177	1.859	1.592
25	Bare	168.7	151.1	0.0171	0.969	0.830
26	Bare	183.9	151.1	0.0152	0.244	0.209
27	Cd	88.9	90.8	0.0156	1.704	1.459
28	Cd	88.9	118.0	0.0146	2.059	1.763
29	Cd	88.9	179.0	0.0137	2.045	1.751
30	Cd	88.9	206.9	0.0164	1.619	1.386

TABLE 7.3

(Continued)

Foil No.	Foil Type	Location Radial (cm)	Location Axial (cm)	Weight (gm)	Specific Activity d/m/gm x 10^{-6}	Local to Foil (X)
Run 1095 (Cont'd)						
31	Cd	61.0	206.9	0.0172	1.628	1.394
32	Cd	81.3	209.5	0.0172	1.637	1.402
33	Cd	15.2	118.0	0.0162	1.217	1.042
34	Cd	15.2	179.0	0.01555	1.222	1.046
Run 1096						
1	Cd	71.1	90.8	0.0188	1.630	
2	Cd	71.1	118.0	0.0187	1.630	
3	Cd	71.1	179.0	0.0164	1.696	
4	Cd	71.1	206.9	0.0180	1.570	
5	Cd	81.3	90.8	0.0179	1.746	
6	Cd	81.3	118.0	0.0186	1.875	
7	Cd	81.3	179.0	0.0221	1.719	
8	Cd	81.3	206.9	0.0212	1.445	
9	Cd	153.5	151.1	0.0169	0.003	
10	Cd	0	29.1	0.0205	0.005	
11	Bare	0	82.5	0.0164	6.141	5.258
12	Bare	100.1	151.1	0.0153	6.421	5.497
Run 1097						
1	Bare	0	67.2	0.02793	6.728	5.760
2	Bare	0	52.0	0.0293	4.959	4.246
3	Bare	115.4	151.1	0.0293	4.964	4.250
4	Bare	130.6	151.1	0.0287	3.637	3.114

TABLE 7.4

Comparison of Bare Gold Data

Infinitely Dilute Activity

Location		Cold Foil Activity d/m/gm x 10^{-6}			
Radial (cm)	Axial (cm)	Cold Poly.	Hot Poly.	Hot/Cold	
15.2	90.8	3.441	3.472	1.009	
	118.0	2.417	2.500	1.034	
	148.5	2.288	2.346	1.025	
	179.0	2.369	2.456	1.037	
	206.9	3.357	3.472	1.034	
61.0	90.8	4.725	4.843	1.025	
	118.0	4.202	4.212	1.002	
	148.5	4.048	4.269	1.054	
	179.0	4.125	4.204	1.019	
	206.9	4.411	4.770	1.081	
71.1	90.8	5.112	5.298	1.036	
	118.0	4.646	4.707	1.013	
	148.5	4.493	4.640	1.033	
	179.0	4.508	4.605	1.022	
	206.9	4.686	4.873	1.040	
81.3	90.8	5.870	6.235	1.062	
	118.0	5.889	6.357	1.079	
	148.5	5.961	6.085	1.021	
	179.0	5.779	6.150	1.064	
	206.9	5.371	5.698	1.061	
88.9	90.8	6.099	6.685	1.096	
	118.0	6.206	6.678	1.076	
	148.5	6.316	6.698	1.060	
	179.0	6.347	6.718	1.058	
	206.9	5.579	5.809	1.041	1.045±0.024
0	89.4	3.980	4.333	1.089	
0	74.9	9.372	9.391	1.002	
0	59.6	7.280	7.247	0.995	
0	44.4	4.762	5.000	1.050	
0	29.1	2.967	2.950	0.994	
0	13.9	1.477	1.608	1.089	
0	0	0.210	0.228	1.086	1.044±0.042
93.2	151.1	7.119	7.851	1.103	
107.7	151.1	6.536	7.215	1.104	
123.0	151.1	4.464	5.056	1.133	
138.2	151.1	2.978	3.359	1.128	
153.5	151.1	1.865	2.101	1.127	
168.7	151.1	0.985	1.094	1.111	
183.9	151.1	0.273	0.275	1.007	1.102±0.044

TABLE 7.5

Comparison of Cadmium Covered Gold Data

Infinitely Dilute Activity

Location		Gold Foil Activity - d/m/gm x 10^{-6}			
Radial (cm)	Axial (cm)	Hot Poly.(1)	Cold Poly.	Hot/Cold	
15.2	90.8	2.878	2.803	1.027	
15.2	118.0	2.395	2.319	1.033	
15.2	148.5	2.352	2.278	1.033	
15.2	179.0	2.372	2.313	1.025	
15.2	206.9	2.734	2.616	1.045	
61.0	90.8	3.259	3.058	1.066	
61.0	118.0	3.008	2.956	1.018	
61.0	148.5	3.204	3.029	1.058	
61.0	179.0	3.087	3.015	1.024	
61.0	206.9	3.269	2.915	1.122	
71.1	90.8	3.367	3.105	1.084	
71.1	118.0	3.382	3.172	1.066	
71.1	148.5	3.411	3.198	1.067	
71.1	179.0	3.351	3.168	1.058	
71.1	206.9	3.203	3.055	1.048	
81.3	90.8	3.555	3.323	1.070	
81.3	118.0	3.869	3.380	1.145	
81.3	148.5	3.782	3.923	0.964	
81.3	179.0	3.774	3.591	1.051	
81.3	206.9	3.288	3.141	1.047	
88.9	90.8	3.311	3.247	1.020	
88.9	118.0	3.915	3.046	1.285	
88.9	148.5	3.796	3.782	1.004	
88.9	179.0	3.810	3.861	0.987	
88.9	209.5	3.199	3.111	1.028	
30.5	148.5	2.405	2.329	1.033	
45.7	148.5	--	2.672	--	1.045±0,038
0	89.4	3.060	2.669	1.146	
0	74.9	3.203	2.909	1.101	
0	59.6	0.755	0.877	0.861	
0	44.4	0.124	0.113	1.097	
0	29.1	0.0107	0.025	0.428	
93.2	151.1	4.016	3.962	1.014	
107.7	151.1	1.426	1.421	1.004	
123.0	151.1	0.256	0.319	0.803	
153.5	151.1	0.00599	0.0105	0.570	

(1) All data from hot polyethylene has been increased by 12.87% to compare both sets of data at the same power level.

TABLE 7.6

Comparison of Cadmium Ratios

Gold Foil Data

Location		Cadmium Ratios			
Radial (cm)	Axial (cm)	Cold Poly.	Hot Poly.	Hot/Cold	
15.2	90.8	1.228	1.207	0.983	
	118.0	1.042	1.044	1.002	
	148.5	1.014	0.997	0.983	
	179.0	1.024	1.035	1.011	
	209.5	1.284	1.269	0.988	
61.0	90.8	1.545	1.485	0.961	
	118.0	1.421	1.400	0.985	
	148.5	1.337	1.332	0.996	
	179.0	1.368	1.362	0.996	
	209.5	1.513	1.459	0.964	
71.1	90.8	1.646	1.585	0.963	
	118.0	1.465	1.397	0.954	
	148.5	1.405	1.360	0.968	
	179.0	1.423	1.374	0.966	
	209.5	1.534	1.521	0.992	
81.3	90.8	1.766	1.754	0.993	
	118.0	1.742	1.643	0.943	
	148.5	1.519	1.608	1.059	
	179.0	1.609	1.629	1.012	
	209.5	1.710	1.733	1.013	
88.9	90.8	1.986	2.018	1.016	
	118.0	1.908	1.705	0.894	
	148.5	1.766	1.764	0.999	
	179.0	1.738	1.762	1.014	
	209.5	1.837	1.815	0.988	
30.5	148.5	1.066	1.060	0.994	0.986±0.031
0	89.4	1.491	1.416	0.950	
0	74.9	3.222	2.931	0.910	
0	59.6	8.299	9.593	1.156	
0	44.4	43.90	40.32	0.918	
0	29.1	118.8	276.2	2.325	
93.2	151.1	1.797	1.955	1.088	
107.7	151.1	4.602	5.059	1.099	
123.0	151.1	13.98	19.67	1.407	
138.2	151.1	92.15	72.85	0.791	
153.5	151.1	177.4	350.8	1.977	

TABLE 7.7

Comparison of Thermal Flux

Gold Foil Data - 36.5 kg Polyethylene and Stainless Steel Liner in Reactor

Location		Thermal Neutron Flux - $n/cm^2/sec/watt \times 10^{-6}$			
Radial (cm)	Axial (cm)	Cold Poly.	Hot Poly.	Hot/Cold	
0	89.4	0.961	0.933	0.971	
0	74.9	4.736	4.534	0.957	
0	59.6	4.692	4.758	1.014	
0	44.4	3.409	3.572	1.048	
0	29.1	2.156	2.154	0.999	0.998±0.036
0	13.9	1.076 (1)	1.178 (1)	1.095	
0	0	0.154 (1)	0.167 (1)	1.084	
93.2	151.1	2.313	2.810	1.215	
107.7	151.1	3.749	4.243	1.132	
123.0	151.1	3.037	3.516	1.158	
138.2	151.1	2.158	2.427	1.125	
153.5	151.1	1.359	1.535	1.130	1.152±0.037
168.7	151.1	0.718 (1)	0.802 (1)	1.117	
183.9	151.1	0.199 (1)	0.202 (1)	1.015	
15.2	90.8	0.467	0.436	0.934	
15.2	118.0	0.0716	0.0763	1.064	
15.2	148.5	0.0058	--		
15.2	179.0	0.0409	0.0609	1.489	
15.2	206.9	0.542	0.539	0.994	0.997±0.065
61.0	90.8	1.222	1.159	0.948	
61.0	118.0	0.913	0.882	0.966	
61.0	148.5	0.747	0.780	1.044	
61.0	179.0	0.814	0.819	1.006	
61.0	206.9	1.097	1.099	1.002	0.993±0.037
71.1	90.8	1.471	1.412	0.960	
71.1	118.0	1.081	0.981	0.907	
71.1	148.5	0.949	0.900	0.948	
71.1	179.0	0.983	0.918	0.934	
71.1	206.9	1.196	1.224	1.023	0.954±0.043
81.3	90.8	1.866	1.963	1.052	
81.3	118.0	1.839	1.823	0.991	
81.3	148.5	1.493	1.687	1.130	
81.3	179.0	1.603	1.741	1.086	
81.3	206.9	1.634	1.766	1.081	1.068±0.051
88.9	90.8	2.159	2.471	1.145	
88.9	118.0	2.225	2.023	0.909	
88.9	148.5	1.939	2.126	1.096	
88.9	179.0	1.910	2.129	1.115	
88.9	206.9	1.808	1.911	1.057	1.103±0.037
30.5	148.5	0.112	0.0939	0.838	
45.7	148.5	0.103	0.171 (1)	1.660	

(1) Based on extrapolated value for cadmium covered data.

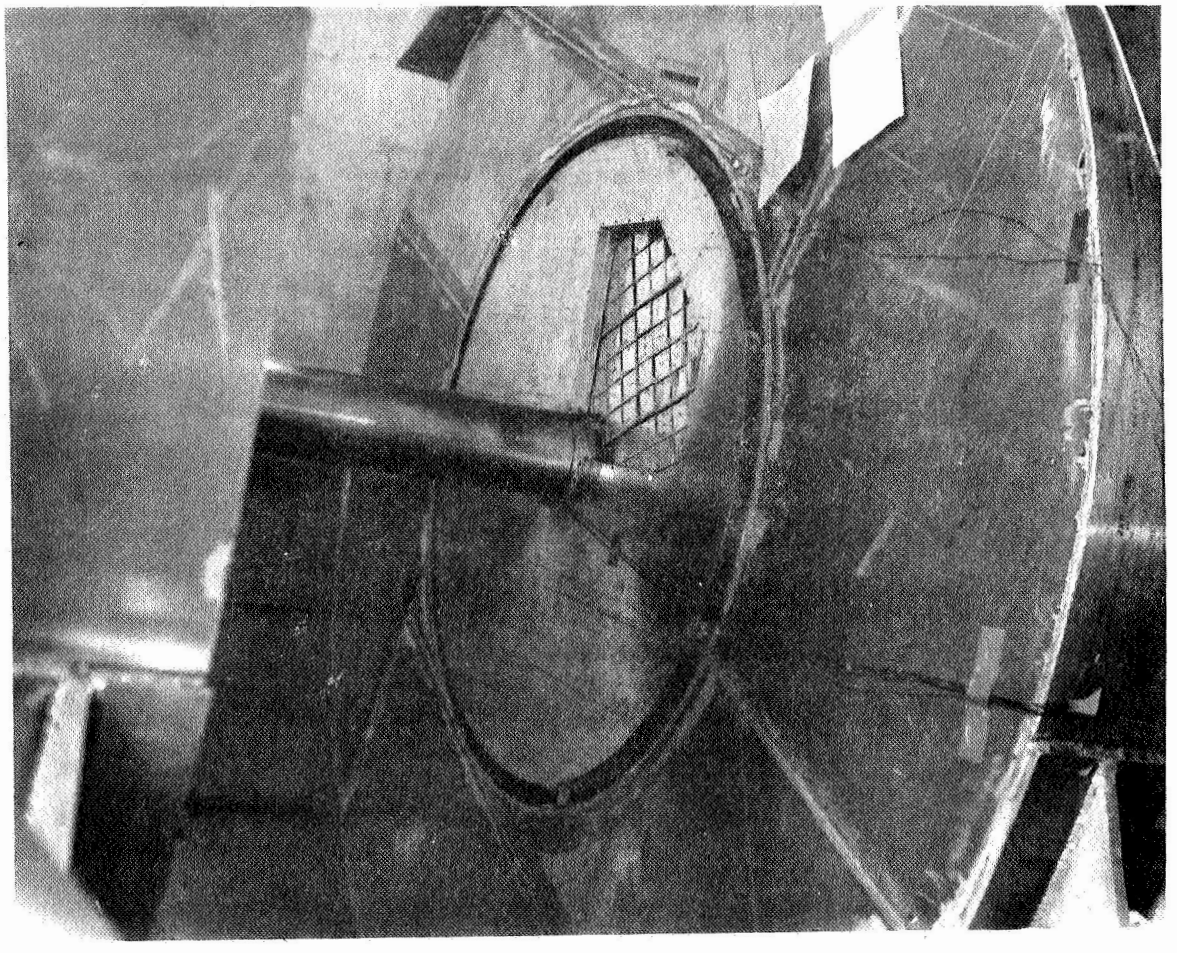

Fig. 7.1 Reactor face - showing hole in air ducting to allow power mapping

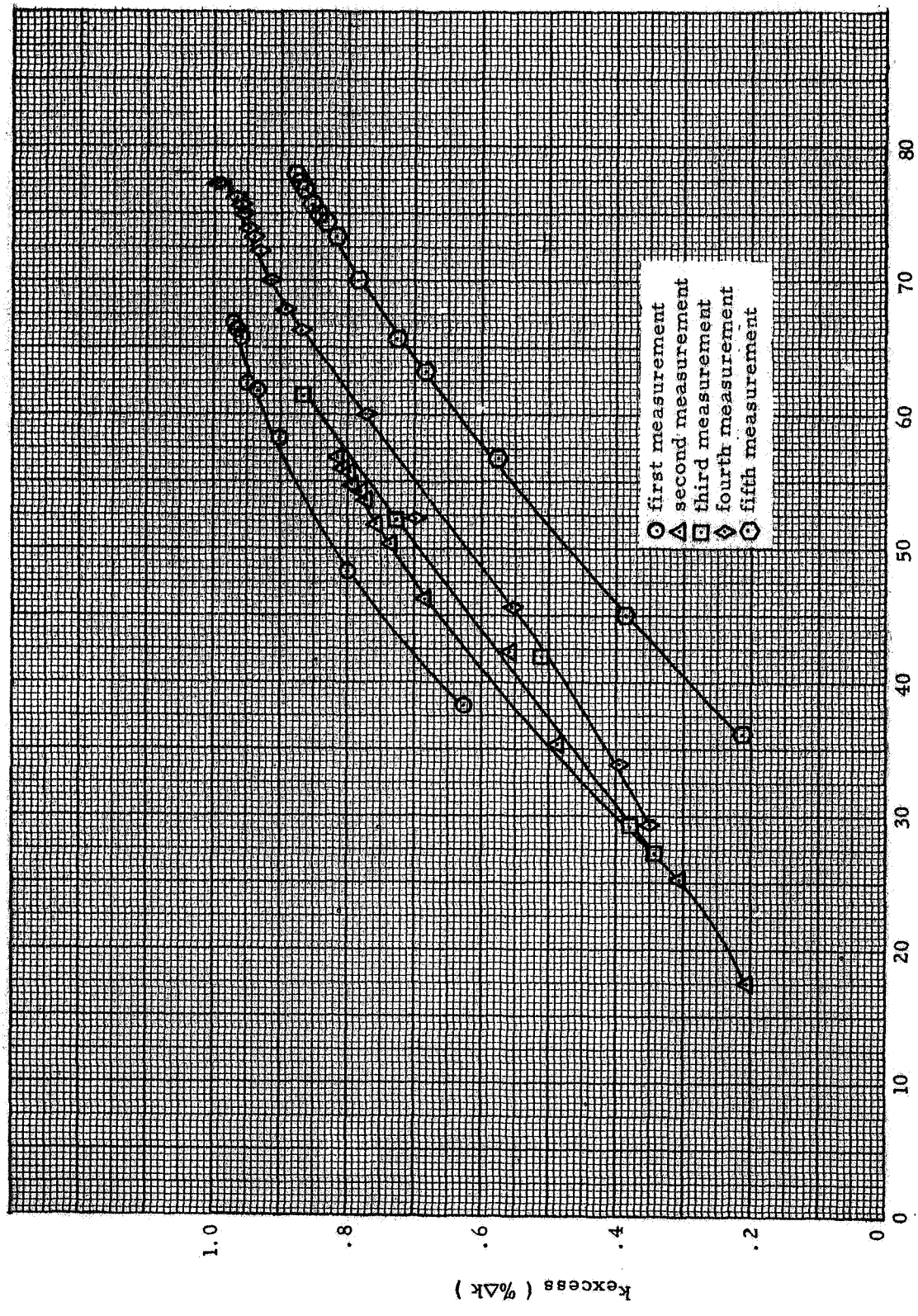

Fig. 7.2 Change in excess multiplication with changes in polyethylene temperature

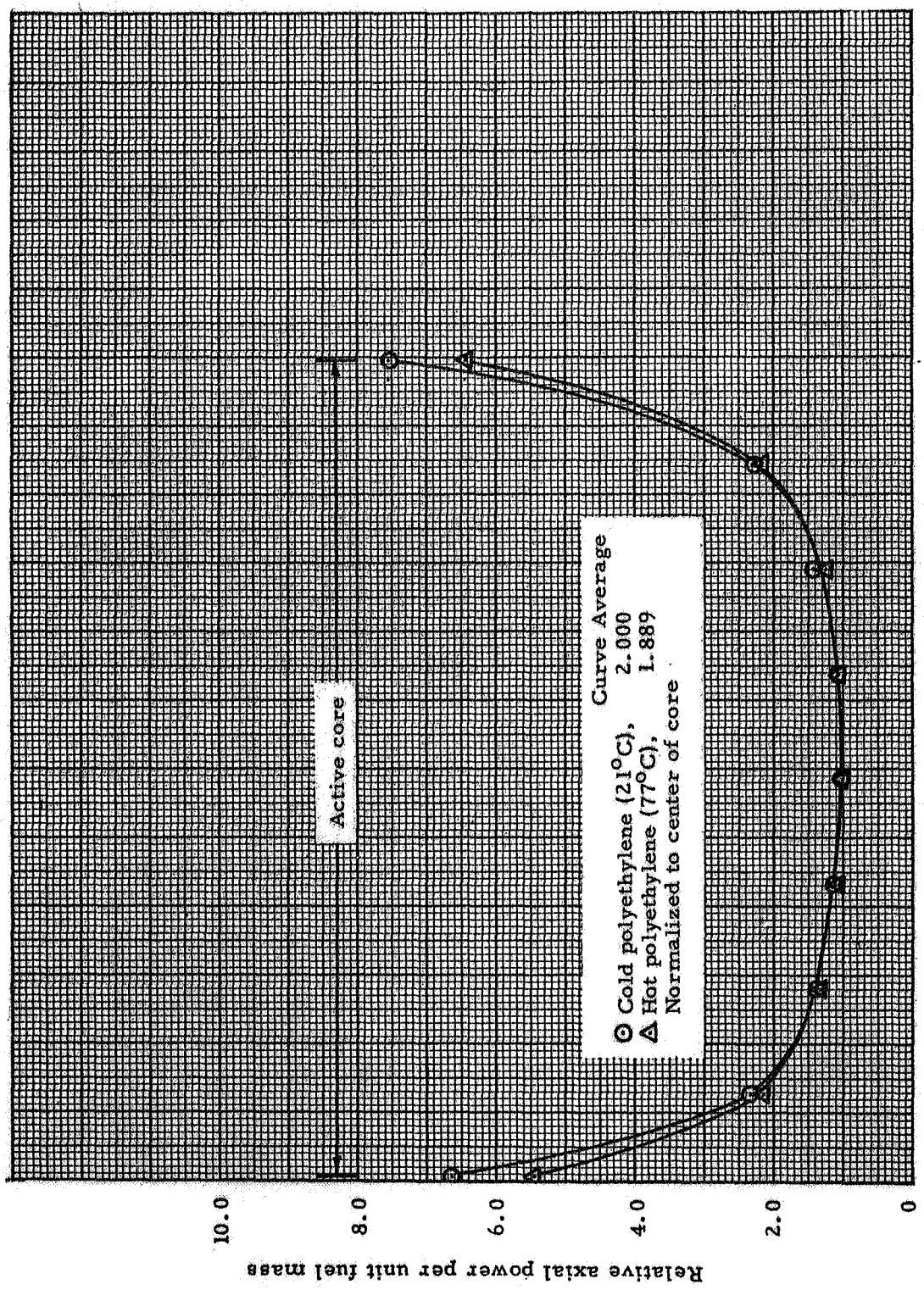

Fig. 7.3 Axial power distribution within the active core region, hot CH_2, bare Au catcher foils

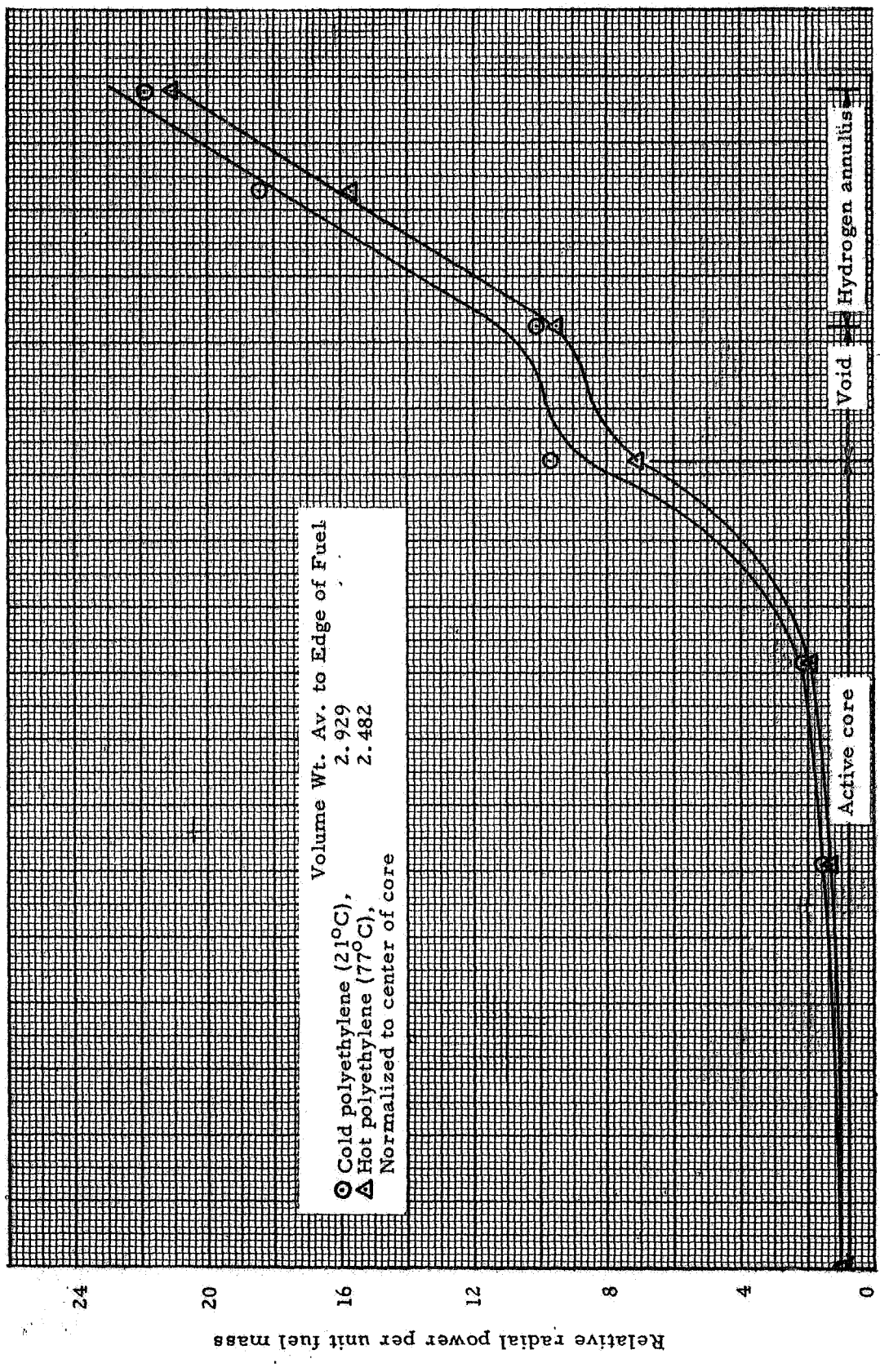

Fig. 7.4 Relative radial power distribution at axial center of core, hot CH_2, bare Au catcher foils

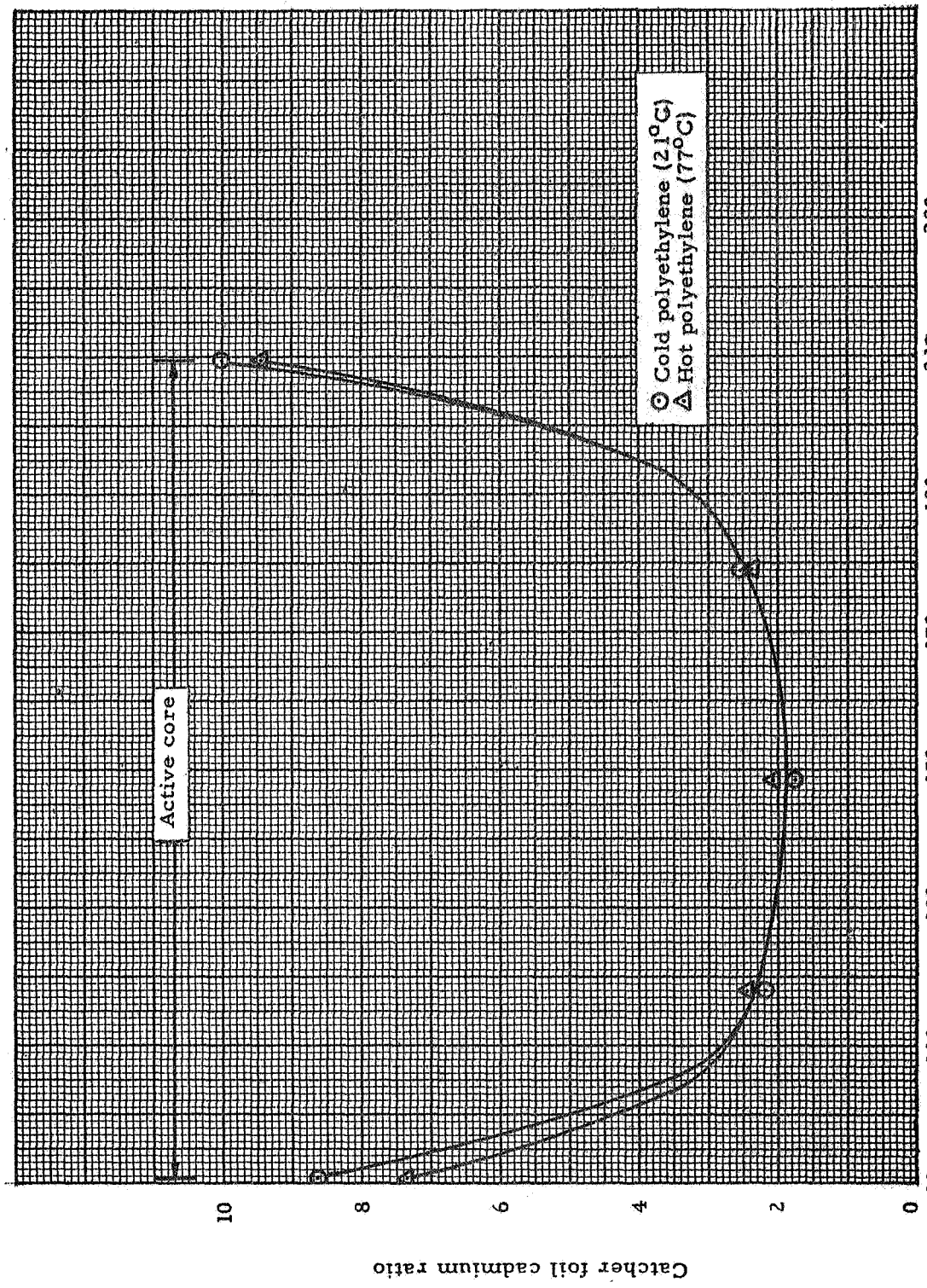

Fig. 7.5 Axial distribution of catcher foil cadmium ratios, hot CH_2

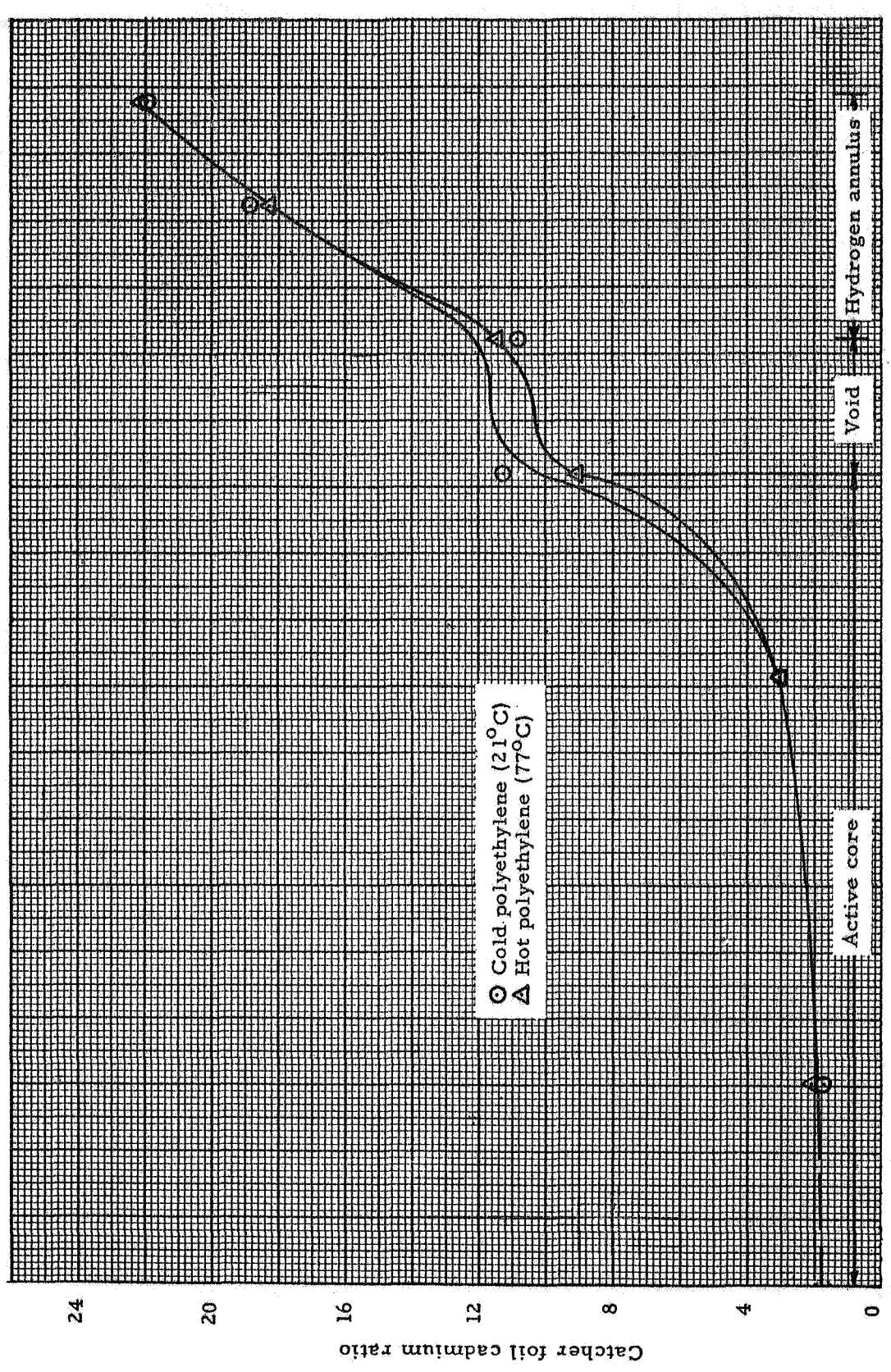

Fig. 7.6 Radial distribution of catcher foil cadmium ratios, hot CH_2

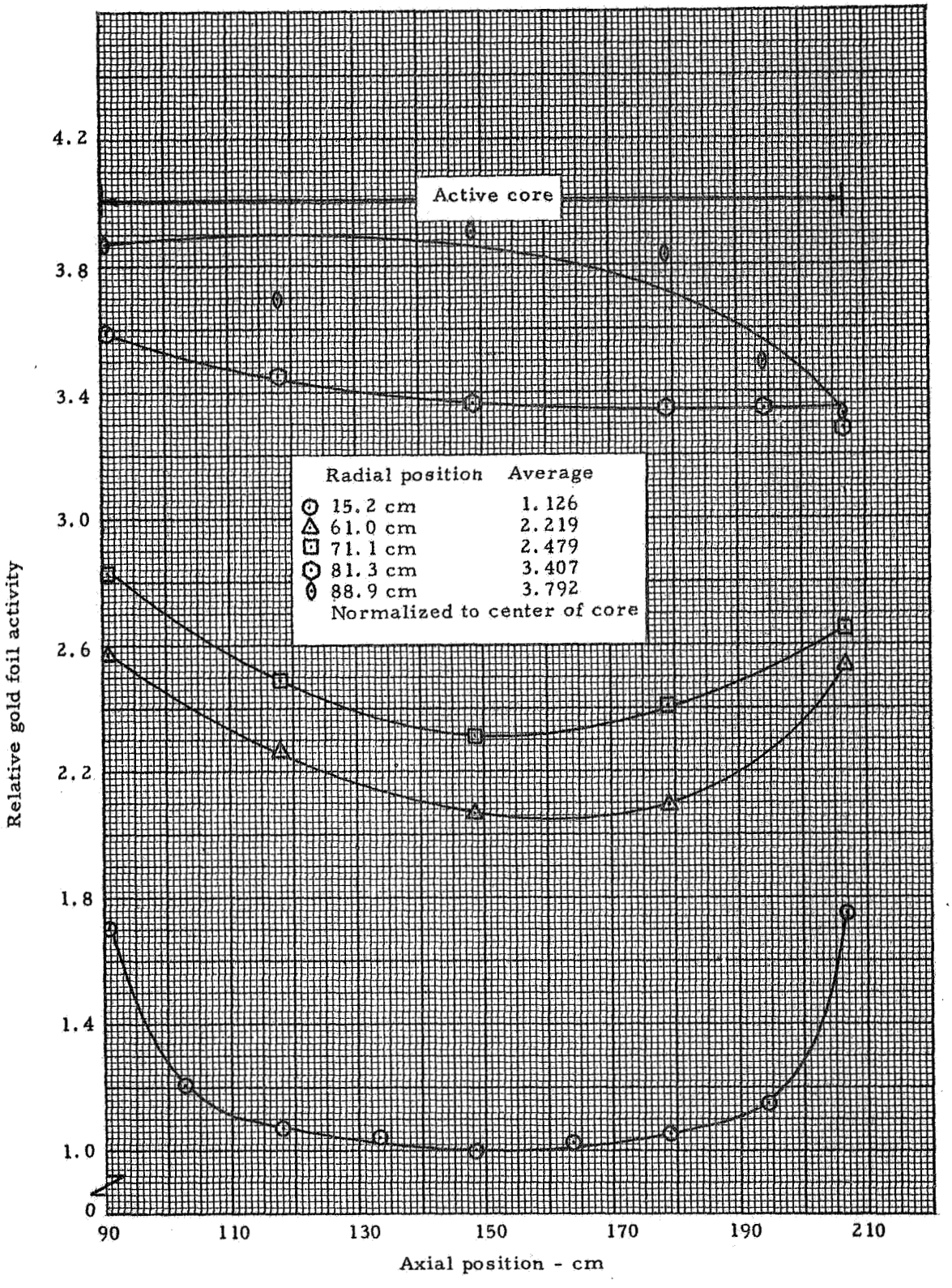

Fig. 7.7 Relative gold foil activity, axial distribution, hot CH_2

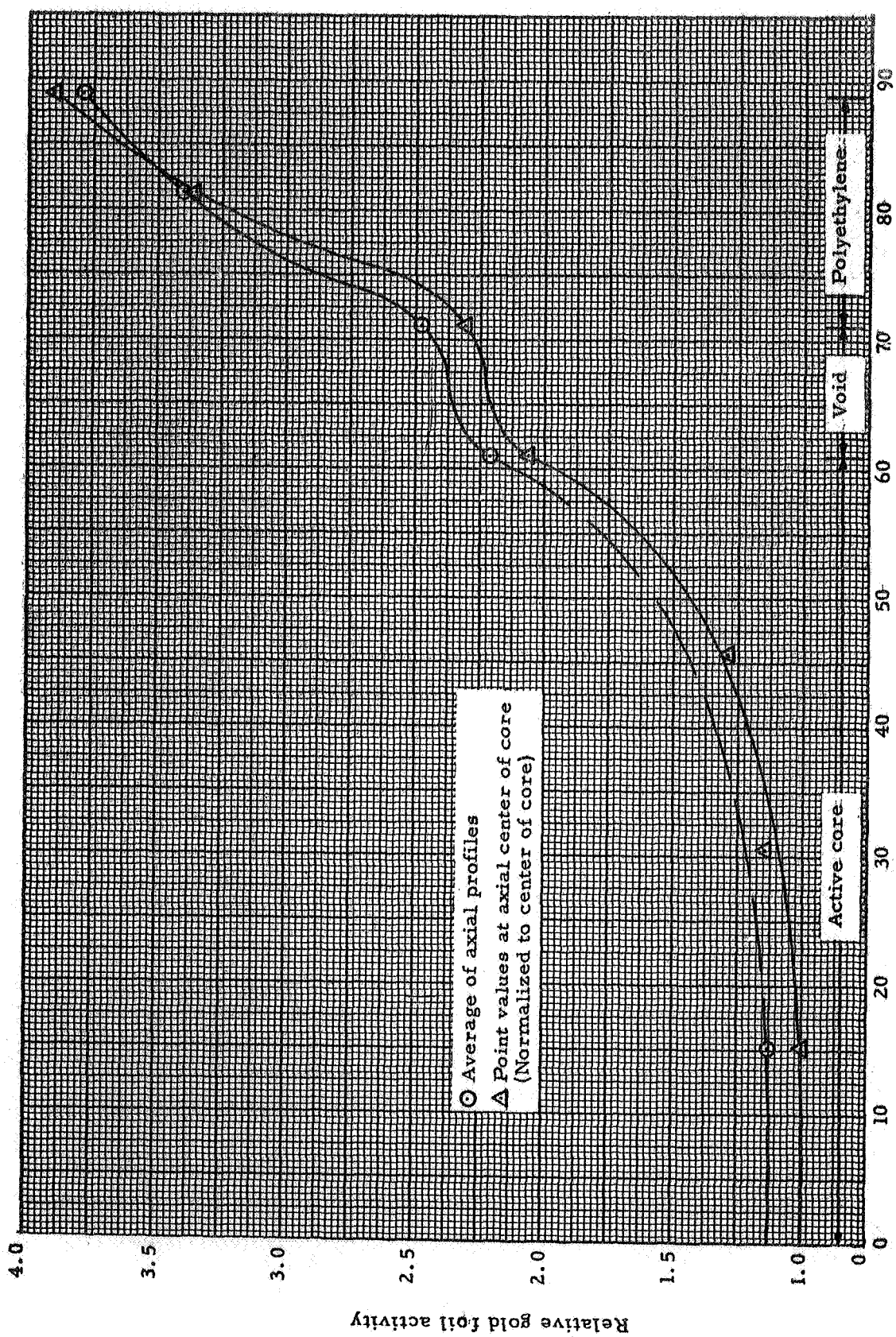

Fig. 7.8 Relative gold foil activity, radial distribution, hot CH_2

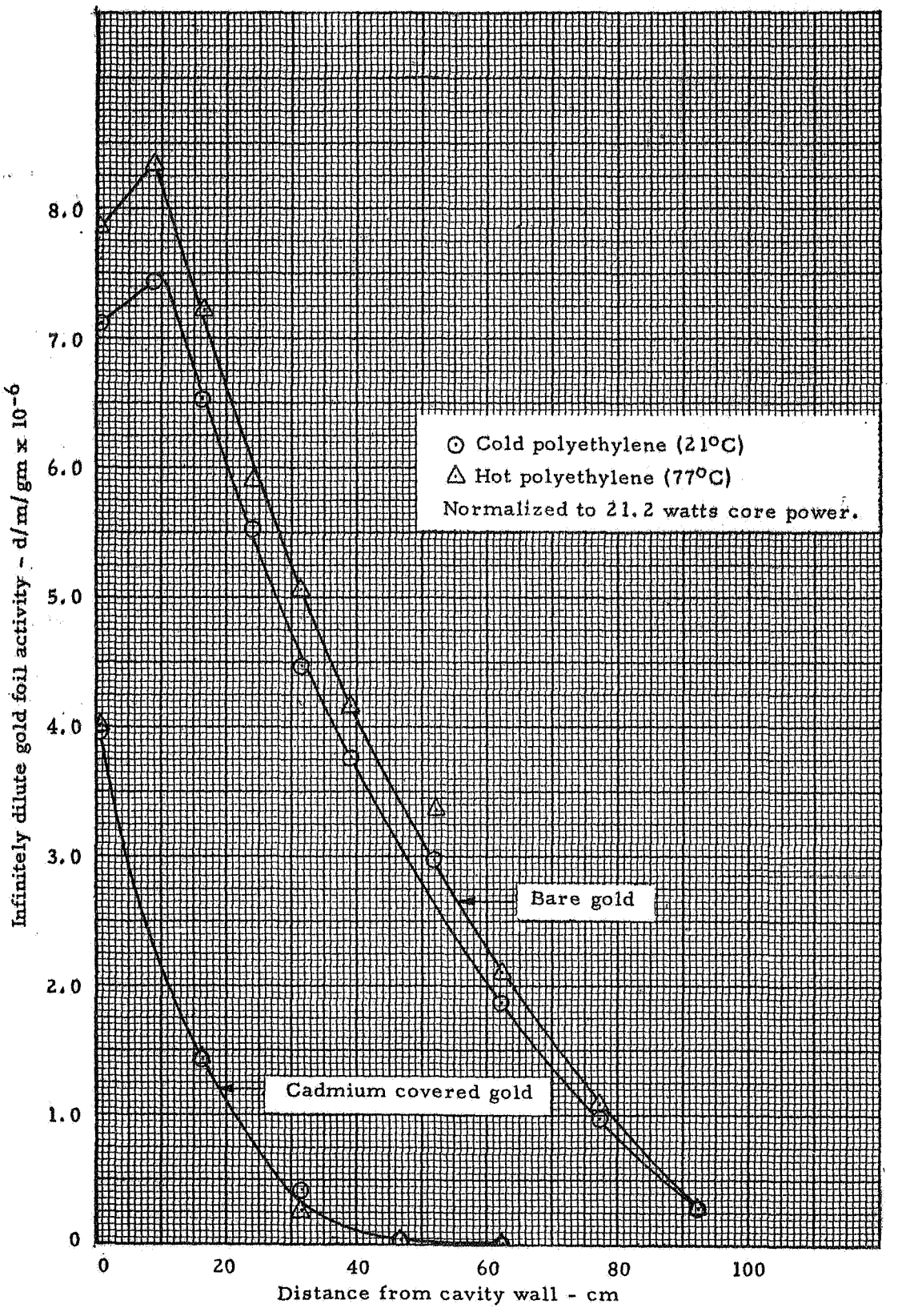

Fig. 7.9 Infinitely dilute gold foil activity, radial reflector, hot CH_2

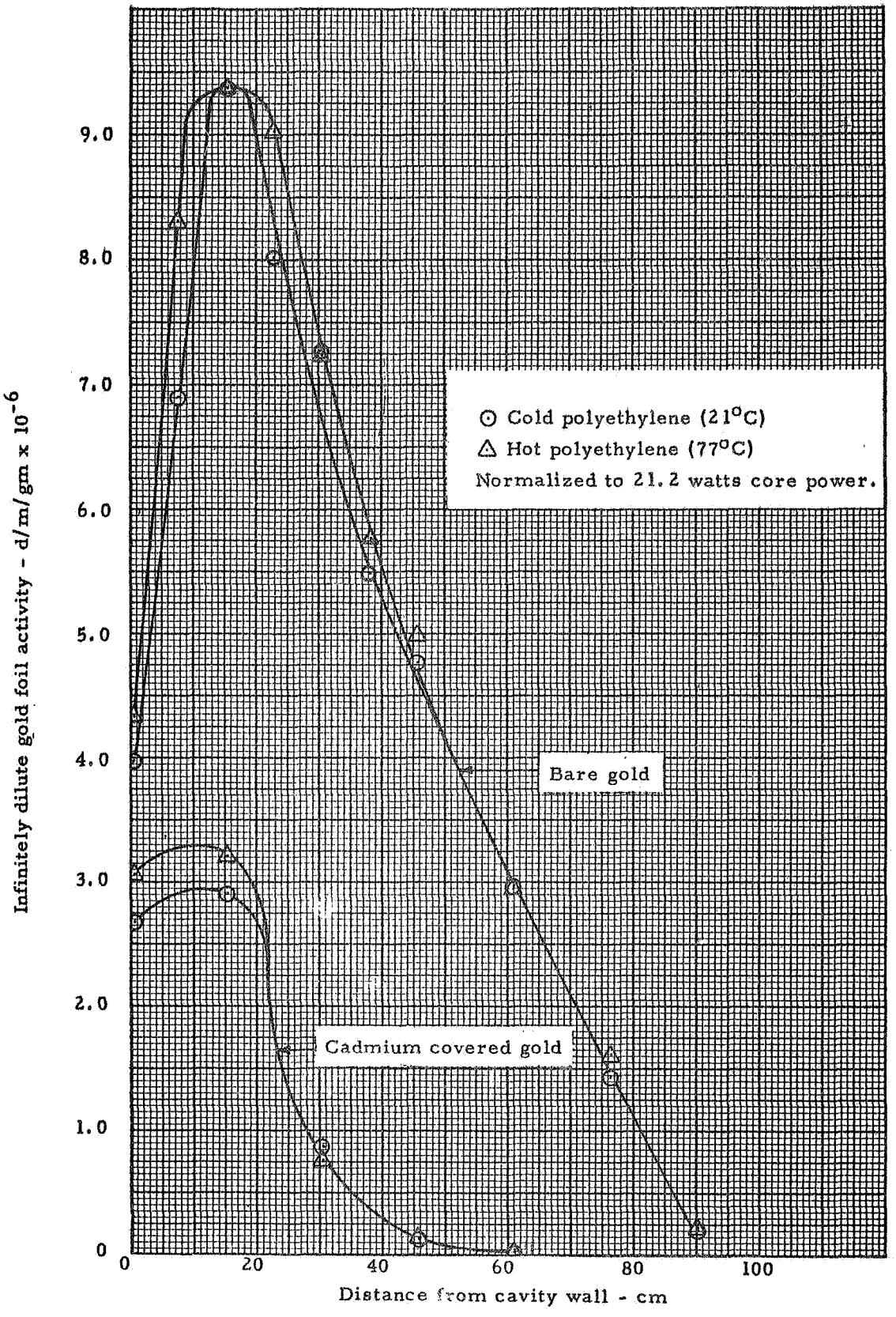

Fig. 7.10 Infinitely dilute gold foil activity, end reflector, hot CH_2

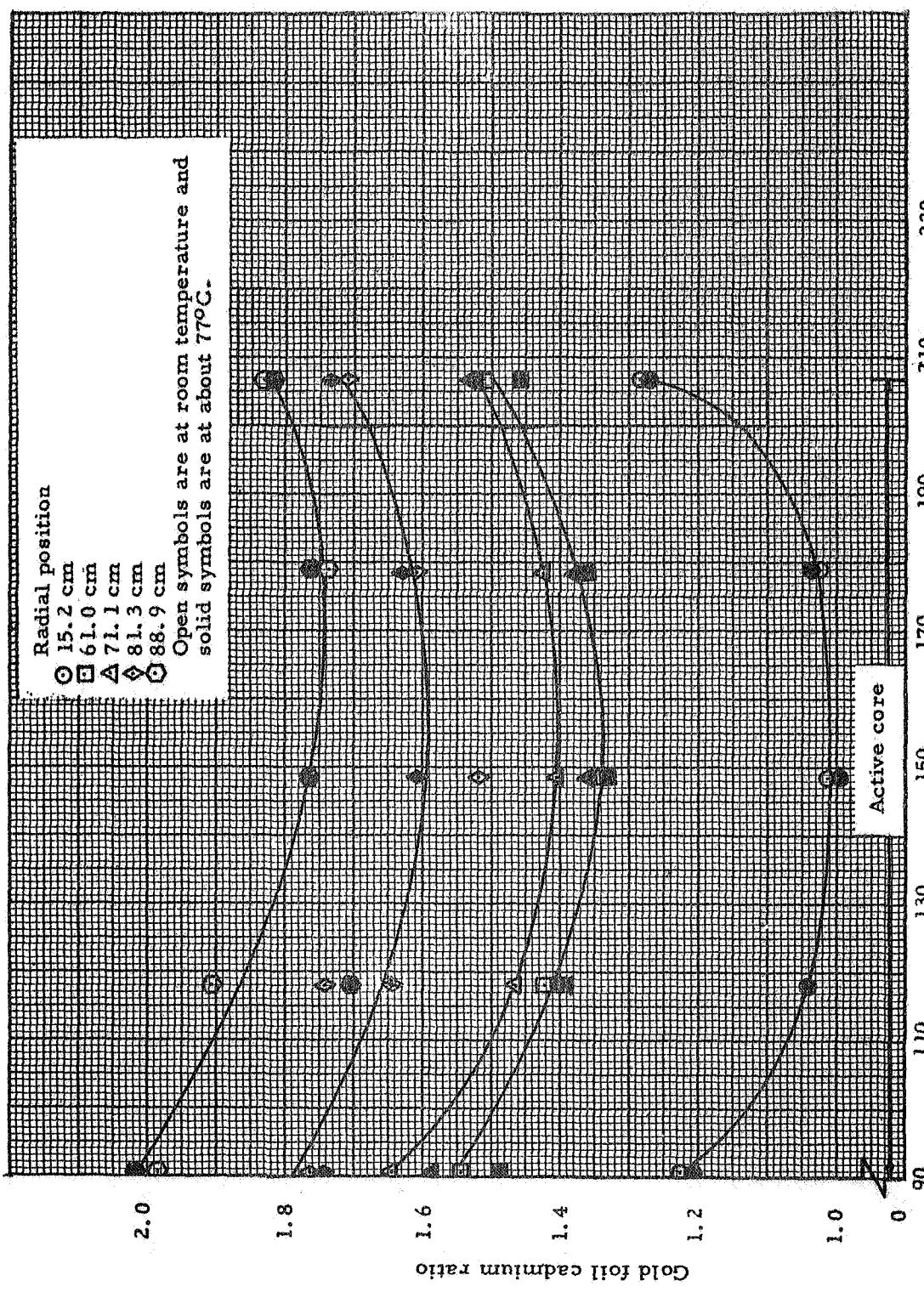

Fig. 7.11 Axial distribution of gold foil cadmium ratios through the cavity region, hot CH_2

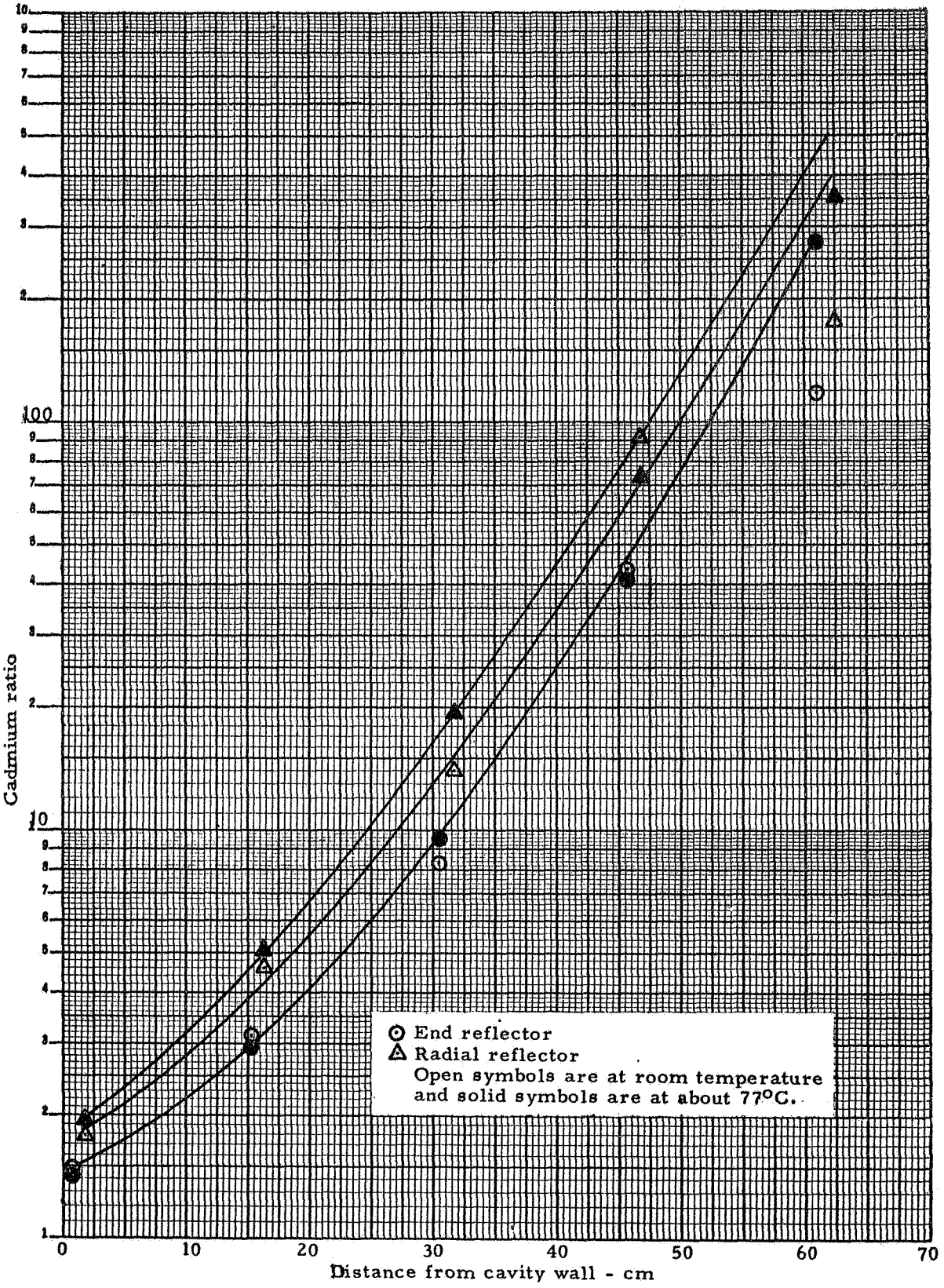

Fig. 7.12 Gold foil cadmium ratio distribution within the reflector regions, hot CH_2

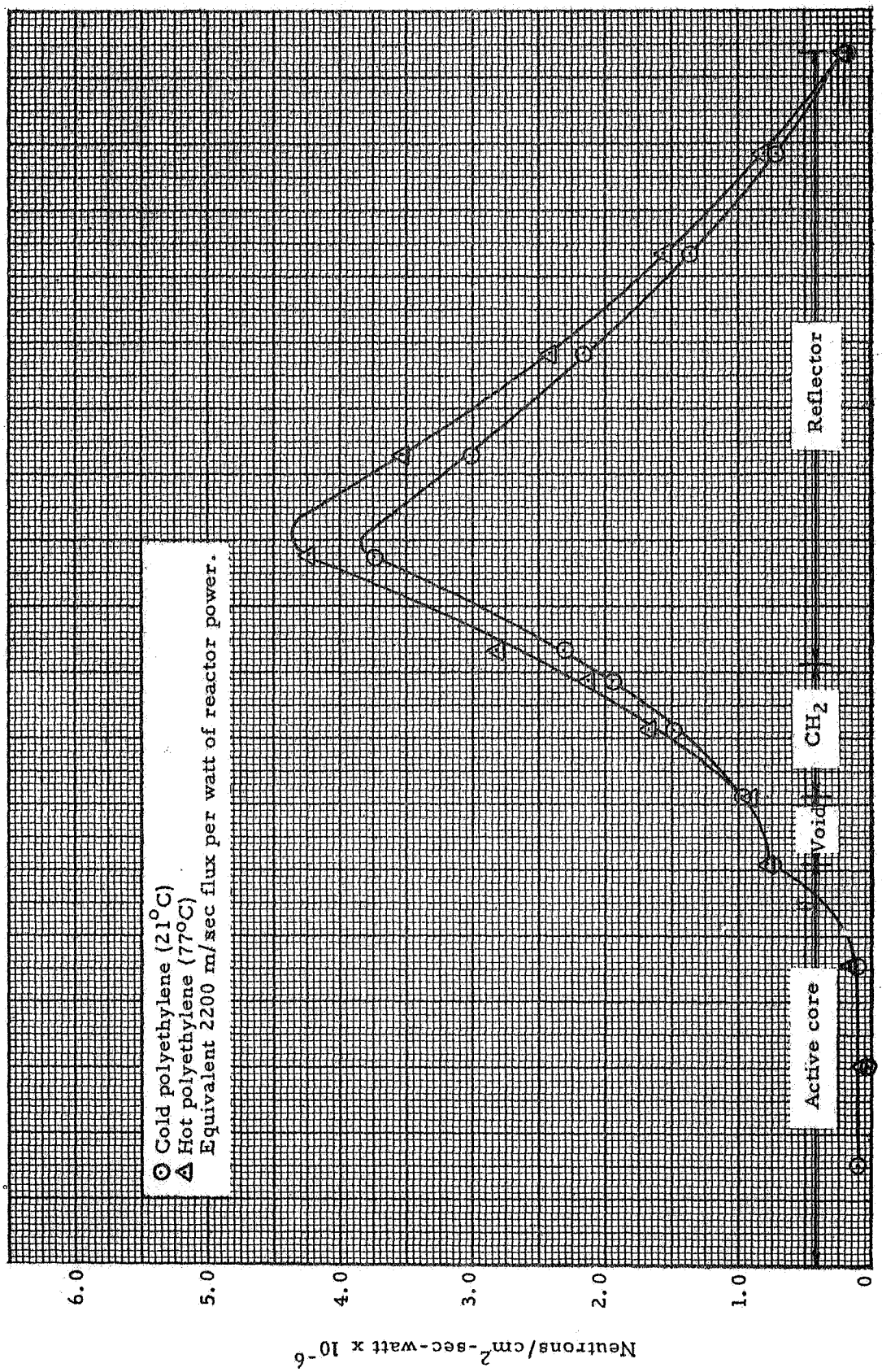

Fig. 7.13 Thermal neutron flux distribution, radial profile, hot CH_2

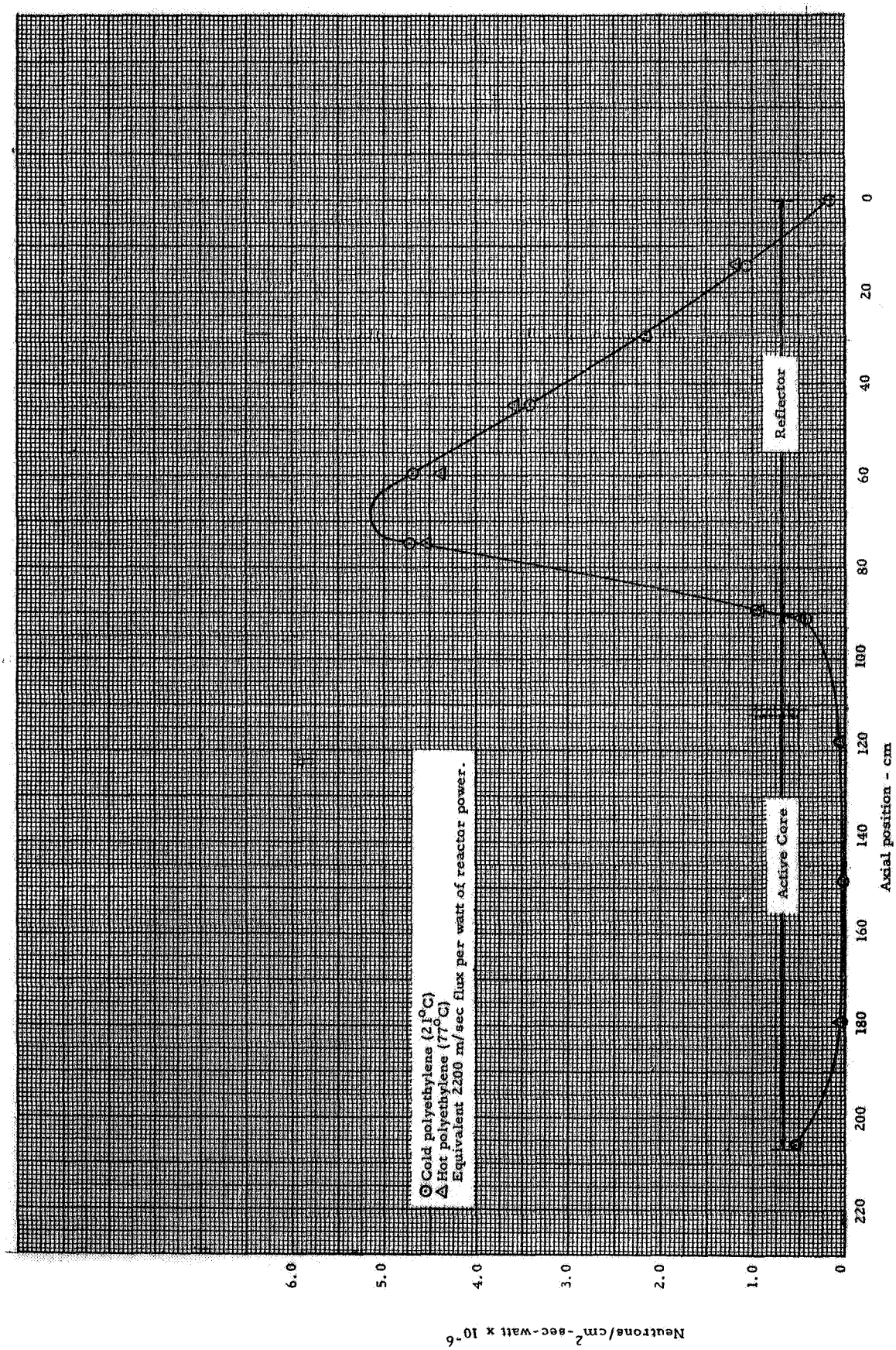

Fig. 7.14 Thermal neutron flux distribution, axial profile, hot CH_2

8.0 VARIABLE HYDROGEN EXPERIMENT

8.1 Description of Reactor

The variable hydrogen experiment was designed to simulate the various hydrogen density distributions that occur in an operating cavity reactor. The hydrogen density specifications were as given in Figure 8.1. Because of the very low density requirements in some regions, it was desirable to use a material less dense than polyethylene. It was decided to go to foamed polystyrene (CH) as the base structure and use that amount which would produce the density requirement for the least dense region (Region 4) in the void between the active core and cavity wall. The hydrogen densities for the other regions (Regions 1, 3, and 6) were then produced by adding polyethylene sheets between the polystyrene. The polystyrene was cut into several thin slabs 117 cm long and thus polyethylene could be placed between the slabs to increase the hydrogen densities over the desired region. Figure 8.2 shows an assembly of polystyrene and polyethylene which occupied 12% of the volume of the region between the active core and cavity wall. As can be seen here, the foam was cut into a swiss-cheese arrangement but was still sufficiently rigid to support the additional polyethylene and fill the void between the core and cavity wall. The plastic material was carefully weighed following the experiment and the weights are given in Table 8.1. It will be noted that all of the densities were very close to those proposed for this mockup experiment. Within the active core region, thin strips of polyethylene were placed on top of each of the fuel elements to achieve the desired low hydrogen density.

All other components were the same as previously described. All of the ducting and air flow channels used for the uniform hydrogen experiments (Sections 6.0 and 7.0) were removed for this experiment.

8.2 Initial Loading

It was initially anticipated that it would require about the same fuel loading for this experiment as for the uniform hydrogen experiments so no change was made to the fuel elements. They were loaded with 166 equivalent size 1.0 fuel sheets, and a total compliment of 208 fuel elements was required to fill the active core region, for a total loading of 89.6 kg of uranium.

Initial loading began with the polyethylene and polystyrene in the region between the active core and cavity wall, and with 86 fuel elements in the reactor. The loading of fuel elements then proceeded incrementally as shown in Table 8.2 and Figure 8.3 until there were 164 fuel elements in the reactor. At this point the reactor was critical and k-excess was 0.1136%Δk. There were approximately 70 kg of fuel in the reactor at this time.

It was obvious that a reduction in the number of fuel sheets per fuel element would be required before continuing the fuel loading. The remaining 44 fuel elements which had not yet been placed in the reactor were altered so that each contained 136 equivalent size 1.0 fuel sheets

instead of 166. The addition and dispersal of these lighter loaded fuel elements throughout the reactor was accomplished with the reactor critical. The final loading was 86.2 kg of uranium and k-excess was $2.203 \pm 0.049\%\Delta k$. The D_2O temperature was 21°C. Figure 8.4 shows the location of the various types of fuel elements in the reactor after the loading was completed.

8.3 Rod and Material Worth Measurements

8.3.1 Rod Worths

Several rod worth measurements were made during the course of this experiment as shown in Table 8.3. Where repeat measurements were available, the values were averaged and the standard error was calculated. The standard error was 2.2% or less which is considered excellent agreement.

8.3.2 Material Worths

The reactivity worth of several materials was measured with this reactor configuration. The results are given in Table 8.4. Polyethylene was determined to have a positive effect on reactivity from the center of the core to beyond 35 cm from the core center. However, near the outside of the core polyethylene is a poison so that in the outer 7 cm of the active core it was worth $-(3.792 \pm 0.130) \times 10^{-5}\%\Delta k/gm$. The core average worth of polyethylene was $+(1.217 \pm 0.105) \times 10^{-5}\%\Delta k/gm$.

The reactivity effects of type 6061 aluminum and magnesium were measured in the radial reflector at two positions for the purpose of evaluating the two metals as core structure material. It was considered that magnesium could be used as structural material in cavity reactors if a substantial savings in neutron absorption would result, compared to aluminum. These data indicate a reduction of a factor of two in absorption of neutrons per unit mass of the structural material if Mg were used instead of Al. The comparison was made on a mass basis since the two metals have approximately equal strength per unit mass.

Because of some uncertainty associated with the earlier teflon (CF_2) and carbon reactivity coefficients (Reference 2, page 52) within the active core, these measurements were repeated. A positive core average worth was measured for teflon in this heavily loaded core. The previous measurements, all in lightly loaded cores (22 to 28 kg), gave a worth of $-1.28 \times 10^{-5}\%\Delta k/gm$ whereas the value given in Table 8.4 shows a value of $+0.281 \times 10^{-5}\%\Delta k/gm$. However, quite different core loadings were involved. In the lightly loaded core, the absorption effect of the fluorine predominates and causes negative worth, but in the heavily loaded cores the small amount of moderation provided by fluorine apparently has a greater effect than the absorption thus its reactivity effect is positive.

Carbon worths were also positive in this 86 kg core, whereas carbon had previously been measured to be negative on the same lightly-loaded configuration as for the earlier teflon measurements. Carbon worth, however, goes negative at the outer edge of the active core as does polyethylene.

Several measurements have been made in the past to determine the worth of the beryllium in the radial reflector but the reactivity effects of the support plates on the end of the beryllium blocks was never measured. A single set of these support plates was worth -0.141 ± 0.005%Δk. There are 14 sets of these in the beryllium ring which would be worth -1.97 ± 0.02 %Δk. This reactivity worth is undoubtedly dependent on the total fuel loading and on other material, such as the stainless steel liner, polyethylene, etc., used in the reactor. The measurement was useful in pointing out that the hardware used on the ends of the beryllium blocks and any other materials (other than the beryllium itself) which were inserted in or removed from the radial reflector with the beryllium were a significant portion of the total reactivity effect.

The reactivity effect of table separation was also measured with this assembly. Excess reactivity was high and it was, therefore, convenient to make such a measurement at this time. The results are given in Table 8.5 and Figure 8.5. Previous measurements showed that with the table against the mechanical stops, the gap at the separation plane was 1.22 cm. The structural material in the cavity prevented the table from closing all the way, leaving an additional gap at the mechanical stops of 0.22 cm. The table separation at the closed position was, therefore, 1.44 cm which is the first point on the curve at a k-excess of 1.933%Δk. The average reactivity worth per cm was measured 0.550 ± 0.020%Δk which agrees with previous results (Reference 1, p. 80) and indicates that the worth of the gap is independent of the amount of fuel or other material in the cavity.

8.4 Power Distribution Measurements

Essentially all of the foil exposure runs were made with Actuators 1, 2, and 3 withdrawn, Actuators 4, 5, and 6 fully inserted and Actuator 7 about 8 cm withdrawn. The D_2O temperature was nominally 20°C.

8.4.1 Bare Catcher Foils

The catcher foil data obtained from this reactor configuration are shown in Table 8.6 and Figures 8.6 and 8.7. The table contains all of the catcher foils, including bare and cadmium covered foils. The axial profiles at the various radial positions within the cavity region, given in Figure 8.6, clearly show the effects of the heavy hydrogen density in Region 1. There was a significant depression in the power near the outer edge of the active core over this region. Near the cavity wall, the fission rate was enhanced (Note, the fuel region did not extend beyond 73 cm) in Region 1.

The hydrogen (polyethylene and polystyrene) acts as a flux trap for thermal neutron incident from the reflector, thus reducing the neutron flux that reaches the active core. The net effect is to suppress the flux in the core and enhance the flux around and at the cavity wall. This has been observed from calculations as discussed in Reference 1, p. 358, 359, and 370.

Figure 8.7 was produced by plotting the axial averages given in Figure 8.6. The volume weighted average specific power over the active core was 3.50 with respect to the value at the core center. The power in the outer cylindrical shell of the fuel was a factor of 9.3 above the core center specific power.

8.4.2 Uranium Cadmium Ratios

Very few cadmium covered catcher foils were exposed on this configuration but sufficient data were obtained to give an axial cadmium ratio profile at the radial center of the core and a radial profile at the axial center of the reactor. These data are given in Table 8.6 and Figures 8.8 and 8.9. At the core center the cadmium ratio was 1.66 and this increased to 9.94 at the outer edge of the fuel. At the ends of the core on the radial centerline, the cadmium ratios were 7.85 and 10.90, with the highest value being at the separation plane. This higher ratio at the separation plane is due to the void in the end reflector which simulates the exhaust nozzle. At the radial cavity wall on the axial centerline the cadmium ratio was 16.57.

8.5 Resonance Detector Measurements

8.5.1 Bare Gold Foil Data

A large number of gold foils, bare and cadmium covered, were exposed within the cavity and reflector regions of the variable hydrogen configuration. These data are given in Table 8.7. As usual, power normalizer foils were obtained from each foil exposure so that all of the resonance detector data could be power normalized to the same total reactor power level. The normalizer foil data along with the normalization factors are presented in Table 8.8. All of the gold data were normalized to Run 1101.

Figures 8.10 and 8.11 show the axial and radial profiles for the bare foils within the cavity region normalized to the center of the core. Each of the nine axial profiles was averaged by integrating under the curve and these averages were used to generate the radial curve given in Figure 8.11. About the same relative distribution was observed as for the catcher foils. The most dramatic effect of the hydrogen (polyethylene and polystyrene) was over Region 1 where the concentration was the heaviest. The outer edge of the active core experienced a significant decrease in neutron flux while a flux trapping effect occurred near and at the outer edge of the hydrogen. The reason for these changes in neutron flux distribution would be the same as given in Section 8.4.1.

The bare gold foil activity distributions within the reflector regions are presented in Figures 8.12 and 8.13. These data are for a power level of 19.6 watts which was the power for Run 1101. Both sets of curves appear to be as expected from previous results. A comparison with the cold, uniform polyethylene experiment shows no measurable change in the end reflector but about a 12% increase in the radial reflector. These data were compared to the same power base of 19.6 watts and only the points which had an accompanying cadmium covered foil at the same location were

compared. The comparison was also based on infinitely dilute foil activities as shown in Table 8.9. The gold activity distribution was not measured through the heavy hydrogen density in Region 1 but instead traversed regions 3, and 4, with an average density of 0.6×10^{21} H/cc. This density is much lower than the 2×10^{21} in the cold, uniform hydrogen experiment. Thus, the poorer flux trapping of the hydrogen was probably responsible for the higher flux in the reflector.

8.5.2 Bare Indium Foil Data

Both bare and cadmium covered indium foils were exposed on this reactor in the center of the active core and in the end and radial reflector. The data obtained are given in Table 8.10. These data were obtained with a 66 degree sector of beryllium removed from the top portion of the radial reflector and the fuel loading reduced in 28 fuel elements position as follows:

Position Number

1-2, 2-7, 2-9, 3-2, 3-12, 4-5, 5-2, 5-12, 6-5, 6-7, 7-2, 7-9, 7-11, 8-7, 9-3, 9-6, 10- 2, 10-9, 11-5, 11-12, 12-2, 12-4, 13-1, 14-1, 14-15, 15-5, 15-11, 16-1

Ten of these fuel elements contained 42 sheets and 19 contained 43 sheets of fuel. The total reduction in fuel was 10.8 kg which gave a core loading of 75.4 kg of uranium.

The bare indium foil data within the active core were normalized to the center of the core. The resulting axial profile through the core center is shown in Figure 8.14. The curve average was 1.101 with peaks at the ends of the core being from 1.60 to 1.65 above the core center. This traverse had a shape similar to that obtained with gold foils.

The indium foil activity distribution within the reflector regions is given in Figures 8.15 and 8.16. Both bare and cadmium covered foil results are shown in these figures. A dashed line was used through the cadmium covered data in the end reflector because of the uncertainty of the curve. The curve which was drawn represents approximately the distribution obtained for cadmium covered gold in the end reflector.

8.5.3 Bare Manganese Foil Data

Manganese foils were also exposed at the same locations and with the same reactor configuration as for the indium foils reported in the previous section. The results are given in Table 8.11. The normalized axial profile through the center of the core is shown in Figure 8.17. The curve average was 1.491 with peaks at the separation plane and back of the core being 5.3 and 4.1, respectively, above the center of the core. The manganese bare activity was much more peaked at the core ends than was observed for gold or indium.

The foil activity distribution in the radial and end reflectors is presented in Figures 8.18 and 8.19. Two sets of bare foil data were obtained in the radial reflector which show quite different results. No

changes were made to the reactor between these measurements. The exact reason for the difference is not known. The cadmium covered foil data in the reflectors were also included in these figures. The activities were low and hard to distinguish on the scale needed for the bare foil activities.

8.5.4 Gold Cadmium Ratios

Where both bare and cadmium covered gold foils were available, cadmium ratios were calculated. The foil counts were reduced to infinitely dilute activities in order to produce corrected cadmium ratios and these data are presented in Table 8.12. The cadmium ratios within the cavity region are shown in Figure 8.20. In general, all of the data fall on a smooth curve (within ±5% or less) which is normal for this type of measurement. The high hydrogen concentration in Region 1 had a most noticeable effect, as was expected from the bare foil data given in Figure 8.10.

The cadmium ratios in the reflectors are shown graphically in Figure 8.21. The distributions were quite normal with the radial reflector showing the higher cadmium ratios.

8.5.5 Indium Cadmium Ratios

Table 8.13 contains the indium cadmium ratios and the infinitely dilute foil activities for the bare and cadmium covered foils. At the core center, the ratio was 1.059. This increased to 1.437 and 1.358 at the separation plane and back of the core, respectively. The higher value at the separation plane was due to the exhaust nozzle hole in the end reflector.

The cadmium ratios in the reflectors are presented in Figure 8.22. The point nearest the separation plane in the radial reflector appears to be in error. The bare foil was too low in activity which resulted in a low cadmium ratio.

8.5.6 Manganese Cadmium Ratios

The manganese cadmium ratios are given in Table 8.14. Included in this table are the infinitely dilute foil activities. The approximate correction to obtain infinitely dilute activity was accomplished by merely applying a 5% increase to the cadmium covered foil activity and adding the increase to the bare foil activity. The cadmium ratio at the center of the core was 1.49. At the separation plane, this ratio increased to 7.03 and at the other end of the core the ratio was 5.00. The difference at the ends of the core was due primarily to the exhaust nozzle at the separation plane.

Figure 8.23 shows the cadmium ratios in the reflectors. The two sets of data in the radial reflector are a result of this repeat bare foil measurements, shown in Figure 8.18.

8.5.7 Comparison of Cadmium Ratios and Spectral Shape

As discussed in Section 6.5, a 1/E flux spectrum would give gold and indium cadmium ratios that were nominally the same, and for manganese the Cd-ratio less 1.0 should be 13 to 14 times the similar value for Au or In. However, the large 1/v component of the manganese resonant integral makes it difficult to infer the shape of the flux if the above ratio does not apply. Table 8.16 lists the cadmium ratios determined for the three detectors. The results indicate a nominal 1/E flux spectrum between the gold and indium resonances except deep into the reflector or near the core center. Manganese comparisons also tend to extend this contention up to the 337 ev manganese resonance. Note that the data is sparse, and appears to be of poorer than average quality, but is good enough to corroborate the results of computer calculations that show that a 1/E spectrum exists only in a limited region of the reactor.

8.6 Thermal Neutron Flux

8.6.1 Gold Results

Thermal flux was calculated from the gold data where both the bare and cadmium covered foil activities were available. These results are given in Table 8.15, and are shown graphically in Figures 8.24, 8.25, and 8.26. It will be noted from the table that some thermal flux values were calculated from an extrapolated cadmium covered foil activity. This was done to help fill in some of the points and give more complete curves for Figures 8.25 and 8.26.

There is evidence from these data as well as the catcher foil data that the thermal flux depression does not penetrate very far beyond the outer boundary of the core. It would seem reasonable to think that this reduced flux would be observed well into the fueled region yet the data show no such penetration. The reason for this is believed to be due to the contribution of neutrons from the end reflector where there is no hydrogen barrier between the D_2O and the active core. The hydrogen shields the outer edge of the fueled region from flux incident from the radial reflector and outer portions of the end reflector. But little of this flux actually penetrates to the axial centerline. Therefore, the depression caused by the hydrogen is rapidly attenuated and virtually disappears a small distance (about 10 cm) from the outer edge of the fuel.

8.6.2 Indium and Manganese Results

The indium and manganese thermal flux values are shown in Table 8.16, and the results from the gold foils are listed for comparison. The comparison is generally poor (±10%, with some points much worse) and there was even a lack of a consistent trend for the indium results to be higher than the gold results, although the low lying resonance of In would yield higher results if cross section corrections were not made (see Section 6.5). The manganese and gold results generally are in agreement except deep within the reflector.

TABLE 8.1

Summary of Hydrogen Densities Actually Used in Variable Hydrogen Experiment

Region No.	Polyethylene (gm)	Polystyrene (gm)	Region Volume ($cm^3 \times 10^{-5}$)	Hydrogen Density atoms/cc $\times 10^{-21}$	
				Actual	Desired
1	14174	3870	4.448	3.14	3.0
2	0	0	0	0	0
3	1797	4024	4.893	0.696	0.75
4	0	3712	4.003	0.429	0.40
5	604.9	0	5.338	0.0972	0.10
6	535	3870	4.448	0.506	0.50
7	427.6	0	2.669	0.1375	0.15

TABLE 8.2

Initial Loading of Variable

Hydrogen Reactor Configuration

Increment	Total No. Elements	Channel No. 1 CPM	Channel No. 1 CPMo/CPM	Channel No. 2 CPM	Channel No. 2 CPMo/CPM	Channel No. 3 CPM	Channel No. 3 CPMo/CPM	Average CPMo/CPM	Rod Positions
decay corrected		793		819		617			In
count rate zeros		883		927		690			Out
1	86	6628	0.120	4817	0.170	5114	0.121	0.137	In
		10328	0.0855	7513	0.123	7898	0.0874	0.0986	Out
2	92	7347	0.108	5382	0.152	5609	0.110	0.123	In
		11844	0.0746	8643	0.107	8926	0.0773	0.0864	Out
3	98	8103	0.0979	5753	0.142	6043	0.102	0.114	In
		13247	0.0667	9663	0.0959	9905	0.0697	0.0774	Out
4	115	11203	0.0708	8061	0.102	8444	0.0731	0.0820	In
		22312	0.0396	15922	0.0582	16397	0.0421	0.0421	Out
5	132	14638	0.0542	10455	0.0783	10932	0.0564	0.0630	In
		37215	0.0237	26946	0.0344	27161	0.0254	0.0278	Out
6	149	19594	0.0405	14086	0.0581	14643	0.0421	0.0469	In
		81545	0.0108	57929	0.0160	58432	0.0129	0.0129	Out
7	164	28781	0.0276	20476	0.0400	21268	0.0290	0.0322	In
		Reactor critical with 0.1136%Δk excess							Out

TABLE 8.3

Rod Worths - Variable Hydrogen Experiment

Run No.	Actuator Combinations and Reactivity Worths (%Δk)					
	1,2,7	3 & 6	1 to 6 (17 rods)	1 to 7 (20 rods)	1	1 & 2
393		-1.422				
394			-3.663			
395			-3.610			
396			-3.681			
397			-3.616			
398			-3.606			
399				-4.034		
400				-4.054		
401				-4.055		
402				-4.066		
403					-0.6707 (shadowed by 2 and 3)	
411				-4.019		
414	-2.004					
415					-0.8060 (unshadowed)	
418				-3.9864		
420				-4.2616		
421						-1.623
422						-1.623
Averages			-3.635±.034	-4.068±.090		-1.623±.000

TABLE 8.4

Summary of Material Worth Measurement

Variable Hydrogen and a Stainless Steel Liner in the Cavity

Material	Location	Material Worth %Δk/gm
Polyethylene	79.8 gm in Region 7 (core) 222.2 gm in Region 5 (core)	$-(2.9 \pm 1.7) \times 10^{-5}$
Polyethylene	Core average	$+(1.217 \pm 0.105) \times 10^{-4}$
Polyethylene	Outer row of fuel elements (59.7 cm from core center)	$-(3.792 \pm 0.130) \times 10^{-4}$
Polyethylene	34.7 cm from core center	$+(2.377 \pm 0.105) \times 10^{-4}$
Teflon	Core average	$+(0.281 \pm 0.035) \times 10^{-5}$
Carbon	5.4 cm from core center	$+(0.516 \pm 0.039) \times 10^{-5}$
Carbon	34.5 cm from core center	$+(0.231 \pm 0.039) \times 10^{-5}$
Aluminum (6061) (1)	On wet surface of cavity wall	$-(1.797 \pm 0.367) \times 10^{-5}$
Aluminum (6061) (1)	7.6 cm from wet surface of cavity wall	$-(4.018 \pm 0.141) \times 10^{-5}$
Magnesium (1)	On wet surface of cavity wall	$-(0.745 \pm 0.372) \times 10^{-5}$
Magnesium (1)	7.6 cm from wet surface of cavity wall	$-(2.924 \pm 0.142) \times 10^{-5}$
End plates on Be blocks	At normal position but removed from Be block	$-(0.141 \pm 0.005)$ (2)

(1) Aluminum and magnesium of equal mass were employed, and the displacement of D_2O is included in the effect of the measurement.

(2) Worth of two plates or the hardware on the ends of a Be block.

TABLE 8.5

Table Separation Measurement

Table Position (cm)	k-excess (1) (%Δk)	Reactivity Difference (%Δk)	Worth/cm (2) (%Δk)
1.44	1.933	0	--
2.37	1.418	0.510	0.548
3.65	0.519	1.409	0.638
4.86	0.029	1.899	0.555
1.74	1.758	0.170	0.567
1.44	1.924	0	--
4.27	0.338	1.590	0.562
2.37	1.447	0.481	0.517
		Average (3)	0.550±0.020

(1) k-excess is based on following rod worths

All rods = -4.034%Δk

Act 1 = -0.806%Δk

Act 1,2,7 = -2.004%Δk

(2) Based on k-excess of 1.928%Δk at 1.44 cm and each position referenced to 1.44 cm.

(3) Average does not include the 0.638%Δk/cm value.

TABLE 8.6

Catcher Foil Data

Variable Hydrogen

Foil No.	Type	Location Radial (cm)	Location Axial (cm)	Normalized Count	Local to Foil (X)
1	Bare	0	90.8	35770	5.916
2	Bare	0	102.8	14780	2.444
3	Bare	0	118.0	8512	1.408
4	Bare	0	133.3	6667	1.103
5	Bare	0	148.5	6046	1.000 (X)
6	Bare	0	163.8	6438	1.065
7	Bare	0	179.0	8183	1.353
8	Bare	0	194.2	14650	2.423
9	Bare	0	206.9	50428	8.340
10	Bare	30.5	90.8	36639	6.060
11	Bare	30.5	102.8	15952	2.638
12	Bare	30.5	118.0	9293	1.537
13	Bare	30.5	133.3	7349	1.215
14	Bare	30.5	148.5	7610	1.259
15	Bare	30.5	163.8	8338	1.379
16	Bare	30.5	179.0	9652	1.596
17	Bare	30.5	194.2	15270	2.526
18	Bare	30.5	206.9	44009	7.279
19	Bare	45.7	90.8	41255	6.823
20	Bare	45.7	102.8	18152	3.002
21	Bare	45.7	118.0	14031	2.321
22	Bare	45.7	133.3	13069	2.161
23	Bare	45.7	148.5	14729	2.436
24	Bare	45.7	163.8	15219	2.517
25	Bare	45.7	179.0	14746	2.439
26	Bare	45.7	194.2	19727	3.264
27	Bare	45.7	206.9	46638	7.717
28	Bare	53.3	90.8	45974	7.604
29	Bare	53.3	102.8	27359	4.525
30	Bare	53.3	118.0	20418	3.377
31	Bare	53.3	133.3	22021	3.642
32	Bare	53.3	148.5	23201	3.837
33	Bare	53.3	163.8	25499	4.217
34	Bare	53.3	179.0	23686	3.917
35	Bare	53.3	194.2	29660	4.905
36	Bare	53.3	206.9	60622	10.03
37	Bare	61.0	90.8	78714	13.02
38	Bare	61.0	102.8	48246	7.979
39	Bare	61.0	118.0	39715	6.568
40	Bare	61.0	133.3	55411	9.164
41	Bare	61.0	148.5	49781	8.233

TABLE 8.6
(Continued)

Foil No.	Type	Locaion Radial (cm)	Axial (cm)	Normalized Count	Local to Foil (X)
42	Bare	61.0	163.8	58718	9.711
43	Bare	61.0	179.0	61378	10.15
44	Bare	61.0	194.2	62542	10.34
45	Bare	61.0	206.9	81033	13.40
46	Bare	73.0	90.8	122947	20.33
47	Bare	73.0	102.8	100714	16.66
48	Bare	73.0	118.0	85278	14.10
49	Bare	73.0	133.3	83360	13.79
50	Bare	73.0	148.5	78926	13.05
51	Bare	73.0	163.8	76795	12.70
52	Bare	73.0	179.0	84146	13.92
53	Bare	73.0	194.2	90603	14.98
54	Bare	73.0	206.9	100583	16.64
55	Bare	79.4	90.8	145929	24.14
56	Bare	79.4	102.8	150221	24.85
57	Bare	79.4	118.0	123912	20.49
58	Bare	79.4	133.3	99264	16.42
59	Bare	79.4	148.5	98303	16.26
60	Bare	79.4	163.8	92923	15.37
61	Bare	79.4	179.0	100501	16.62
62	Bare	79.4	194.2	94389	15.61
63	Bare	79.4	206.9	107297	17.75
64	Bare	85.1	90.8	152738	25.26
65	Bare	85.1	102.8	137217	22.69
66	Bare	85.1	118.0	137674	22.77
67	Bare	85.1	133.3	115980	19.18
68	Bare	85.1	148.5	108548	17.95
69	Bare	85.1	163.8	94175	15.58
70	Bare	85.1	179.0	108803	17.99
71	Bare	85.1	194.2	104346	17.26
72	Bare	85.1	206.9	108949	18.02
73	Bare	90.8	90.8	147483	24.39
74	Bare	90.8	102.8	142727	23.61
75	Bare	90.8	118.0	125536	20.76
76	Bare	90.8	133.3	106587	17.63
77	Bare	90.8	148.5	103053	17.04
78	Bare	90.8	163.8	101351	16.76
79	Bare	90.8	179.0	103732	17.16
80	Bare	90.8	194.2	102814	17.00
81	Bare	90.8	206.9	103340	17.09

TABLE 8.6

(Continued)

Foil No.	Type	Location Radial (cm)	Location Axial (cm)	Normalized Count	Cadmium Ratio
Run 1106					
1	Cd	0	90.8	4556	7.85
2	Cd	0	118.0	3841	2.22
3	Cd	0	148.5	3638	1.66
4	Cd	0	179.0	3782	2.16
5	Cd	0	206.9	4626	10.90
6	Cd	30.5	148.5	3985	1.91
7	Cd	61.0	148.5	5010	9.94
8	Cd	90.8	148.5	6221	16.57

TABLE 8.7

Gold Foil Data

Variable Hydrogen

Foil No.	Foil Type	Location Radial (cm)	Location Axial (cm)	Foil Weight (gm)	Specific Activity d/m/gm x 10^{-6}	Local to Foil (X)
Run 1101						
1	Bare	0	89.4	0.0210	2.714	2.042
2	Bare	0	74.9	0.0186	7.272	5.472
3	Bare	0	59.6	0.0172	6.168	4.641
4	Bare	0	44.4	0.0187	4.343	3.268
5	Bare	0	29.1	0.0142	2.653	1.996
6	Bare	0	13.9	0.0199	1.329	1.000
7	Bare	0	0	0.0194	0.184	0.138
8	Bare	107.7	151.1	0.0207	6.064	4.563
9	Bare	123.0	151.1	0.0198	4.680	3.521
10	Bare	138.0	151.1	0.0169	3.116	2.345
11	Bare	153.5	151.1	0.0161	1.937	1.457
12	Bare	168.7	151.1	0.0193	1.013	0.762
13	Bare	183.9	151.1	0.0149	0.231	0.174
14	Bare	73.0	90.8	0.0167	4.601	3.462
15	Bare	73.0	102.8	0.0150	4.251	3.199
16	Bare	73.0	118.0	0.01695	3.952	2.974
17	Bare	73.0	133.3	0.0194	3.720	2.799
18	Bare	73.0	148.5	0.0216	3.585	2.697
19	Bare	73.0	163.8	0.0163	3.738	2.813
20	Bare	73.0	179.0	0.0213	3.583	2.696
21	Bare	73.0	194.2	0.0161	3.869	2.911
22	Bare	73.0	206.9	0.0125	4.144	3.118
23	Bare	79.4	90.8	0.0204	4.858	3.655
24	Bare	79.4	102.8	0.0189	5.070	3.815
25	Bare	79.4	118.0	0.0211	4.707	3.542
26	Bare	79.4	133.3	0.0175	4.392	3.305
27	Bare	79.4	148.5	0.0184	4.059	3.054
28	Bare	79.4	163.8	0.0192	4.073	3.065
29	Bare	79.4	179.0	0.0191	4.001	3.011
30	Bare	79.4	194.2	0.0187	3.925	2.953
31	Bare	79.4	206.9	0.0139	4.124	3.103
32	Bare	85.1	90.8	0.0152	4.900	3.687
33	Bare	85.1	102.8	0.0186	5.020	3.777
34	Bare	85.1	118.0	0.0167	4.885	3.676
35	Bare	85.1	133.3	0.0158	4.512	3.395
36	Bare	85.1	148.5	0.0166	4.357	3.278
37	Bare	85.1	163.8	0.0169	4.143	3.117
38	Bare	85.1	179.0	0.0172	4.126	3.105
39	Bare	85.1	194.2	0.0182	3.563	2.681

TABLE 8.7
(Continued)

Foil No.	Foil Type	Location Radial (cm)	Location Axial (cm)	Foil Weight (gm)	Specific Activity d/m/gm x 10^{-6}	Local to Foil (X)
Run 1101 (Cont'd)						
40	Bare	85.1	206.9	0.0182	4.099	3.084
41	Bare	90.8	90.8	0.0211	5.152	3.877
42	Bare	90.8	102.8	0.0159	5.439	4.093
43	Bare	90.8	118.0	0.0174	4.945	3.721
44	Bare	90.8	133.3	0.0185	4.379	3.295
45	Bare	90.8	148.5	0.0159	4.319	3.250
46	Bare	90.8	163.8	0.0136	4.325	3.254
47	Bare	90.8	179.0	0.0208	4.116	3.097
49	Bare	90.8	194.2	0.0152	3.666	2.758
48	Bare	90.8	206.9	0.0152	4.273	3.215
50	Cd	0	118.0	0.0139	1.350	--
51	Cd	0	148.5	0.0175	1.210	--
52	Cd	0	179.0	0.0129	1.322	--
53	Cd	30.5	90.8	0.0131	1.717	--
54	Cd	30.5	148.5	0.0177	1.278	--
55	Cd	30.5	206.9	0.0143	1.698	--
56	Cd	61.0	118.0	0.0210	1.646	--
57	Cd	61.0	148.5	0.0189	1.658	--
58	Cd	61.0	179.0	0.0179	1.680	--
59	Bare	93.2	151.1	0.0175	5.220	3.928
Run 1102						
1	Bare	30.5	90.8	0.0175	2.289	1.722
2	Bare	30.5	102.8	0.0184	1.588	1.195
3	Bare	30.5	118.0	0.0191	1.481	1.114
4	Bare	30.5	133.3	0.0164	1.417	1.066
5	Bare	30.5	148.5	0.0155	1.463	1.101
6	Bare	30.5	163.8	0.0185	1.436	1.081
7	Bare	30.5	179.0	0.0193	1.459	1.098
8	Bare	30.5	194.2	0.0157	1.733	1.304
9	Bare	30.5	206.9	0.0175	2.507	1.886
10	Bare	45.7	90.8	0.0155	2.551	1.919
11	Bare	45.7	102.8	0.0176	1.842	1.386
12	Bare	45.7	118.0	0.0162	1.764	1.327
13	Bare	45.7	133.3	0.0151	1.723	1.246
14	Bare	45.7	148.5	0.0146	1.725	1.298
15	Bare	45.7	163.8	0.0176	1.680	1.264
16	Bare	45.7	179.0	0.0200	1.666	1.254
17	Bare	45.7	194.2	0.0180	1.910	1.437
18	Bare	45.7	206.9	0.0163	2.783	2.094
19	Bare	53.3	90.8	0.0182	2.767	2.082

TABLE 8.7

(Continued)

Foil No.	Type	Location Radial (cm)	Location Axial (cm)	Foil Weight (gm)	Specific Activity d/m/gm x 10^{-6}	Local to Foil (X)
Run 1102 (Cont'd)						
20	Bare	53.3	102.8	0.0203	2.024	1.523
21	Bare	53.3	118.0	0.0123	2.079	1.564
22	Bare	53.3	133.3	0.0198	1.817	1.367
23	Bare	53.3	148.5	0.0210	1.849	1.391
24	Bare	53.3	163.8	0.0142	2.034	1.530
25	Bare	53.3	179.0	0.0182	1.996	1.502
26	Bare	53.3	194.2	0.0166	2.207	1.661
27	Bare	53.3	206.9	0.0158	2.953	2.222
28	Bare	61.0	90.8	0.0156	3.278	2.466
29	Bare	61.0	102.8	0.0206	2.570	1.934
30	Bare	61.0	118.0	0.0174	2.567	1.932
31	Bare	61.0	133.3	0.0184	2.829	2.129
32	Bare	61.0	148.5	0.0184	2.865	2.156
33	Bare	61.0	163.8	0.0165	2.881	2.168
34	Bare	61.0	179.0	0.0162	2.907	2.187
35	Bare	61.0	194.2	0.0140	3.053	2.297
36	Bare	61.0	206.9	0.0171	3.404	2.561
37	Cd	73.0	90.8	0.01355	2.004	
38	Cd	73.0	118.0	0.0205	1.883	
39	Cd	73.0	148.5	0.01625	1.991	
40	Cd	73.0	179.0	0.0180	1.931	
41	Cd	73.0	206.9	0.0190	1.836	
42	Cd	90.8	90.8	0.0178	1.751	
43	Cd	90.8	118.0	0.0196	2.042	
44	Cd	90.8	148.5	0.0134	2.248	
45	Cd	90.8	179.0	0.0171	2.040	
46	Cd	90.8	206.9	0.0158	1.863	
47	Cd	123.0	151.1	0.0163	0.160	
48	Cd	153.5	151.1	0.0202	0.004	
49	Cd	0	206.9	0.0136	1.534	
50	Cd	0	90.8	0.0149	1.615	
51	Cd	0	59.6	0.0189	0.425	
52	Cd	0	29.1	0.0175	0.016	
53	Bare	79.4	90.8	0.01395	5.166	3.887
54	Bare	79.4	120.8	0.0156	4.974	3.743
55	Bare	79.4	118.0	0.01165	4.892	3.681
56	Bare	79.4	133.3	0.01975	4.156	3.127
57	Bare	79.4	148.5	0.0167	4.065	3.059
58	Bare	79.4	163.8	0.0136	4.181	3.146
59	Bare	79.4	179.0	0.0191	3.956	2.977
60	Bare	79.4	194.2	0.0172	4.102	3.087
61	Bare	79.4	206.9	0.0133	4.234	3.186

TABLE 8.7
(Continued)

Foil No.	Foil Type	Location Radial (cm)	Location Axial (cm)	Foil Weight (gm)	Specific Activity d/m/gm x 10^{-6}	Local to Foil (X)
Run 1103						
1	Bare	0	90.8	0.0177	2.265	1.704
2	Bare	0	102.8	0.0199	1.520	1.144
3	Bare	0	118.0	0.0163	1.415	1.065
4	Bare	0	133.3	0.01615	1.303	0.980
5	Bare	0	148.5	0.0160	1.329	1.000 (X)
6	Bare	0	163.8	0.0169	1.311	0.986
7	Bare	0	179.0	0.0161	1.365	1.027
8	Bare	0	194.2	0.0141	1.631	1.227
9	Bare	0	206.9	0.0153	2.517	1.894
10	Cd	0	74.9	0.0174	1.622	
11	Cd	0	44.4	0.0152	0.071	
12	Cd	30.5	118.0	0.0187	1.308	
13	Cd	30.5	179.0	0.0183	1.273	
14	Cd	45.7	102.8	0.0144	1.546	
15	Cd	45.7	148.5	0.0130	1.484	
16	Cd	45.7	194.2	0.0172	1.492	
17	Cd	61.0	90.8	0.0163	1.768	
18	Cd	61.0	206.9	0.0201	1.683	
19	Cd	73.0	133.3	0.0157	1.996	
20	Cd	73.0	163.8	0.0185	1.888	
21	Cd	79.4	102.8	0.0145	2.079	
22	Cd	79.4	148.5	0.0148	2.132	
23	Cd	79.4	194.2	0.0159	1.998	
24	Cd	90.8	133.3	0.0164	2.066	
25	Cd	90.8	163.8	0.0153	2.097	
26	Cd	107.7	151.1	0.0161	0.853	
27	Cd	138.2	151.1	0.0154	0.022	
Run 1104						
1	Bare	0	82.5	0.0185	5.848	4.400
2	Bare	0	67.2	0.0187	7.017	5.280
3	Bare	0	52.0	0.0208	5.144	3.871
4	Bare	100.1	151.1	0.0164	6.547	4.926
5	Bare	115.4	151.1	0.01995	5.374	4.044
6	Bare	130.16	151.1	0.0168	3.853	2.899
Run 1105						
1	Cd	0	89.4	0.0154	1.620	
2	Cd	45.7	90.8	0.0178	1.613	
3	Cd	45.7	206.9	0.0196	1.591	

TABLE 8.7

(Continued)

Foil No.	Foil Type	Location Radial (cm)	Location Axial (cm)	Foil Weight (gm)	Specific Activity d/m/gm x 10^{-6}	Local to Foil (X)
Run 1105 (Cont'd)						
4	Cd	61.0	102.8	0.0203	1.660	
5	Cd	61.0	194.2	0.0168	1.741	
6	Cd	73.0	102.8	0.0152	2.017	
7	Cd	73.0	194.2	0.0155	1.978	
8	Cd	79.4	102.8	0.0163	2.066	
9	Cd	79.4	163.8	0.0164	2.012	
10	Cd	79.4	194.2	0.0170	1.935	
11	Cd	85.1	90.8	0.0180	1.783	
12	Cd	85.1	118.0	0.0188	2.061	
13	Cd	85.1	179.0	0.0136	2.159	
14	Cd	85.1	206.9	0.0169	1.786	
15	Cd	93.2	151.1	0.0150	2.142	
Run 1106						
1	Cd	53.3	133.3	0.0160	1.508	
2	Cd	53.3	163.8	0.0164	1.526	
3	Cd	61.0	102.8	0.0177	1.683	
4	Cd	61.0	194.2	0.0168	1.699	
5	Cd	90.8	102.8	0.0183	1.975	
6	Cd	90.8	194.2	0.0148	1.998	

TABLE 8.8

Power Normalization Factors

Variable Hydrogen Experiment

Run	Time	Decay Time (min)	Decay Factor	Activity (CPM)	Corrected Activity (CPM) (1)		Norm. Factor
1101	1632.00	28.01	0.541	514907	278565		
	1634.27	30.28	0.583	477344	278292		
	1636.41	32.42	0.624	447032	278948		
					278602		1.000
1102	1314.90	56.96	1.167	237338	276973		
	1316.90	58.96	1.217	227430	276782		
	1318.90	60.96	1.269	218644	277459		
					277071	$\frac{278602}{277071}$ =	1.006
1103	1554.00	35.93	0.693	402079	278641		
	1556.23	38.16	0.739	376835	278481		
	1558.01	39.94	0.776	358424	278137		
					278419	$\frac{278602}{278419}$ =	0.997
1104	1309.80	48.44	0.963	291111	280340		
	1311.80	50.44	1.010	278228	281010		
	1313.80	52.44	1.056	265043	279885		
					280411		
Counting system calibration correction 2.33/2.31 x 28041 =						$\frac{278602}{282839}$ =	0.985
1105	1550.48	43.47	0.851	329357	280283		
	1552.60	45.59	0.899	312915	281311		
	1554.35	47.34	0.938	298975	280439		
					280677	$\frac{278602}{280677}$ =	0.993
1106	1259.30	53.54	1.084	256138	277654		
	1301.30	55.54	1.132	244867	277189		
	1303.50	57.74	1.188	233639	277563		
					277469		
Counting system calibration correction 2.33/2.31 x 277469 =						$\frac{278602}{279871}$ =	0.995
1107	1341.50	56.39	1.149	243615	279914		
	1343.30	58.19	1.197	234181	280315		
	1345.00	59.89	1.244	227128	282547		
					280925		
Counting system calibration correction 2.34/2.31 x 280925 =						$\frac{278602}{284573}$ =	0.979
1108	1530.00	43.89	0.861	325296	280080		
	1531.50	45.39	0.894	312859	279696		
	1533.00	46.89	0.928	301862	280128		
					279968	$\frac{278602}{279968}$ =	0.995

TABLE 8.8

(Continued)

Run	Time	Decay Time (min)	Decay Factor	Activity (CPM)	Corrected Activity (CPM) (1)		Norm. Factor
1109	1235.22	48.69	0.973	293019	285107		
	1236.84	50.31	1.001	281647	281929		
	1238.47	51.94	1.043	271187	282848		
				Av =	283295	$\frac{278602}{283295}$	0.983
1110	1433.05	41.19	0.803	348789	280078		
	1435.25	43.39	0.850	329596	280157		
	1436.90	45.04	0.886	315392	279437		
				Av =	279891	$\frac{278602}{279891}$	0.995
1111	1552.90	30.03	0.578	478355	276489		
	1554.94	32.07	0.616	448743	276426		
	1556.88	34.01	0.655	423255	277232		
				Av =	276716	$\frac{278602}{276716}$	1.007

(1) Corrected to shutdown time

TABLE 8.9

Comparison of Bare Gold Foil

Data in the Radial Reflector Variable Hydrogen Experiment

Location		Infinitely dilute foil activity - d/m/gm at 19.6 watts		
Radial (cm)	Axial (cm)	Uniform Hydrogen (cold)	Variable Hydrogen	Variable H / Uniform H
0	89.4	3.680	4.036	1.097
0	74.9	8.664	8.585	0.991
0	59.6	6.730	6.510	0.967
0	44.4	4.402	4.398	0.999
0	29.1	2.743	2.664	0.971
93.2	151.1	6.582	6.827	1.027
107.7	151.1	6.043	6.767	1.120
123.0	151.1	4.127	4.810	1.165
138.2	151.1	2.753	3.132	1.138
153.5	151.1	1.724	1.940	1.125

TABLE 8.10

Indium Foil Data

Variable Hydrogen Experiment

Foil No.	Type	Location Radial (cm)	Location Axial (cm)	Foil Weight (gm)	Specific Activity d/m/gm x 10^{-8}	Local to Foil (X)
Run 1107						
404	Bare	0	90.8	0.00229	4.682	1.601
492	Bare	0	102.8	0.00222	3.538	1.210
620	Bare	0	118.0	0.00231	3.083	1.054
632	Bare	0	133.3	0.00231	2.943	1.007
642	Bare	0	148.5	0.00229	2.924	1.000 (X)
664	Bare	0	163.8	0.00228	2.914	0.997
729	Bare	0	179.0	0.00231	2.930	1.002
763	Bare	0	194.2	0.00233	3.258	1.114
812	Bare	0	206.9	0.00228	4.892	1.673
Run 1108						
11	Cd	0	90.8	0.00584	3.510	
12	Cd	0	118.0	0.00518	3.509	
13	Cd	0	148.5	0.00512	3.376	
14	Cd	0	179.0	0.00649	3.157	
15	Cd	0	206.9	0.00515	3.479	
Run 1109						
404	Bare	0	89.4	0.00229	10.07	3.444
492	Bare	0	74.9	0.00222	14.41	4.928
620	Bare	0	59.6	0.00231	10.23	3.499
632	Bare	0	44.4	0.00230	6.863	2.347
11	Bare	0	29.1	0.00584	4.056	1.387
12	Bare	0	13.9	0.00518	2.008	0.687
13	Bare	0	0	0.00512	0.252	0.086
642	Bare	93.2	151.1	0.00229	5.291	1.810
664	Bare	107.7	151,1	0.00228	14.60	4.993
729	Bare	123.0	151.1	0.00231	12.17	4.162
763	Bare	138.2	151.1	0.00233	8.470	2.897
14	Bare	153.5	151.1	0.00649	5.430	1.857
15	Bare	168.7	151.1	0.00515	2.699	0.923
17	Bare	183.9	151.1	0.00740	0.379	0.130

TABLE 8.10

(Continued)

Foil No.	Foil Type	Location Radial (cm)	Location Axial (cm)	Foil Weight (gm)	Specific Activity d/m/gm x 10^{-8}	Local to Foil (X)
Run 1110						
812	Cd	0	89.4	0.00228	3.087	
18	Cd	0	59.6	0.00510	1.054	
19	Cd	0	29.1	0.00679	0.0353	
20	Cd	93.2	151.1	0.00519	4.247	
21	Cd	123.0	151.1	0.00562	0.508	
22	Cd	153.5	151.1	0.00516	0.0161	
Run 1111						
822	Cd	0	89.4	0.00228	3.149	
29	Cd	0	59.6	0.00230	0.813	

Note: The light weight foils were all 0.625 cm diameter foils and the heavy foil were 1.429 cm in diameter. Foil activities are corrected to reactor shutdown time.

TABLE 8.11

Manganese Foil Data

Variable Hydrogen Experiment

Foil No.	Foil Type	Location Radial (cm)	Location Axial (cm)	Foil Weight (gm)	Specific Activity d/m/gm x 10^{-7}	Local to Foil (X)
Run 1107						
3	Bare	0	89.4	0.04150	1.407	5.673
5	Bare	0	74.9	0.04255	6.480	26.13
8	Bare	0	59.6	0.04304	6.627	26.72
9	Bare	0	44.4	0.04270	4.833	19.49
10	Bare	0	29.1	0.04586	2.808	11.32
11	Bare	0	13.9	0.04800	1.518	6.121
12	Bare	93.2	151.1	0.04150	5.641	22.75
13	Bare	107.7	151.1	0.04230	5.812	23.44
16	Bare	123.0	151.1	0.04558	5.896	23.77
17	Bare	138.2	151.1	0.04320	5.367	21.64
18	Bare	153.5	151.1	0.04235	4.027	16.24
19	Bare	168.7	151.1	0.04340	2.533	10.21
Run 1108						
20	Cd	0	89.4	0.04385	0.208	
21	Cd	0	59.6	0.04330	0.0389	
23	Cd	0	29.1	0.04370	0.0022	
24	Cd	93.2	151.1	0.04070	0.229	
25	Cd	123.0	151.1	0.04590	0.0176	
26	Cd	153.5	151.1	0.04380	0.00124	
Run 1109						
3	Bare	0	90.8	0.04150	1.019	4.109
9	Bare	0	102.8	0.04270	0.433	1.746
10	Bare	0	118.0	0.04586	0.279	1.125
11	Bare	0	133.3	0.04800	0.253	1.020
12	Bare	0	148.5	0.04150	0.248	1.000 (X)
17	Bare	0	163.8	0.04320	0.273	1.101
18	Bare	0	179.0	0.04235	0.308	1.242
19	Bare	0	194.2	0.04340	0.475	1.915
28	Bare	0	206.9	0.04670	1.319	5.319
Run 1110						
20	Cd	0	90.8	0.04385	0.186	
21	Cd	0	118.0	0.04330	0.174	
23	Cd	0	148.5	0.04370	0.163	
24	Cd	0	179.0	0.04070	0.168	
25	Cd	0	206.9	0.04590	0.180	

TABLE 8.11

(Continued)

Foil No.	Foil Type	Location Radial (cm)	Location Axial (cm)	Foil Weight (gm)	Specific Activity d/m/gm x 10^{-7}	Local to Foil (X)
Run 1111						
5	Bare	93.2	151.1	0.04255	3.832	15.45
8	Bare	107.7	151.1	0.04304	6.759	27.25
13	Bare	123.0	151.1	0.04230	5.645	22.76
16	Bare	138.2	151.1	0.04558	3.869	15.60
26	Bare	153.5	151.1	0.04380	2.385	9.617

Note: All foil activities are corrected to reactor shutdown time

TABLE 8.12

Gold Cadmium Ratios

Variable Hydrogen

Location		Infinitely Dilute Foil Activity		
Radial (cm)	Axial (cm)	Bare Foil Activity d/m/gm x 10^{-6}	Cd Foil Activity d/m/gm x 10^{-6}	Cadmium Ratio
0	90.8	3.480	2.739	1.270
0	118.0	2.372	2.239	1.060
0	148.5	2.247	2.166	1.038
0	179.0	2.276	2.142	1.063
0	209.5	3.567	2.526	1.412
30.5	90.8	3.522	2.795	1.260
30.5	118.0	2.578	2.396	1.076
30.5	148.5	2.423	2.296	1.055
30.5	179.0	2.524	2.314	1.091
30.5	209.5	3.761	2.842	1.324
45.7	90.8	3.765	2.904	1.296
45.7	102.8	2.989	2.593	1.153
45.7	148.5	2.704	2.410	1.122
45.7	194.2	3.096	2.655	1.166
45.7	209.5	4.050	2.963	1.367
53.0	133.3	3.034	2.618	1.159
53.0	163.8	3.106	2.672	1.162
61.0	90.8	4.573	3.089	1.480
61.0	102.8	3.999	3.024	1.322
61.0	102.8	4.049	3.130	1.293
61.0	118.0	3.950	3.142	1.257
61.0	148.5	4.239	3.048	1.391
61.0	179.0	4.199	3.031	1.386
61.0	194.2	4.248	2.999	1.416
61.0	194.2	4.277	3.073	1.392
61.0	209.5	4.786	3.163	1.513
73.0	90.8	6.026	3.297	1.828
73.0	118.0	5.503	3.563	1.544
73.0	133.3	5.308	3.444	1.541
73.0	148.5	5.258	3.475	1.513
73.0	163.8	5.211	3.445	1.513
73.0	179.0	5.254	3.490	1.506
73.0	209.5	5.418	3.382	1.602
79.4	102.8	6.439	3.495	1.842
79.4	102.8	6.487	3.610	1.797
79.4	148.5	5.625	3.608	1.559
79.4	163.8	5.565	3.522	1.580
79.4	194.2	5.618	3.462	1.623
79.4	194.2	5.607	3.436	1.632
85.1	90.8	6.235	3.223	1.935
85.1	118.0	6.520	3.782	1.724

TABLE 8.12

(Continued)

Location		Infinitely Dilute Foil Activity		
Radial (cm)	Axial (cm)	Bare Foil Activity d/m/gm x 10^{-6}	Cd Foil Activity d/m/gm x 10^{-6}	Cadmium Ratio
85.1	179.0	5.683	3.556	1.598
85.1	209.5	5.517	3.159	1.746
90.8	90.8	6.656	3.152	2.111
90.8	102.8	6.940	3.549	1.955
90.8	118.0	6.619	3.803	1.741
90.8	133.3	6.014	3.617	1.663
90.8	148.5	5.877	3.685	1.595
90.8	163.8	5.734	3.587	1.598
90.8	179.0	5.834	3.622	1.611
90.8	194.2	5.673	3.381	1.678
90.8	209.5	5.000	3.221	1.553
0	89.4	4.036	2.777	1.453
0	74.9	8.585	2.897	2.963
0	59.6	6.510	0.781	8.332
0	44.4	4.398	1.209	36.37
0	29.1	2.664	0.029	93.04
93.2	151.1	6.827	3.641	1.875
107.7	151.1	6.767	1.484	4.559
123.0	151.1	4.810	0.280	17.21
138.2	151.1	3.132	0.038	83.05
153.5	151.1	1.940	0.0075	257.7

TABLE 8.13

Indium Cadmium Ratios

Variable Hydrogen Reactor

Location		Infinitely Dilute Foil Activity d/m/gm x 10^{-8}		
Radial (cm)	Axial (cm)	Bare Foil Activity	Cd Foil Activity	Cadmium Ratio
0	90.8	6.984	5.143	1.358
0	118.0	5.322	4.984	1.068
0	148.5	5.064	4.781	1.059
0	179.0	5.069	4.761	1.065
0	206.9	7.092	4.934	1.437
0	89.4	12.56	5.628	2.232
0	59.6	10.90	1.482	7.355
0	29.1	4.073	0.0539	75.57
93.2	151.1	7.992	6.035	1.324
123.0	151.1	12.50	0.737	16.96
153.5	151.1	5.438	0.0228	238.5

TABLE 8.14

Manganese Cadmium Ratios

Variable Hydrogen Reactor

Location		Infinitely Dilute Foil Activity $d/m/gm \times 10^{-7}$		
Radial (cm)	Axial (cm)	Bare Foil	Cadmium Foil	Cadmium Ratio
0	89.4	1.417	0.218	6.50
0	59.6	6.629	0.0408	162.0
0	29.1	2.808	0.0023	121.6
93.2	151.1	5.652	0.240	23.5
123.0	151.1	5.897	0.0185	319.0
153.5	151.1	4.027	0.00130	309.3
0	90.8	1.029	0.206	5.00
0	118.0	0.288	0.183	1.57
0	148.5	0.256	0.172	1.49
0	179.0	0.316	0.176	1.79
0	206.9	1.328	0.189	7.03
Repeat Measurement				
93.2	151.1	3.841	0.240	16.0
123.0	151.1	5.654	0.0185	306.0
153.5	151.1	2.385	0.00130	1832.0

TABLE 8.15

Thermal Neutron Flux

Gold Data

Variable Hydrogen Reactor

Location		
Radial (cm)	Axial (cm)	Thermal Neutron Flux $n/cm^2/sec/watt \times 10^{-6}$
0	90.8	0.587
0	102.8	0.185 (1)
0	118.0	0.106
0	133.3	0.041 (1)
0	148.5	0.065
0	163.8	0.072 (1)
0	179.8	0.106
0	194.2	0.223 (1)
0	206.9	0.824
30.5	90.8	0.577
30.5	118.0	0.145
30.5	148.5	0.100
30.5	179.0	0.166
30.5	206.9	0.729
45.7	90.8	0.682
45.7	102.8	0.314
45.7	148.5	0.234
45.7	179.0	0.271
45.7	194.2	0.350
45.7	206.9	0.862
53.3	133.3	0.330
53.3	148.5	0.370 (1)
53.3	163.8	0.344
61.0	90.8	1.176
61.0	102.8	0.750
61.0	118.0	0.640
61.0	148.5	0.944
61.0	179.0	0.926
61.0	194.2	0.972
61.0	206.9	1.286
73.0	90.8	2.163
73.0	102.8	1.764
73.0	118.0	1.537
73.0	133.3	1.477
73.0	148.5	1.413
73.0	163.8	1.400
73.0	179.0	1.398
73.0	194.2	1.518
73.0	206.9	1.614
79.4	102.8	2.308
79.4	148.5	1.599

TABLE 8.15

(Continued)

Location		
Radial (cm)	Axial (cm)	Thermal Neutron Flux $n/cm^2/sec/watt \times 10^{-6}$
79.4	163.8	1.619
79.4	194.2	1.715
85.1	90.8	2.387
85.1	118.0	2.170
85.1	148.5	1.831 (1)
85.1	179.0	1.686
85.1	206.9	1.869
90.8	90.8	2.777
90.8	102.8	2.688
90.8	118.0	2.232
90.8	133.3	1.900
90.8	148.5	1.737
90.8	163.8	1.702
90.8	179.0	1.753
90.8	194.2	1.817
90.8	206.9	1.410
0	89.4	0.998
0	82.5	3.372 (1)
0	74.9	4.508
0	67.2	4.588 (1)
0	59.6	4.541
0	52.0	3.900 (1)
0	44.4	3.384
0	29.1	2.089
0	13.9	1.051 (1)
0	0	0.145 (1)
93.2	151.1	2.525
100.1	151.1	2.066 (1)
107.7	151.1	4.187
115.4	151.1	3.913 (1)
123.0	151.1	3.591
130.6	151.1	3.013 (1)
138.2	151.1	2.453
153.5	151.1	1.532
168.7	151.1	0.802 (1)
183.9	151.1	0.183 (1)

(1) These values are based on an extrapolated cadmium covered gold foil activity.

TABLE 8.16

Comparison of In, Mn, Au Detectors

Variable Hydrogen Reactor

Location		Cadmium Ratios			Thermal Neutron Flux $n/cm^2/sec/watt \times 10^{-6}$		
Radial (cm)	Axial (cm)	In	Mn	Au	In	Mn	Gold
0	90.8 wall	1.358	5.00	1.270	0.82	0.57	0.59
0	118.0 core	1.068	1.57	1.060	0.15	0.07	0.11
0	148.5 core	1.059	1.49	1.038	0.13	0.06	0.06
0	179.0 core	1.065	1.79	1.063	0.14	0.10	0.22
0	206.9 wall	1.437	7.03	1.412	0.96	0.78	0.82
0	89.4 wall	2.232	6.50	1.453	--	0.82	1.00
0	59.6 refl	7.355	162.0	8.332	4.17	4.53	4.54
0	29.1 refl	75.6	1216.0	93.0	1.78	1.92	2.09
93.2	151.1 wall	1.324	23.5	1.875	0.90	3.2	2.5
123.0	151.1 refl	16.96	319.0	17.21	5.2	4.0	3.4
153.5	151.1 refl	238.5	3093	256.0	2.4	2.8	1.5

The radial reflector measurements were made in a sector where the Be slab had been removed.

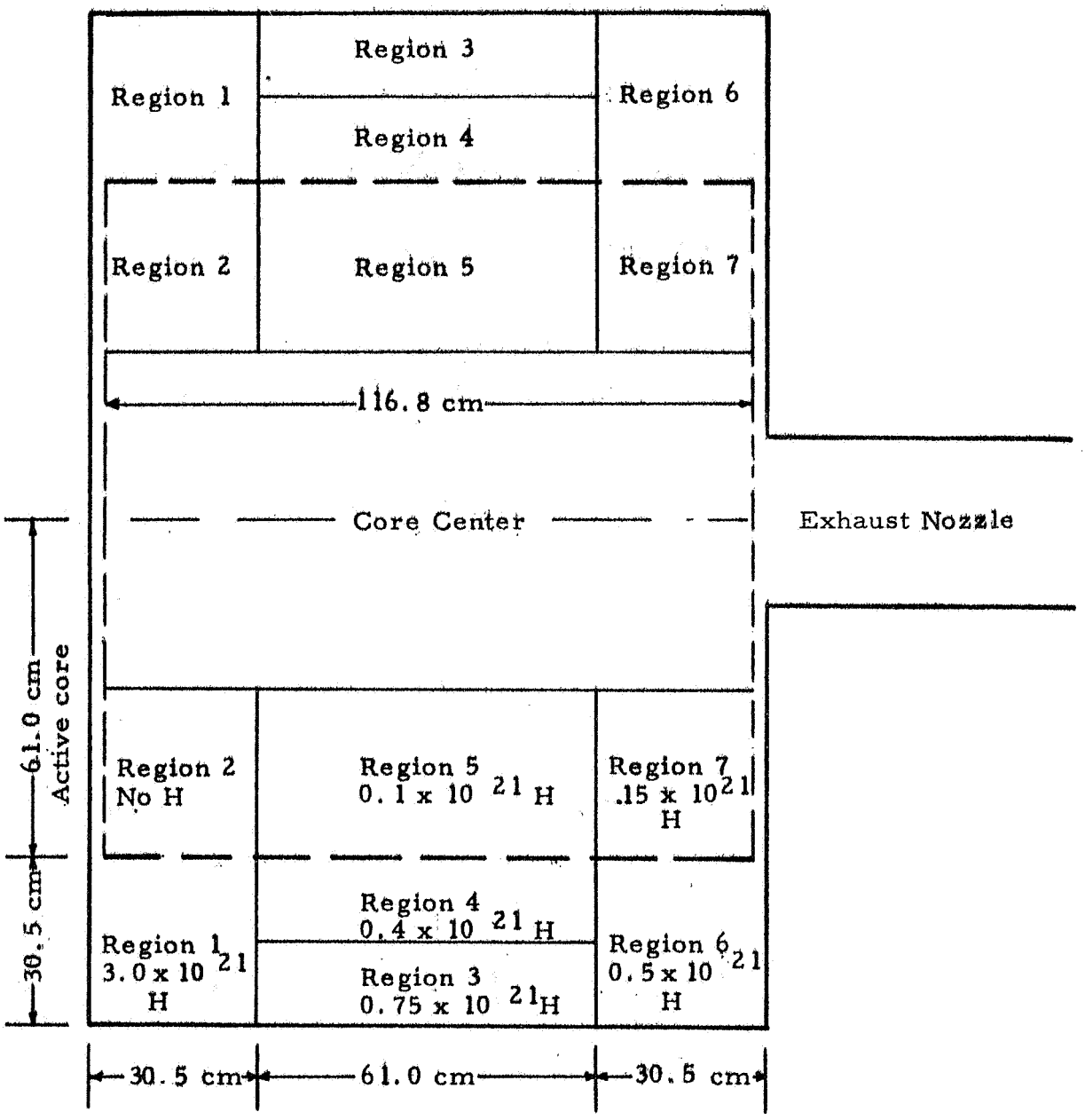

Fig. 8.1 Hydrogen density distribution within the reactor, variable hydrogen experiment

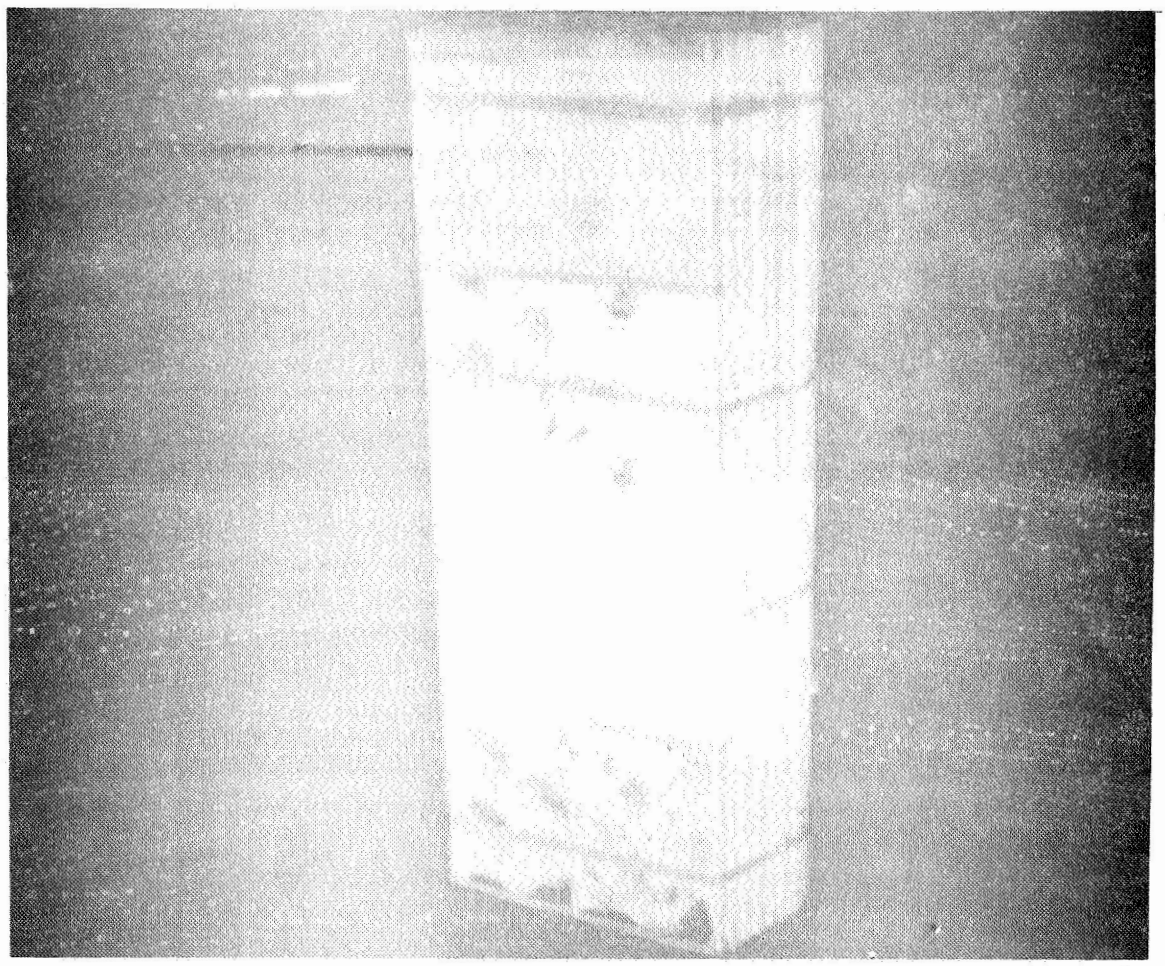

Fig. 8.2 Polyethylene - Polystyrene "swiss cheese" assembly, variable hydrogen experiment

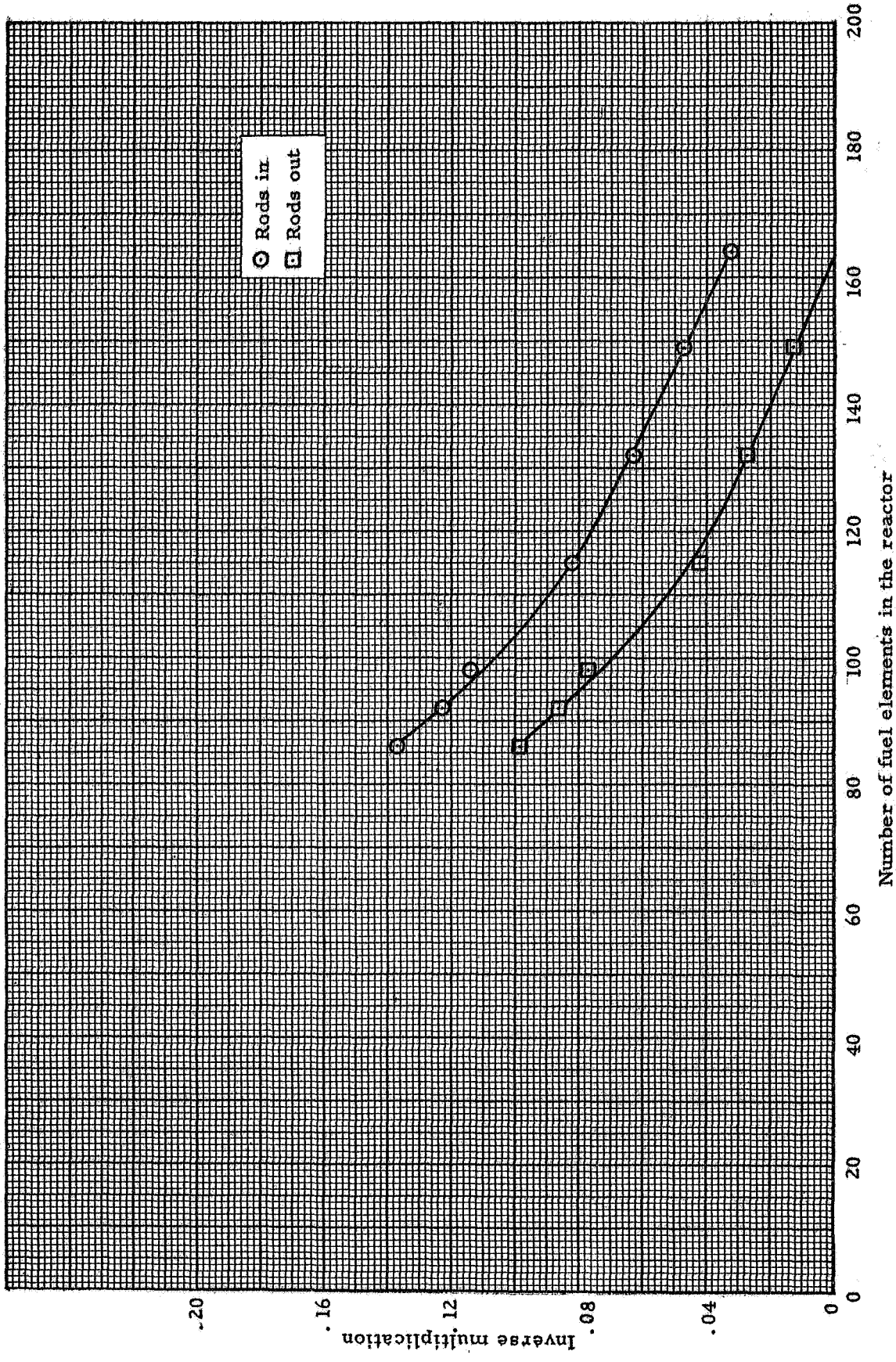

Fig. 8.3 Inverse multiplication curves, variable hydrogen experiment

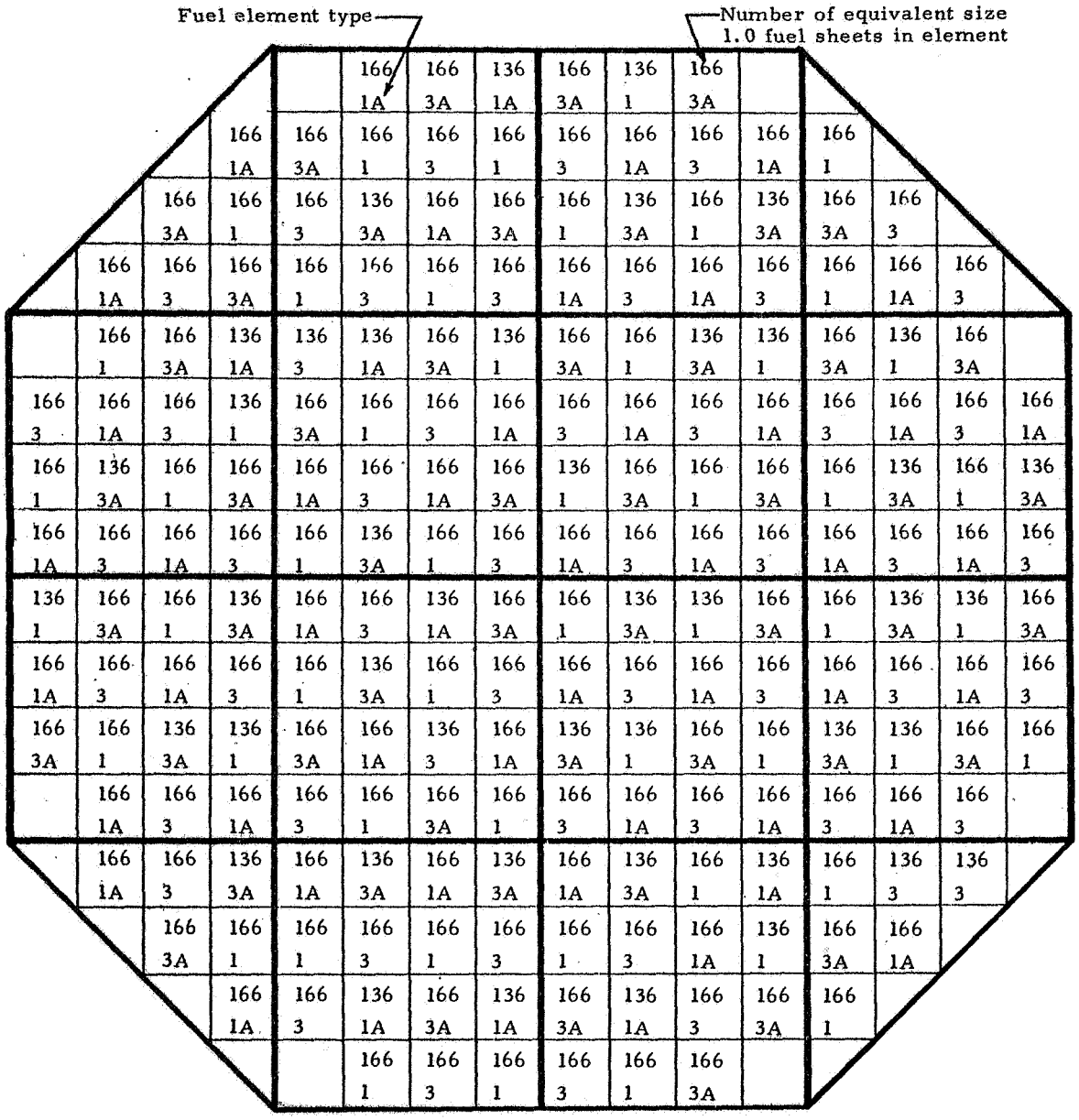

					166 1A	166 3A	136 1A	166 3A	136 1	166 3A					
			166 1A	166 3A	166 1	166 3	166 1	166 3	166 1A	166 3	166 1A	166 1			
		166 3A	166 1	166 3	136 3A	166 1A	166 3A	166 1	136 3A	166 1	136 3A	166 3A	166 3		
	166 1A	166 3	166 3A	166 1	166 3	166 1	166 3	166 1A	166 3	166 1A	166 3	166 1	166 1A	166 3	
	166 1	166 3A	136 1A	136 3	136 1A	166 3A	136 1	166 3A	166 1	136 3A	136 1	166 3A	136 1	166 3A	
166 3	166 1A	166 3	136 1	166 3A	166 1	166 3	166 1A	166 3	166 1A	166 3	166 1A	166 3	166 1A	166 3	166 1A
166 1	136 3A	166 1	166 3A	166 1A	166 3	166 1A	166 3A	136 1	166 3A	166 1	166 3A	166 1	136 3A	166 1	136 3A
166 1A	166 3	166 1A	166 3	166 1	136 3A	166 1	166 3	166 1A	166 3	166 1A	166 3	166 1A	166 3	166 1A	166 3
136 1	166 3A	166 1	136 3A	166 1A	166 3	136 1A	166 3A	166 1	136 3A	136 1	166 3A	166 1	136 3A	136 1	166 3A
166 1A	166 3	166 1A	166 3	166 1	136 3A	166 1	166 3	166 1A	166 3	166 1A	166 3	166 1A	166 3	166 1A	166 3
166 3A	166 1	136 3A	136 1	166 3A	166 1A	136 3	166 1A	136 3A	136 1	166 3A	166 1	136 3A	136 1	166 3A	166 1
	166 1A	166 3	166 1A	166 3	166 1	166 3A	166 1	166 3	166 1A	166 3	166 1A	166 3	166 1A	166 3	
	166 1A	166 3	136 3A	166 1A	136 3A	166 1A	136 3A	166 1A	166 3A	166 1	166 1A	166 1	136 3	136 3	
		166 3A	166 1	166 1	166 3	166 1	166 3	166 1	166 3	166 1A	136 1	166 3A	166 1A		
			166 1A	166 3	136 1A	166 3A	136 1A	166 3A	136 1A	166 3	166 3A	166 1			
					166 1	166 3	166 1	166 3	166 1	166 3A					

Fig. 8.4 Fuel element location, final loading, variable hydrogen experiment

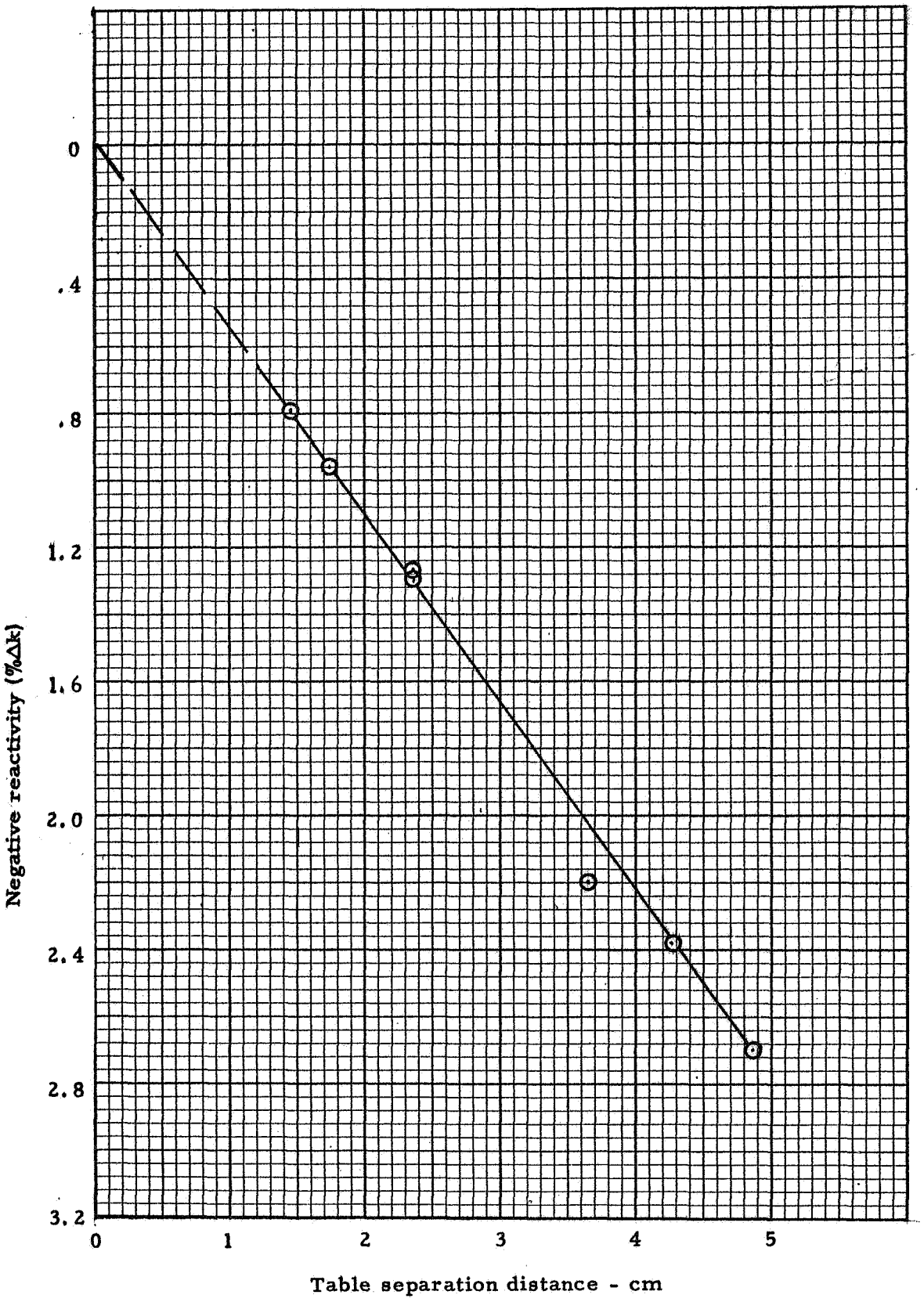

Fig. 8.5 The effect of table separation on excess reactivity, variable hydrogen

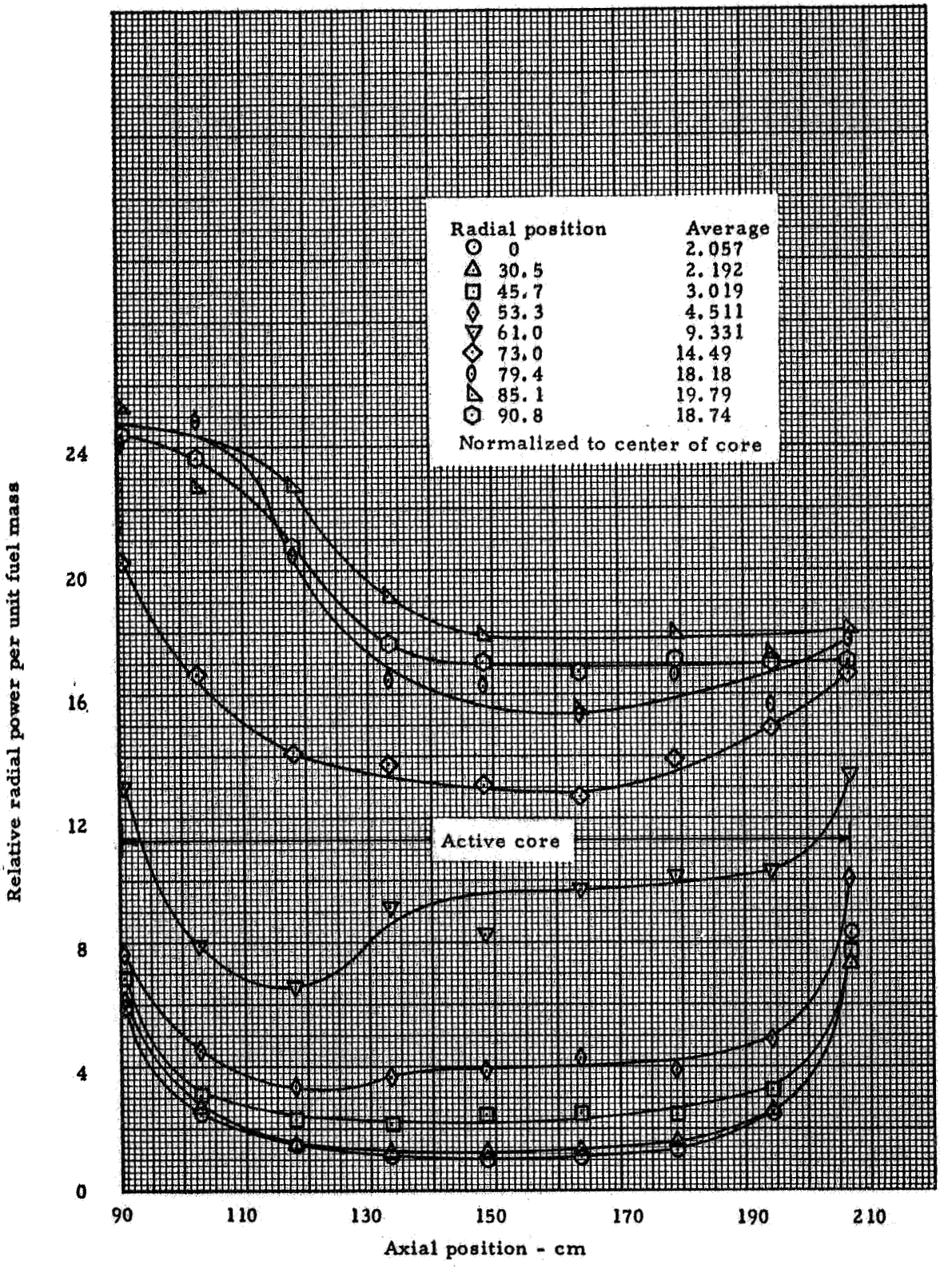

Fig. 8.6 Relative axial power distribution, variable hydrogen

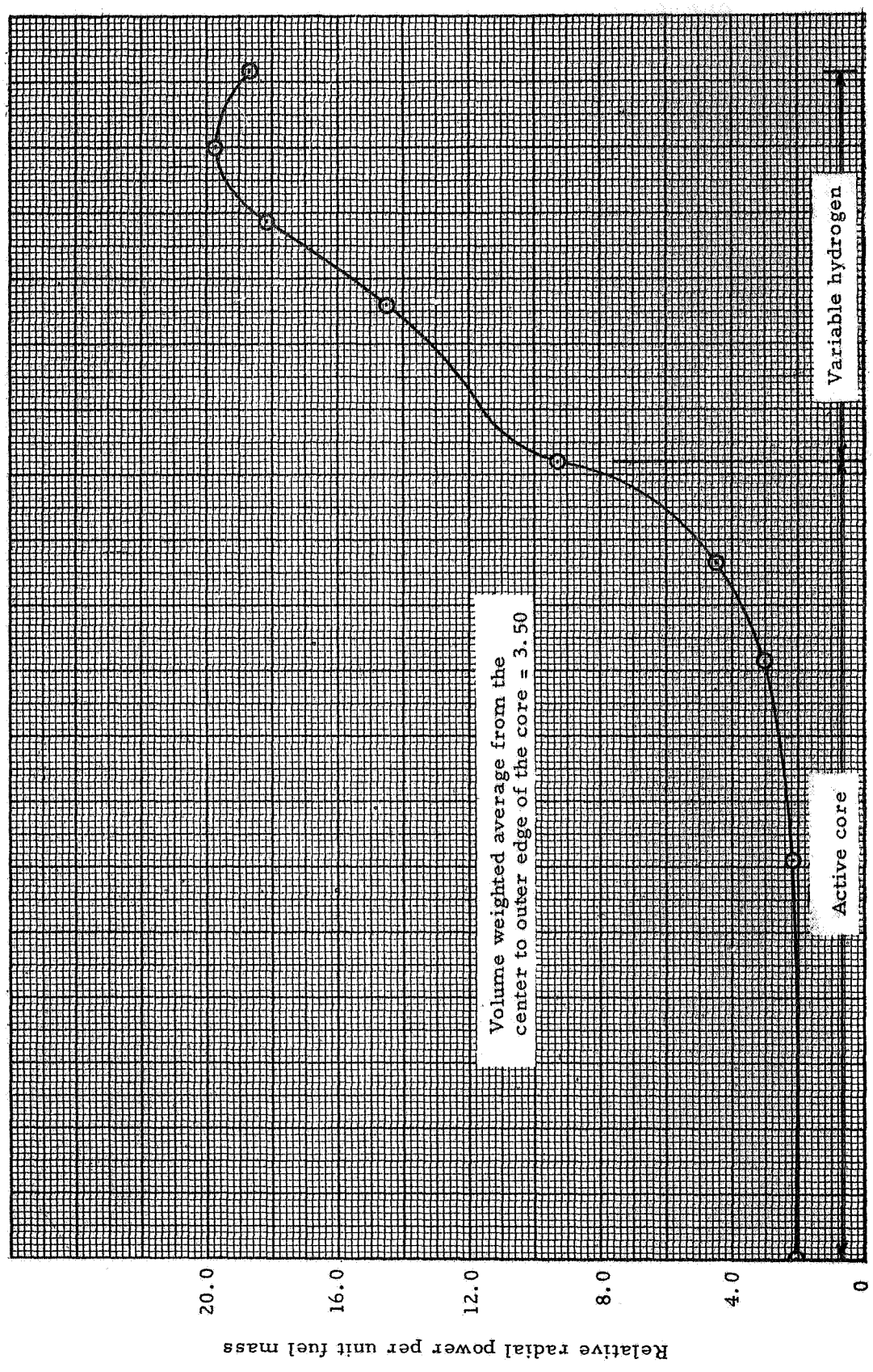

Fig. 8.7 Relative radial power distribution, variable hydrogen

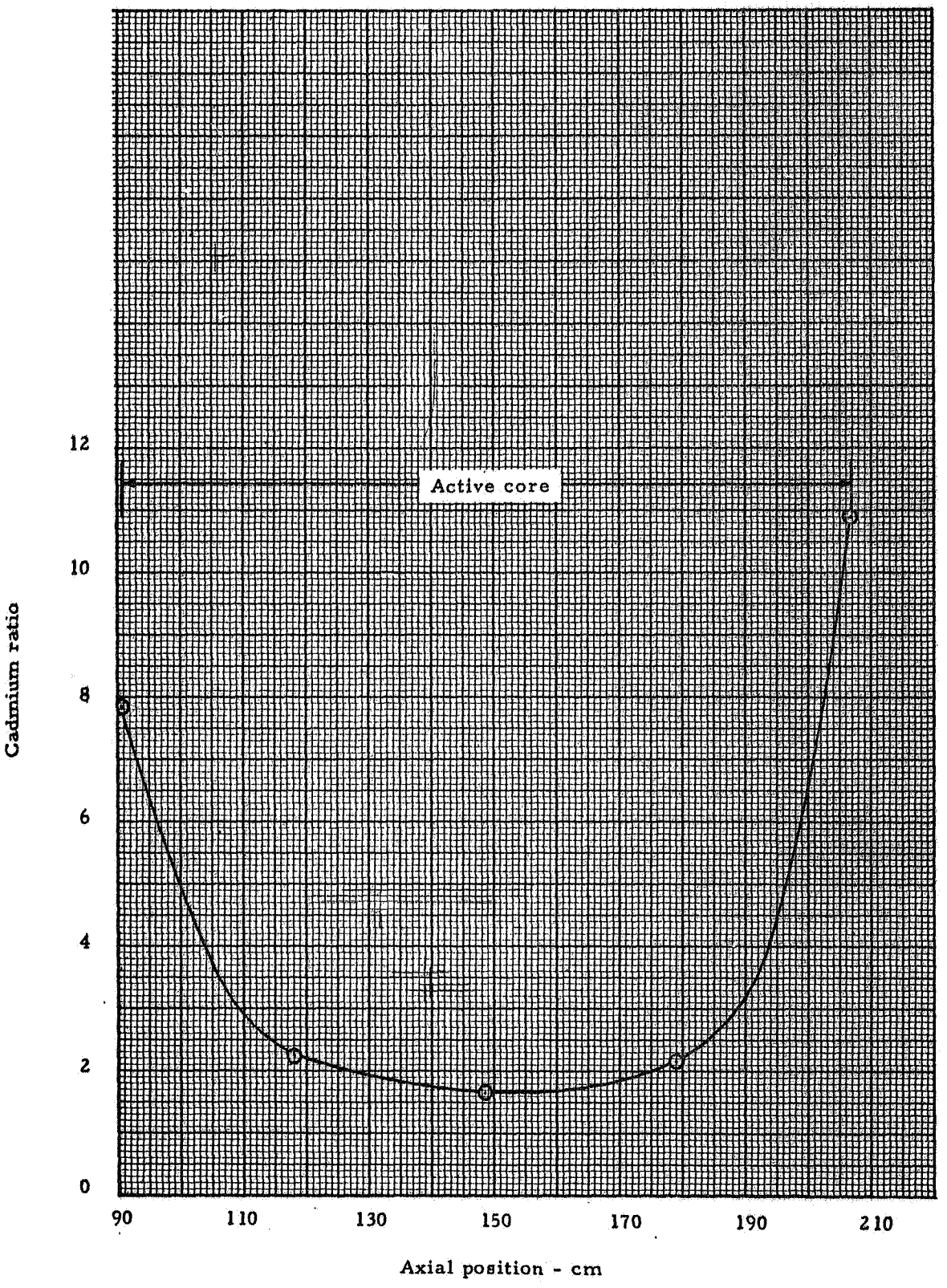

Fig. 8.8 Catcher foil cadmium ratio distribution, axial profile, variable hydrogen

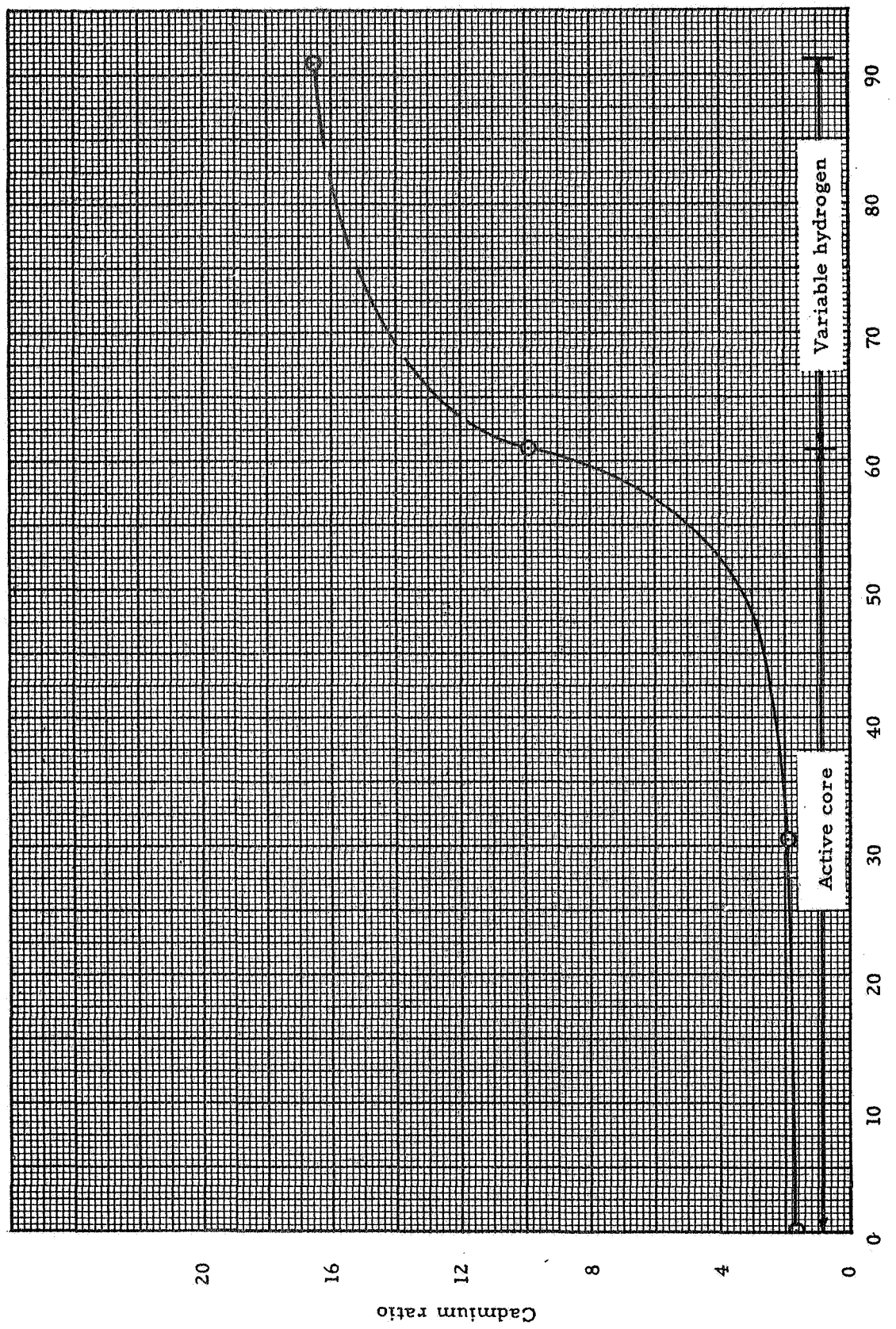

Fig. 8.9 Catcher foil cadmium ratio distribution, radial profile, variable hydrogen

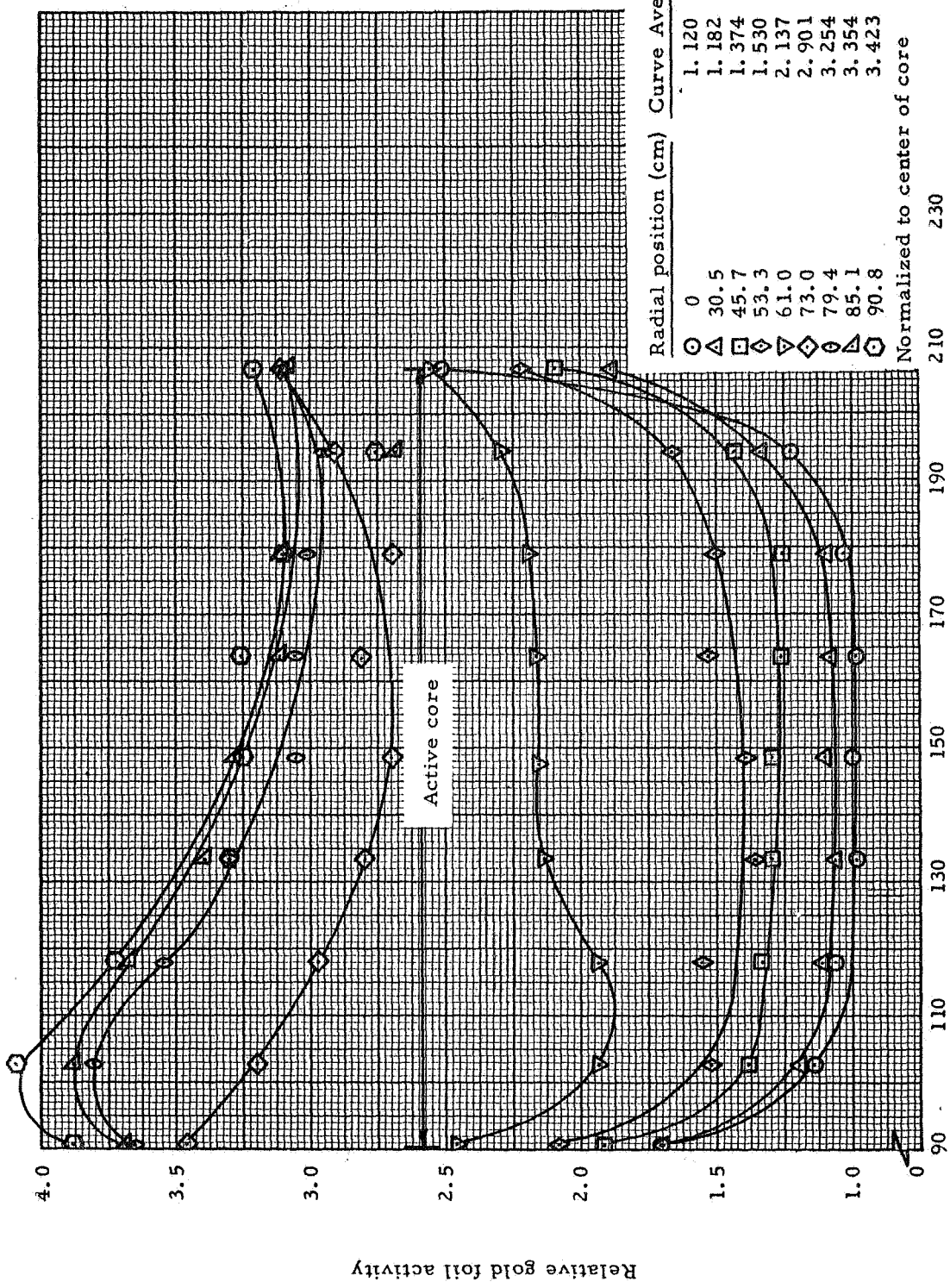

Fig. 8.10 Relative gold foil activity, axial profiles, variable hydrogen

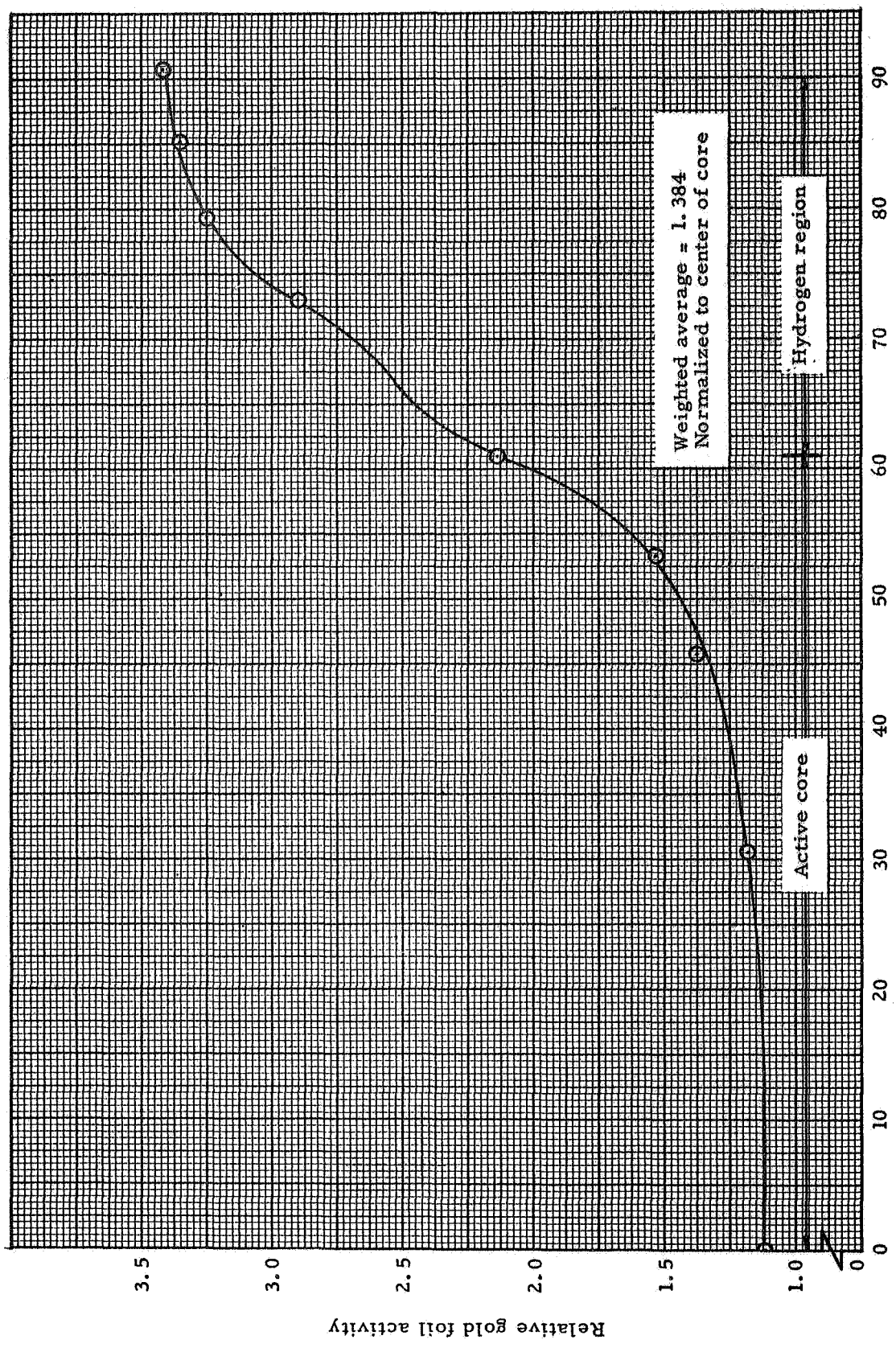

Fig. 8.11 Relative gold foil activity, radial profile, variable hydrogen

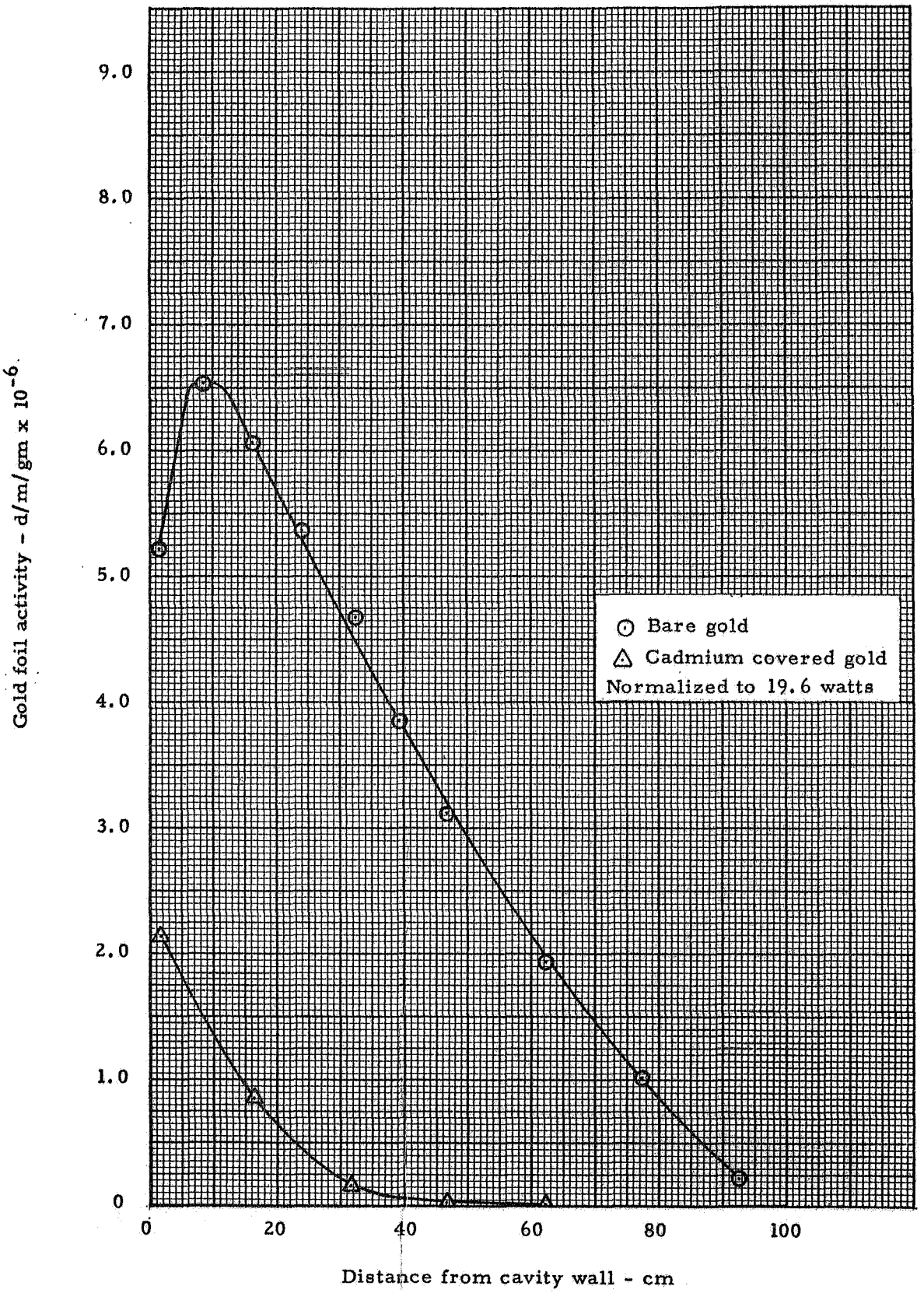

Fig. 8.12 Gold foil activity, radial reflector, variable hydrogen

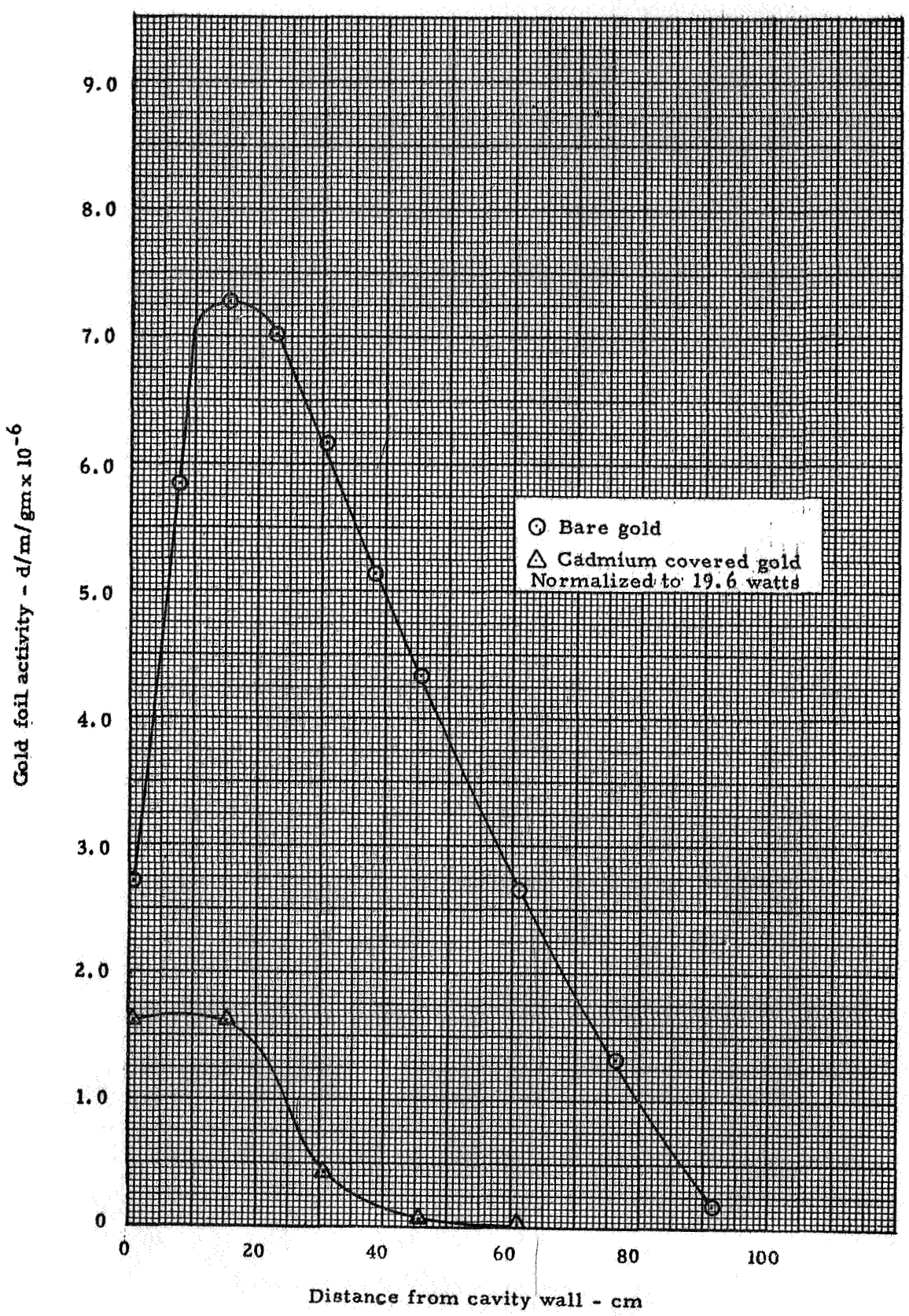

Fig. 8.13 Gold foil activity, end reflector, variable hydrogen

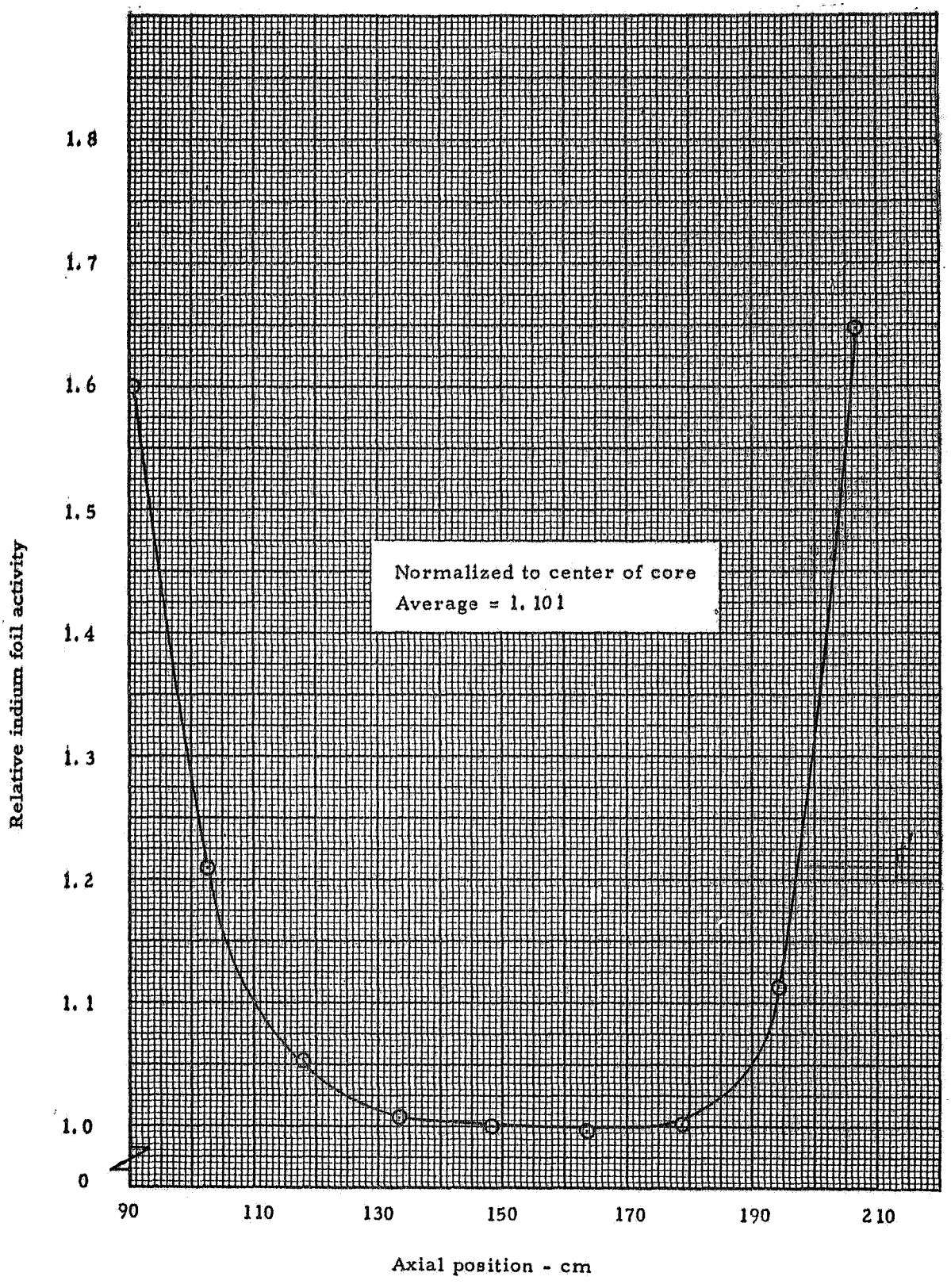

Fig. 8.14 Bare indium foil activity, axial profile through center of active core, variable hydrogen

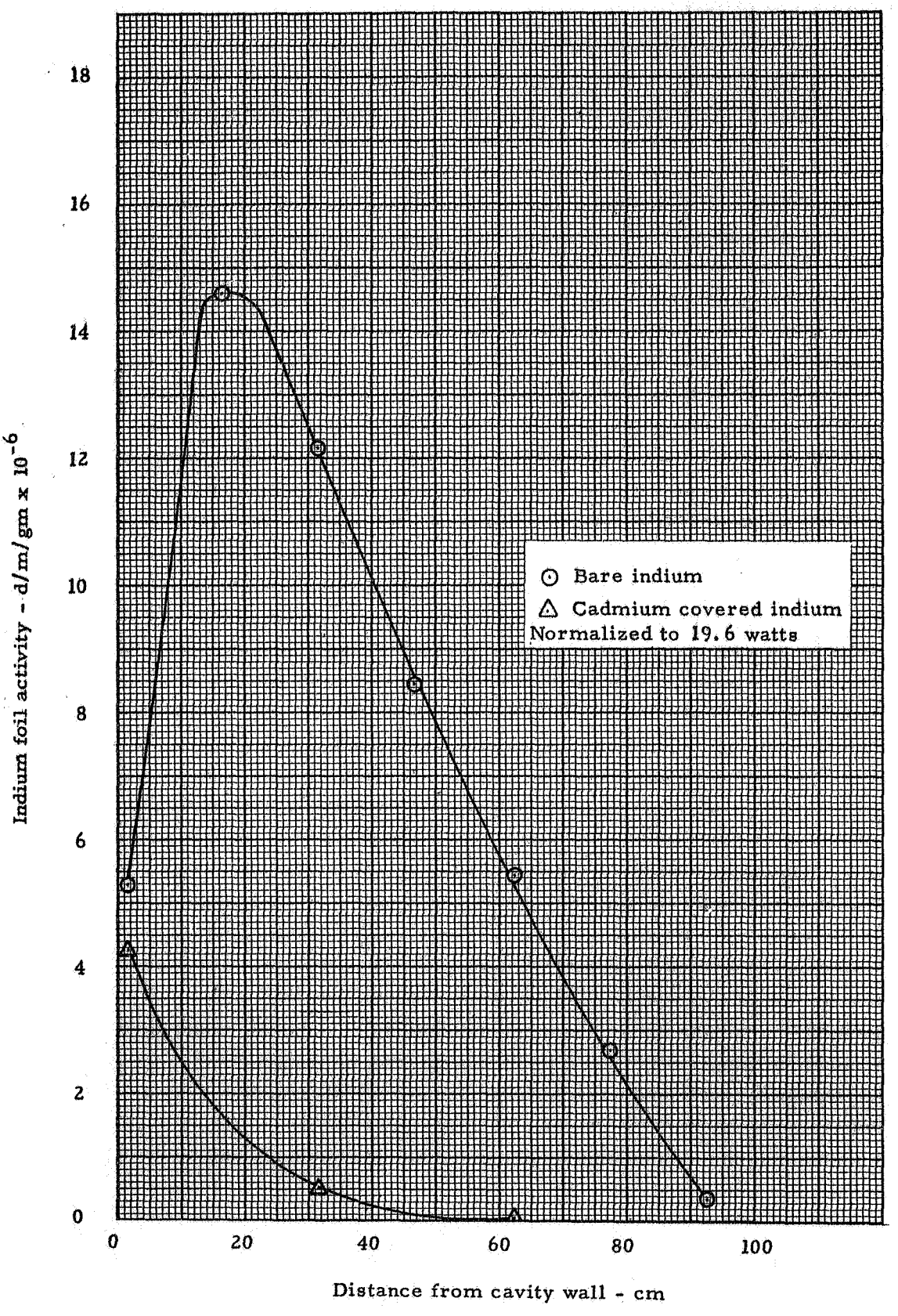

Fig. 8.15 Indium foil activity, radial reflector, variable hydrogen

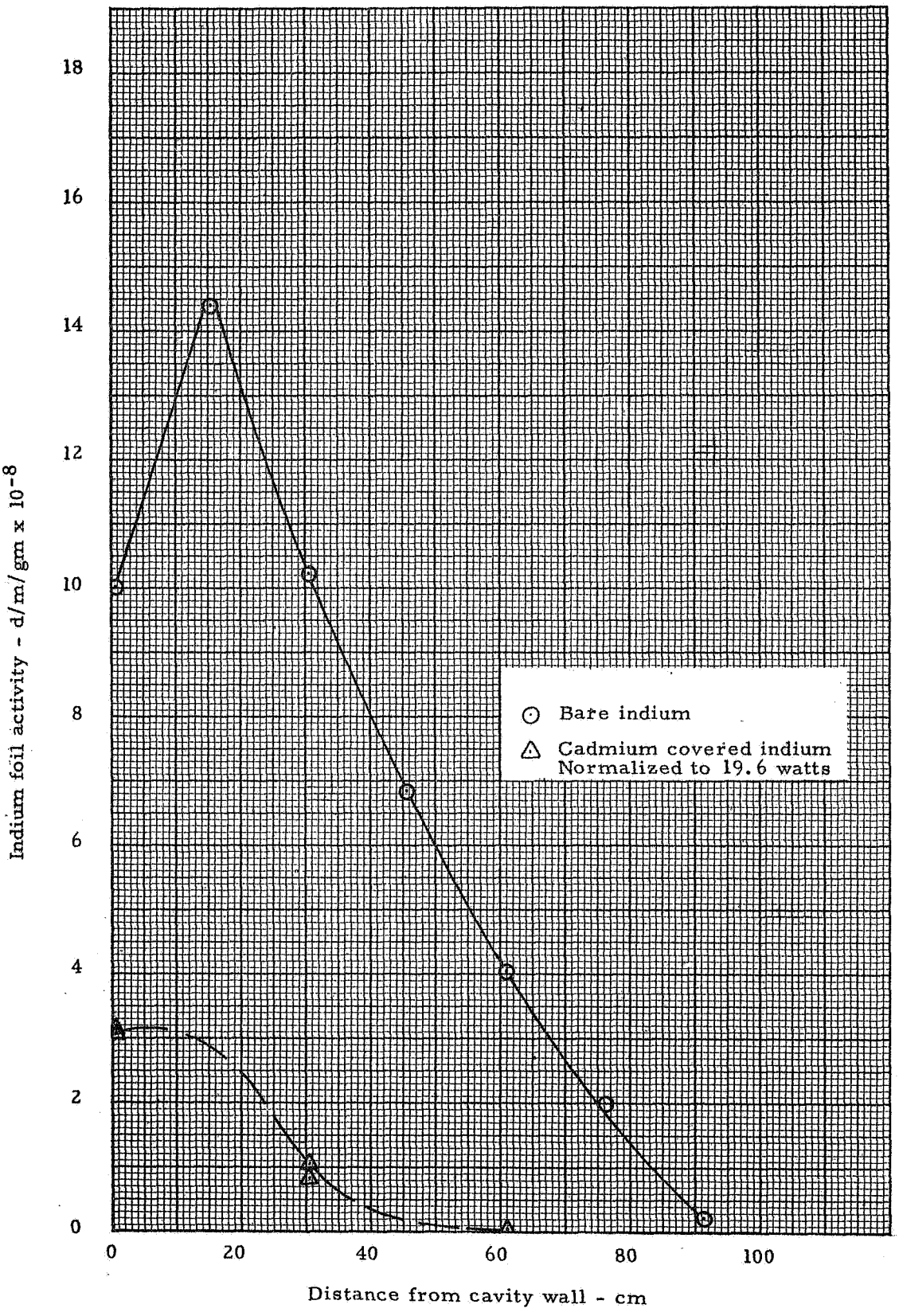

Fig. 8.16 Indium foil activity, end reflector, variable hydrogen

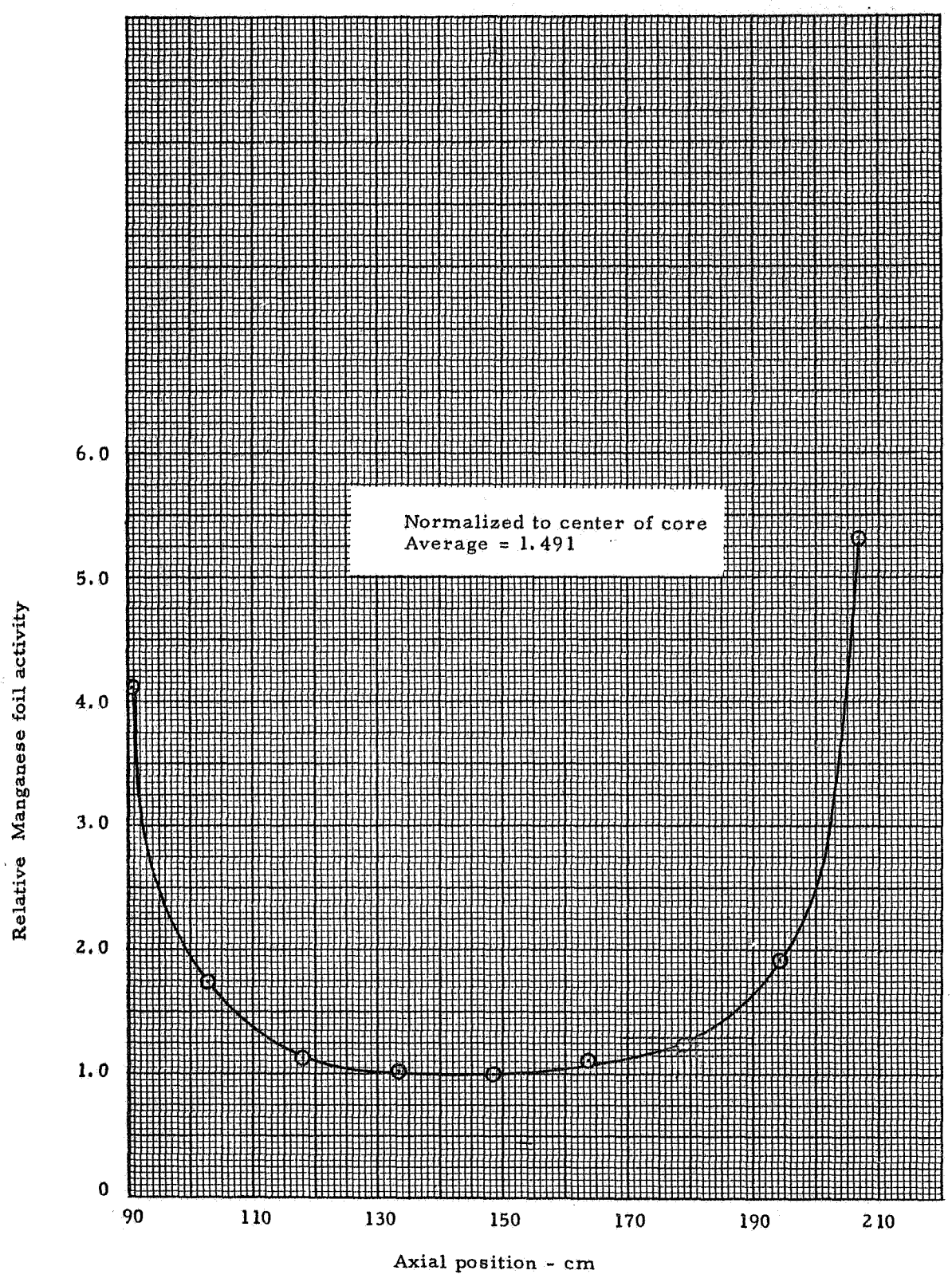

Fig. 8.17 Bare manganese foil activity, axial profile through center of active core, variable hydrogen

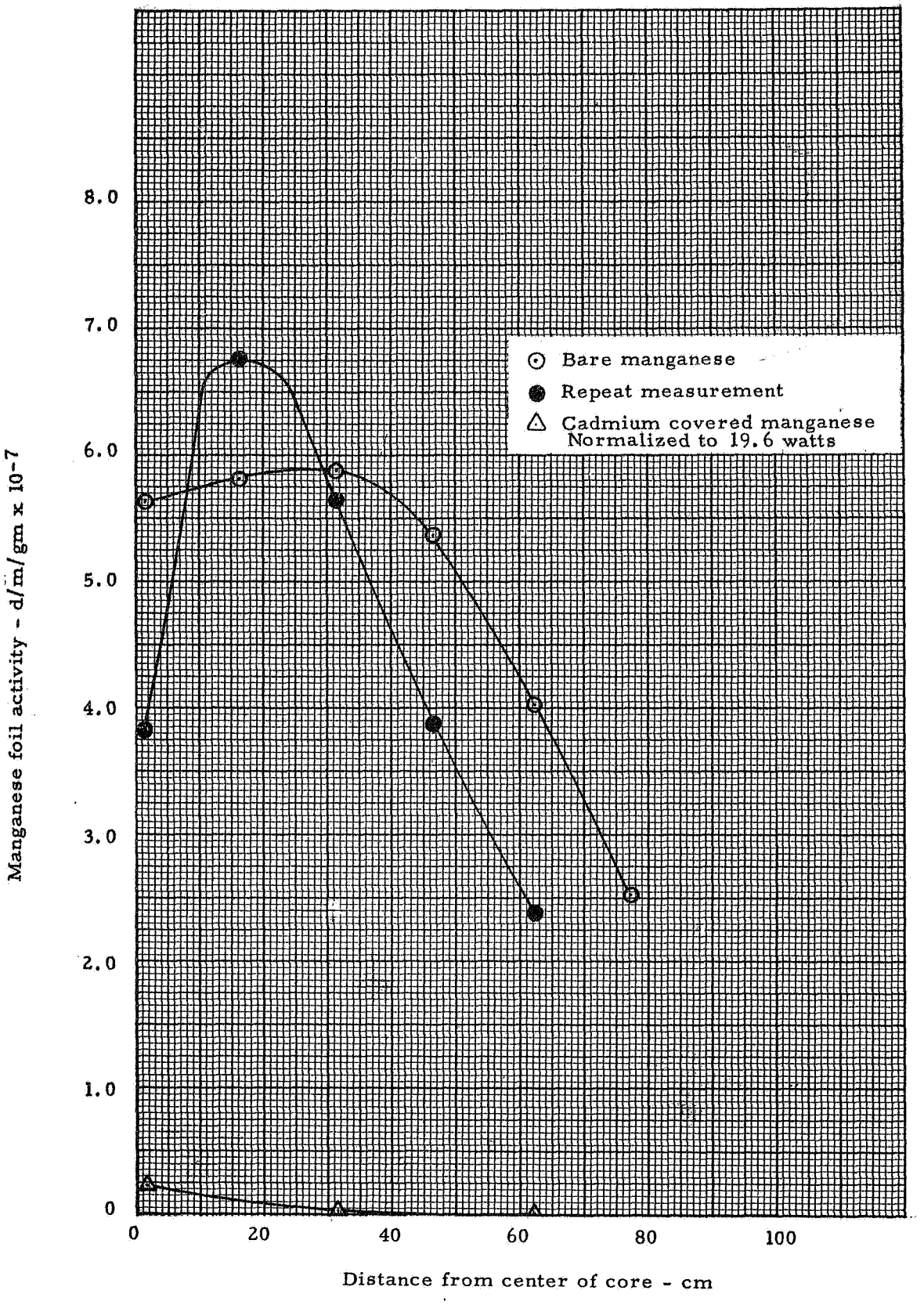

Fig. 8.18 Manganese foil activity, radial reflector, variable hydrogen

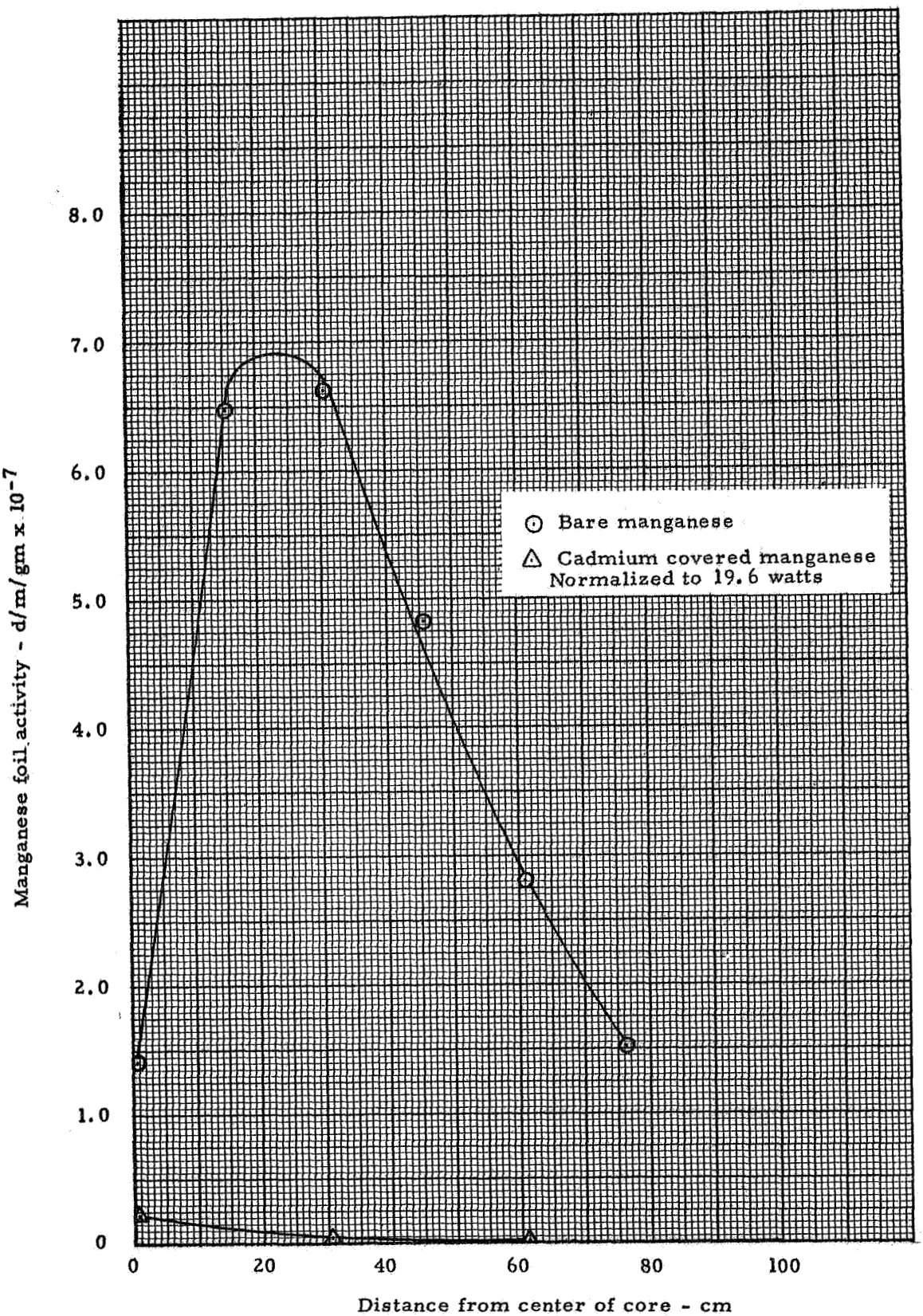

Fig. 8.19 Manganese foil activity, end reflector, variable hydrogen

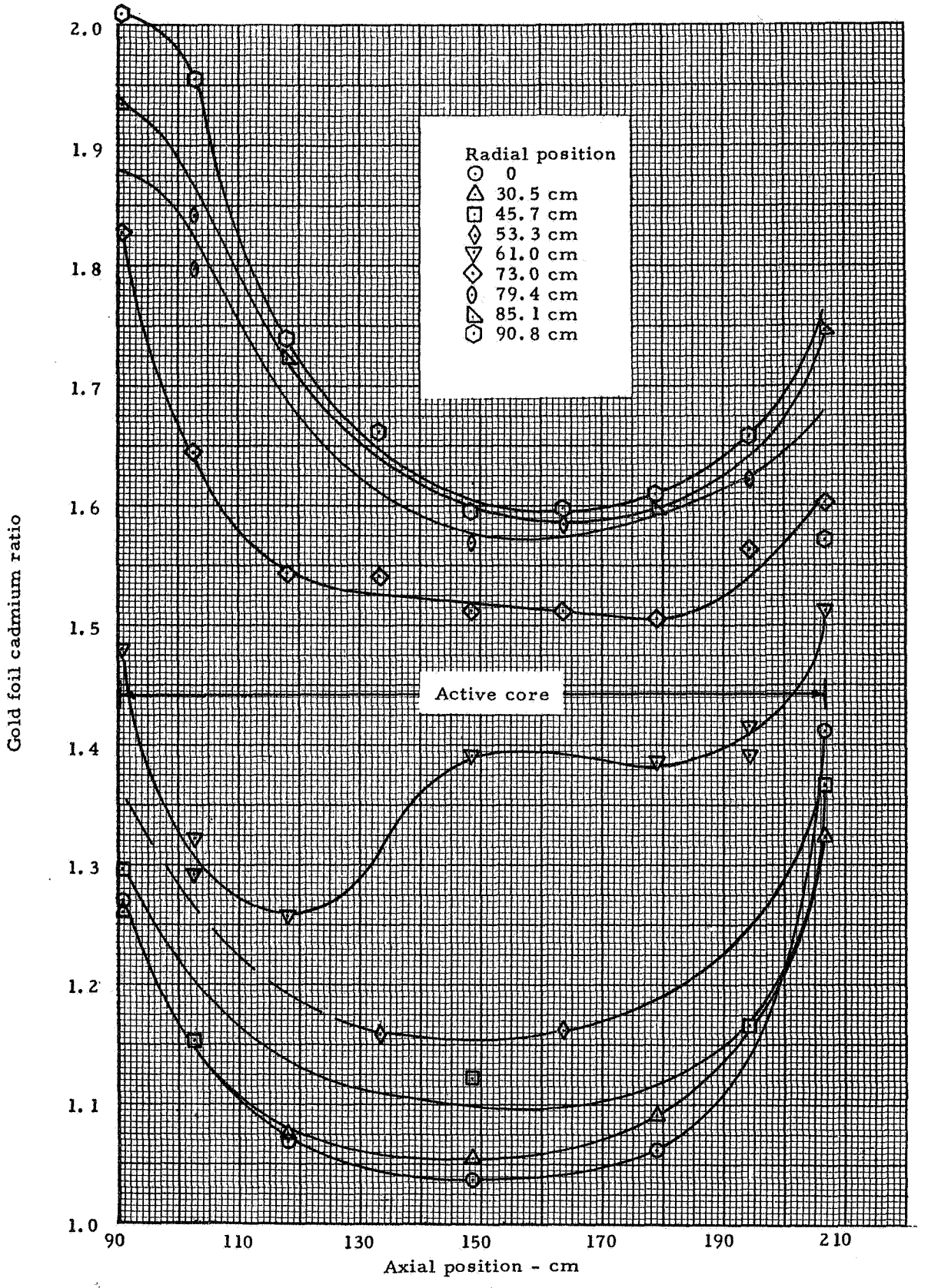

Fig. 8.20 Gold foil cadmium ratio distribution in the cavity region, variable hydrogen

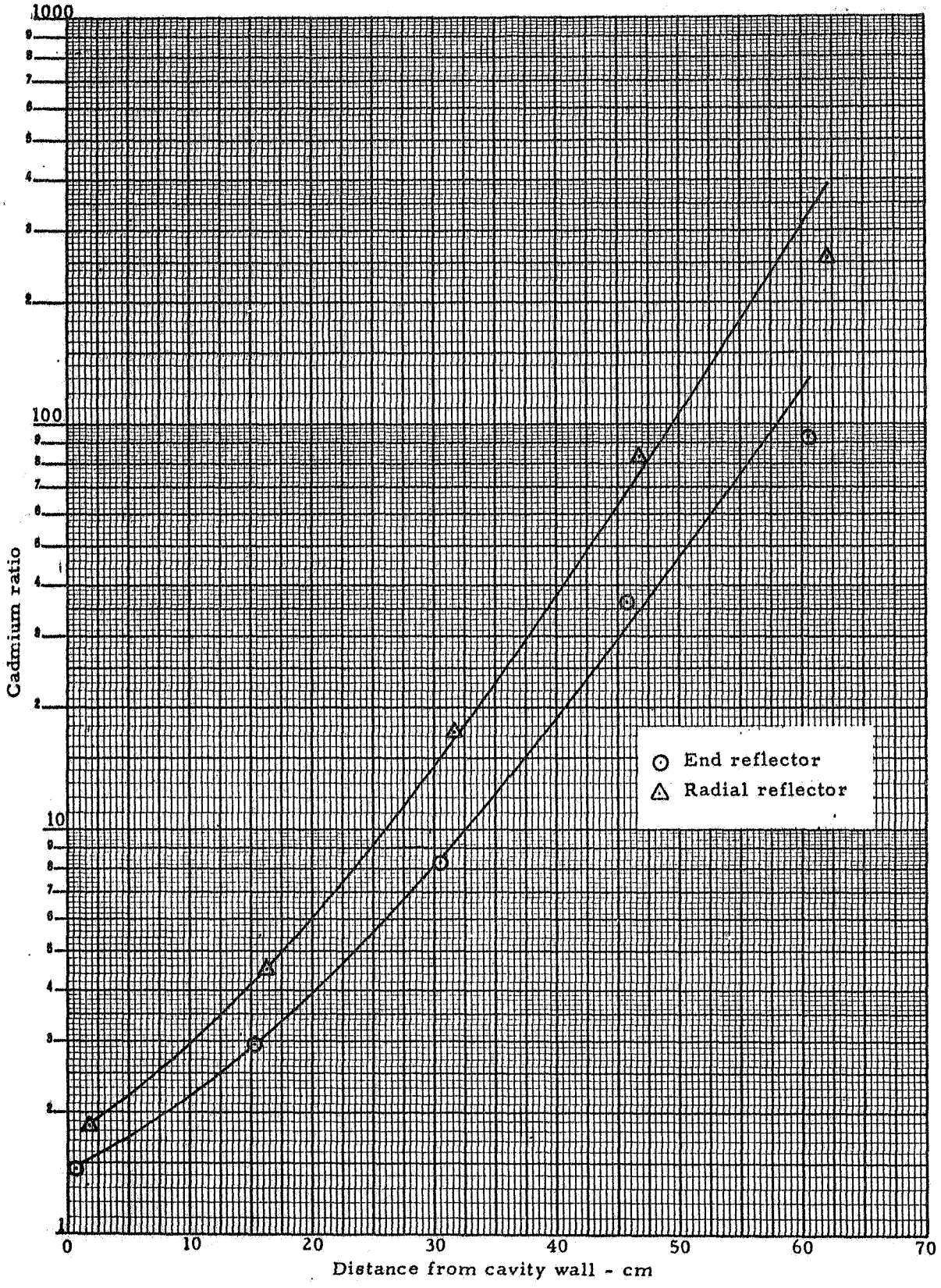

Fig. 8.21 Gold foil cadmium ratios, reflector regions, variable hydrogen

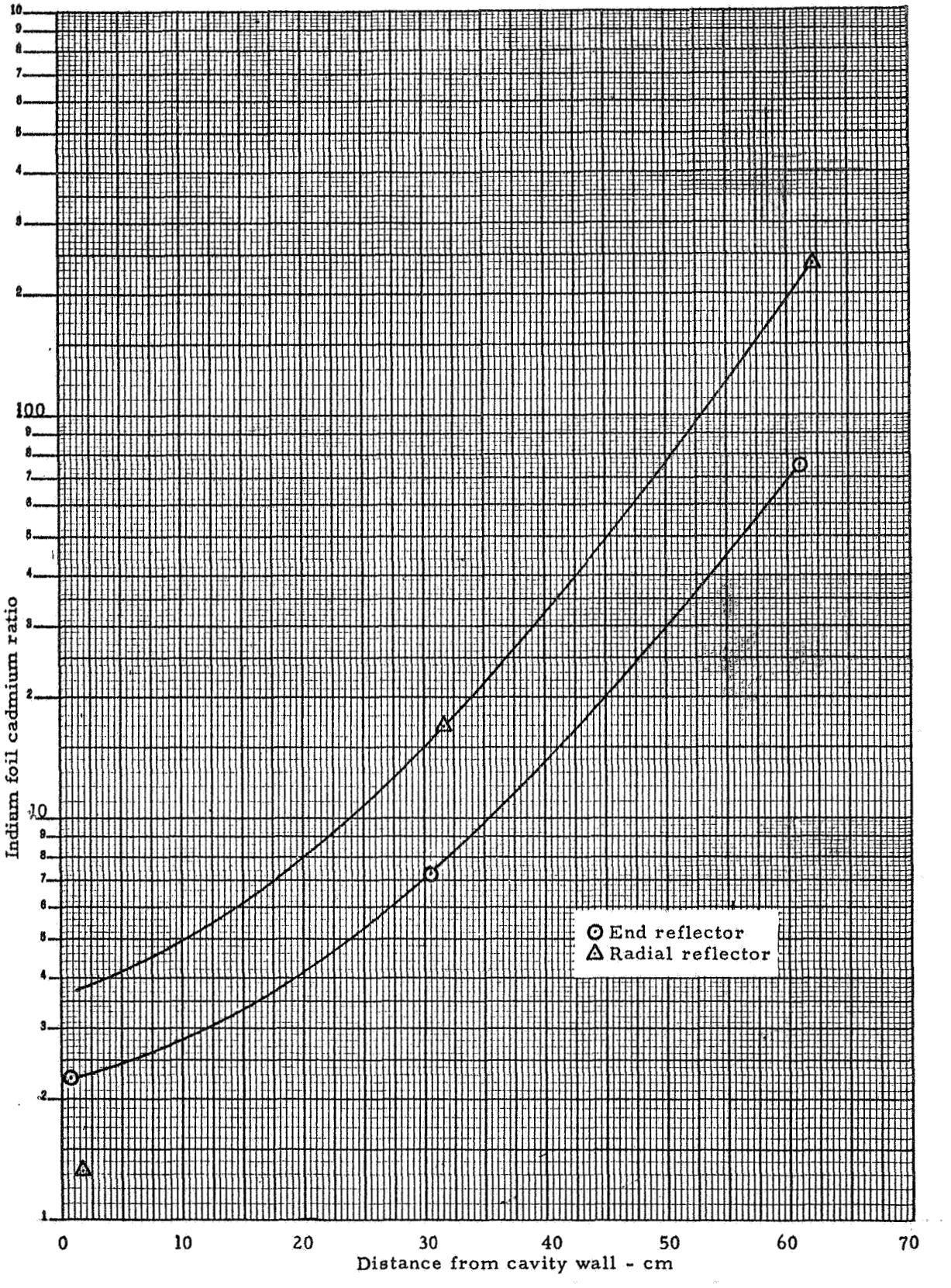

Fig. 8.22 Indium foil cadmium ratios, reflector regions, variable hydrogen

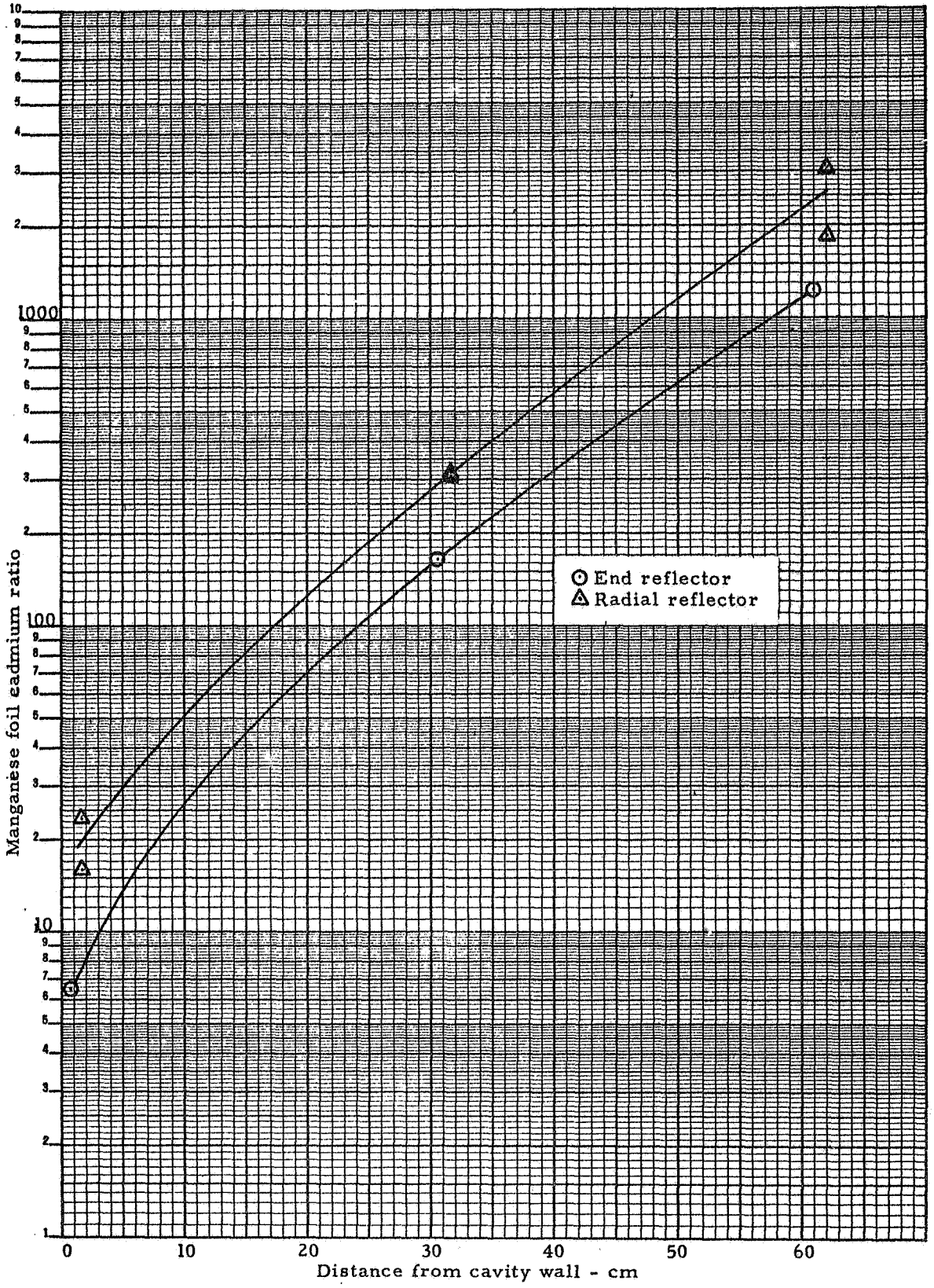

Fig. 8.23 Manganese foil cadmium ratios, reflector regions, variable hydrogen

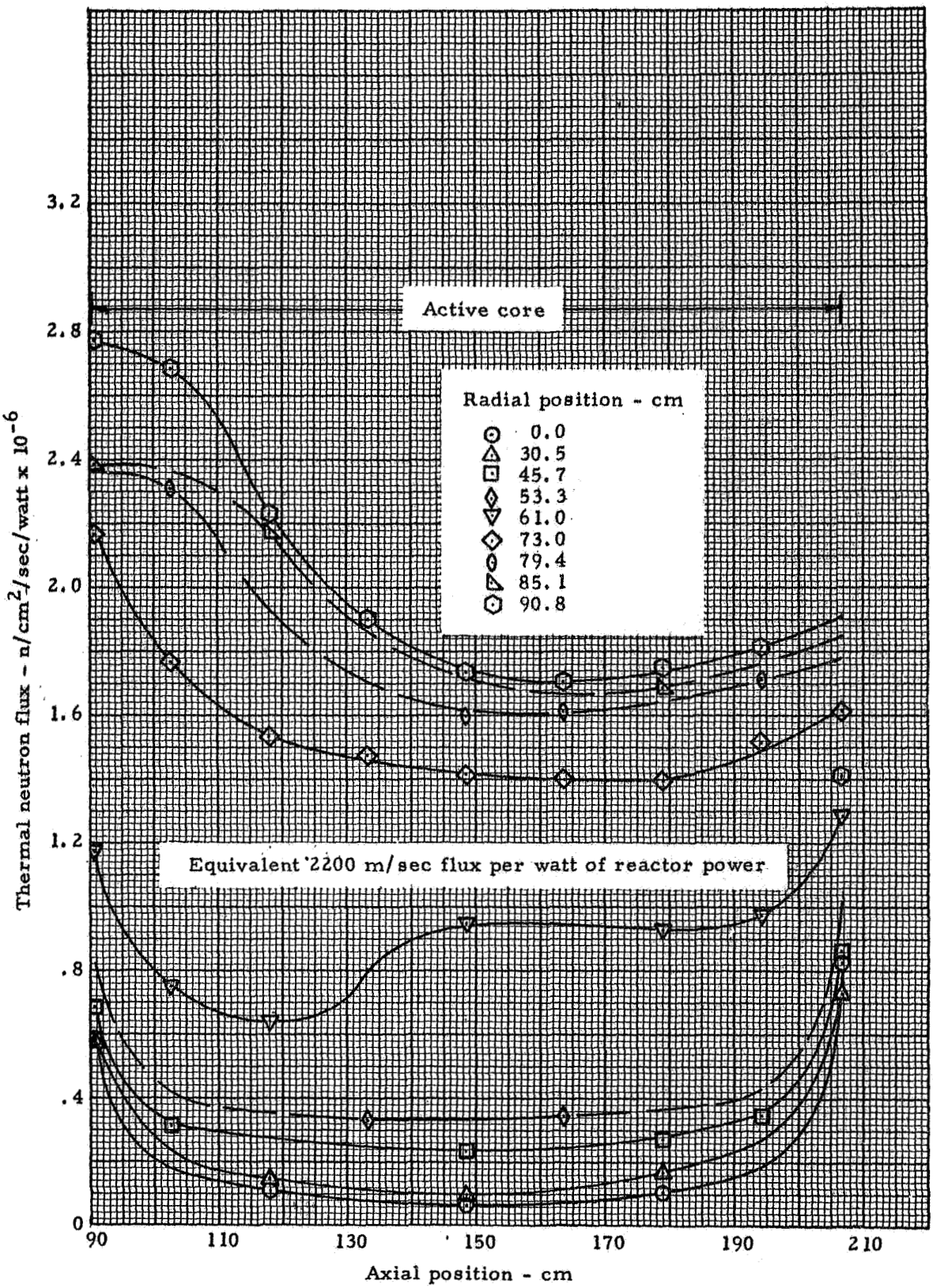

Fig. 8.24 Thermal neutron flux axial distributions in the cavity region, gold foils, variable hydrogen

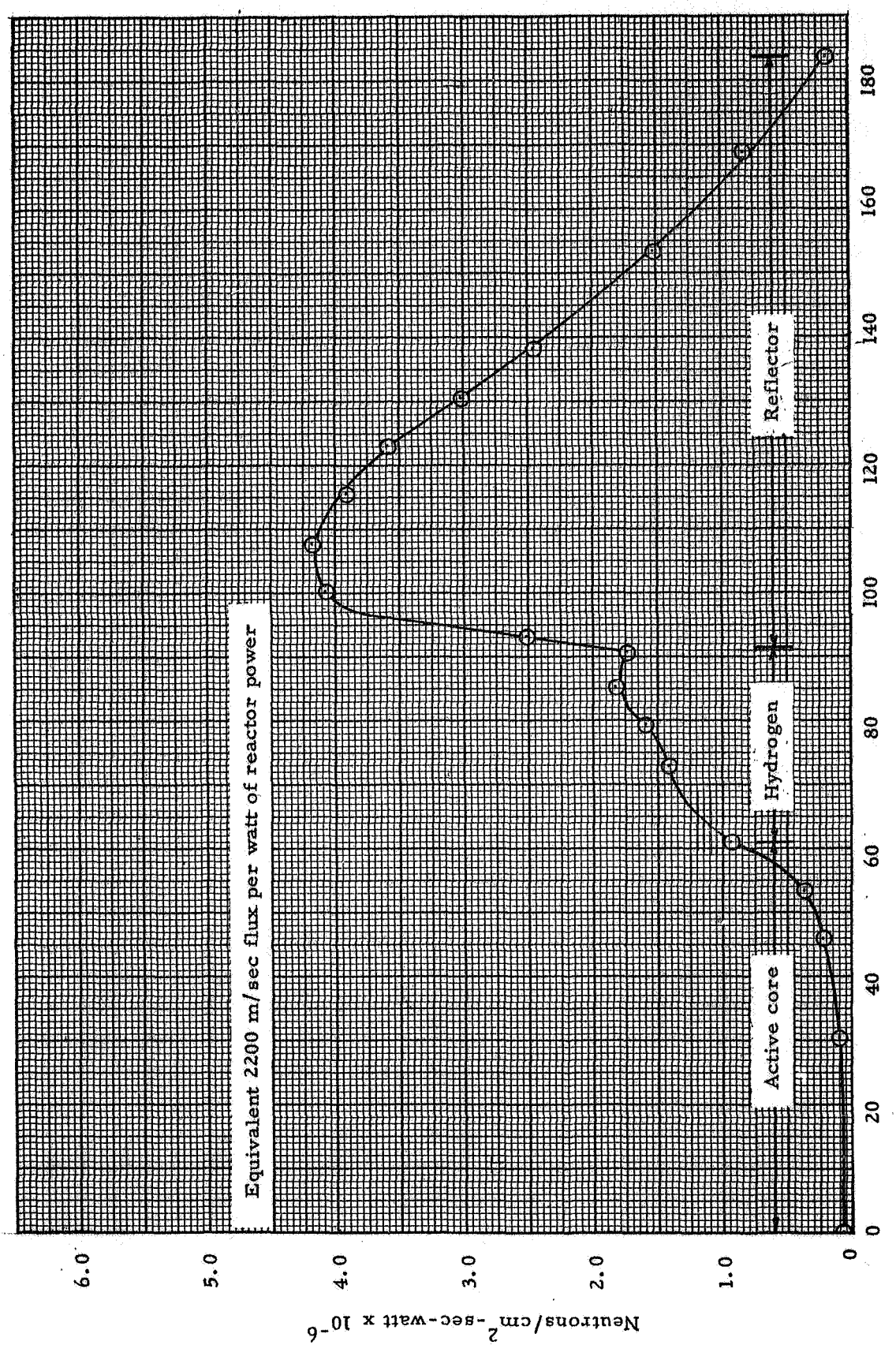

Fig. 8.25 Thermal neutron flux, radial profile, gold foils, variable hydrogen

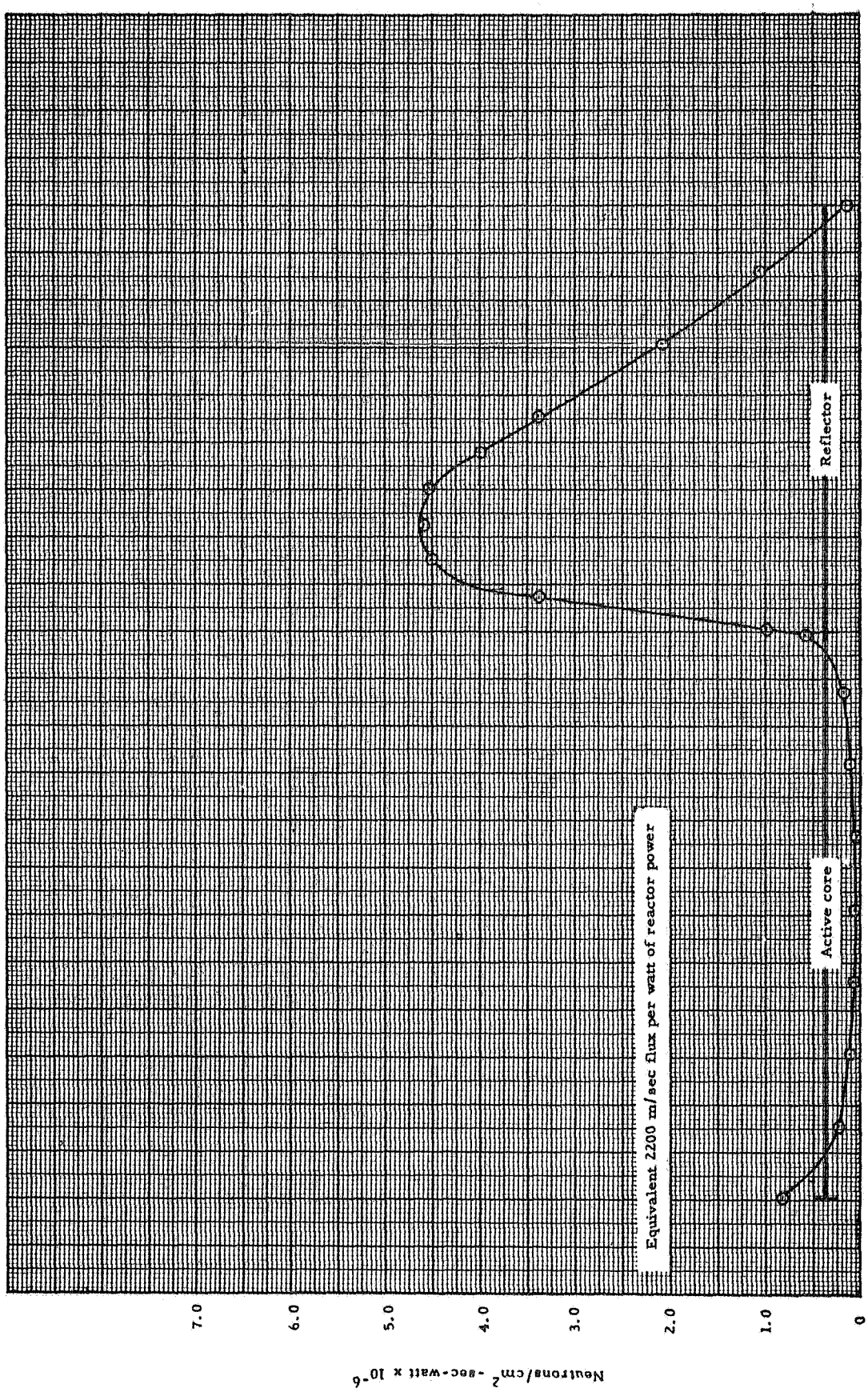

Fig. 8.26 Thermal neutron flux, gold foils, axial profile, variable hydrogen

9.0 FUEL ANNULUS IN RADIAL REFLECTOR

9.1 Description of Reactor

A series of experiments were performed to evaluate the effects of a fuel annulus in the radial reflector on critical mass and power distribution in the core. A significant reduction in critical mass was very desirable as this would reduce the operating pressure in the cavity of the power reactor. Earlier measurements (Section 6.2.2) were made in the radial reflector to determine the approximate worth of uranium vs position in the reflector. These data indicated a peak reactivity gain at about 7.6 cm from the cavity wall, thus this position was chosen as the position for the full ring of MTR type fuel plates. These fuel plates are described in Section 6.2.2. Each plate contained 8.4 gm of U^{235} and 88 of these plates were placed around the cavity region 7.6 cm from the wet surface of the cavity wall. This formed a single layer of fuel plates 50.8 cm in length which were centered axially over the cavity as shown in Figure 9.1.

The beryllium which had been in the reflector for the previous experiments was removed from the reactor and the fuel plates were installed, mounted on special holders and clamped to the same rails which held the beryllium in place.

The fuel elements were also removed and reloaded. The type 1 and 3 orientation stages were loaded with three sheets of fuel per stage and the type 2 orientation stage contained two sheets of fuel per stage. These were all size 1.0 fuel sheets so all of the type 1, 1A, 3, and 3A fuel elements were loaded with a total of 43 sheets of fuel and all type 2 and 2A fuel elements were loaded with 42 sheets of fuel.

The stainless steel liner was left in the cavity but all hydrogenous materials were removed for this experiment.

9.2 Initial Loading

Initial loading began with the fuel annulus in the radial reflector 7.6 cm from the wet surface of the cavity wall. The loading proceeded in increments, as shown in Table 9.1 and Figure 9.2, until 197 fuel elements were in the reactor. At this point the reactor was critical with 0.198%Δk excess reactivity. The loading continued until all 208 fuel elements were in the reactor. The resulting k-excess was 1.251 $\pm$ 0.018%Δk with 23.25 kg of uranium in the cavity region and 739.2 gm of U^{235} in the radial reflector. The D_2O temperature at this time was 21°C.

Figure 9.3 shows the core layout and the types of fuel elements placed in each of the positions in the active core. There were 8875 size 1.0 sheets of fuel in the reactor contained in 69 fuel elements with 42 sheets per element and 139 fuel elements with 43 sheets per element.

9.3 Rod Worth and Reactivity Measurements

9.3.1 Rod Worths

The worth of Actuators 3 and 6 equally withdrawn together with all other rods withdrawn from the reactor was measured eight times, resulting in an average worth of -1.3924±0.0229%Δk. Actuators 1 to 7 as a bank were measured once to be worth -4.1602%Δk and Actuator 5 was worth -0.5168%Δk, also a single measurement.

9.3.2 Material Worths

The reactivity worth of several materials was measured while testing this configuration and Table 9.2 contains the results. The worth of aluminum and magnesium was measured in the radial reflector region on an earlier configuration but no measurements were made within the cavity. It will be noted from Table 9.2 that these two materials were worth about the same at the outer edge of the active core.

The worth of teflon was again repeated because the fuel loading was reasonably close to the loading of the UF_6 fueled reactor (Reference 2). There was still some uncertainty as to the worth of fluorine and since teflon consisted of CF_2, the fluorine component could be extracted from the worth of teflon and carbon. Based on a core average worth of $-(0.369 \pm 0.155) \times 10^{-2}\%\Delta k/kg$ for carbon and $-(1.260 \pm 0.139) \times 10^{-3}\%\Delta k/kg$ for teflon, fluorine calculates to be worth $-(1.54 + 0.33) \times 10^{-2}\%\Delta k/kg$. This compares to $-(0.96 \pm 0.42) \times 10^{-2}\%\Delta k/kg$ reported on page 52 of Reference 2. There was, of course, some questions concerning the proper core average worth of carbon. It was not feasible to spread the carbon throughout the reactor as it was with teflon in order to measure a true core average. The only reactor grade carbon (graphite) on hand was in the form of slabs about 7.5 cm wide by 117 cm long by 1.27 cm thick. The carbon component represents 24% of the teflon worth and a 10% change in carbon worth represents only about 2% change in fluorine worth. An earlier teflon worth measurement with a much heavier fuel loading was positive, indicating a change of sign and a significant change in worth with changes in core loading.

The worth of fuel was again measured through the active core region by interchanging light and heavy-loaded fuel elements and also by removing complete fuel elements at the outer edge of the active core. These data are contained in Table 9.2 and Figure 9.4. When completely removing a fuel element, an open streaming path is created for the neutrons passing through the cavity and likewise, the fuel is self-shielded so that heavy loaded fuel elements give lower fuel worths than would lightly loaded elements. These facts account for higher values for fuel worth when removing fuel elements than when interchanging the fuel elements with different concentrations of fuel. The true values for this particular fuel loading should be between the two curves shown in Figure 9.4 and close to the bottom curve except possibly near the outer edge of the fuel where the self-shielding is greatest. The core average using the curve for the interchanging of the fuel elements was $0.756\%\Delta k/kg$. If the other curve is used beyond 50 cm from the core center this average increases to $0.770\%\Delta k/kg$. The latter value should be nearest the true core average for this reactor.

The worth of the support end plates for the beryllium reflector slabs was again repeated at this lighter loading with a measured worth of $-0.169 \pm 0.007\%\Delta k$. This compares to $-0.141 \pm 0.005\%\Delta k$ measured on the variable hydrogen experiment.

Measurements had never been made in the past to determine if the cell dividers of the core structure provided low absorption streaming paths for neutrons. Four fuel elements were loaded with an extra layer of fuel against one wall of the fuel elements. The fuel elements were then placed in positions next to one of the section walls and reactivity measurements were made as the fuel elements were rotated to the four possible positions, one of which was next to the cell or section wall. The results are given in Table 9.3. There was no trend indicating fuel to be worth more next to the section divider than on the surfaces away from the section wall.

The critical mass for this reactor calculates to be 21.7 kg of uranium after correcting for a k-excess of 1.250%Δk. The above fuel worth fits very well the curve of fuel worth for the UF_6 reactor (Reference 2, p. 212), so this curve was used to make the correction. The hardware holding the fuel annulus in place was estimated to be worth -0.35%Δk based on measurements of the hardware at 19.0 cm from the cavity wall. Correcting for this, reduces the critical loading to 21.3 kg of uranium.

9.4 Power Distribution Measurements

The power distribution measurements were all made with Actuators 4, 5, and 6 equally withdrawn about 4 cm and the other actuators fully withdrawn. The D_2O temperature was maintained at 21°C.

The cavity region was thoroughly power mapped with bare catcher foils and sufficient cadmium covered catcher foils were exposed to give a single radial at the axial center and a single axial at the radial center of the reactor as will be noted from Table 9.4. The bare foil data were normalized to the center of the core and the resulting axial profiles are shown in Figure 9.5. Figure 9.6 presents the radial distribution of the axial averages out to the cavity wall and, it will be noted that the volume weighted average over the fueled region was 1.631 with respect to the center of the core.

The cadmium ratios are given in Table 9.4. The core center showed a cadmium ratio of 7.84 which increased to 17.38 at the outer surface of the fueled region. At the separation plane and back end of the core on the radial centerline, this ratio was 16.35 and 10.81, respectively. The high value at the separation plane was due to the exhaust nozzle.

Bare catcher foils were also exposed on the fuel annulus in the D_2O to determine the power generation in the annulus. The average ratio of the foil activity in the annulus to the center of the core was 5.716. The calculated power in the active core region was 12.91 watts and in the annulus was 2.11 watts for 1 kg of U^{235} or 1.56 watts for the 739.2 gm U^{235} actually installed. The total reactor power with 1 kg of U^{235} in the annulus would, therefore, be 15.02 watts and 14.0% of this would be generated in the annulus alone.

9.5 Resonance Detector Measurements

9.5.1 Bare Gold Data

Quite extensive mapping was done with bare gold foils both in the cavity and reflector regions. Table 9.5 contains the data and this table also includes several cadmium covered foil counts. All of the gold data were power normalized to Run 1112 and the normalizer factors are given in Table 9.6.

Before plotting the bare foil data within the cavity, the data were normalized to the center of the core. Figure 9.7 shows the normalized axial profiles within the cavity along with the integrated average value for each curve. These averages were then plotted to give the radial profile in Figure 9.8. The foil activity at the center of the core appears to have been high by about 4.5% which, if corrected by this amount would have shifted all of the axial curves up by 4.5%.

The axial distribution of bare gold foil activity at the cavity wall shows a shift in distribution over that observed at the other positions. The activation flux was highest on the cavity wall at the axial center of the core whereas the ends of the cavity are the highest points on axial traverses inside the fueled region. The presence of the fuel plates near the cavity wall undoubtedly caused this change. It should be remembered that the fuel plates were 50.8 cm long and centered over the cavity. This peaking effect is apparently washed out across the void between the cavity wall and active core because of the flux contribution from the end reflectors.

The bare and cadmium covered foil activity distributions in the reflectors are shown in Figures 9.9 and 9.10. These data all appear to be normal with no appreciable change in distribution over previous measurements. The neutron flux level in the radial reflector was about the same as in the end reflector whereas the end reflector flux had been higher than the radial reflector on previous configurations with about the same fuel loading. See page 130 of Reference 1. The extra fuel in the radial reflector, however, did not produce any significant changes in the flux shape and the peak is essentially at the same point as indicated by previous data.

In Section 9.3.2, data were given on reactivity measurements that had been made to determine if the section or cell walls of the core structure provided streaming paths for neutrons. Foil exposures were also made to further evaluate this item. One fuel element was chosen near the center of the core and one near the edge of the active core and gold foils 0.0127 cm thick were placed across the elements on stages 1, 4, and 7. The results obtained from this measurement are given in Table 9.7 and Figure 9.11. The data were normalized to the center of stage 7 of the fuel element in position 10-4. It will be noted here that the flux level is lower at the cell walls thus substantiating the conclusion drawn from the reactivity measurements that there was no streaming of low energy neutrons down the cell dividers.

9.5.2 Gold Cadmium Ratios

The gold cadmium ratios are given in Table 9.8 and Figures 9.12 and 9.13. At the core center the ratio was 1.26 which increased to 1.56 at the outer edge of the fuel. At the ends of the core on the radial centerline, the ratios were 1.503 and 1.392 for the separation plane and back end of the core, respectively. There appears to be a slightly lower cadmium ratio in the radial reflector due to the fuel annulus if one compares the data to that obtained on Mockup No. 2 with a pure D_2O reflector (Reference 2, page 196). This would be expected since the fuel annulus would contribute to the fast neutron components of the neutron spectrum particularly near the region of the fuel plates.

9.5.3 Thermal Neutron Flux

Where both bare and cadmium covered gold foils were available, the thermal neutron flux was calculated. Table 9.9 contains these values and the distributions are plotted in Figure 9.14 and 9.15. Except for the region near the cavity wall, the radial reflector has a higher thermal flux level than does the end reflector. With no fuel in the radial reflector the thermal flux was normally lower than that in the end reflector. However, the total change in the relative flux levels in the two reflectors was not large and there really isn't any configuration that one can compare with exactly because of differences in fuel loading, control rod positions and other core constituents.

TABLE 9.1

Initial Loading of Reactor with

Fuel Annulus in Radial Reflector

Increment	Total Number Elements	Channel No. 1		Channel No. 2		Channel No. 3		Average CPMo/CPM	Rod Positions
		CPM	CPMo/CPM	CPM	CPMo/CPM	CPM	CPMo/CPM		
0	0	1018	1.000	656	1.000	797	1.000	1.000	In
0	0	1129	1.000	744	1.000	914	1.000	1.000	Out
1	31	1955	0,521	1274	0.515	1556	0.512	0.516	In
1	31	2284	0.494	1562	0.476	1872	0.488	0.486	Out
2	47	2526	0.403	1682	0.390	1983	0.402	0.398	In
2	47	3140	0.360	2072	0.359	2460	0.372	0.372	Out
3	73	3691	0.276	2491	0.263	2931	0.272	0.270	In
3	73	4891	0.231	3240	0.230	3805	0.240	0.234	Out
4	100	5322	0.191	3525	0.186	4254	0.187	0.188	In
4	100	7576	0.149	5024	0.148	5877	0.156	0.151	Out
5	125	7735	0.132	5163	0.127	6020	0.132	0.130	In
5	125	12393	0.091	8285	0.090	9568	0.096	0.092	Out
6	146	10254	0.099	6953	0.094	8105	0.098	0.097	In
6	146	19428	0.058	13198	0.056	15192	0.060	0.058	Out
7	167	14374	0.0708	9725	0.0675	11218	0.0710	0.0698	In
7	167	38829	0.0291	26114	0.0285	29467	0.0310	0.0295	Out
8	188	21816	0.0467	14664	0.0447	17012	0.0468	0.0461	In
8	188	172959	0.0065	113941	0.0065	123213	0.0074	0.0068	Out
9	197	27032	0.0377	18166	0.0361	20360	0.0391	0.0376	In

Reactor was critical with 0.1976%Δk excess reactivity

TABLE 9.2

Summary of Reactivity Measurements

Fuel Annulus in the Radial Reflector

Material	Location	Material Worth (%Δk/kg)
Mg	Outer edge of active core	$-(2.550\pm0.058)\times10^{-2}$
Al (type 1100)	Outer edge of active core	$-(2.508\pm0.331)\times10^{-2}$
Al (type 6061)	Outer edge of active core	$-(2.670\pm0.212)\times10^{-2}$
Teflon	Core average	$-(1.260\pm0.130)\times10^{-3}$
Carbon	5.4 cm from core center (position 11-1)	$+(0.178\pm0.155)\times10^{-3}$
Carbon	34.5 cm from core center (position 12-1)	$-(0.369\pm0.155)\times10^{-3}$
Uranium	57.3 cm from core center (position 8-16)	+1.024±0.024
Uranium	50.8 cm from core center (position 8-11)	+0.832±0.027
Uranium	60.2 cm from core center (position 3-3)	+1.162±0.088
Uranium	34.5 cm from core center (position 8-13)	+0.617±0.027
Uranium	19.4 cm from core center (position 7-5)	+0.498±0.027
Uranium	5.4 cm from core center (position 11-1)	+0.450±0.027
Fuel Element	Position 4-1 - 43-sheet fuel element	+1.276±0.036
Fuel Element	Position 4-3 - 42-sheet fuel element	+1.163±0.036
Fuel Element	Position 8-8 - 42-sheet fuel element	+1.269±0.036
Fuel Element	Position 3-1 - 43-sheet fuel element	+1.056±0.036
Fuel Element	Position 3-2 - 43-sheet fuel element	+1.121±0.036
2 Be end plates	Radial reflector	-0.169±0.007

TABLE 9.3

Fuel Element Rotation Measurement with Extra Fuel on One Surface

Fuel Annulus in Radial Reflector

Positions in Core	Location of Extra Fuel	Reactivity Change (%Δk)
3-9, 5-15, 8-14, 15-5 (3 fuel elements from outer edge of core)	Facing towards center of core	0.0
	Facing away from center of core	+0.0056
	Facing section wall	+0.0051
	Facing away from section wall	+0.0007
8-16, 15-13, 3-1, 5-13 (outer edge of core)	Facing towards center of core	0.0
	Facing away from center of core *	+0.0527
	Facing section wall	+0.0202
	Facing away from section wall	+0.0287

Note: The possible minimum standard error on these reactivity differences is about ±0.004%Δk. The average total worth of the fuel that was rotated is 0.15%Δk for position 3-9. amd 0.20%Δk for position 8-16.

* Also on outer section wall

TABLE 9.4

Catcher Foil Data

Fuel Annulus in D_2O Reflector at 7.6 cm

No.	Type	Radial (cm)	Axial (cm)	Normalized Counts	Local to Foil (X)
Run 1112					
1	Bare	0	90.8	58477	1.683
2	Bare	0	102.8	46934	1.351
3	Bare	0	118.0	41191	1.185
4	Bare	0	133.3	39606	1.140
5	Bare	0	148.5	34741	1.000 (X)
6	Bare	0	163.8	37447	1.078
7	Bare	0	179.0	36432	1.049
8	Bare	0	194.2	49049	1.412
9	Bare	0	206.9	74622	2.148
10	Bare	15.2	90.8	27464	1.654
11	Bare	15.2	102.8	48609	1.399
12	Bare	15.2	118.0	41659	1.199
13	Bare	15.2	133.3	37667	1.084
14	Bare	15.2	148.5	35484	1.021
15	Bare	15.2	163.8	35647	1.026
16	Bare	15.2	179.0	41459	1.193
17	Bare	15.2	194.2	45571	1.312
18	Bare	15.2	206.9	65692	1.891
19	Bare	30.5	90.8	66416	1.911
20	Bare	30.5	102.8	51887	1.493
21	Bare	30.5	118.0	44824	1.290
22	Bare	30.5	133.3	42567	1.225
23	Bare	30.5	148.5	41937	1.207
24	Bare	30.5	163.8	42400	1.220
25	Bare	30.5	179.0	46449	1.337
26	Bare	30.5	194.2	52920	1.523
27	Bare	30.5	206.9	68291	1.965
28	Bare	45.7	90.8	71511	2.058
29	Bare	45.7	102.8	58536	1.685
30	Bare	45.7	118.0	52080	1.499
31	Bare	45.7	133.3	52508	1.511
32	Bare	45.7	148.5	49692	1.430
33	Bare	45.7	163.8	50984	1.467
34	Bare	45.7	179.0	52368	1.507
35	Bare	45.7	194.2	58172	1.674
36	Bare	45.7	206.9	72709	2.093
37	Bare	61.0	90.8	96482	2.777
38	Bare	61.0	102.8	91448	2.632
39	Bare	61.0	118.0	88158	2.537

TABLE 9.4
(Continued)

No.	Type	Location Radial (cm)	Location Axial (cm)	Normalized Counts	Local to Foil (X)
Run 1112 (Cont'd)					
40	Bare	61.0	133.3	84341	2.427
41	Bare	61.0	148.5	87339	2.514
42	Bare	61.0	163.8	82867	2.385
43	Bare	61.0	179.0	84267	2.425
44	Bare	61.0	194.2	91007	2.619
45	Bare	61.0	206.9	94877	2.731
46	Bare	76.2	90.8	110104	3.169
47	Bare	76.2	102.8	104755	3.015
48	Bare	76.2	118.0	104622	3.011
49	Bare	76.2	133.3	100925	2.905
50	Bare	76.2	148.5	101440	2.919
51	Bare	76.2	163.8	99392	2.861
52	Bare	76.2	179.0	102250	2.943
53	Bare	76.2	194.2	106895	3.076
54	Bare	76.2	206.9	105391	3.033
55	Bare	91.4	90.8	115533	3.325
56	Bare	91.4	102.8	116339	3.348
57	Bare	91.4	118.0	101679	2.926
58	Bare	91.4	133.3	105119	3.025
59	Bare	91.4	148.5	99694	2.869
60	Bare	91.4	163.8	103155	2.969
61	Bare	91.4	179.0	101414	2.919
62	Bare	91.4	194.2	97948	2.819
63	Bare	91.4	206.9	107164	3.084
Run 1113					Cadmium Ratios
1	Cd	0	90.8	5409	10.81
2	Cd	0	118.0	4773	8.63
3	Cd	0	148.5	4432	7.84
4	Cd	0	179.0	4807	7.58
5	Cd	0	206.9	4563	16.35
6	Cd	30.5	148.5	4675	8.97
7	Cd	61.0	148.5	5026	17.38
8	Cd	91.4	148.5	5530	18.03
Run 1115					Local to Foil (X)
1	Bare	99.7	125.7	194979	5.613
2	Bare	100.2	125.7	200171	5.763
3	Bare	99.7	151.1	203984	5.873
4	Bare	100.2	151.1	192643	5.546
5	Bare	99.7	176.5	195915	5.640
6	Bare	100.2	176.5	203694	5.864

TABLE 9.5

Gold Foil Data

Fuel Annulus in Radial Reflector at 7.6 cm

Foil No.	Foil Type	Location Radial (cm)	Location Axial (cm)	Foil Weight (gm)	Specific Activity d/m/gm x 10^{-6}	Local to Foil (X)
Run 1112						
1	Bare	0	89.4	0.0159	3.081	1.454
2	Bare	0	74.9	0.0199	6.462	3.050
3	Bare	0	59.6	0.0193	5.370	2.534
4	Bare	0	44.4	0.0164	3.655	1.725
5	Bare	0	29.1	0.0160	2.118	1.000
6	Bare	0	13.9	0.0161	1.111	0.524
7	Bare	0	0	0.0167	0.162	0.076
8	Bare	93.2	151.1	0.0173	4.336	2.046
9	Bare	107.7	151.1	0.0178	6.365	3.004
10	Bare	123.0	151.1	0.0152	5.040	2.378
11	Bare	138.2	151.1	0.0190	3.262	1.539
12	Bare	153.5	151.1	0.0173	1.947	0.919
13	Bare	168.7	151.1	0.0182	0.904	0.427
14	Bare	183.9	151.1	0.0189	0.119	0.056
Run 1113						
1	Cd	0	89.4	0.0183	1.721	
2	Cd	93.2	151.1	0.0184	1.801	
Run 1114						
1	Cd	0	90.8	0.0153	1.598	
2	Cd	0	118.0	0.0164	1.503	
3	Cd	0	148.5	0.0205	1.304	
4	Cd	0	179.0	0.0169	1.398	
5	Cd	0	206.9	0.0212	1.320	
6	Cd	0	74.9	0.0221	1.227	
7	Cd	0	44.4	0.0186	0.054	
8	Cd	30.5	148.5	0.0179	1.411	
9	Cd	61.0	148.5	0.0180	1.499	
10	Cd	91.4	148.5	0.0164	1.684	
11	Cd	107.7	151.1	0.0187	1.104	
12	Cd	138.2	151.1	0.0188	0.033	
Run 1115						
1	Bare	0	90.8	0.0153	2.669	1.260
2	Bare	0	102.8	0.0142	2.377	1.122
3	Bare	0	118.0	0.0158	2.134	1.007

TABLE 9.5
(Continued)

Foil No.	Type	Location Radial (cm)	Location Axial (cm)	Foil Weight (gm)	Specific Activity d/m/gm x 10^{-6}	Local to Foil (X)
Run 1115 (Cont'd)						
4	Bare	0	133.3	0.0155	2.076	0.980
5	Bare	0	148.5	0.0143	2.119	1.000 (X)
6	Bare	0	163.8	0.0177	2.040	0.963
7	Bare	0	179.0	0.0163	2.142	1.011
8	Bare	0	194.2	0.0171	2.230	1.052
9	Bare	0	206.9	0.0193	2.636	1.244
10	Bare	15.2	90.8	0.0211	2.568	1.212
11	Bare	15.2	102.8	0.0154	2.393	1.129
12	Bare	15.2	118.0	0.0182	2.170	1.024
13	Bare	15.2	133.3	0.0163	2.093	0.988
14	Bare	15.2	148.5	0.0170	1.987	0.938
15	Bare	15.2	163.8	0.0161	2.060	0.972
16	Bare	15.2	179.0	0.0182	2.131	1.006
17	Bare	15.2	194.2	0.0160	2.297	1.084
18	Bare	15.2	206.9	0.0176	2.596	1.225
19	Bare	30.5	90.8	0.0171	2.775	1.310
20	Bare	30.5	102.8	0.0145	2.461	1.161
21	Bare	30.5	118.0	0.0186	2.262	1.067
22	Bare	30.5	133.3	0.0151	2.210	1.043
23	Bare	30.5	148.5	0.0159	2.149	1.014
24	Bare	30.5	163.8	0.0171	2.145	1.012
25	Bare	30.5	179.0	0.0134	2.353	1.110
26	Bare	30.5	194.2	0.0183	2.415	1.140
27	Bare	30.5	206.9	0.0200	2.756	1.301
28	Bare	45.7	90.8	0.0171	2.863	1.351
29	Bare	45.7	102.8	0,0143	2.667	1.259
30	Bare	45.7	118.0	0.0177	2.425	1.144
31	Bare	45.7	133.3	0.0162	2.458	1.160
32	Bare	45.7	148.5	0.0202	2.286	1.079
33	Bare	45.7	163.8	0.0152	2.451	1.157
34	Bare	45.7	179.0	0.0177	2.422	1.143
35	Bare	45.7	194.2	0.0147	2.634	1.243
36	Bare	45.7	206.9	0.0163	2.862	1.351
37	Bare	61.0	90.8	0.0204	3.184	1.503
38	Bare	61.0	102.8	0.0161	3.124	1.474
39	Bare	61.0	118.0	0.0160	3.085	1.456
40	Bare	61.0	133.3	0.0197	2.991	1.412
41	Bare	61.0	148.5	0.0200	2.965	1.399
42	Bare	61.0	163.8	0.0216	2.957	1.395
43	Bare	61.0	179.0	0.0148	3.045	1.437
44	Bare	61.0	194.2	0.0178	3.137	1.480
45	Bare	61.0	206.9	0.0170	3.222	1.521
46	Bare	76.2	90.8	0.0169	3.536	1.669

TABLE 9.5

(Continued)

Foil No.	Type	Location Radial (cm)	Location Axial (cm)	Foil Weight (gm)	Specific Activity $d/m/gm \times 10^{-6}$	Local to Foil (X)
Run 1115 (Cont'd)						
47	Bare	76.2	102.8	0.0169	3.536	1.669
48	Bare	76.2	118.0	0.0166	3.484	1.644
49	Bare	76.2	133.3	0.0175	3.341	1.577
50	Bare	76.2	148.5	0.0187	2.890	1.364
51	Bare	76.2	163.8	0.0202	3.411	1.610
52	Bare	76.2	179.0	0.0145	3.548	1.674
53	Bare	76.2	194.2	0.01555	3.660	1.727
54	Bare	76.2	206.9	0.0162	3.481	1.643
55	Bare	91.4	90.8	0.0172	3.468	1.637
56	Bare	91.4	102.8	0.0178	3.515	1.659
57	Bare	91.4	118.0	0.0164	3.606	1.702
58	Bare	91.4	133.3	0.0137	3.545	1.672
59	Bare	91.4	148.5	0.0146	3.528	1.665
60	Bare	91.4	163.8	0.0156	3.473	1.639
61	Bare	91.4	179.0	0.0147	3.463	1.634
62	Bare	91.4	194.2	0.01735	3.271	1.544
63	Bare	91.4	206.9	0.0162	3.346	1.579
64	Cd	0	59.6	0.0198	0.322	
65	Cd	0	29.1	0.0194	0.011	
66	Cd	123.0	151.1	0.0206	0.255	
67	Cd	153.5	151.1	0.0161	0.005	
Run 1116						
1	Bare	0	82.5	0.0156	5.566	2.627
2	Bare	0	67.2	0.0141	6.151	2.903
3	Bare	0	52.0	0.01965	4.377	2.066
4	Bare	101.1	151.1	0.0175	5.505	2.598
5	Bare	115.4	151.1	0.0146	5.791	2.733
6	Bare	130.6	151.1	0.0163	4.024	1.899
7	Cd	30.5	90.8	0.0206	1.470	
8	Cd	30.5	206.9	0.0156	1.542	
9	Cd	61.0	90.8	0.0154	1.577	
10	Cd	61.0	209.5	0.0161	1.501	
11	Cd	91.4	90.8	0.0165	1.376	
12	Cd	91.4	206.9	0.0194	1.306	

TABLE 9.6

Power Normalization Factors

Fuel Annulus in D_2O Reflector at 7.6 cm

Run No.	Time	Decay Time (min)	Decay Factor	Activity (CPM)	Corrected Activity (CPM)	Norm. Factor
1112	1209.55	48.89	0.974	258902	252171	
	1211.40	50.74	1.017	247741	251953	
	1213.10	52.44	1.057	238245	251825	
					251983	1.000
1113	1509.56	46.41	0.917	266764	244623	
	1511.75	48.60	0.967	253166	244812	
	1513.90	50.75	1.017	240318	244403	
					244613	1.030
1114	1709.06	68.40	1.457	170976	249112	
	1711.20	70.54	1.515	164750	249596	
	1713.57	72.91	1.578	157698	248847	
					249185	1.011
1115	1304.30	47.18	0.935	260916	243956	
	1305.90	48.78	0.971	251142	243859	
	1307.50	50.38	1.009	241599	243773	
					243863	
			243863 x 2.37/2.33 =		248049	1.016
1116	1543.10	49.76	0.994	251279	249771	
	1544.90	51.56	1.035	240980	249414	
	1546.50	53.16	1.075	232254	249673	
					249619	
			249619 x 2.37/2.33 =		253904	0.992
1117	1448.30	49.96	0.999	257132	256875	
	1450.10	51.76	1.041	246057	256145	
	1452.00	53.66	1.087	235959	256487	
					256502	
			256502 x 2.35/2.33 =		258704	0.974
1118	1233.50	49.30	0.983	263897	259411	
	1235.40	51.20	1.029	251219	258504	
	1237.20	53.00	1.071	241846	259017	
					258977	
			258977 x 2.35/2.33 =		261200	0.965
1119	1124.45	25.50	0.496	532659	264199	
	1126.45	27.50	0.532	501899	267010	
	1135.45	36.50	0.705	378933	267148	
					266119	
			266119 x 2.30/2.33 =		262693	0.959

TABLE 9.6

(Continued)

Run No.	Time	Decay Time (Min)	Decay Factor	Activity (CPM)	Corrected Activity (CPM)	Norm. Factor
1120	1428.20	52.50	1.059	255065	270114	
	1429.70	54.00	1.095	244915	268182	
	1431.20	55.50	1.132	237472	268818	
					269038	
			269038 x 2.30/2.33 =		265574	0.949
1121	1037.73	51.02	1.023	263077	269128	
	1039.73	53.02	1.071	251847	269728	
	1041.73	55.02	1.120	240150	268968	
					269274	
			269274 x 2.26/2.33 =		261184	0.965
1122	1509.97	35.50	0.685	355538	243544	
	1511.97	37.50	0.725	335264	243066	
	1513.97	39.50	0.767	316533	242781	
					243130	
			243130 x 2.208/2.33 =		230400	1.094

TABLE 9.7

Measurement of Streaming Effects

Along Section Dividers - Gold Data

Foil No.	Fuel Element Position	Stage No.	Distance from Center of element (cm)	Foil Weight (gm)	Normalized Counts	Local to No. 1976	Counts/ gm
1953	10-4	1	3.81 (cell wall)	0.3978	25977	1.306	65302
1812	10-4	1	1.75	0.4064	28016	1.379	68937
1904	10-4	1	0.00	0.3955	26772	1.354	67692
1927	10-4	1	1.75	0.3986	29433	1.477	73841
1935	10-4	1	3.81	0.3942	25281	1.283	64132
1916	10-4	4	3.81 (cell wall)	0.3913	21086	1.078	53887
1909	10-4	4	1.75	0.3845	23958	1.246	62309
1947	10-4	4	0.00	0.4050	22000	1.086	54321
1901	10-4	4	1.75	0.3950	24060	1.218	60911
1816	10-4	4	3.81	0.4042	20747	1.027	51329
1941	10-4	7	3.81 (cell wall)	0.3960	20158	1.018	50904
1965	10-4	7	1.75	0.4055	23751	1.171	58572
1976	10-4	7	0.00	0.4125	20618	1.000	49983
1969	10-4	7	1.75	0.3887	27772	1.429	71448
1906	10-4	7	3.81	0.3807	20176	1.060	52997
1971	12-3	1	3.81	0.3814	30711	1.610	80522
1968	12-3	1	1.75	0.3973	34365	1.730	86496
1907	12-3	1	0.00	0.3841	30977	1.613	80648
1960	12-3	1	1.75	0.4134	33793	1.635	81744
1993	12-3	1	3.81 (cell wall)	0.4098	29220	1.426	71303
1998	12-3	4	3.81	0.4084	30603	1.499	74934
1945	12-3	4	1,75	0.3866	28621	1.481	74033
1944	12-3	4	0.00	0.3971	27990	1.410	70486
1996	12-3	4	1.75	0.3845	30197	1.571	78536
1973	12-3	4	3.81 (cell wall)	0.3848	26414	1.373	68643
1989	12-3	7	3.81	0.3871	30276	1.564	78212
1959	12-3	7	1.75	0.3883	33393	1.720	85998
1992	12-3	7	0.00	0.4035	28247	1.400	70005
1977	12-3	7	1.75	0.3848	31343	1.629	81453
1902	12-3	7	3.81 (cell wall)	0.3860	25972	1.346	67285

TABLE 9.8

Gold Foil Cadmium Ratios

Fuel Annulus in Radial Reflector 7.6 cm from Cavity Wall

Location		Infinitely Dilute Foil Activity $d/m/gm \times 10^{-6}$		
Radial (cm)	Axial (cm)	Bare Foils	Cadmium Foils	Cadmium Ratios
0	90.8	3.805	2.734	1.392
0	118.0	3.243	2.631	1.233
0	148.5	3.112	2.468	1.261
0	179.0	3.199	2.473	1.294
0	206.9	3.799	2.529	1.503
30.5	90.8	3.992	2.787	1.433
30.5	148.5	3.225	2.545	1.267
30.5	206.9	3.996	2.655	1.505
61.0	90.8	4.456	2.704	1.648
61.0	148.5	4.230	2.709	1.561
61.0	206.9	4.360	2.612	1.669
91.4	90.8	4.525	2.414	1.875
91.4	148.5	4.726	2.948	1.603
91.4	206.9	4.379	2.423	1.807
0	89.4	4.404	3.128	1.408
0	74.9	7.574	2.386	3.174
0	59.6	5.647	0.602	9,383
0	44.4	3.697	0.0987	37.45
0	29.1	2.127	0.0204	104.2
93.2	151.1	5.776	3,280	1.761
107.7	151.1	7.264	2.022	3.592
123.0	151.1	5.240	0.483	10.84
138.2	151.1	3.290	0.0606	54.33
153.5	151.1	1.952	0.0087	224.4

TABLE 9.9

Thermal Neutron Flux

Fuel Annulus in Radial Reflector 7.6 cm from Cavity Wall

Location		Thermal Neutron Flux
Radial (cm)	Axial (cm)	$n/cm^2/sec/watt \times 10^{-6}$
0	90.8	1.290
0	118.0	0.737
0	148.5	0.776
0	179.0	0.875
0	206.9	1.530
30.5	90.8	1.452
30.5	148.5	0.818
30.5	206.9	1.615
61.0	90.8	2.111
61.0	148.5	1.831
61.0	206.9	2.105
91.4	90.8	2.542
91.4	148.5	2.141
91.4	206.9	2.356
0	89.4	1.535
0	74.9	6.247
0	59.6	6.075
0	44.4	4.333
0	29.1	2.536
93.2	151.1	3.006
107.7	151.1	1.213
123.0	151.1	5.728
138.2	151.1	3.888
153.5	151.1	2.340

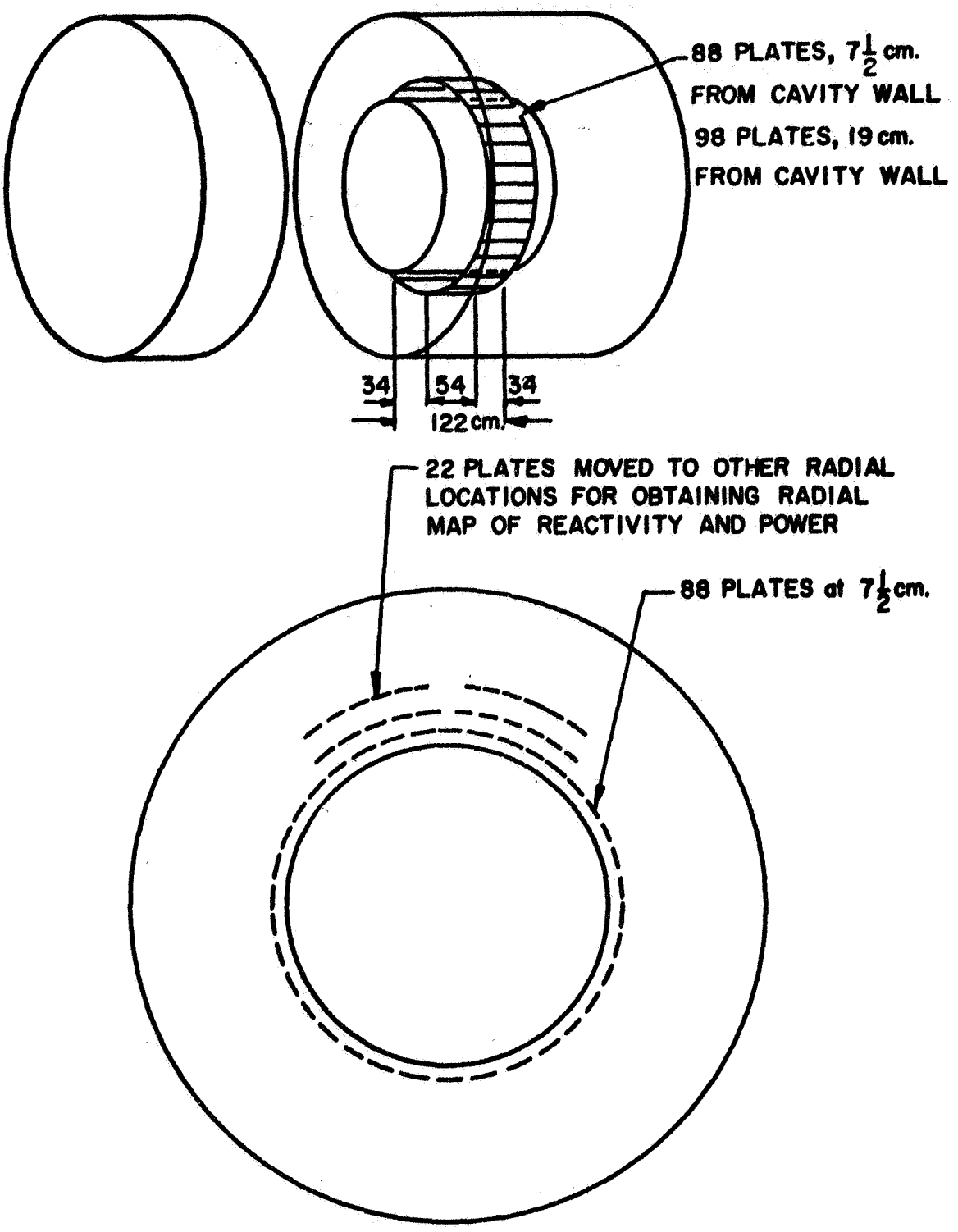

Fig. 9.1 Reactor with fuel annulus in radial reflector

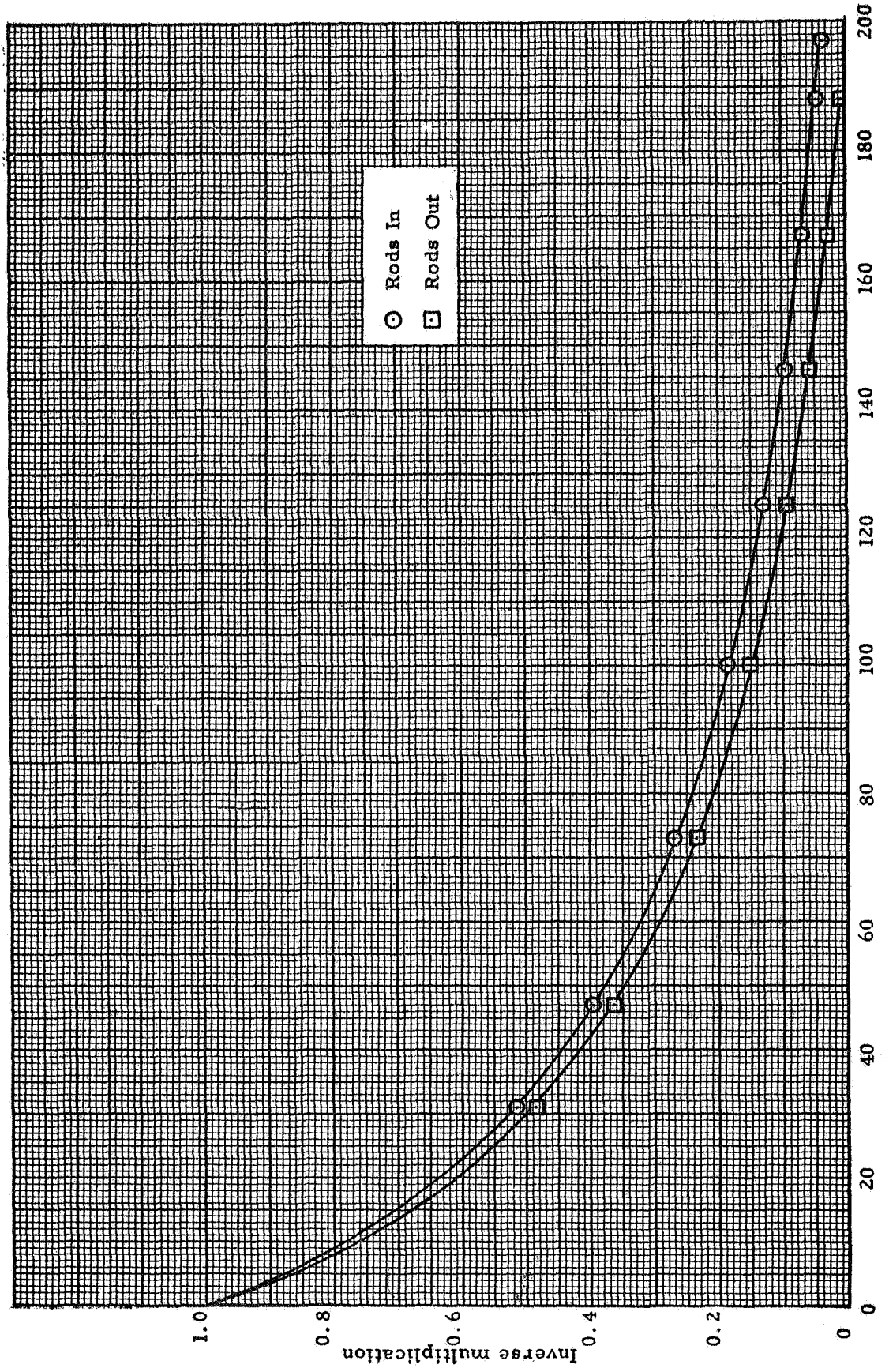

Fig. 9.2 Inverse multiplication curves, fuel in reflector

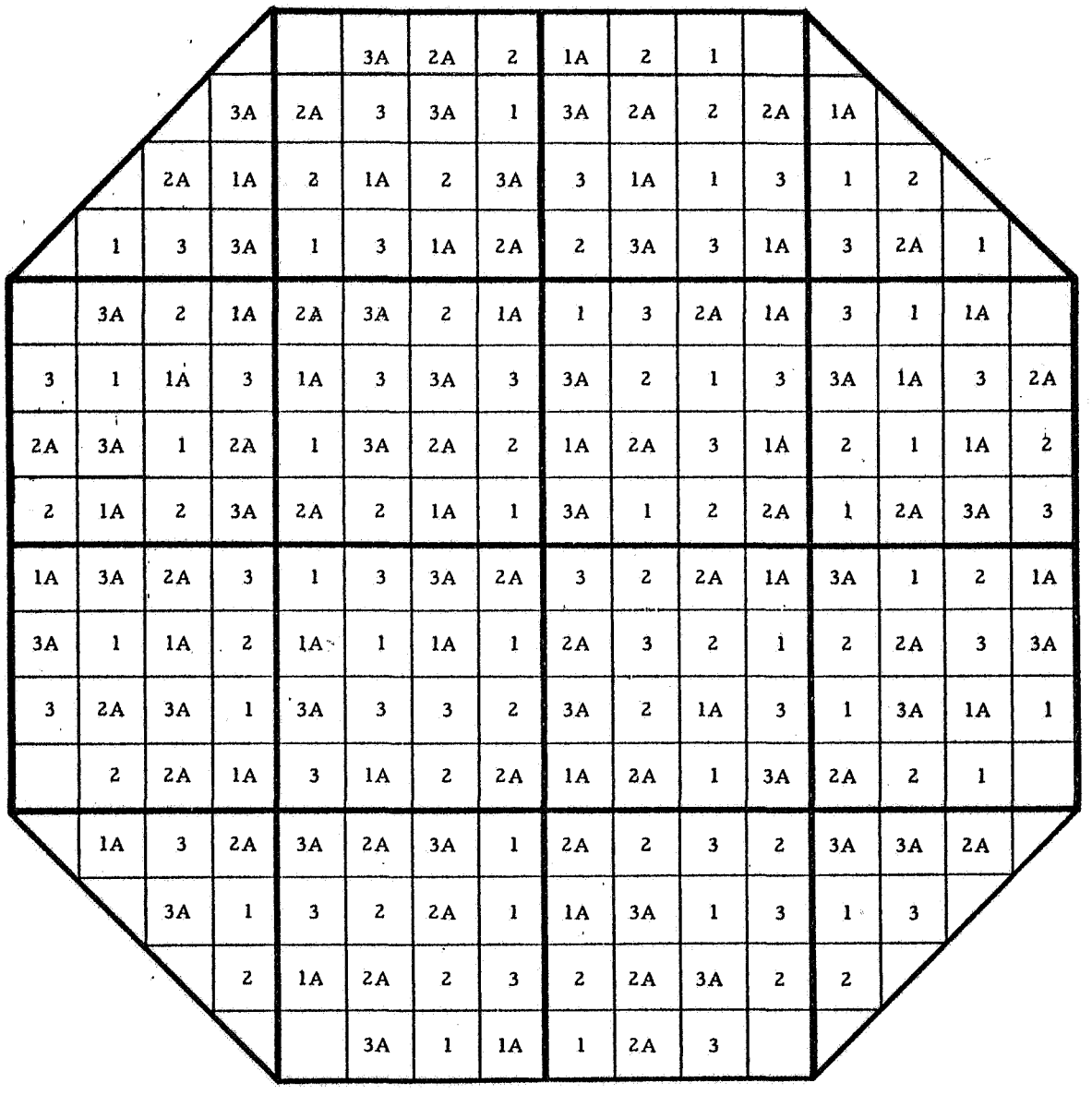

				3A	2A	2	1A	2	1						
			3A	2A	3	3A	1	3A	2A	2	2A	1A			
		2A	1A	2	1A	2	3A	3	1A	1	3	1	2		
	1	3	3A	1	3	1A	2A	2	3A	3	1A	3	2A	1	
	3A	2	1A	2A	3A	2	1A	1	3	2A	1A	3	1	1A	
3	1	1A	3	1A	3	3A	3	3A	2	1	3	3A	1A	3	2A
2A	3A	1	2A	1	3A	2A	2	1A	2A	3	1A	2	1	1A	2
2	1A	2	3A	2A	2	1A	1	3A	1	2	2A	1	2A	3A	3
1A	3A	2A	3	1	3	3A	2A	3	2	2A	1A	3A	1	2	1A
3A	1	1A	2	1A	1	1A	1	2A	3	2	1	2	2A	3	3A
3	2A	3A	1	3A	3	3	2	3A	2	1A	3	1	3A	1A	1
	2	2A	1A	3	1A	2	2A	1A	2A	1	3A	2A	2	1	
	1A	3	2A	3A	2A	3A	1	2A	2	3	2	3A	3A	2A	
		3A	1	3	2	2A	1	1A	3A	1	3	1	3		
			2	1A	2A	2	3	2	2A	3A	2	2			
					3A	1	1A	1	2A	3					

Fig. 9.3 Fuel element layout in active core, fuel in reflector

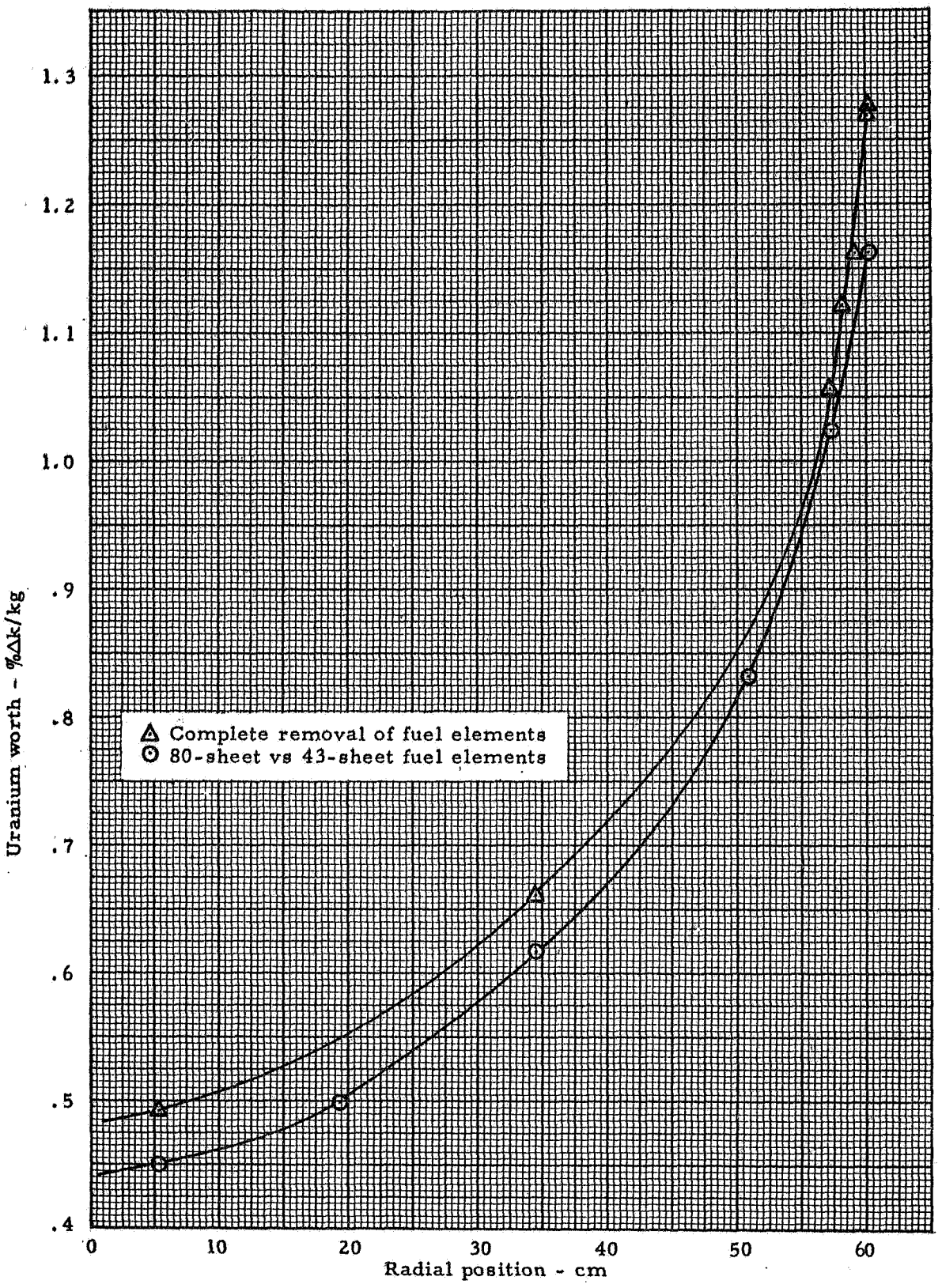

Fig. 9.4 Uranium reactivity worth in the active core, fuel in reflector

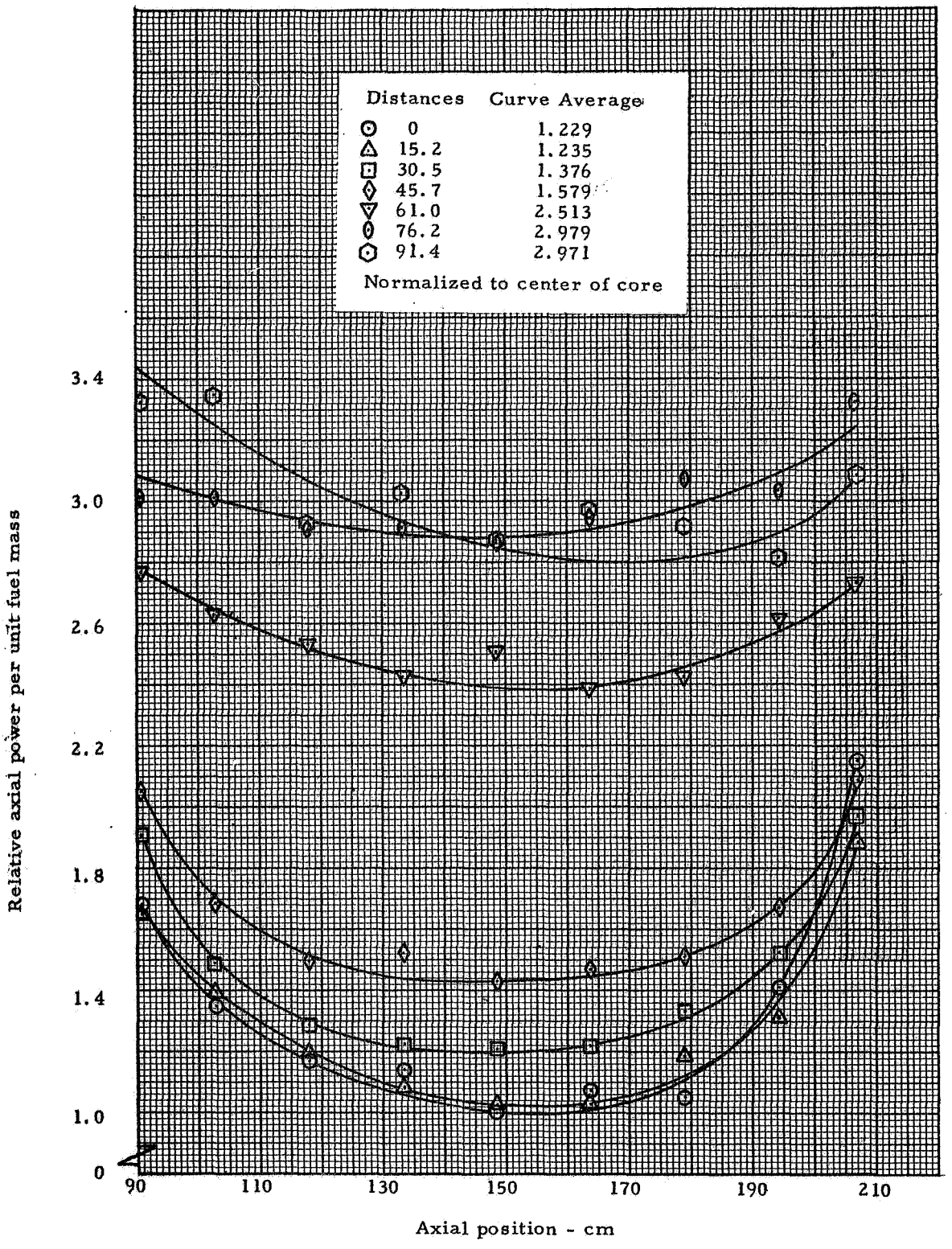

Fig. 9.5 Relative axial power distribution from bare catcher foils within the cavity region, fuel in reflector.

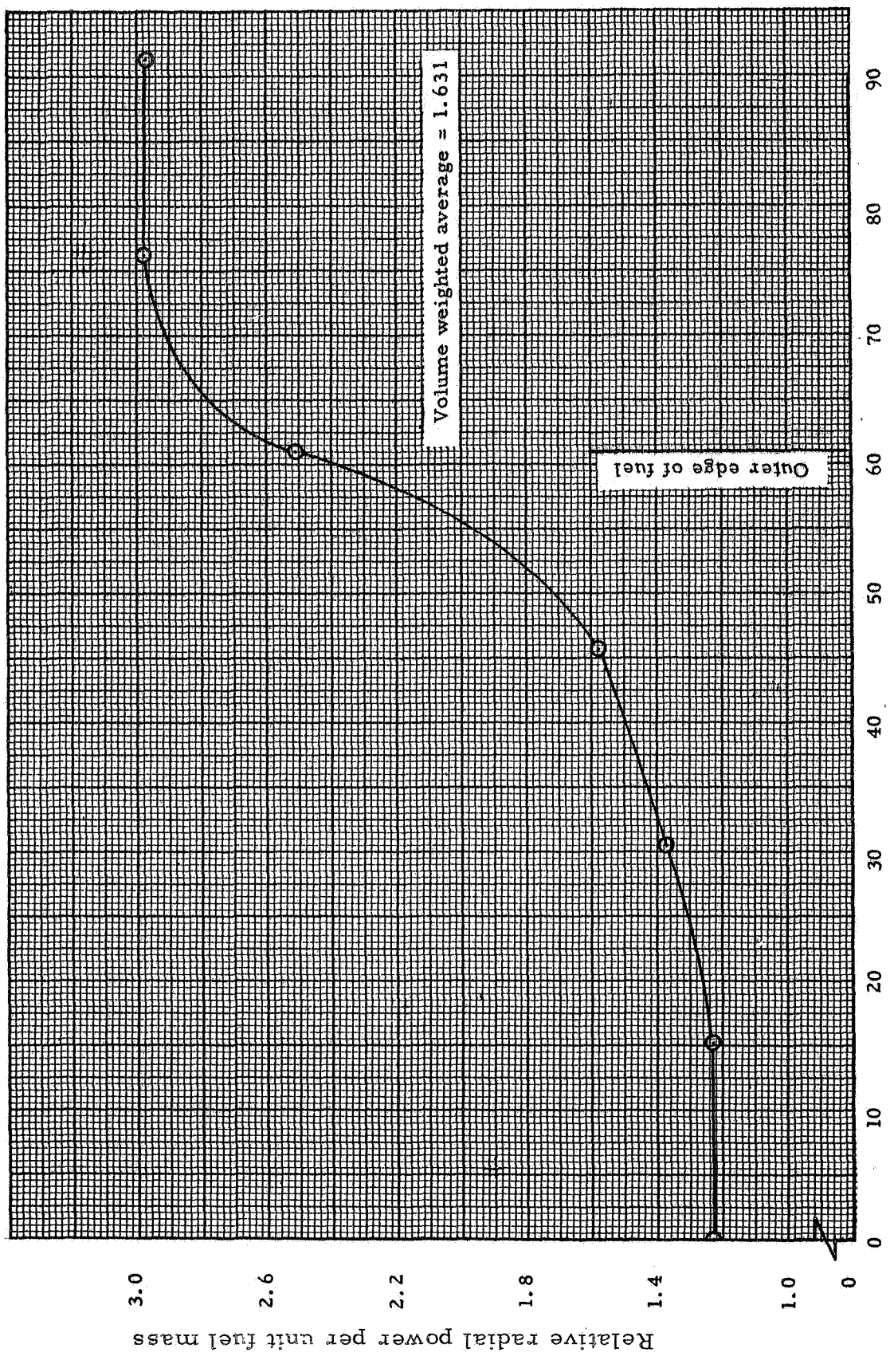

Fig. 9.6 Relative radial distribution from bare catcher foils within the cavity region using the axial averages from Figure 2.1, Fuel in reflector

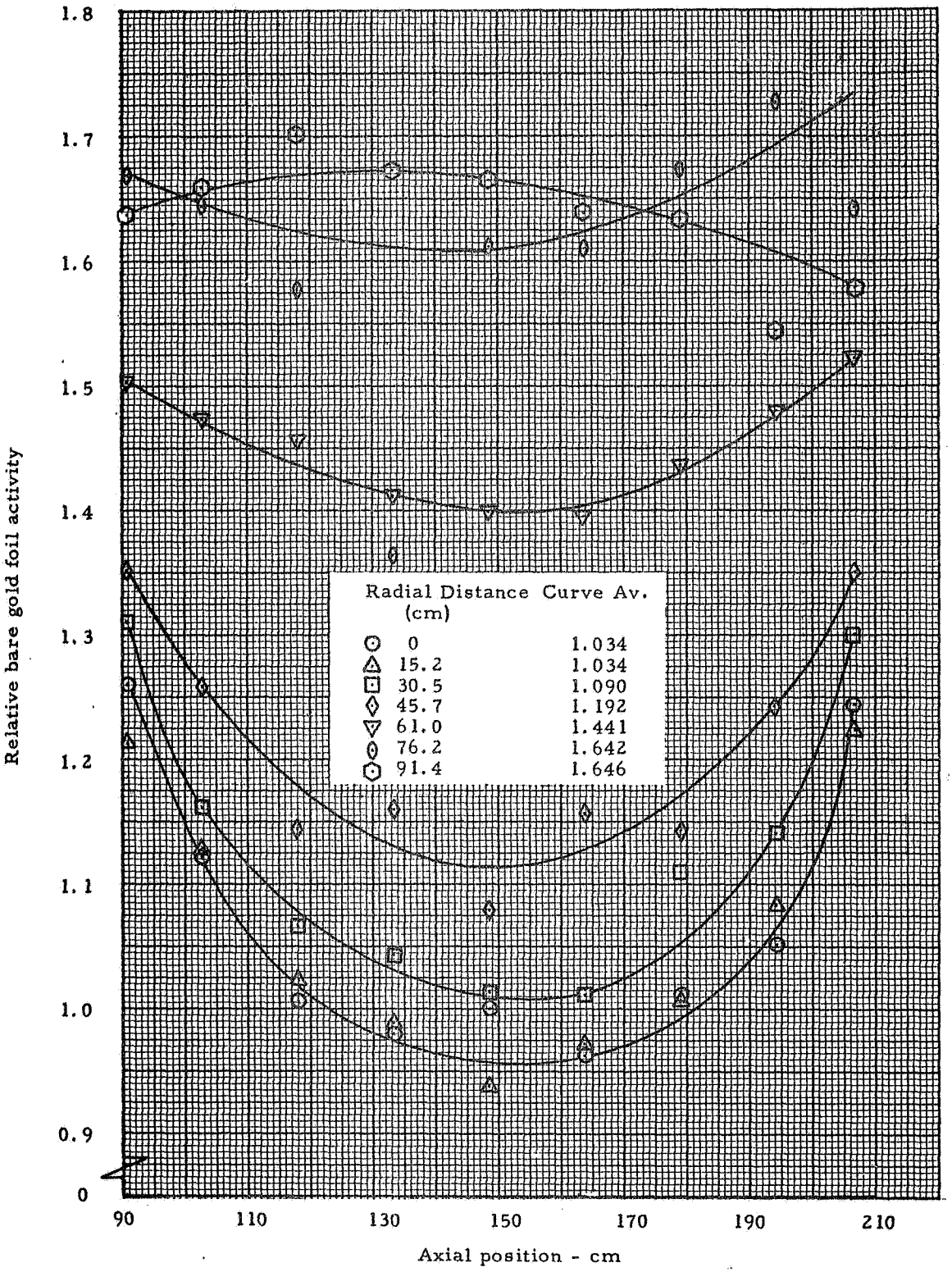

Fig. 9.7 Relative bare gold foil activity, axial distributions in the cavity region, fuel to reflector

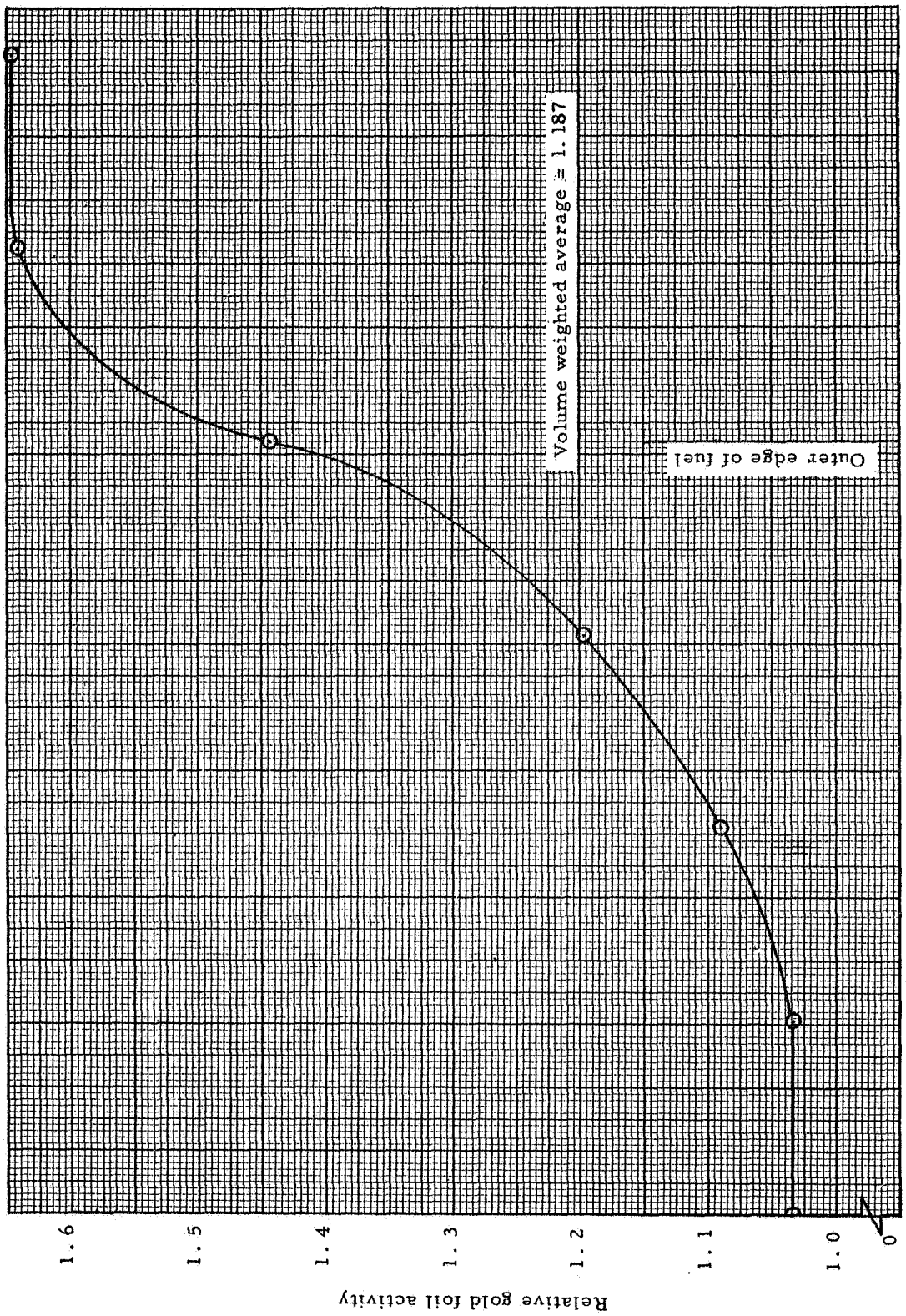

Fig. 9.8 Bare gold foil activity, radial profile in the cavity region, fuel in reflector

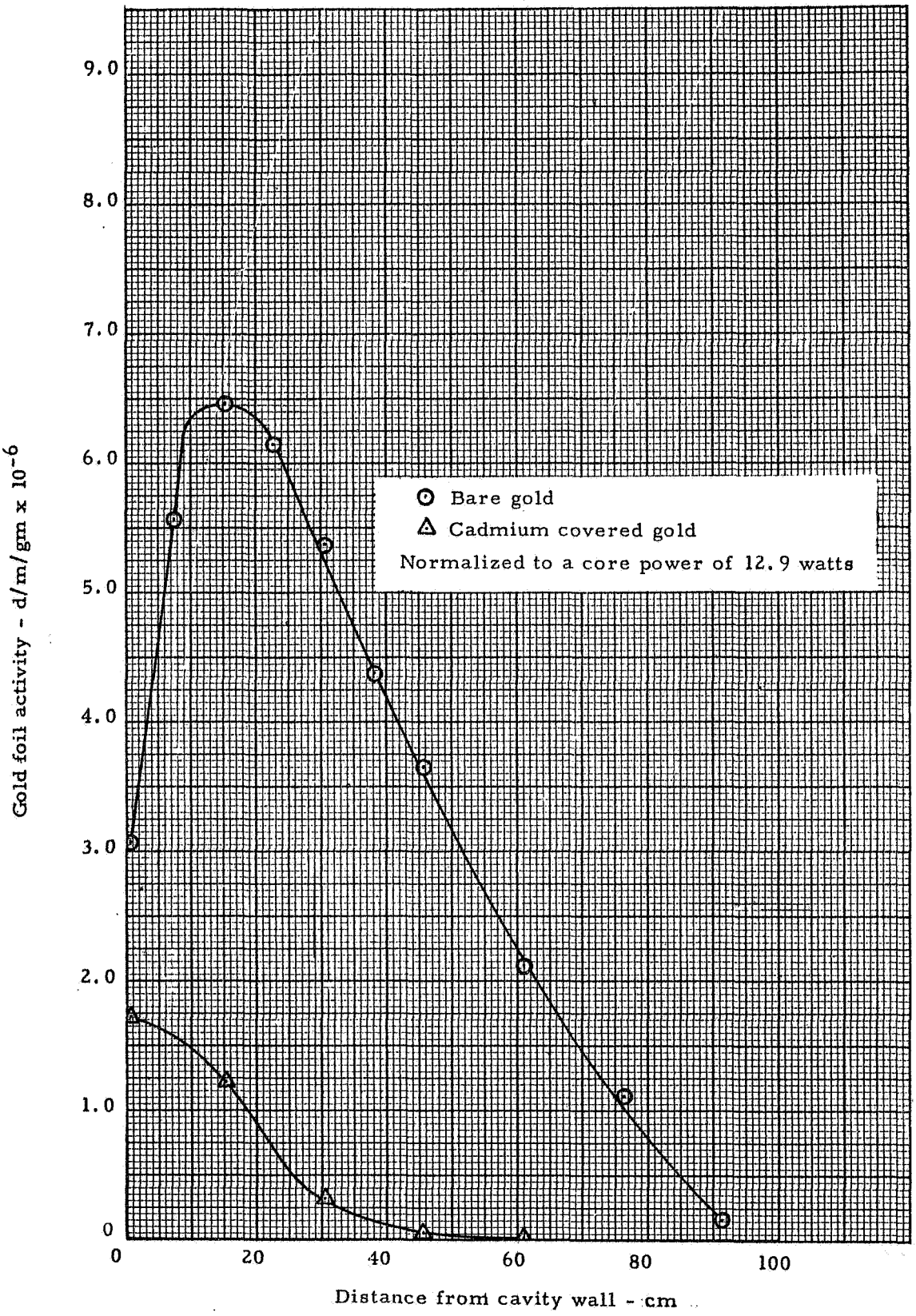

Fig. 9.9 Gold foil activity, end reflector, fuel in radial reflector

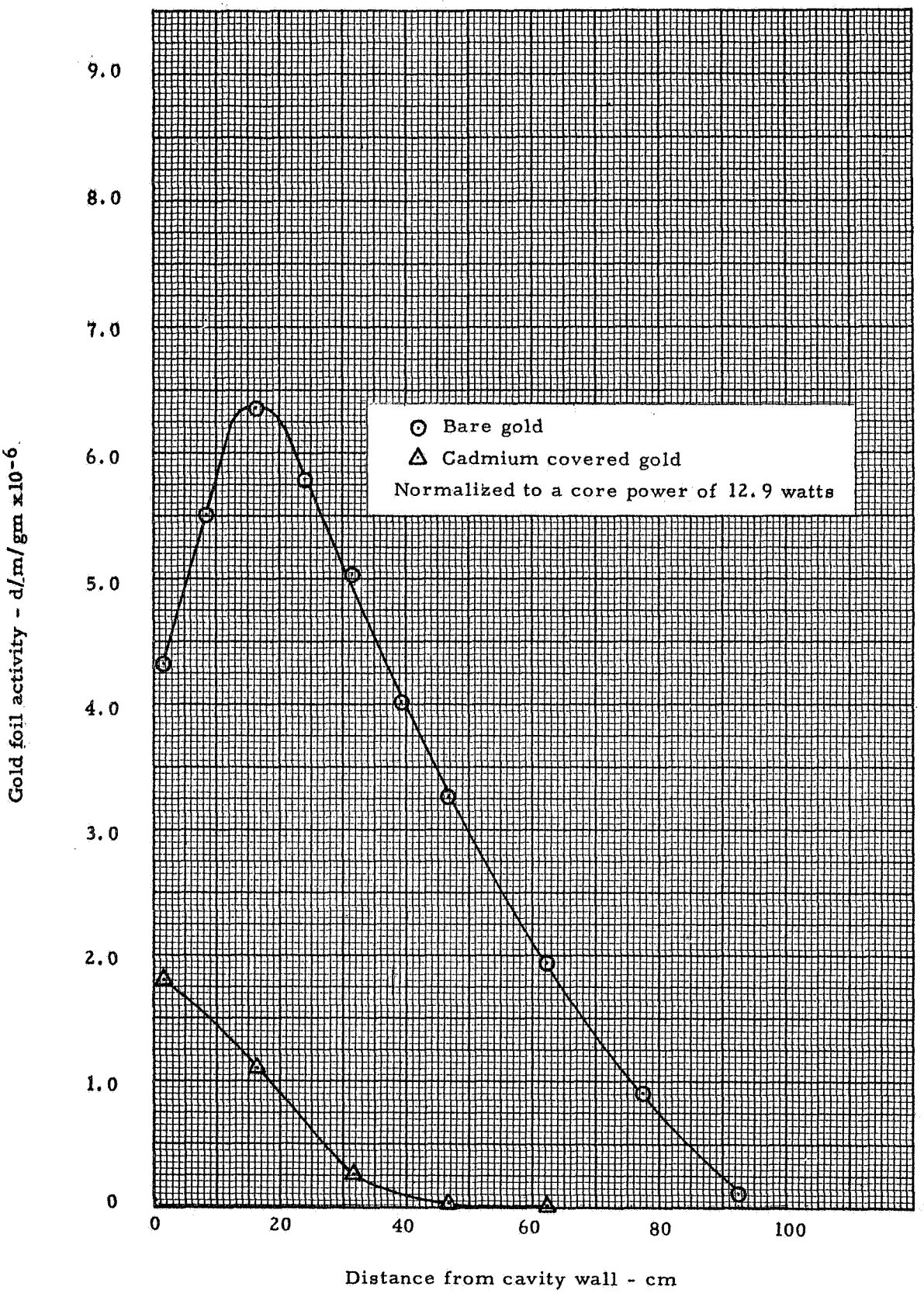

Fig. 9.10 Gold foil activity, radial reflector, fuel in radial reflector

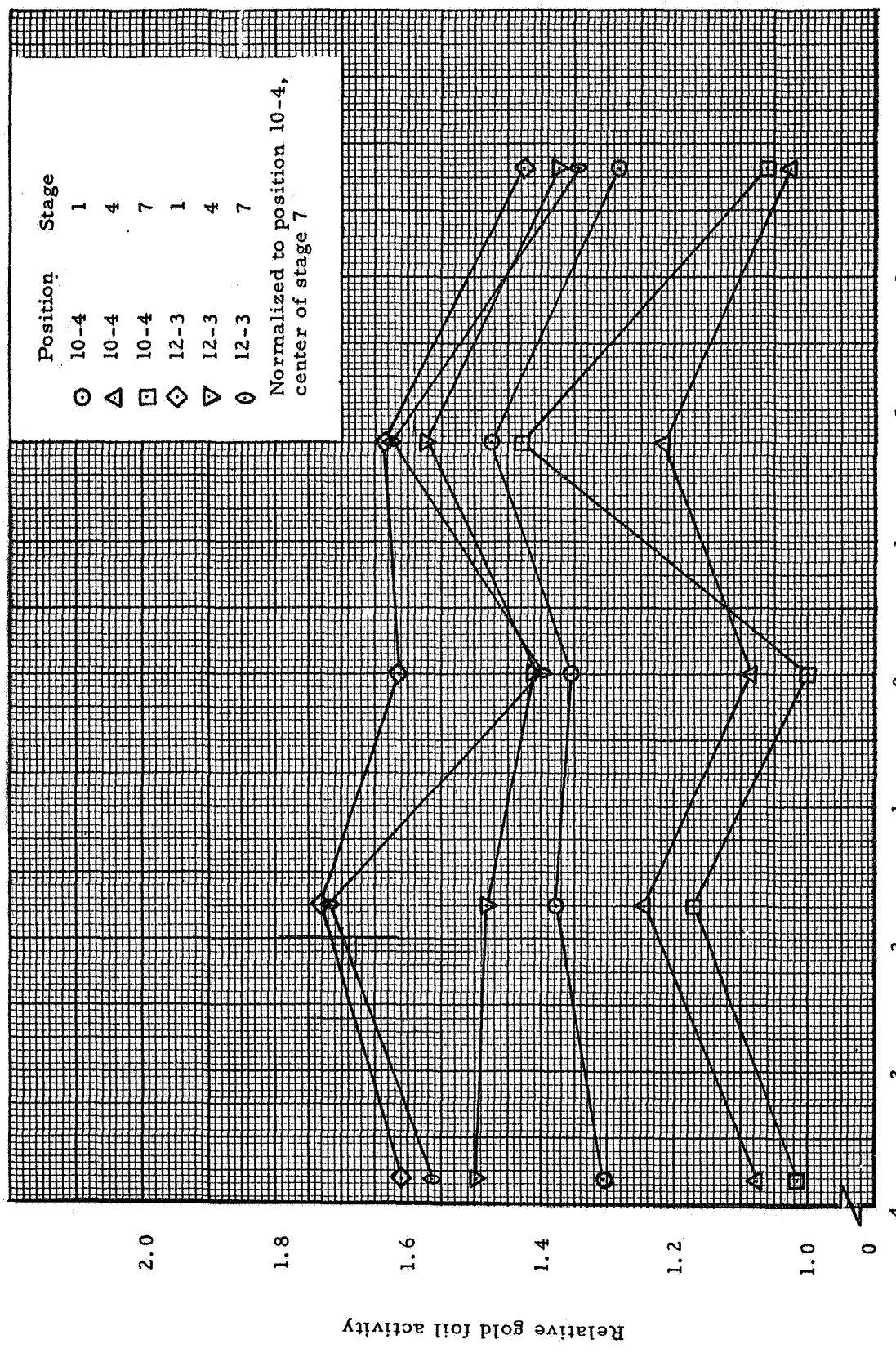

Fig. 9.11 Relative distribution of bare gold foil activities across fuel elements to determine neutron streaming along fuel element and cell boundaries. Fuel in reflector

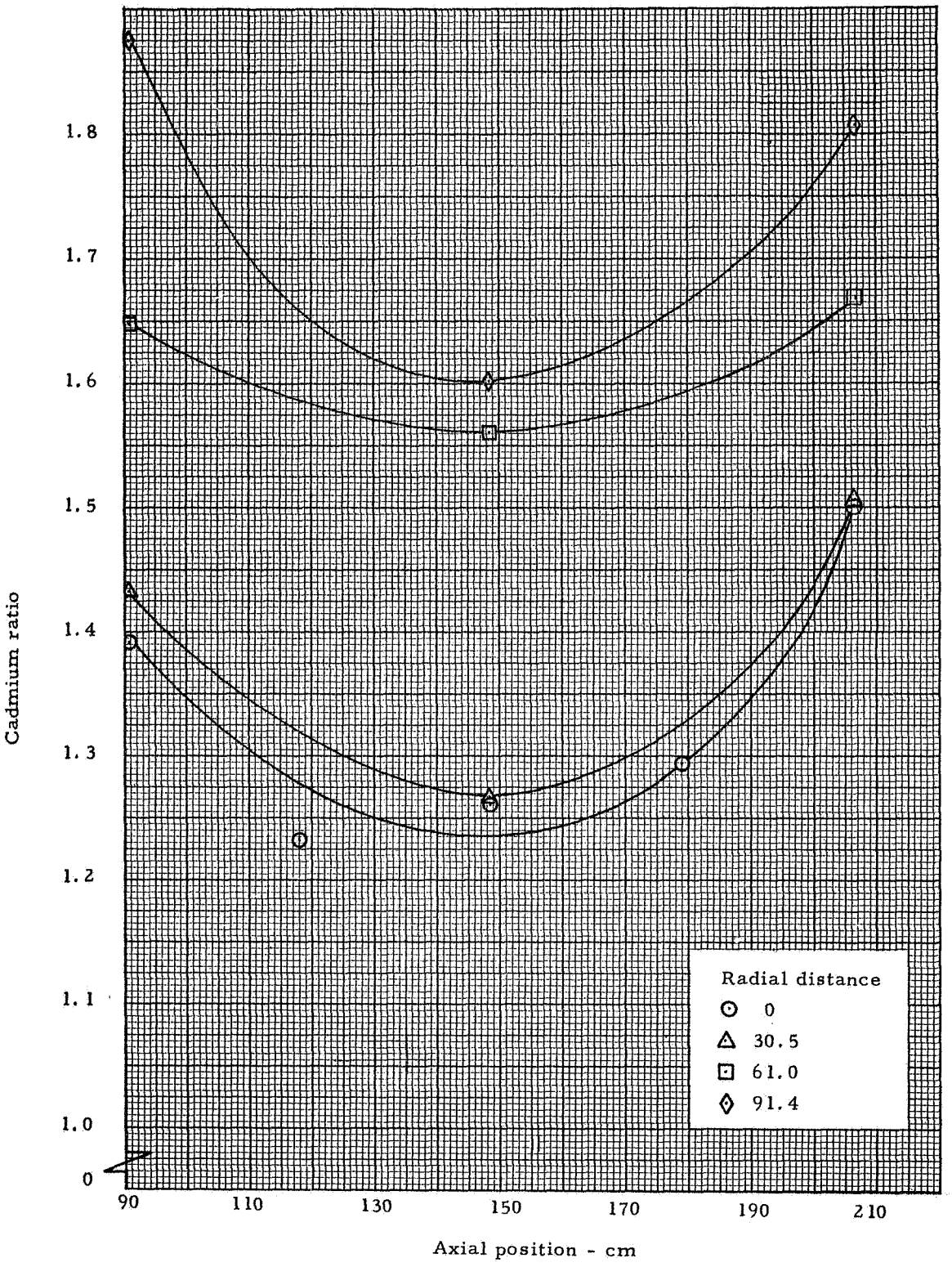

Fig. 9.12 Gold foil cadmium ratios, axial profiles in the cavity region, fuel in reflector

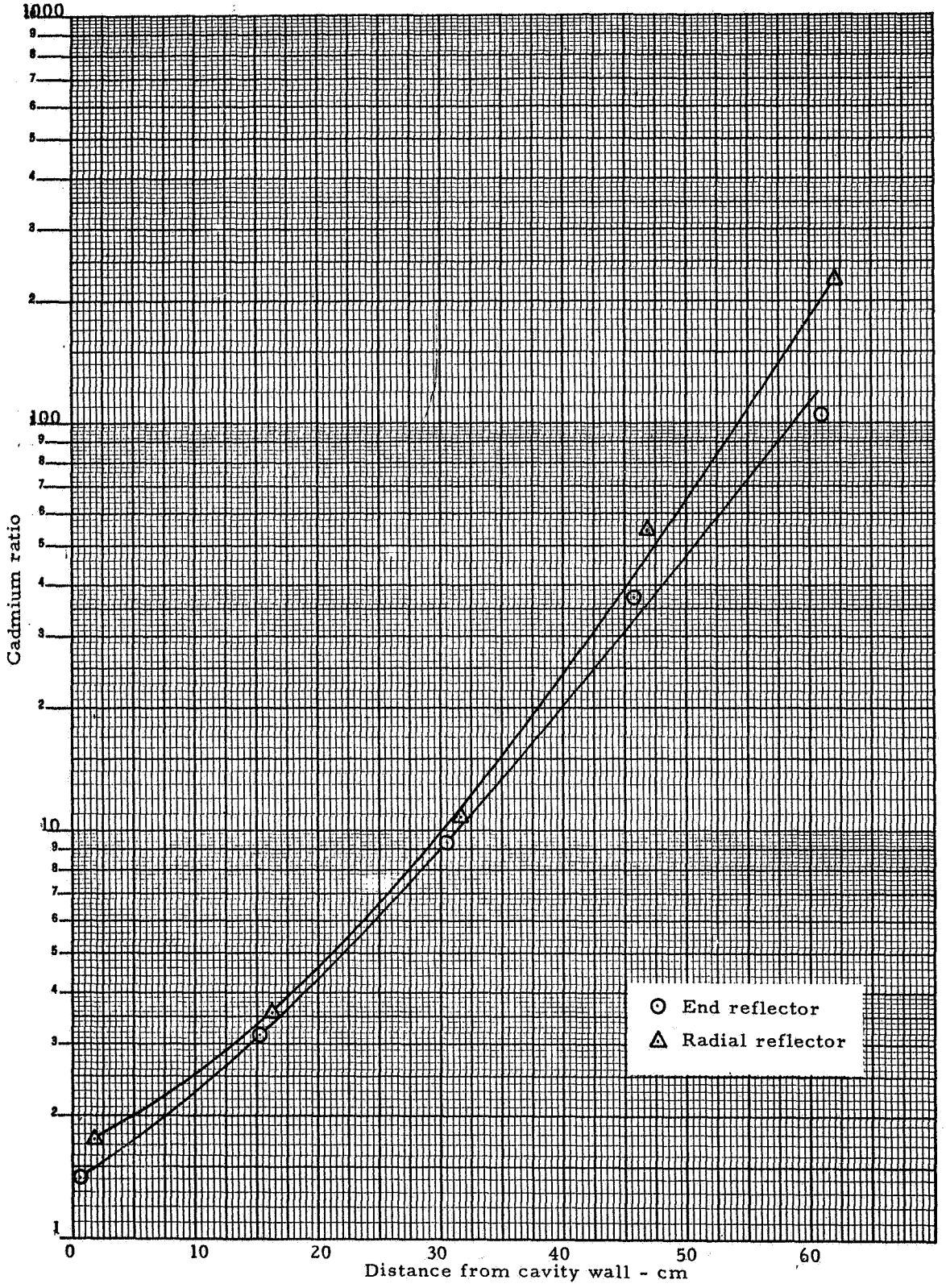

Fig. 9.13 Gold foil cadmium ratios, reflector regions, fuel in radial reflector

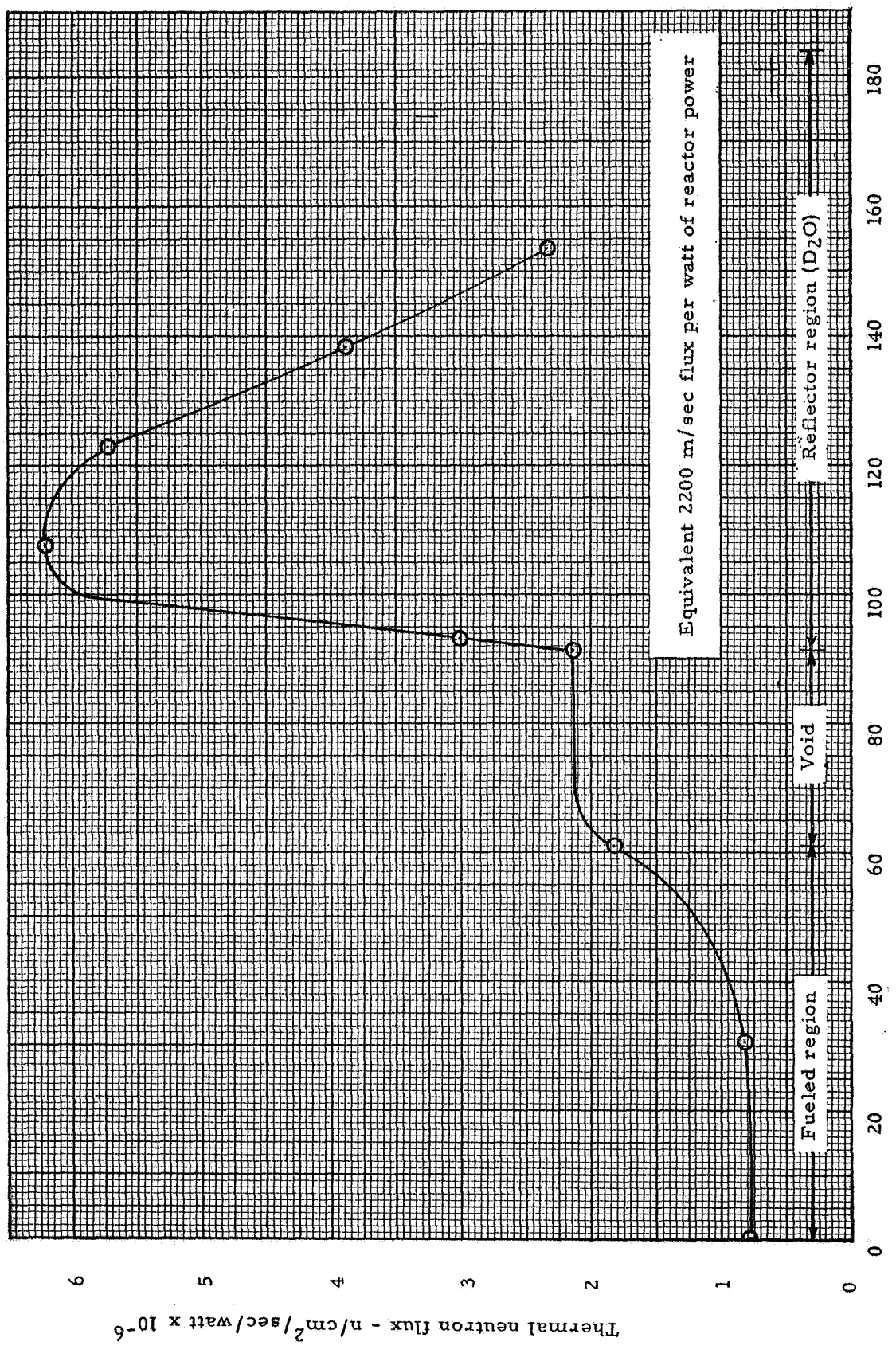

Fig. 9.14 Thermal neutron flux, radial distributions, fuel in radial reflector

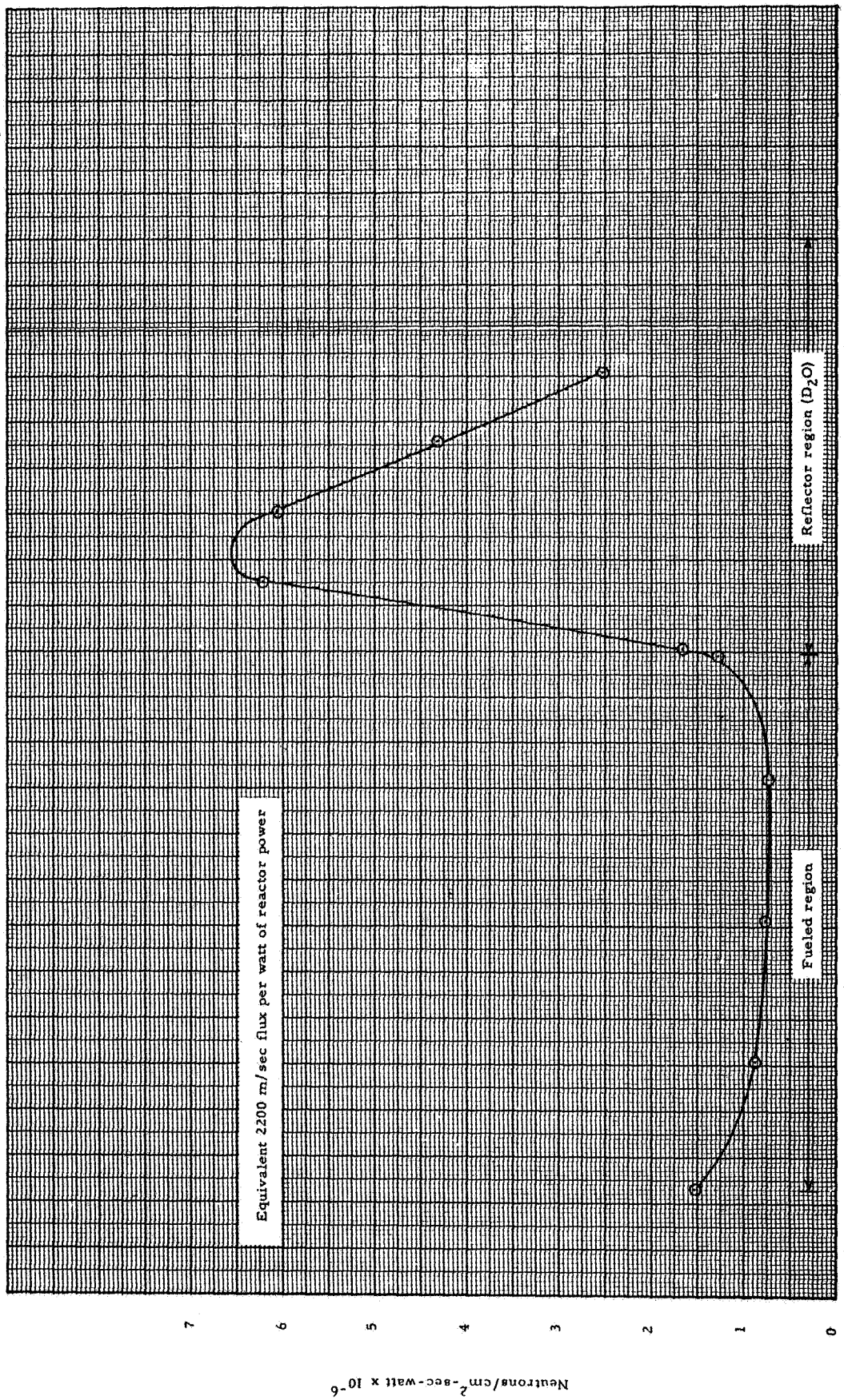

Fig. 9.15 Thermal neutron flux, axial distributions, fuel in radial reflector

10.0 MOVEMENT OF A SECTOR OF FUEL ANNULUS IN RADIAL REFLECTOR

A 90^{o} sector of the fuel annulus at 7.6 cm from the cavity wall was moved to several other positions in the radial reflector to measure the change in annulus power and the effect on reactivity. These data were then normalized to the effect of 1 kg of U^{235} in the fuel annulus. The measurements involved 22 fuel plates which contained 184.8 gm of U^{235}. The remaining 270^{o} of the fuel annulus was at the 7.6 cm position. The core contained 23.25 kg of fuel.

10.1 Reactivity Effects

Table 10.1 gives the reactivity values and the extrapolated critical masses for an annulus of fuel containing 1 kg of U^{235} at each of the positions tested. In order to extrapolate to the various loadings, it was necessary to use a fuel worth vs core loading curve. The core average fuel worth for this configuration fits very well with the data for the UF_6 reactor given on page 214 of Reference 2.

Therefore, this curve was used to correct the critical masses. Figure 10.1 shows the relationship of critical mass and annulus worth vs annulus distance from the wet surface of the cavity wall. The peak reactivity and likewise the minimum critical mass occurs between 15 and 20 cm from the cavity wall. As can be seen from these curves, a savings of 11 kg of uranium (40% of the core loading) from the core region can be achieved with one kg of U^{235} in the radial reflector at about 19 cm from the cavity wall.

10.2 Power Distribution Measurements

Bare catcher foils were exposed in the cavity region and on the movable fuel sector at each of the positions noted in Table 10.1. Since a large sector of the fuel annulus was being moved (90 degrees), there was some concern as to the overall power distribution in the active core. It has been assumed on previous configurations that the power distribution was essentially uniform around the core as all components were essentially symetrical about the center of the core. However, the radial reflector was no longer azimuthally symetrical so, on each power map, sufficient foils were exposed to give both radial and axial power profiles directly opposite the sector of the fuel annulus being moved and also 180 degrees from this region.

Excess reactivity varied considerably over the experiments. The D_2O temperature was maintained at $21^{o}C$. The rod positions were as follows:

Sector Position cm from cavity wall	Actuator Position - cm withdrawn	
	Actuators 1, 2, 3	Actuators 4, 5, 6
15.2	Withdrawn	2.3
19.0	75.6	0.0
30.5	Withdrawn	8.0
45.7	Withdrawn	18.9
61.0	Withdrawn	27.7

The catcher foil data obtained during all of these measurements are contained in Table 10.2. Each set of data was normalized to the center of core and the axial profiles were plotted and averaged. The radial profiles were then plotted from the axial averages and the volume weighted average over the active core was calculated. The catcher foil data from the fuel annulus for each of the five positions are presented in Figures 10.2 to 10.21.

Active core and annulus power were calculated for each of the fuel annulus positions and the ratio of annulus to total core power was determined. The annulus power was based on 1 kg of U^{235} in the annulus. Sufficient catcher foil data were obtained within the cavity at each of the fuel annulus positions to determine if there was any change in power distribution adjacent to the sector where the fuel annulus was moved compared to a region 180 degrees from that sector in the direction of the fixed 7.6 cm annulus. Table 10.2 lists foils exposed at locations towards the top and bottom of the core. Those foils designated "top" were opposite the region where the sector of the fuel annulus was moved and those specified as "bottom" were 180 degrees from that point. As the fuel in the reflector was moved further and further from the cavity wall, the difference in the radial profiles at the top and bottom of the core became larger. In calculating the core power, the volume weighted average radial at the bottom of the core was weighted by a factor of three and the one at the top by a factor of one since the portion of the fuel annulus being moved was a 90 degree sector from the full ring at 7.6 cm from the cavity wall, the location of the remainder of the annulus. Table 10.3 and Figure 10.22 show the results of the power calculations and the fraction of total core power generated in the fuel annulus. The peak power fraction in the annulus occurs around 20 cm from the cavity wall. The power fraction in the fuel annulus would, of course, depend on the amount of uranium as well as position. In the power reactor, these variables (position and loading) would be fixed by the amount of power generation which could be tolerated in the reflector. In addition to the heat generated from fissioning in the fuel annulus, the neutron, gamma, and radiant heating from the active core region would have to be considered in the total power in the reflector.

TABLE 10.1

Reactivity Effects per kg of U^{235} in Radial Reflector

Distance from cavity wall (cm)	Worth of hardware plus fuel plates %Δk/k	Worth of Hardware %Δk	Sector (degrees)	Worth of Annulus %Δk/kg U^{235}	Critical Mass in cavity kg U
7.6	1.0305	-0.2096	90.0	6.710	18.8
15.2	1.2543	-0.2878	83.6	8.344	17.2
19.0	1.2340	-0.2837	80.7	8.212	17.3
30.5	1.0375	-0.2080	73.1	6.739	18.8
45.7	0.4601	-0.0810	65.0	2.928	23.2
61.0	0.1849	-0.0271	58.5	1.147	25.9
91.4 (removed)	0.0	0.0	48.7	0.0	28.1

The measurement involved 22 fuel plates containing 184.8 gm of U^{235}.

TABLE 10.2

Catcher Foil Data

Motion of Fuel Annulus Sector in Radial Reflector

Foil No.	Foil Type	Location Radial (cm)	Location Axial (cm)	Normalized Counts	Local to Foil (X)
Run 1117 (Fuel sector at 15.2 cm from cavity wall)					
1	Bare	91.4	90.8	114137	3.382
2	Bare	Bottom	102.8	102954	3.051
3	Bare	Bottom	118.0	95381	2.826
4	Bare	Bottom	148.5	95044	2.816
5	Bare	Bottom	179.0	96479	2.859
6	Bare	Bottom	194.2	102432	3.035
7	Bare	Bottom	206.9	99535	2.949
8	Bare	61.0	90.8	92784	2.749
9	Bare	Bottom	102.8	90131	2.671
10	Bare	Bottom	118.0	85727	2.540
11	Bare	Bottom	148.5	81933	2.428
12	Bare	Bottom	179.0	82272	2.438
13	Bare	Bottom	194.2	87179	2.583
14	Bare	Bottom	206.9	100292	2.972
15	Bare	45.7	90.8	65274	1.934
16	Bare	Bottom	102.8	59526	1.764
17	Bare	Bottom	118.0	54011	1.600
18	Bare	Bottom	148.5	51468	1.525
19	Bare	Bottom	179.0	50583	1.499
20	Bare	Bottom	194.2	57470	1.703
21	Bare	Bottom	206.9	78778	2.334
22	Bare	30.5	90.8	61692	1.828
23	Bare	Bottom	102.8	52289	1.549
24	Bare	Bottom	118.0	45364	1.344
25	Bare	Bottom	148.5	44234	1.311
26	Bare	Bottom	179.0	45180	1.339
27	Bare	Bottom	194.2	52955	1.569
28	Bare	Bottom	206.9	66474	1.970
29	Bare	0	90.8	61622	1.826
30	Bare	0	102.8	44478	1.318
31	Bare	0	118.0	42030	1.245
32	Bare	0	148.5	33753	1.000 (X)
33	Bare	0	179.0	37946	1.124
34	Bare	0	194.2	47282	1.401
35	Bare	0	206.9	73571	2.180
36	Bare	30.5	90.8	62306	1.846
37	Bare	Top	102.8	49026	1.453
38	Bare	Top	118.0	44050	1.305
39	Bare	Top	148.5	41009	1.215
40	Bare	Top	179.0	45689	1.354

TABLE 10.2

(Continued)

Foil No.	Type	Location Radial (cm)	Axial (cm)	Normalized Counts	Local to Foil (X)
Run 1117 (Cont'd)					
41	Bare	Top	194.2	55908	1.657
42	Bare	Top	206.9	70313	2.083
43	Bare	45.7	90.8	74734	2.214
44	Bare	Top	102.8	57609	1.707
45	Bare	Top	118.0	52476	1.555
46	Bare	Top	148.5	52691	1.561
47	Bare	Top	179.0	56517	1.675
48	Bare	Top	194.2	59694	1.769
49	Bare	Top	206.9	80325	2.380
50	Bare	61.0	90.8	88165	2.612
51	Bare	Top	120.8	75078	2.225
52	Bare	Top	118.0	86171	2.553
53	Bare	Top	148.5	80263	2.378
54	Bare	Top	179.0	81228	2.407
55	Bare	Top	194.2	84079	2.491
56	Bare	Top	206.9	95825	2.839
57	Bare	91.4 (1)	90.8	115490	3.422
58	Bare	91.4	102.8	104755	3.104
59	Bare	91.4	118.0	104691	3.102
60	Bare	91.4	148.5	103013	3.052
61	Bare	91.4	179.0	104242	3.089
62	Bare	91.4	194.2	109981	3.259
63	Bare	91.4	206.9	113390	3.360
64	Bare	107.4	126.0	246157	7.294
65	Bare	107.8	126.0	226795	6.720
66	Bare	107.8	151.1	234342	6.944
67	Bare	107.4	151.1	249050	7.379
68	Bare	107.8	176.0	229186	6.791
69	Bare	107.4	176.0	234427	6.946

(1) Foil 56 to 63 at 91.4 cm were placed between stainless steel liner and cavity wall. All other such traverses at 91.4 cm were with the catcher foils on the cavity side of this liner.

Run 1118 (Fuel sector at 30.5 cm from cavity wall)

1	Bare	91.4	90.8	115982	3.320
2	Bare	Bottom	102.8	102425	2.932
3	Bare	Bottom	118.0	89399	2.559
4	Bare	Bottom	148.5	100145	2.867
5	Bare	Bottom	179.0	97528	2,792
6	Bare	Bottom	194.2	103472	2.962
7	Bare	Bottom	206.9	99255	2.841

TABLE 10.2

(Continued)

Foil No.	Type	Location Radial (cm)	Location Axial (cm)	Normalized Counts	Local to Foil (X)
Run 1118 (Cont'd)					
8	Bare	61.0	90.8	92293	2.642
9	Bare	61.0	102.8	88404	2.530
10	Bare	61.0	118.0	90695	2.596
11	Bare	61.0	148.5	91473	2.332
12	Bare	61.0	179.0	80158	2.294
13	Bare	61.0	194.2	85272	2.441
14	Bare	61.0	206.9	93390	2.673
15	Bare	45.7	90.8	67384	1.929
16	Bare	Bottom	102.8	56814	1.626
17	Bare	Bottom	118.0	49887	1.428
18	Bare	Bottom	148.5	55212	1.580
19	Bare	Bottom	179.0	55305	1.583
20	Bare	Bottom	194.2	61337	1.756
21	Bare	Bottom	206.9	74241	2.125
22	Bare	30.5	90.8	70279	2.012
23	Bare	Bottom	102.8	51261	1.467
24	Bare	Bottom	118.0	43899	1.257
25	Bare	Bottom	148.5	41514	1.188
26	Bare	Bottom	179.0	42227	1.209
27	Bare	Bottom	194.2	53693	1.537
28	Bare	Bottom	206.9	66590	1.906
29	Bare	0	90.8	62953	1.802
30	Bare	0	102.8	44968	1.287
31	Bare	0	118.0	40341	1.155
32	Bare	0	148.5	34935	1.000 (X)
33	Bare	0	179.0	39991	1.145
34	Bare	0	194.2	46428	1.329
35	Bare	0	206.9	72549	2.077
36	Bare	30.5	90.8	63386	1.814
37	Bare	Top	102.8	50557	1.447
38	Bare	Top	118.0	48480	1.388
39	Bare	Top	148.5	40937	1.172
40	Bare	Top	179.0	44803	1.282
41	Bare	Top	194.2	53583	1.534
42	Bare	Top	206.9	67686	1.937
43	Bare	45.7	90.8	71321	2.041
44	Bare	Top	102.8	57010	1.632
45	Bare	Top	118.0	59717	1.709
46	Bare	45.7	148.5	49155	1.407
47	Bare	Top	179.0	55860	1.599
48	Bare	Top	194.2	60944	1.744
49	Bare	Top	206.9	81795	2.341
50	Bare	61.0	90.8	99754	2.855

TABLE 10.2

(Continued)

Foil No.	Type	Location Radial (cm)	Location Axial (cm)	Normalized Counts	Local to Foil (X)
Run 1118 (Cont'd)					
51	Bare	61.0	102.8	91570	2.621
52	Bare	61.0	118.0	84820	2.428
53	Bare	61.0	148.5	78952	2.260
54	Bare	61.0	179.0	88610	2.536
55	Bare	61.0	194.2	89418	2.560
56	Bare	61.0	206.9	93623	2.680
57	Bare	91.4	90.8	119325	3.417
58	Bare	91.4	102.8	108436	3.104
59	Bare	91.4	118.0	114542	3.279
60	Bare	91.4	148.5	104959	3.004
61	Bare	91.4	179.0	113144	3.239
62	Bare	91.4	194.2	112031	3.207
63	Bare	91.4	206.9	103816	2.972
64	Bare	122.6	126.0	210197	6.017
65	Bare	123.0	126.0	205043	5.869
66	Bare	123.0	151.1	206712	5.917
67	Bare	122.6	151.1	216387	6.194
68	Bare	123.0	176.0	191373	5.478
69	Bare	122.6	176.0	193770	5.546
Run 1119 (Fuel sector at 45.7 cm from cavity wall)					
1	Bare	91.4	90.8	112460	3.099
2	Bare	Bottom	102.8	105855	2.917
3	Bare	Bottom	118.0	105152	2.898
4	Bare	Bottom	148.5	102122	2.814
5	Bare	Bottom	179.0	103099	2.841
6	Bare	Bottom	194.2	102783	2.833
7	Bare	Bottom	206.9	95514	2.632
8	Bare	61.0	90.8	90190	2.486
9	Bare	61.0	102.8	89830	2.476
10	Bare	61.0	118.0	83885	2.312
11	Bare	61.0	148.5	83675	2.306
12	Bare	61.0	179.0	76494	2.108
13	Bare	61.0	194.2	84744	2.336
14	Bare	61.0	206.9	90834	2.503
15	Bare	45.7	90.8	71607	1.973
16	Bare	Bottom	102.8	60605	1.670
17	Bare	Bottom	118.0	49699	1.370
18	Bare	Bottom	148.5	51023	1.406
19	Bare	Bottom	179.0	51092	1.408
20	Bare	Bottom	194.2	56095	1.546
21	Bare	Bottom	206.9	69012	1.902

TABLE 10.2

(Continued)

Foil No.	Type	Location Radial (cm)	Location Axial (cm)	Normalized Counts	Local to Foil (X)
Run 1119 (Cont'd)					
22	Bare	30.5	90.8	65486	1.805
23	Bare	Bottom	102.8	48906	1.348
24	Bare	Bottom	118.0	42574	1.173
25	Bare	Bottom	148.5	40966	1.129
26	Bare	Bottom	179.0	42396	1.168
27	Bare	Bottom	194.2	53118	1.464
28	Bare	Bottom	206.9	61416	1.693
29	Bare	0	90.8	60618	1.671
30	Bare	0	102.8	47766	1.316
31	Bare	0	118.0	42234	1.164
32	Bare	0	148.5	36312	1.000 (X)
33	Bare	0	179.0	37250	1.027
34	Bare	0	194.2	47875	1.319
35	Bare	0	206.9	71057	1.958
36	Bare	30.5	90.8	68572	1.890
37	Bare	Top	102.8	52672	1.452
38	Bare	Top	118.0	40558	1.118
39	Bare	Top	148.5	42059	1.159
40	Bare	Top	179.0	44737	1.233
41	Bare	Top	194.2	52611	1.450
42	Bare	Top	206.9	72015	1.985
43	Bare	45.7	90.8	77841	2.145
44	Bare	Top	102.8	58594	1.615
45	Bare	Top	118.0	60783	1.675
46	Bare	45.7	148.5	50513	1.392
47	Bare	Top	179.0	62761	1.730
48	Bare	Top	194.2	61674	1.700
49	Bare	Top	206.9	79624	2.194
50	Bare	61.0	90.8	96478	2.659
51	Bare	61.0	102.8	91853	2.531
52	Bare	61.0	118.0	89552	2.468
53	Bare	61.0	148.5	93776	2.584
54	Bare	61.0	179.0	89290	2.461
55	Bare	61.0	194.2	89370	2.463
56	Bare	61.0	206.9	102327	2.820
57	Bare	91.4	90.8	118034	3.253
58	Bare	91.4	102.8	110372	3.042
59	Bare	91.4	118.0	105218	2.900
60	Bare	91.4	148.5	106192	2.927
61	Bare	91.4	179.0	104193	2.872
62	Bare	91.4	194.2	103609	2.855
63	Bare	91.4	206.9	100599	2.773
64	Bare	122.6	126.0	141311	3.895

TABLE 10.2

(Continued)

Foil No.	Type	Location Radial (cm)	Location Axial (cm)	Normalized Counts	Local to Foil (X)
Run 1119 (Cont'd)					
65	Bare	123.0	126.0	147501	4.065
66	Bare	123.0	151.1	147715	4.071
67	Bare	122.6	151.1	150056	4.136
68	Bare	123.0	176.0	136180	3.753
69	Bare	122.6	176.0	134191	3.698
Run 1120 (Fuel sector at 61.0 cm from cavity wall)					
1	Bare	91.4	90.8	125648	3.324
2	Bare	Bottom	102.8	103575	2.740
3	Bare	Bottom	118.0	p05740	2.797
4	Bare	Bottom	148.5	102160	2.703
5	Bare	Bottom	179.0	106654	2.822
6	Bare	Bottom	194.2	105786	2.799
7	Bare	Bottom	206.9	105076	2.780
8	Bare	61.0	90.8	93506	2.477
9	Bare	Bottom	102.8	86989	2.301
10	Bare	Bottom	118.0	81923	2.167
11	Bare	Bottom	148.5	79195	2.095
12	Bare	Bottom	179.0	78060	2.065
13	Bare	Bottom	194.2	81906	2.167
14	Bare	Bottom	206.9	93109	2.463
15	Bare	45.7	90.8	65154	1.724
16	Bare	Bottom	102.8	56289	1.489
17	Bare	Bottom	118.0	53056	1.404
18	Bare	Bottom	148.5	51883	1.373
19	Bare	Bottom	179.0	51133	1.353
20	Bare	Bottom	194.2	56093	1.484
21	Bare	Bottom	206.9	73670	1.949
22	Bare	30.5	90.8	69489	1.838
23	Bare	Bottom	102.8	46809	1.238
24	Bare	Bottom	118.0	43470	1.150
25	Bare	Bottom	148.5	43686	1.156
26	Bare	Bottom	179.0	36682	0.970
27	Bare	Bottom	194.2	49837	1.318
28	Bare	Bottom	206.9	65789	1.740
29	Bare	0	90.8	62812	1.662
30	Bare	0	102.8	45154	1.195
31	Bare	0	118.0	43082	1.140
32	Bare	0	148.5	37800	1.000 (X)
33	Bare	0	179.0	39231	1.038
34	Bare	0	194.2	51229	1.355
35	Bare	0	206.9	70565	1.867

TABLE 10.2

(Continued)

Foil No.	Type	Location Radial (cm)	Location Axial (cm)	Normalized Counts	Local to Foil (X)
Run 1120 (Cont'd)					
36	Bare	30.5	90.8	67534	1.787
37	Bare	Top	102.8	49062	1.298
38	Bare	Top	118.0	45156	1.195
39	Bare	Top	148.5	43877	1.161
40	Bare	Top	179.0	45749	1.210
41	Bare	Top	194.2	56198	1.487
42	Bare	Top	206.9	72211	1.910
43	Bare	45.7	90.8	75052	1.986
44	Bare	Top	102.8	59307	1.569
45	Bare	Top	118.0	56250	1.488
46	Bare	Top	148.5	55621	1.471
47	Bare	45.7	179.0	60374	1.597
48	Bare	Top	194.2	59337	1.570
49	Bare	Top	206.9	78015	2.064
50	Bare	61.0	90.8	102964	2.724
51	Bare	Top	102.8	89623	2.371
52	Bare	Top	118.0	88741	2.348
53	Bare	Top	148.5	88459	2.340
54	Bare	Top	179.0	86516	2.289
55	Bare	Top	194.2	87190	2.307
56	Bare	Top	206.9	93135	2.464
57	Bare	91.4	90.8	114594	3.032
58	Bare	Top	102.8	104509	2.765
59	Bare	Top	118.0	106058	2.806
60	Bare	Top	148.5	101331	2.681
61	Bare	Top	179.0	103212	2.730
62	Bare	Top	194.2	102206	2.704
63	Bare	Top	206.9	102077	2.700
64	Bare	122.6	126.0	87063	2.303
65	Bare	123.0	126.0	75796	2.005
66	Bare	123.0	151.1	76182	2.015
67	Bare	122.6	121.1	78784	2.084
68	Bare	123.0	176.0	69597	1.841
69	Bare	122.6	176.0	70044	1.853
Run 1121 (Fuel sector at 19.0 cm from cavity wall)					
1	Bare	91.4	90.8	110773	3.107
2	Bare	Bottom	102.8	105744	2.966
3	Bare	Bottom	118.0	95928	2.690
4	Bare	Bottom	148.5	98770	2.798
5	Bare	Bottom	179.0	98926	2.775
6	Bare	Bottom	194.2	97113	2.724

TABLE 10.2

(Continued)

Foil No.	Type	Location Radial (cm)	Location Axial (cm)	Normalized Counts	Local to Foil (X)
Run 1121 (Cont'd)					
7	Bare	Bottom	206.9	98120	2.752
8	Bare	61.0	90.8	91248	2.559
9	Bare	61.0	102.8	90236	2.531
10	Bare	61.0	118.0	87509	2.454
11	Bare	61.0	148.5	82299	2.308
12	Bare	61.0	179.0	77923	2.186
13	Bare	61.0	194.2	90945	2.551
14	Bare	61.0	206.9	94225	2.643
15	Bare	45.7	90.8	68685	1.926
16	Bare	Bottom	102.8	57155	1.603
17	Bare	Bottom	118.0	51258	1.438
18	Bare	Bottom	148.5	54238	1.521
19	Bare	Bottom	179.0	56441	1.583
20	Bare	Bottom	194.2	62411	1.750
21	Bare	Bottom	206.9	73374	2.058
22	Bare	30.5	90.8	57398	1.610
23	Bare	Bottom	102.8	52299	1.467
24	Bare	Bottom	118.0	46214	1.296
25	Bare	Bottom	148.5	43654	1.224
26	Bare	Bottom	179.0	41661	1.168
27	Bare	Bottom	194.2	49402	1.386
28	Bare	Bottom	206.9	65124	1.827
29	Bare	0	90.8	65282	1.831
30	Bare	0	102.8	42542	1.193
31	Bare	0	118.0	38991	1.094
32	Bare	0	148.5	35654	1.000 (X)
33	Bare	0	179.0	37632	1.055
34	Bare	0	194.2	47196	1.324
35	Bare	0	206.9	68345	1.917
36	Bare	30.5	90.8	66980	1.879
37	Bare	Top	102.8	48669	1.365
38	Bare	Top	118.0	45315	1.271
39	Bare	Top	148.5	48141	1.174
40	Bare	Top	179.0	47879	1.343
41	Bare	Top	194.2	53931	1.513
42	Bare	Top	206.9	73733	2.068
43	Bare	45.7	90.8	74316	2.084
44	Bare	Top	102.8	58569	1.643
45	Bare	Top	118.0	55851	1.566
46	Bare	45.7	148.5	52458	1.471
47	Bare	45.7	179.0	53902	1.512
48	Bare	45.7	194.2	64789	1.817
49	Bare	45.7	206.9	73315	2.056

TABLE 10.2

(Continued)

Foil No.	Type	Location Radial (cm)	Location Axial (cm)	Normalized Counts	Local to Foil (X)
50	Bare	61.0	90.8	85277	2.392
51	Bare	Top	102.8	85125	2.388
52	Bare	Top	118.0	83754	2.349
53	Bare	Top	148.5	83401	2.399
54	Bare	Top	179.0	83746	2.349
55	Bare	Top	194.2	91455	2.565
56	Bare	Top	206.9	102925	2.887
57	Bare	91.4	90.8	122836	3.445
58	Bare	Top	102.8	103554	2.904
59	Bare	Top	118.0	104490	2.931
60	Bare	Top	148.5	112249	3.148
61	Bare	Top	179.0	109702	3.077
62	Bare	Top	194.2	101348	2.843
63	Bare	Top	206.9	101574	2.849
64	Bare	122.6	126.0	242990	6.815
65	Bare	123.0	126.0	22075	6.229
66	Bare	123.0	151.1	247094	6.930
67	Bare	122.6	151.1	246920	6.925
68	Bare	123.0	176.0	247225	6.934
69	Bare	122.6	176.0	214240	6.009

TABLE 10.3

Fuel Annulus and Core Power Results

Motion of Fuel Annulus Sector in the Radial Reflector

Position of Annulus Distance from Cavity Wall (cm)	Active Core Power-watts	Annulus Power-watts (1)	Ratio Annulus/ Total Power
7.6	12.91	2.11	0.140
15.2	13.29	2.50	0.158
19.0	12.74	2.48	0.163
30.5	13.06	2.21	0.145
45.7	12.60	1.52	0.108
61.0	12.86	0.80	0.059

(1) Based on 1 kg of U^{235} in annulus

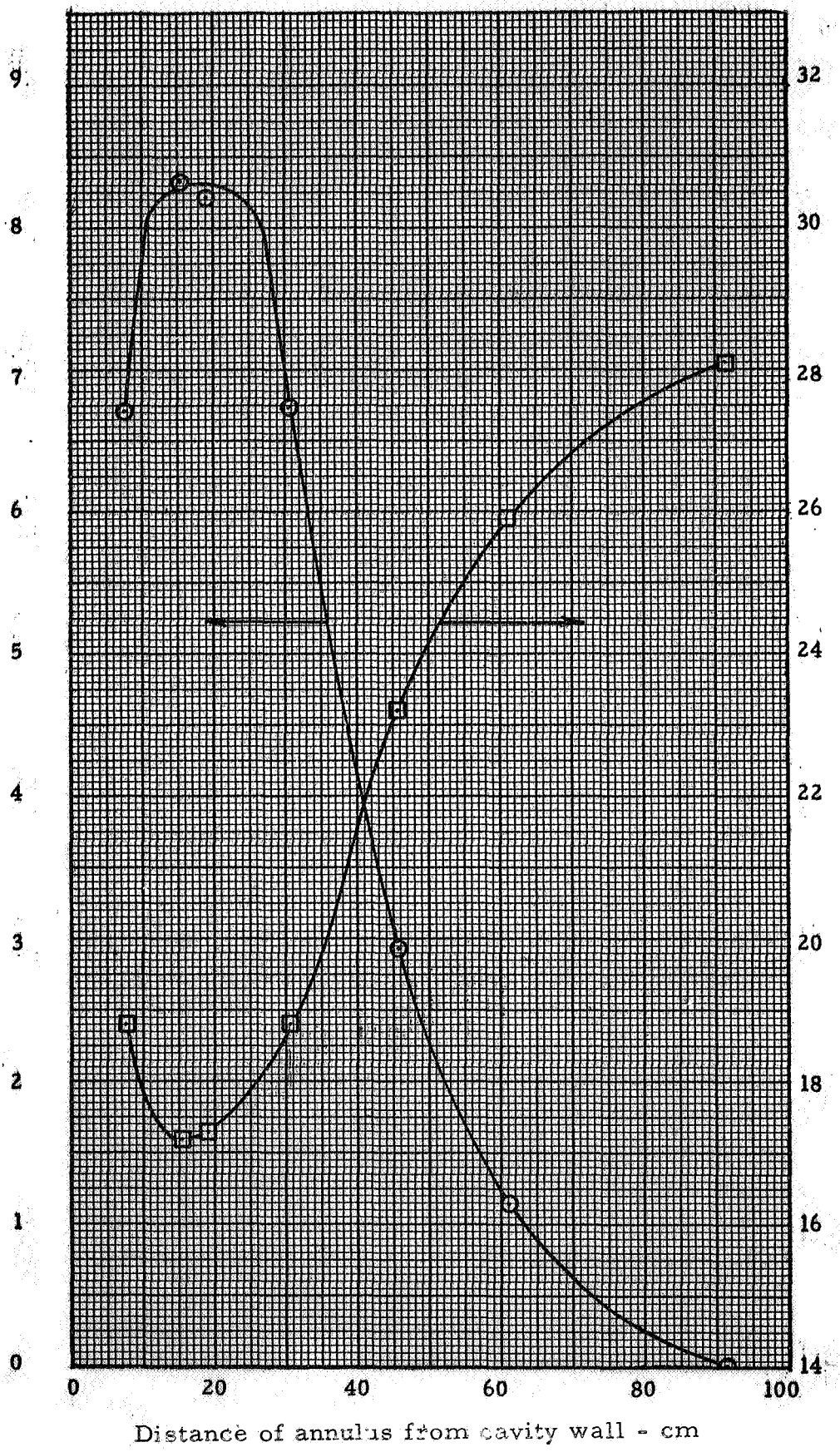

Fig. 10.1 The effect of U-235 in the reflector regions on core loading requirements

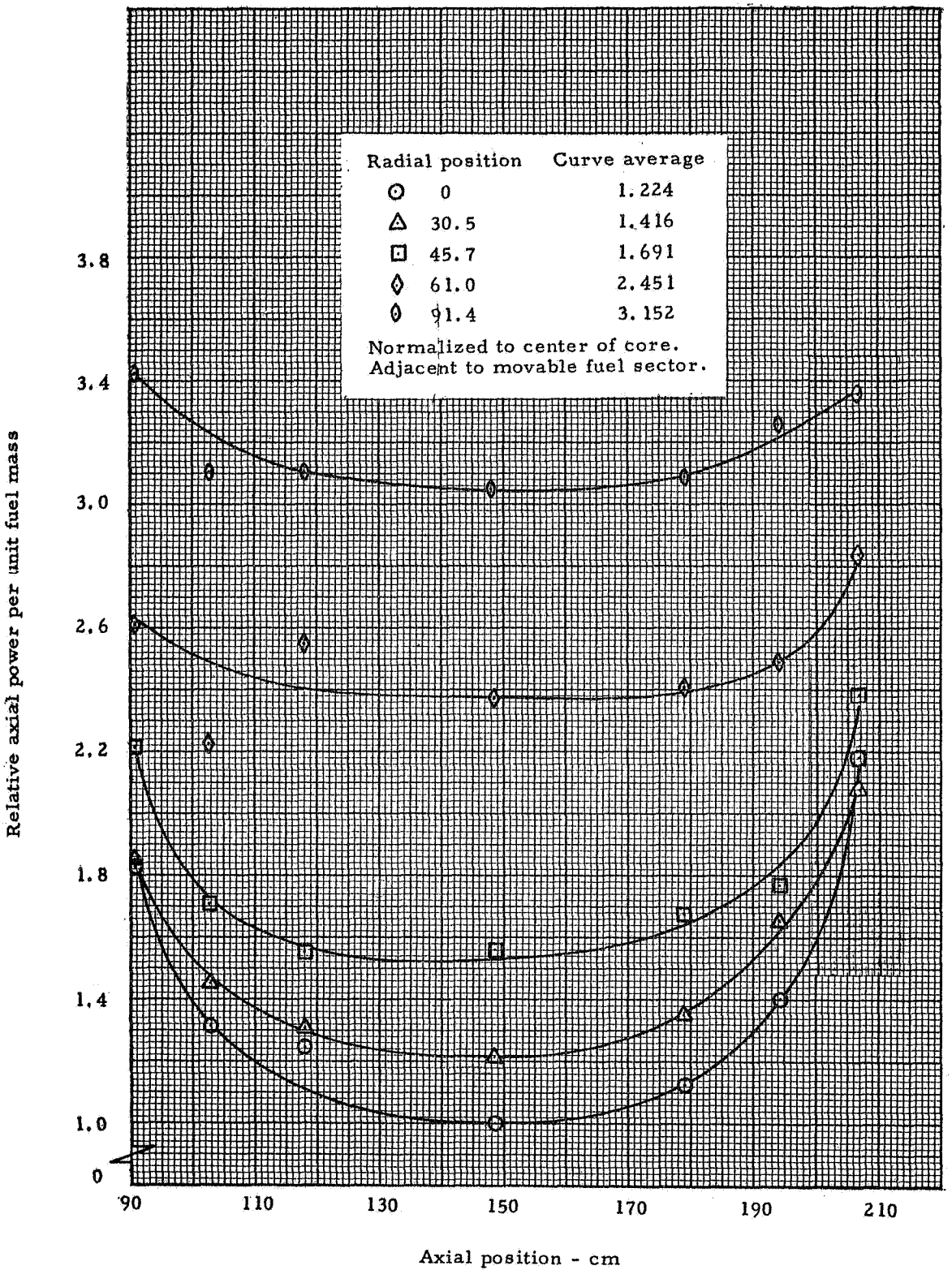

Fig. 10.2 Relative axial power profiles in cavity region adjacent to fuel sector, fuel sector 15.2 cm from cavity wall in reflector

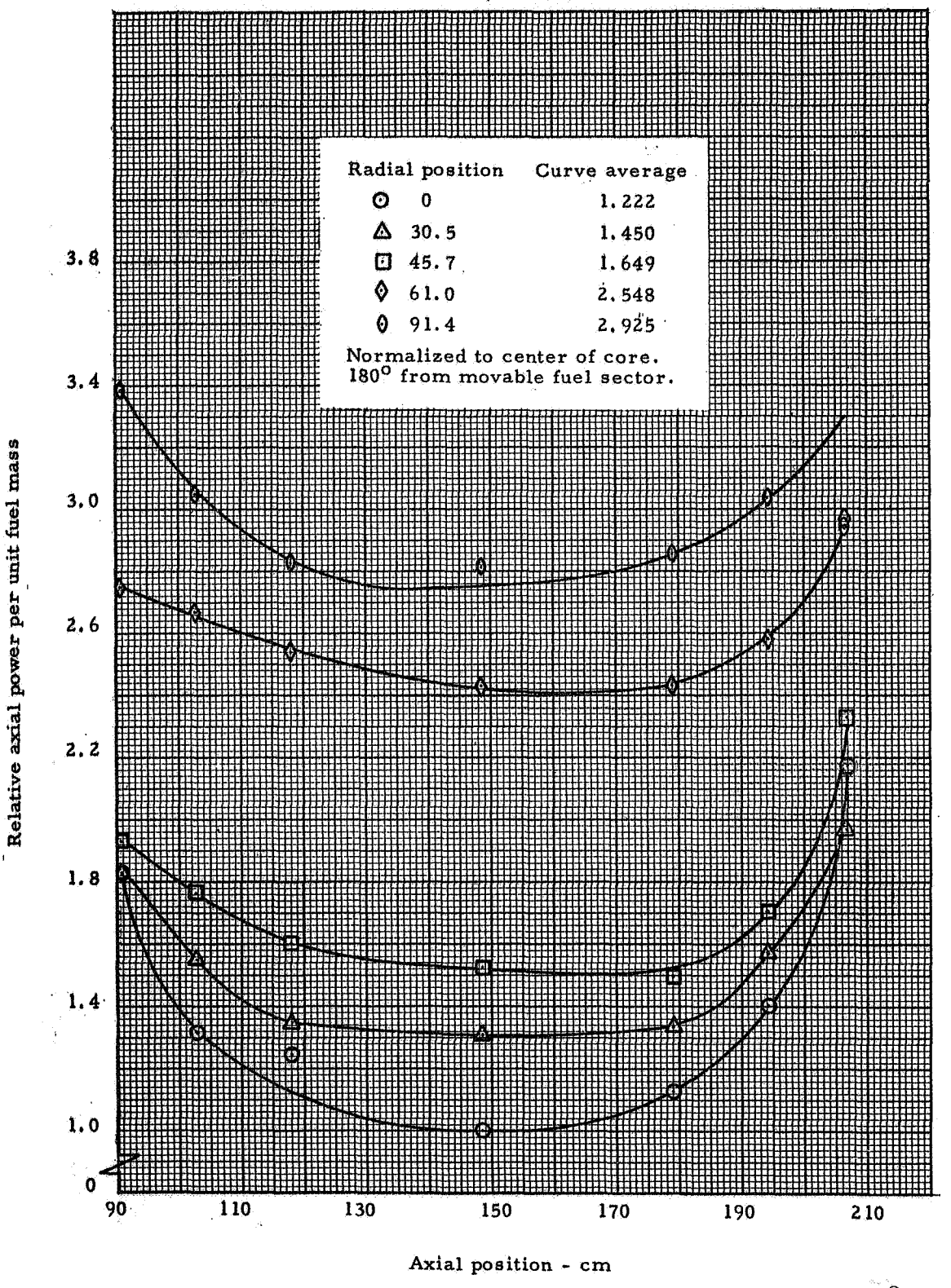

Fig. 10.3 Relative axial power profiles in the cavity region 180°, from sector, fuel sector 15.2 cm from cavity wall in reflector

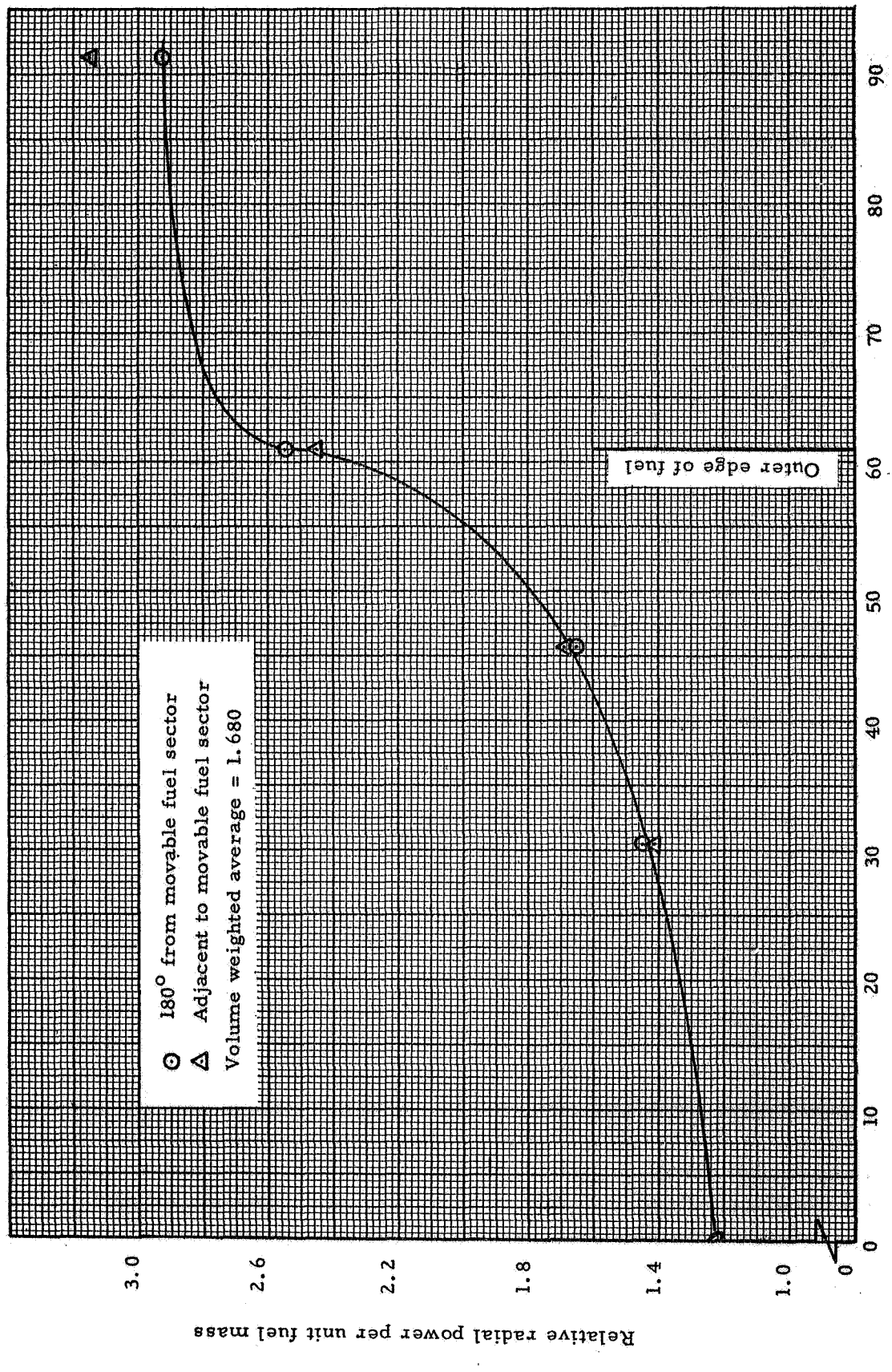

Fig. 10.4 Relative radial power profile in cavity region, averages of axial profiles from Figures 10.2 and 10.3

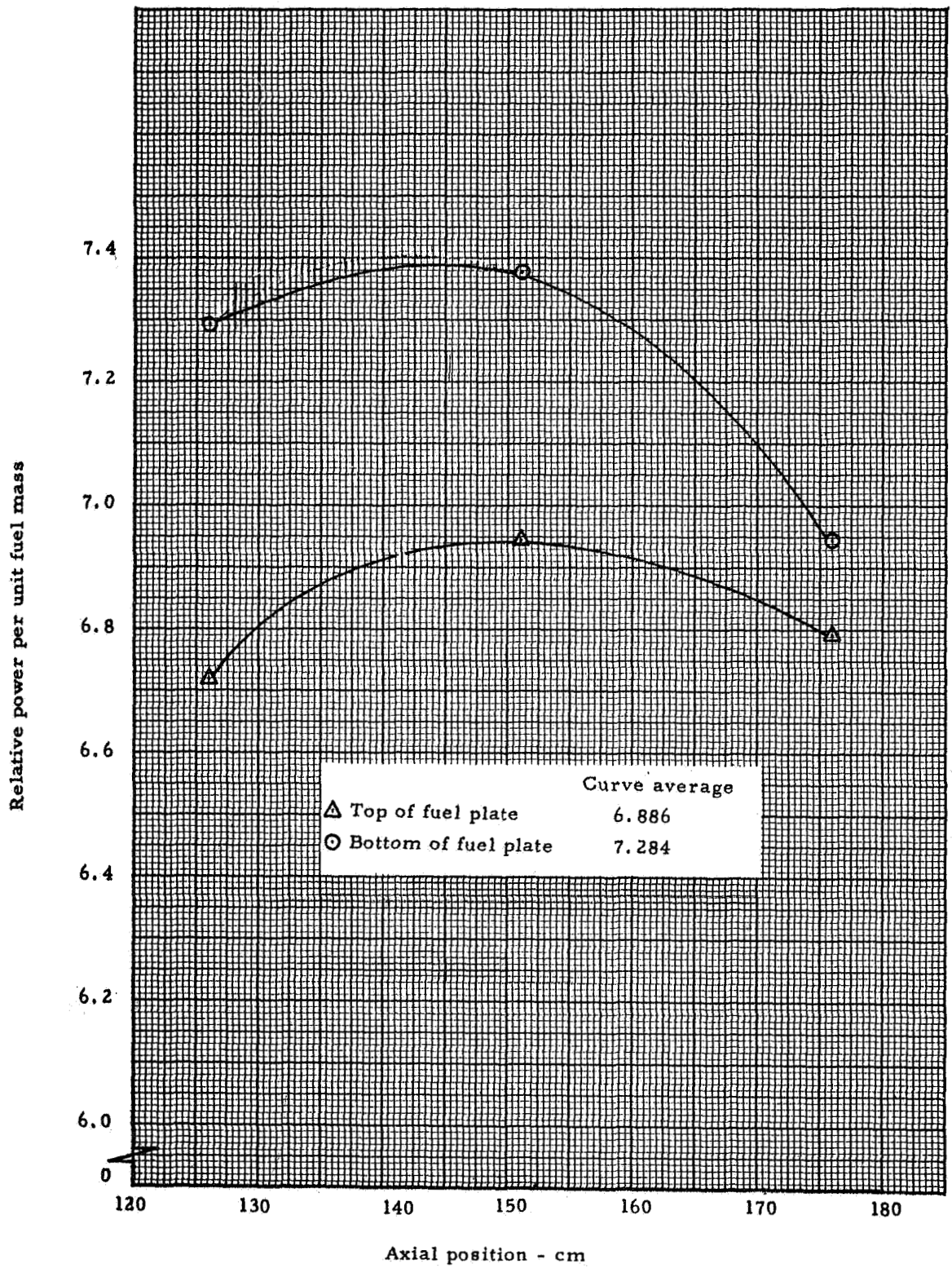

Fig. 10.5 Relative axial power profiles on fuel plates in the reflector with fuel sector 15.2 cm from cavity wall

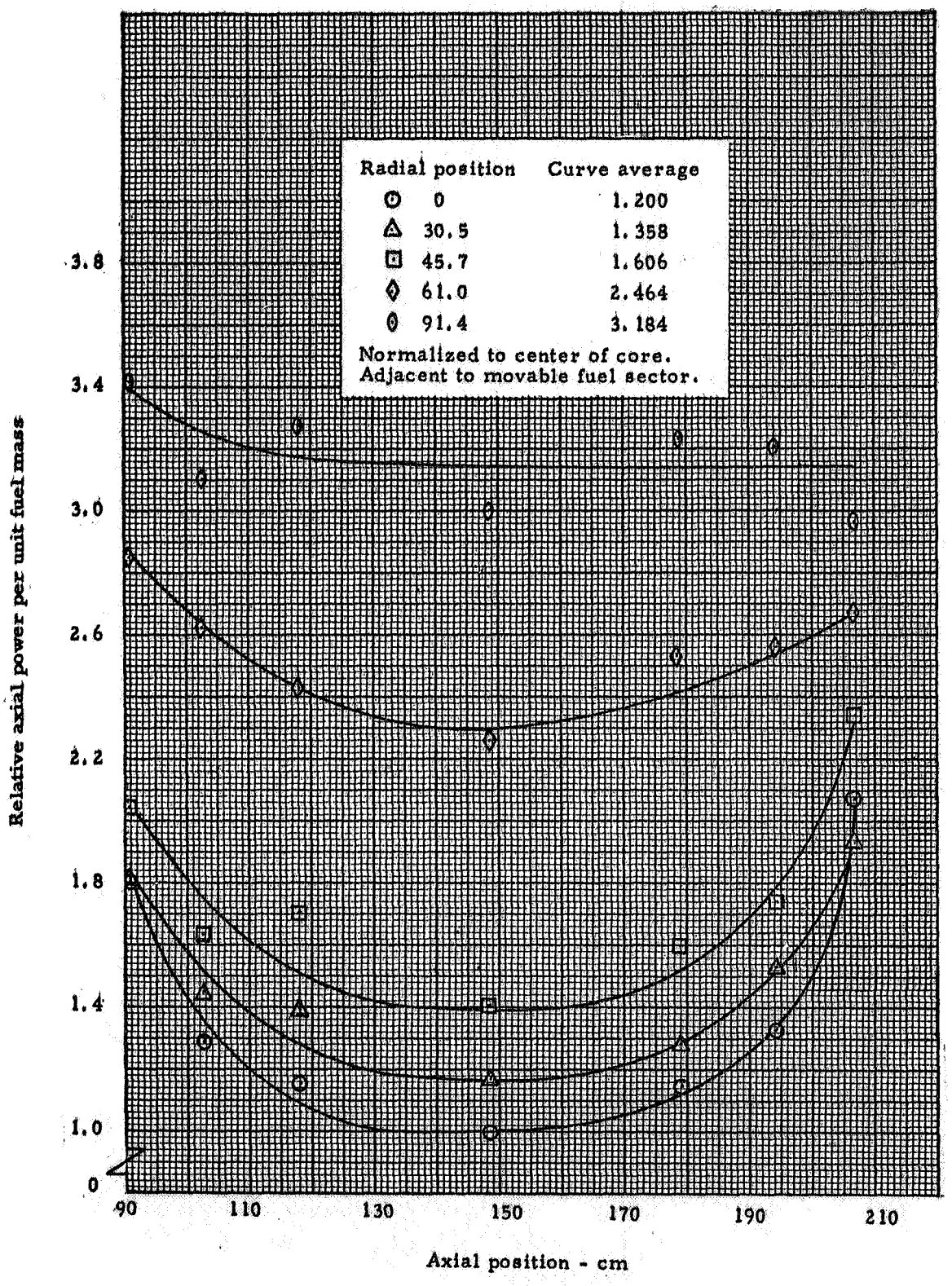

Fig. 10.6 Relative axial power profiles in cavity region adjacent to fuel sector, fuel sector 30.5 cm from cavity wall in reflector

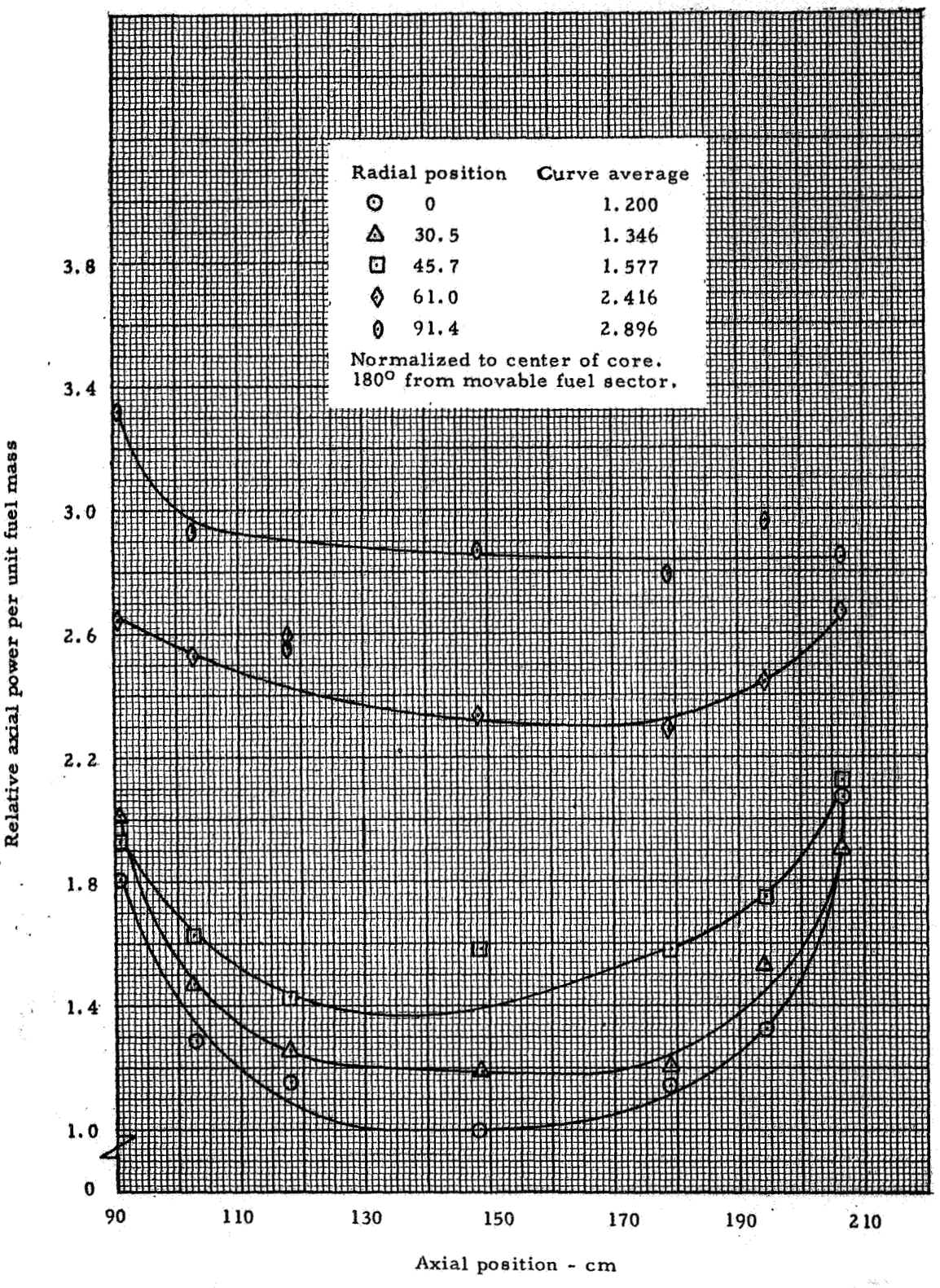

Fig. 10.7 Relative axial power profiles in cavity region 180° from sector, fuel sector 30.5 cm from cavity wall in reflector

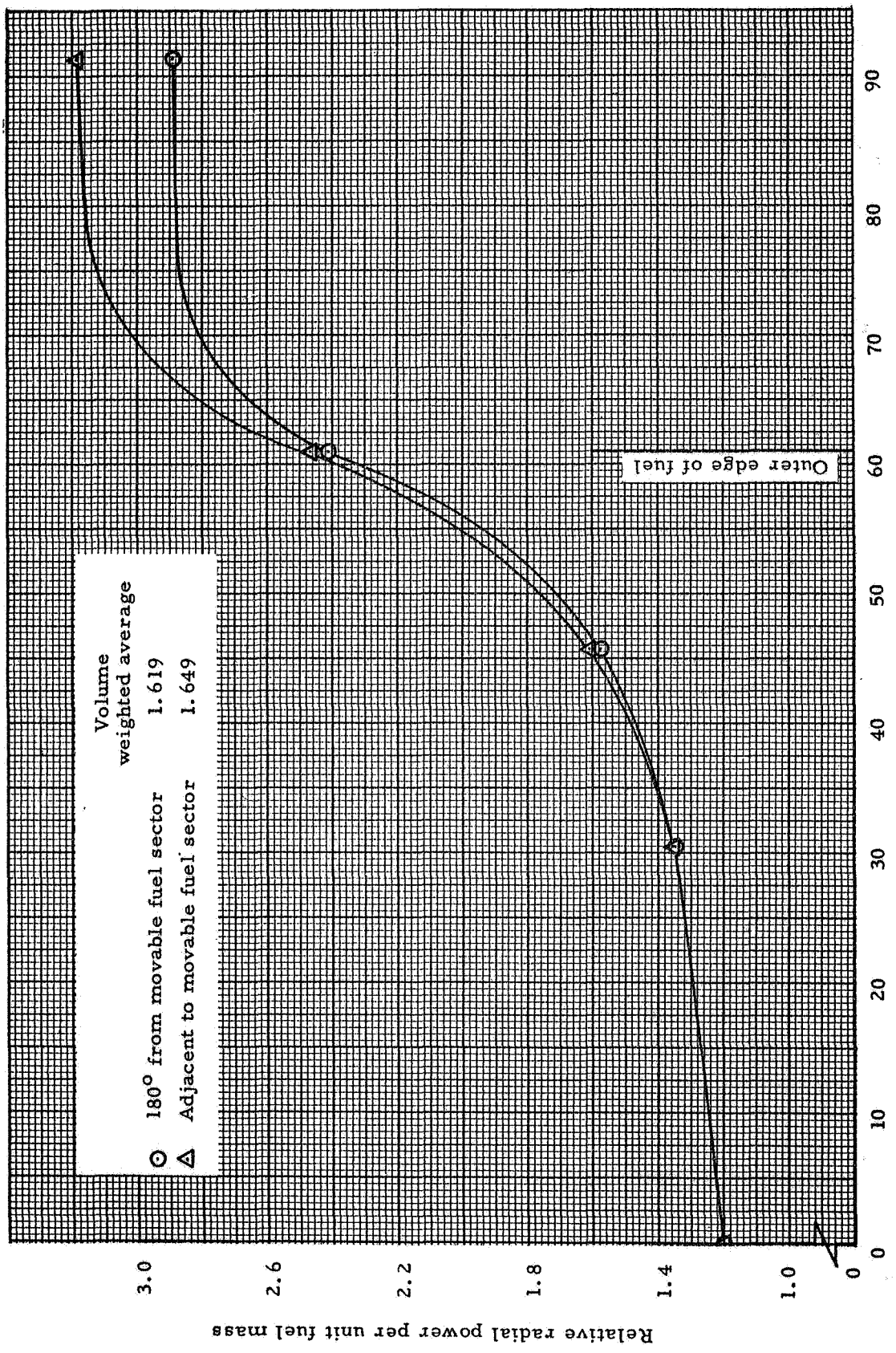

Fig. 10.8 Relative radial power profiles in cavity region, averages of axial profiles from Figures 10.6 and 10.7

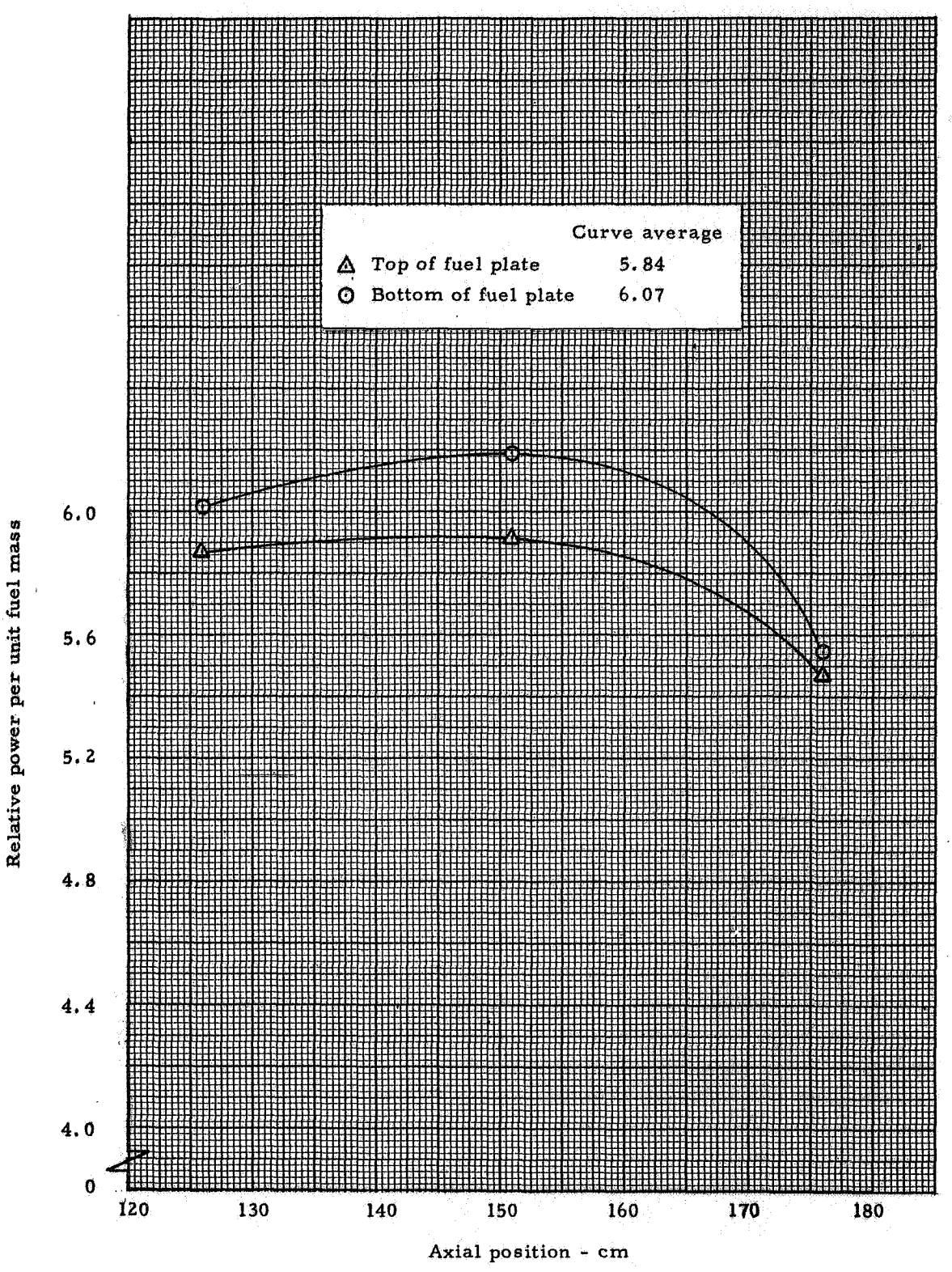

Fig. 10.9 Relative axial power profiles on fuel plates in the reflector with fuel sector 30.5 cm from cavity wall

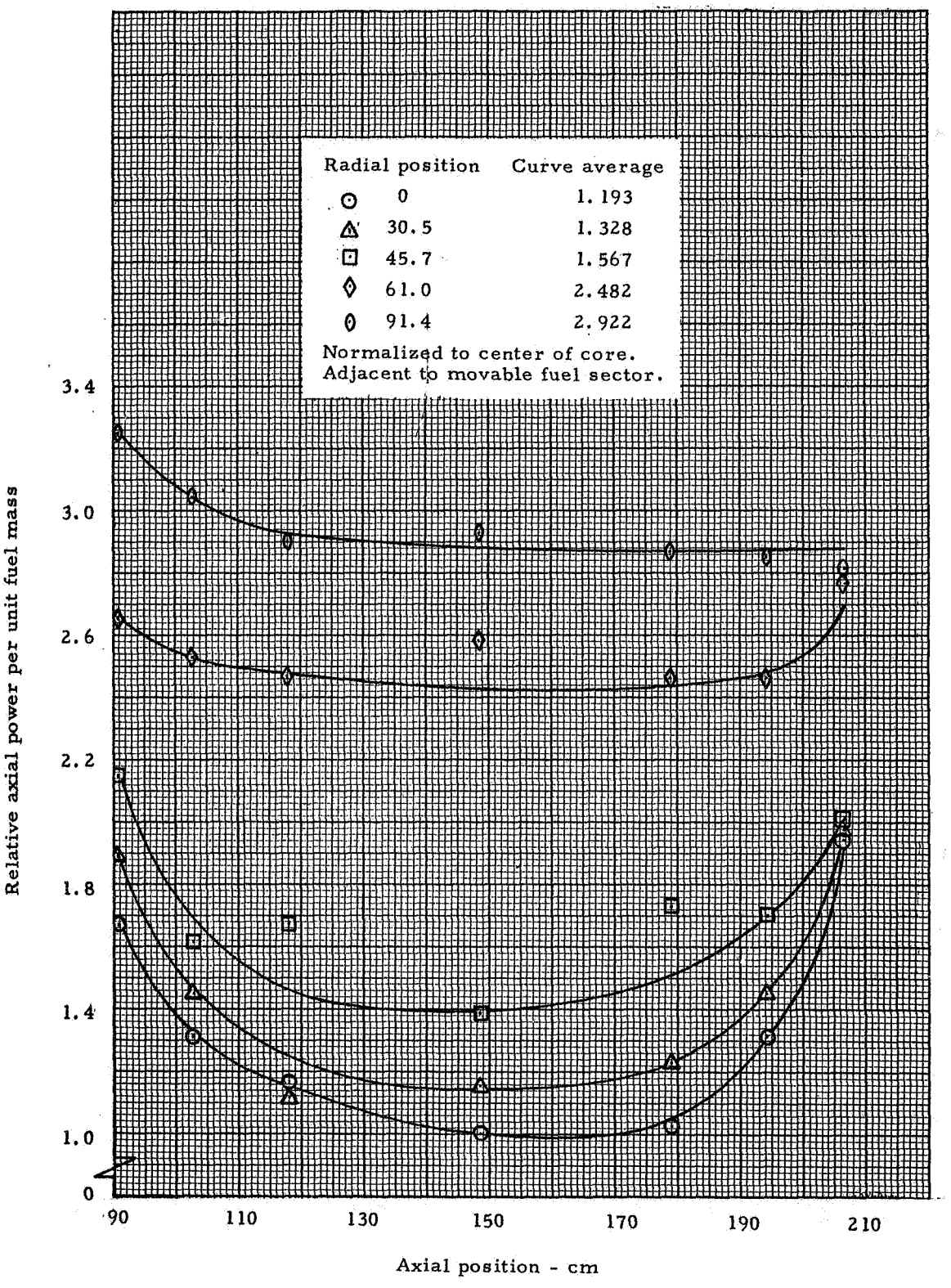

Fig. 10.10 Relative axial power profiles in cavity region adjacent to fuel sector, fuel sector 45.7 cm from cavity wall in reflector

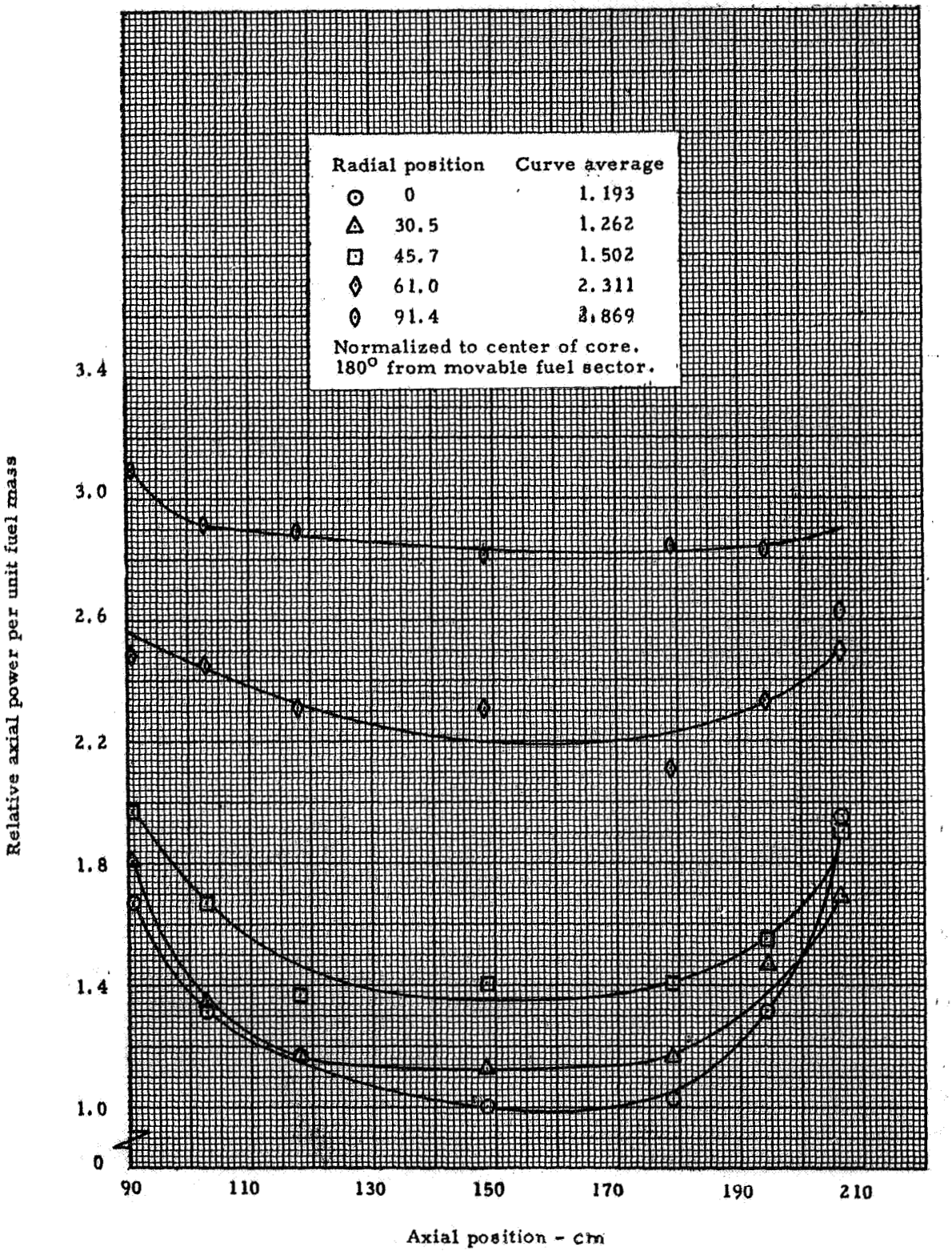

Fig. 10.11 Relative axial power profiles in cavity region 180° from sector, fuel sector 45.7 cm from cavity wall in reflector

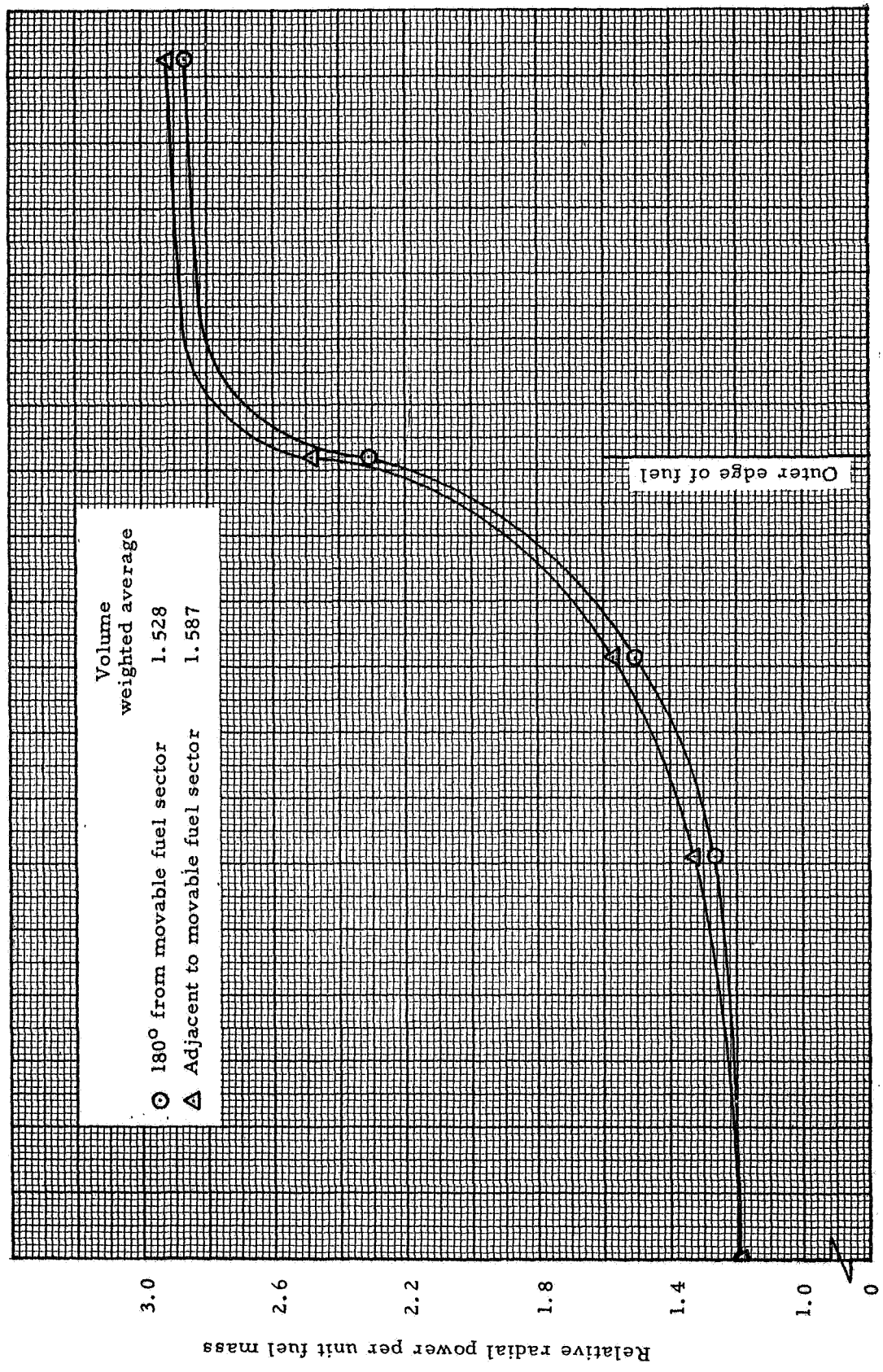

Fig. 10.12 Relative radial power profiles in cavity region, averages of axial profiles from Figures 10.10 and 10.11

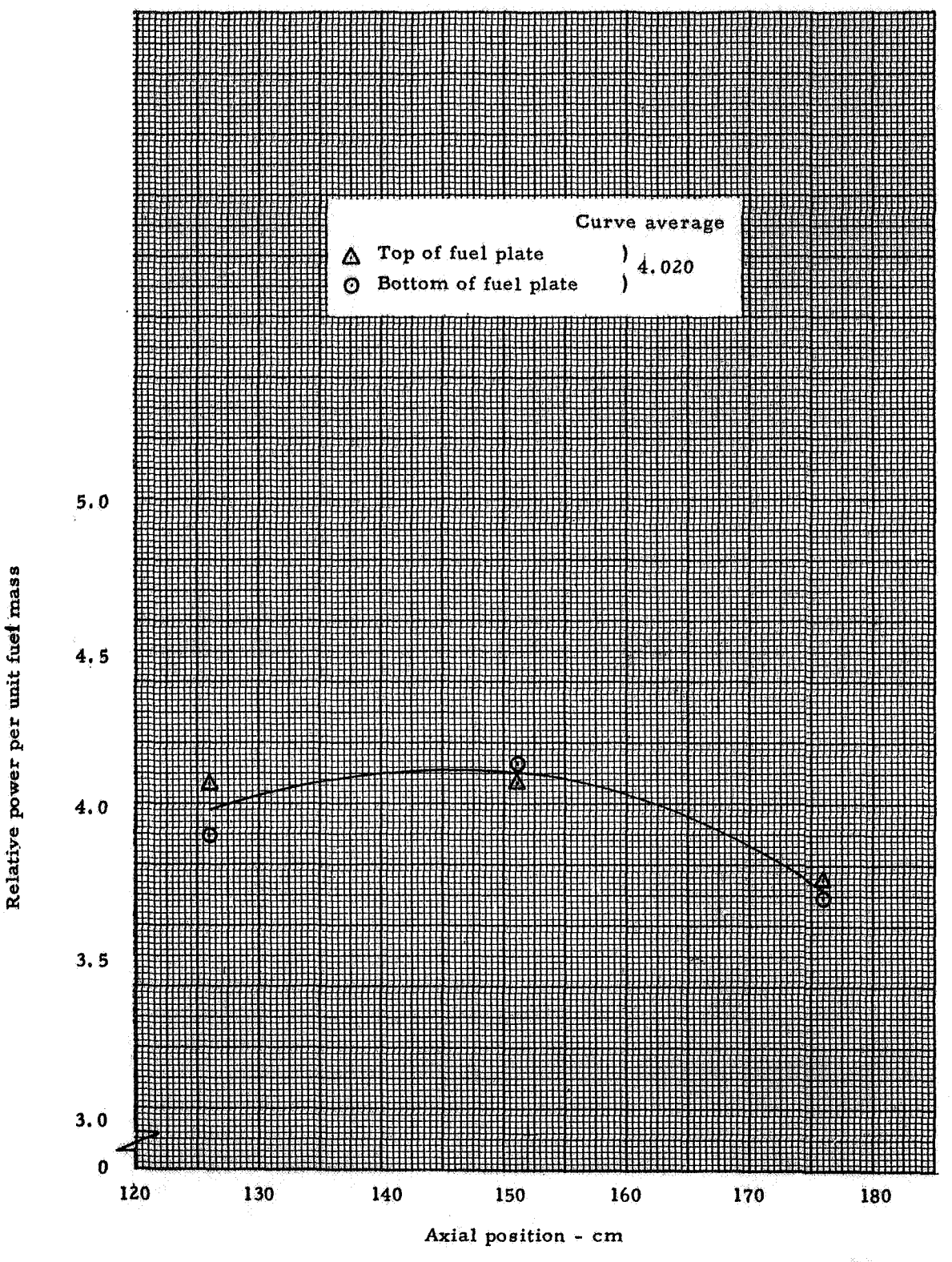

Fig. 10.13 Relative axial power profiles on fuel plates in the reflector with fuel sector 45.7 cm from cavity wall

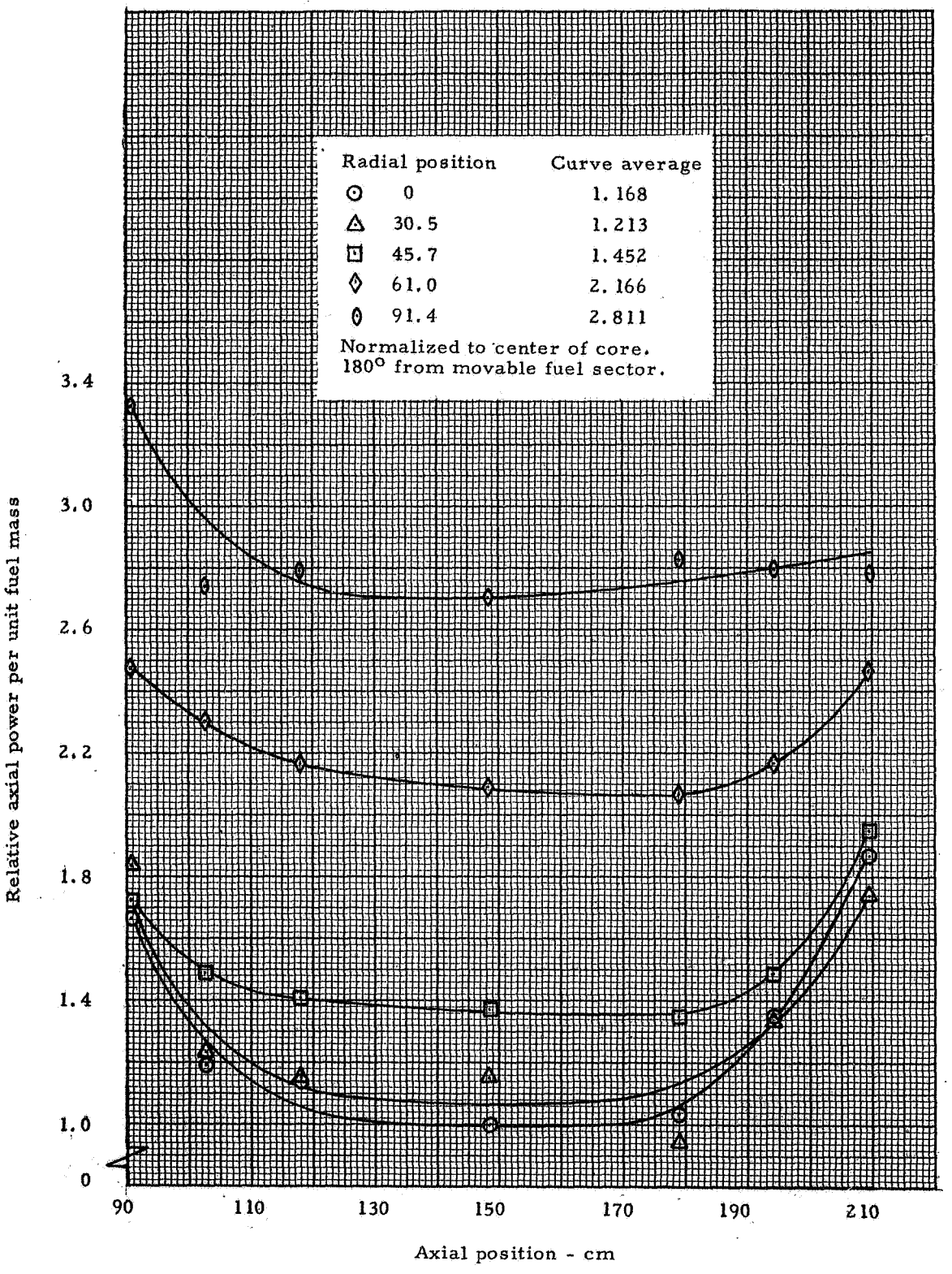

Fig. 10.14 Relative axial power profiles in cavity region adjacent to fuel sector, fuel sector 61 cm from cavity wall in reflector

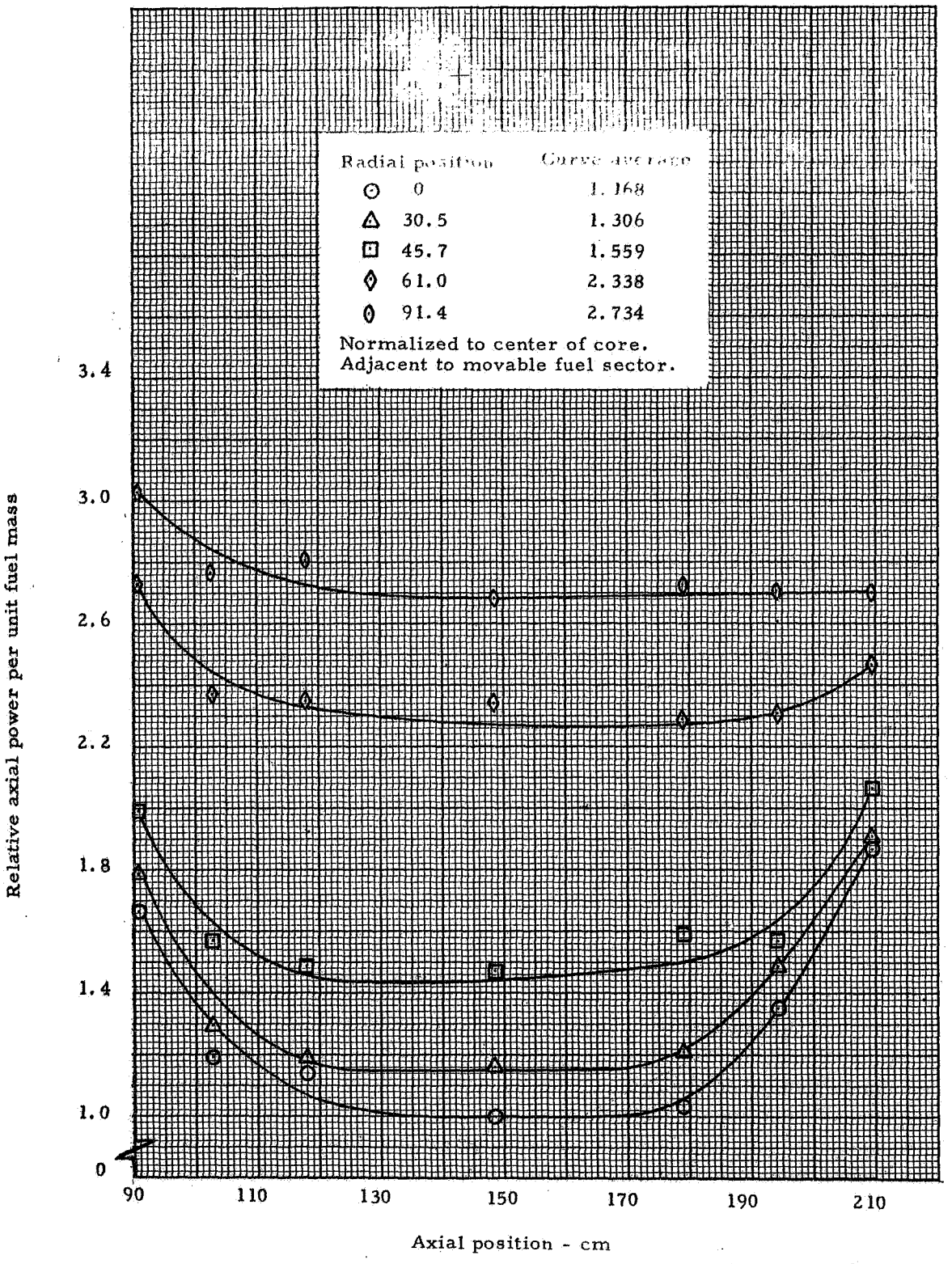

Fig. 10.15 Relative axial power profiles in cavity region 180° from sector, fuel sector 61 cm from cavity wall in reflector

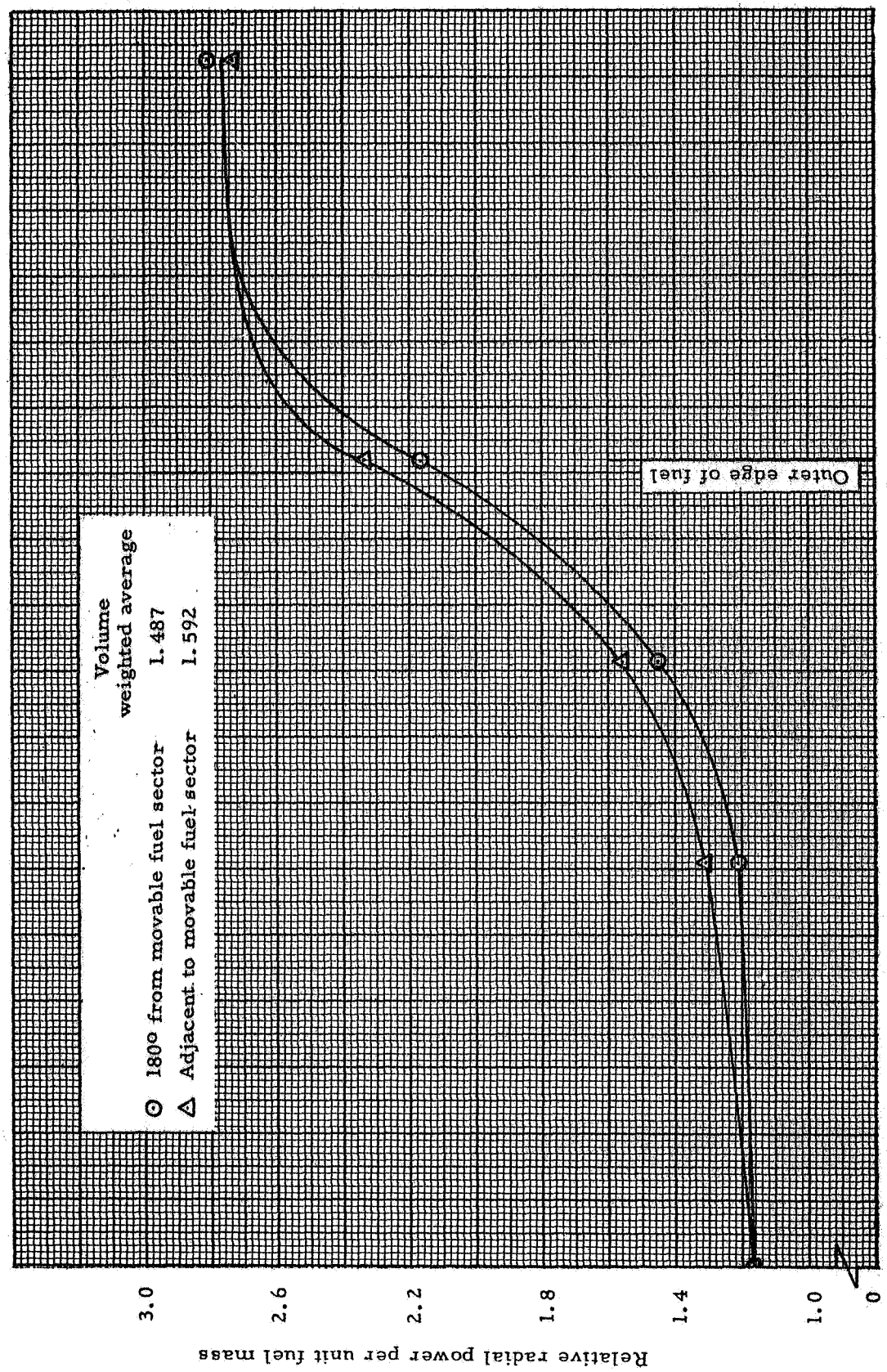

Fig. 10.16 Relative radial power profiles in cavity region, averages of axial profiles from Figures 10.14 and 10.15

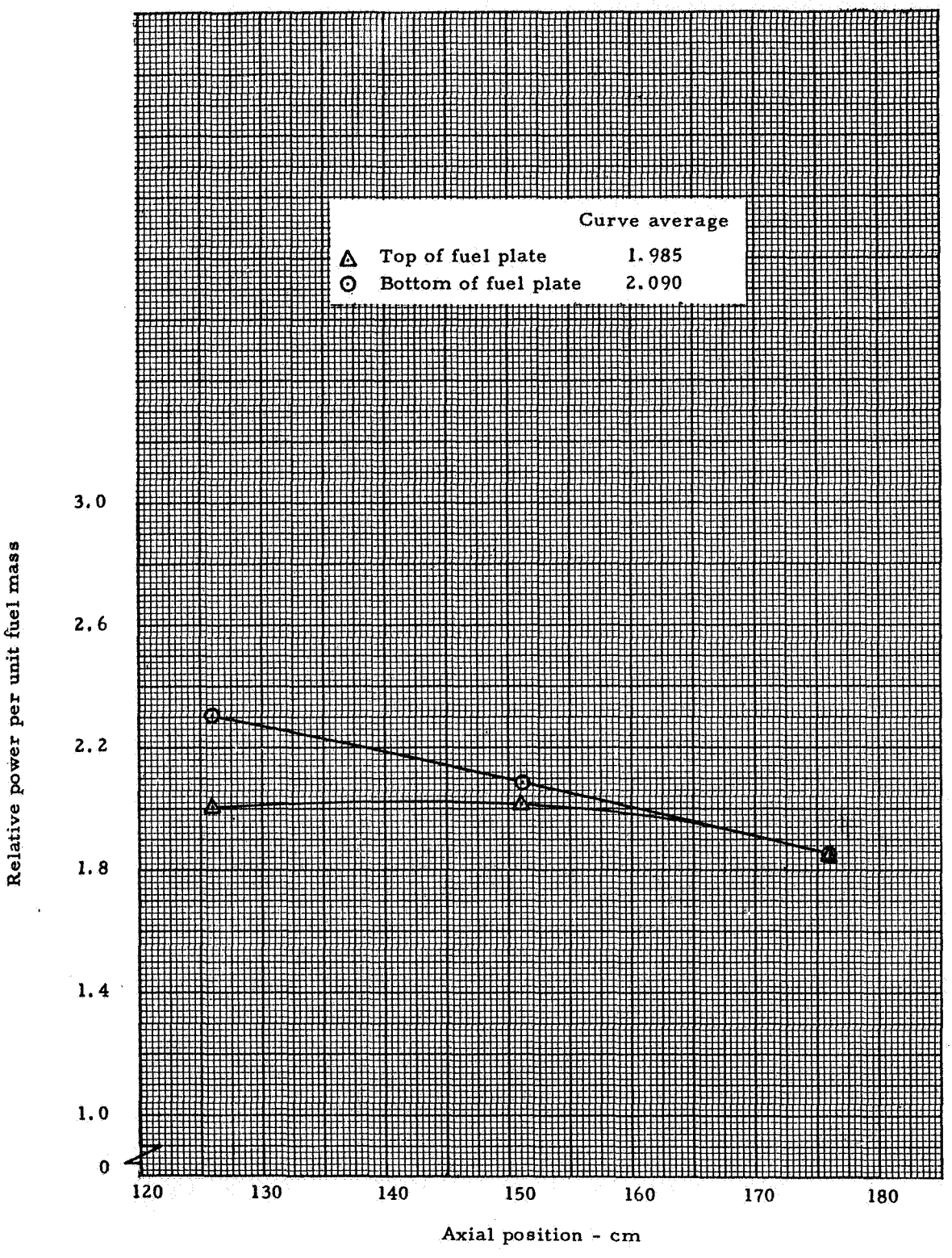

Fig. 10.17 Relative axial power profiles on fuel plates in the reflector with fuel sector 61 cm from cavity wall

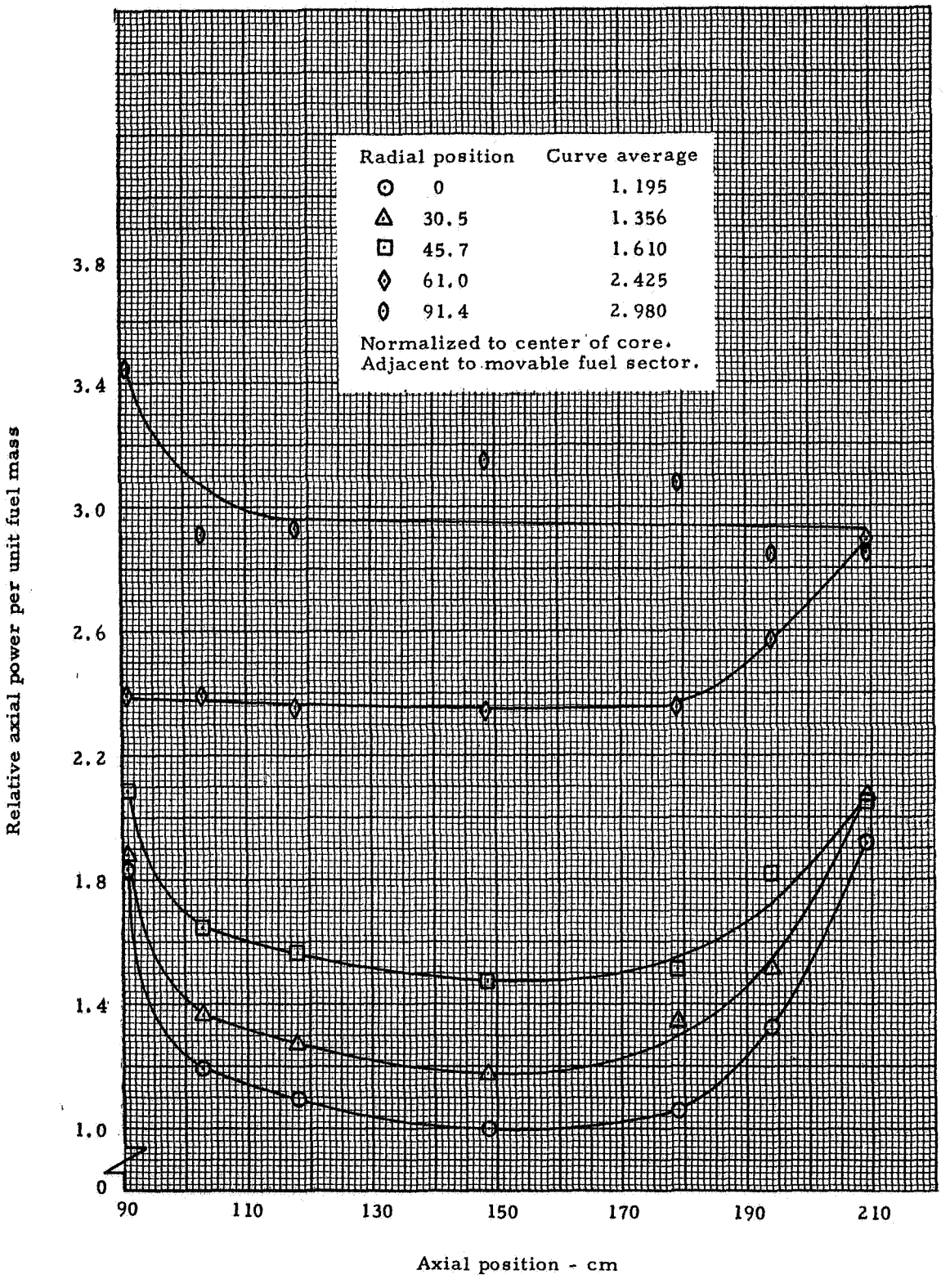

Fig. 10.18 Relative axial power profiles in cavity region adjacent to fuel sector, fuel sector 19 cm from cavity wall in reflector

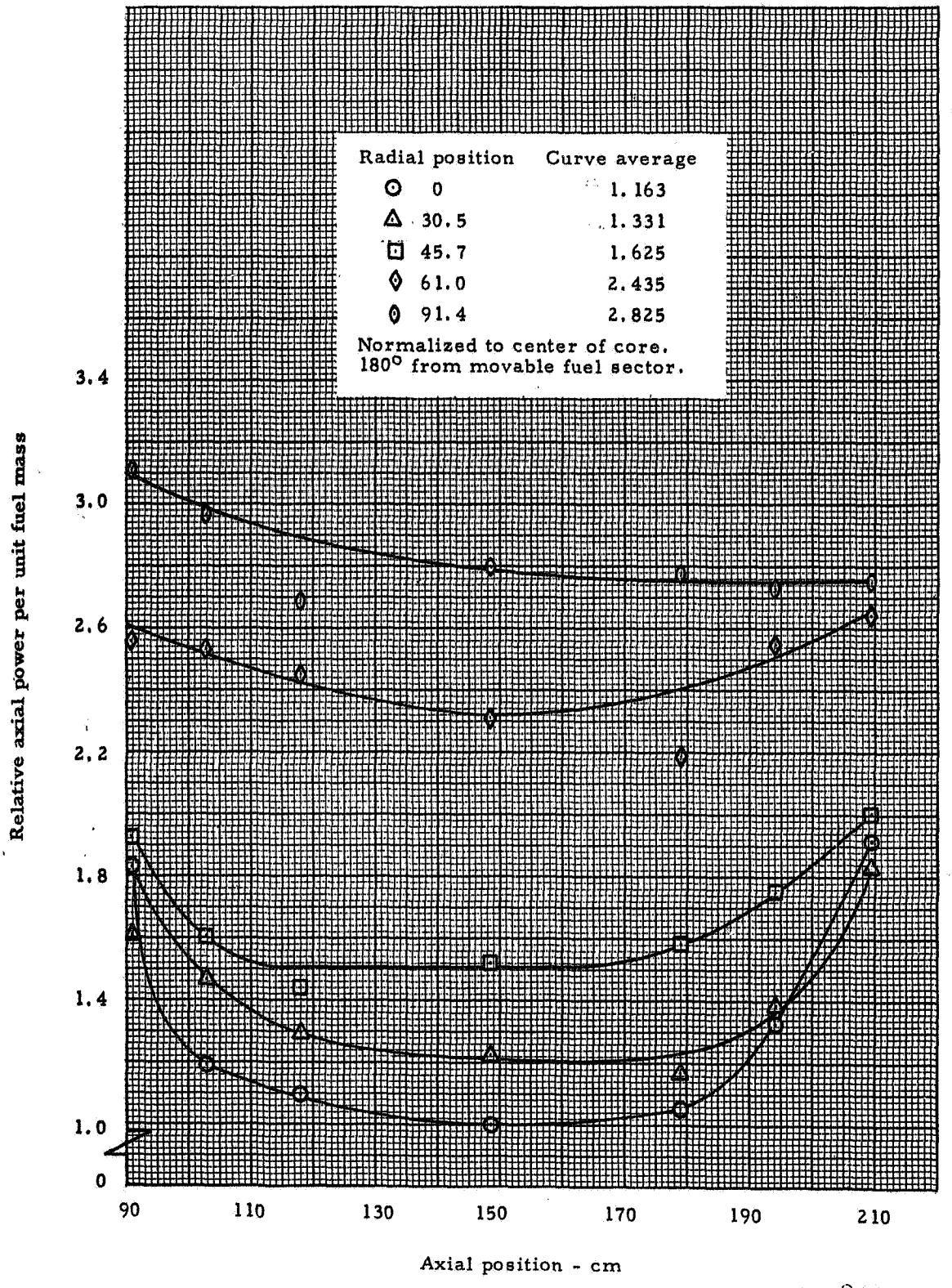

Fig. 10.19 Relative axial power profiles in cavity region 180° from movable fuel sector, fuel sector 19 cm from cavity wall in reflector

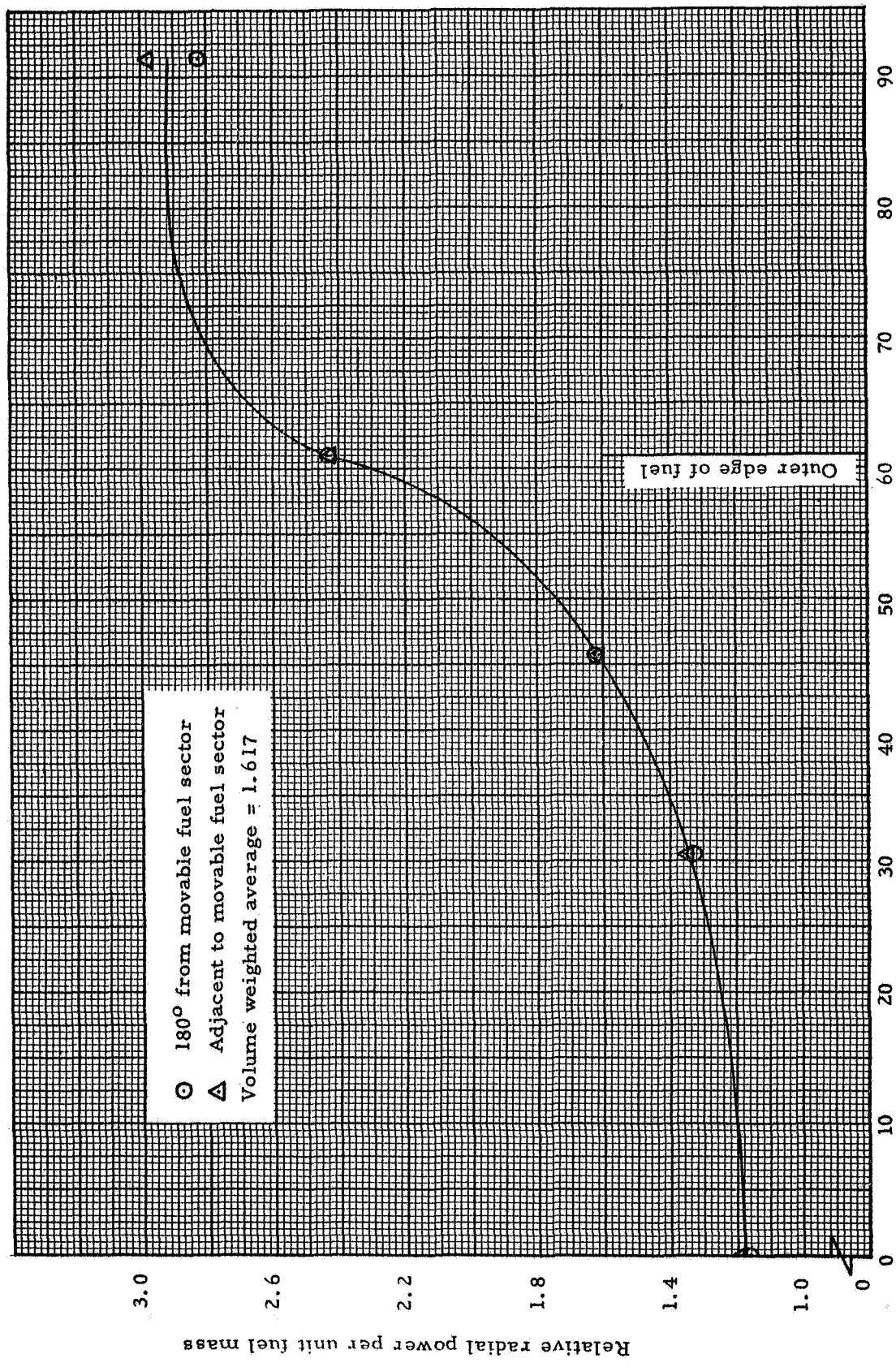

Fig. 10.20 Relative radial power profiles in cavity region, averages of axial profiles from Figures 10.18 and 10.19

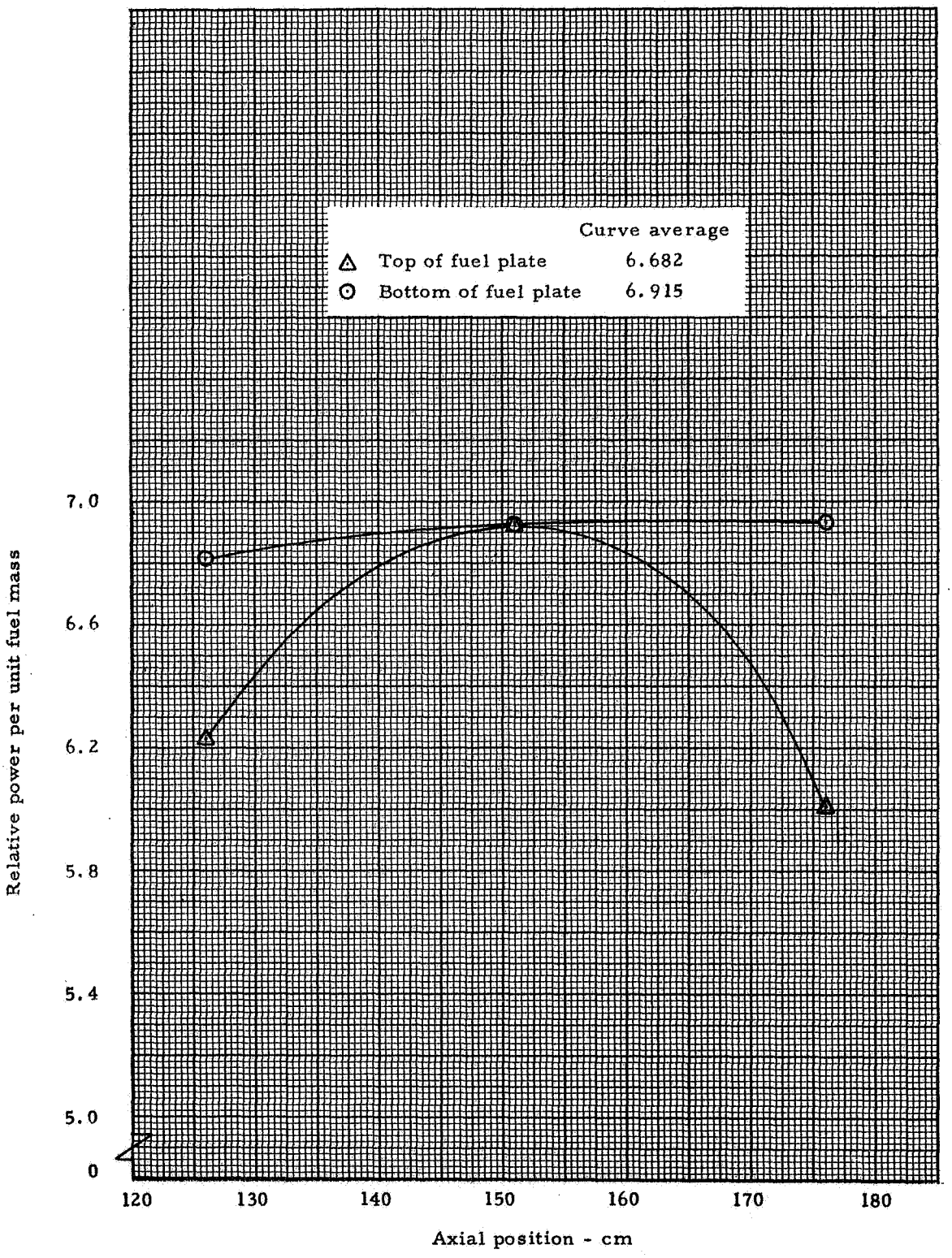

Fig. 10.21 Relative axial power profiles on fuel plates in the reflector with fuel sector 19 cm from cavity wall

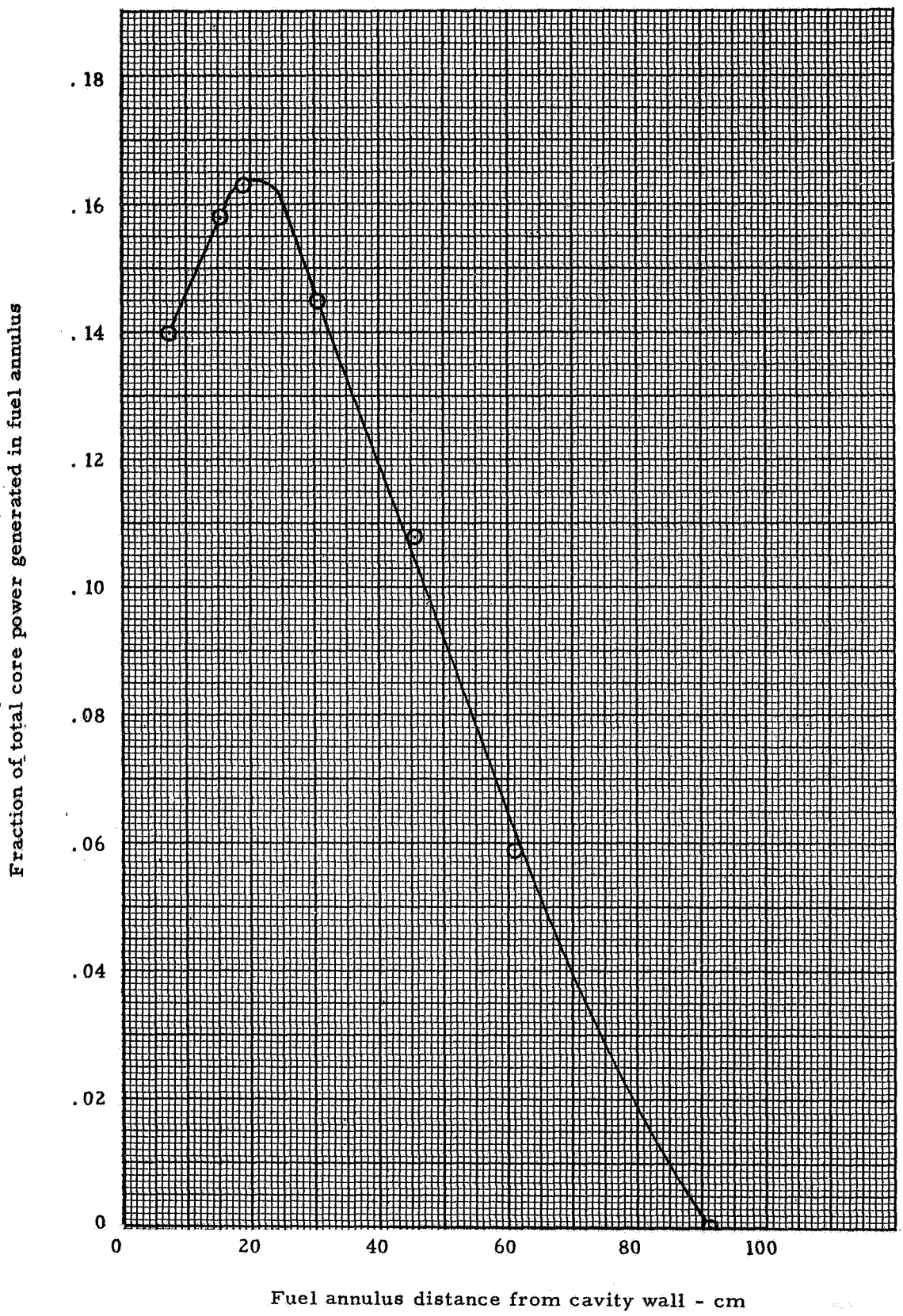

Fig. 10.22 Fraction of total core power generated in 1 kg of U-235 in the radial reflector vs distance from cavity wall

11.0 ADDITIONAL MEASUREMENTS WITH URANIUM IN REFLECTOR REGIONS

Several other measurements not covered in Section 10.0 were performed to evaluate both reactivity and specific power associated with uranium at locations in the radial and end reflector regions. These measurements, however, were made with a different reflector configuration and with a special fuel plate and positioning device. The reactor modification involved a change in the position of the fuel annulus in the radial reflector. Sixty six of the MTR type fuel plates were moved from 7.6 to 19.0 cm from the wet surface of the cavity wall. A total ring of fuel at 19.0 cm required 98 fuel plates, however, only 66 were placed in the reflector at this time in order to keep k-excess down (so that control rods would not seriously perturb the end reflector) and to leave an open sector over the top of the core where measurements could be made in the radial reflector.

A special fuel plate was made which consisted of two thin aluminum plates. A single layer of sheet fuel, 0.00254 cm (0.001 in.) thick by 7.3 cm wide by 29.2 cm long containing 8.54 gm of uranium was placed between these aluminum plates and tape was wrapped around the edges to hold the plates together and prevent D_2O from getting to the uranium. Each of the aluminum plates was 34 cm long by 7.6 cm wide by 0.165 cm thick. This assembly was fastened to a wand which could be handled from the top of the reactor and yet position the fuel plate at the desired locations.

11.1 Initial Loading

Prior to changing the position of the fuel annulus, the D_2O was removed from the fixed tank and half of the fuel was removed from the active core. The 66 fuel plates were then moved to 19.0 cm from the cavity, the tank filled and the core reloaded. The inverse multiplication data obtained during the fuel re-loading are presented in Table 11.1 and Figure 11.1. The fuel element loading was the same as with the full fuel annulus at 7.6 cm from the cavity wall described in Section 9.2. The fully loaded core containing 23.25 kg of uranium in the active core and 554.4 gm U^{235} in the radial reflector 19.0 cm from the wet surface of the cavity wall. Excess reactivity was $1.573 \pm 0.012\%\Delta k$ and the D_2O temperature was $20^{\circ}C$.

There was a 118 degree sector over the top portion of the radial reflector, (measurement access region), where there were no fuel plates. Thus, only 66 of the 98 MTR type fuel plates required for what would make a complete ring were in the radial reflector at the 19 cm location.

After completion of the fuel worth measurements in the reflector, the remaining portion of the fuel annulus was added to the reflector region. The fuel loading in the active core was maintained at 23.25 kg and the annulus in the D_2O contained 23.2 gm U^{235}. In order to maintain the two dollar shutdown requirement in the control rods initially seven actuators and 20 rods, it was necessary to add four manual rods before the fuel annulus could be completed. When fully loaded, there was $1.123\%\Delta k$ held in manual rods and $2.420\%\Delta k$ in driven rods for a total k-excess of $3.543\%\Delta k$. The hardware holding the fuel plate assemblies was worth $-0.525\%\Delta k$, but a correction for this was not included in the above k-excess.

Based on an average fuel worth of 0.89%Δk/kg (taken from UF_6 worth curve on page 212 of Reference 2) of fuel, the critical mass was 18.7 kg of uranium with an 823 gm fuel annulus at 19.0 cm from the cavity wall. Correcting for the hardware in the fuel annulus reduces the critical mass to 18.2 kg.

11.2 Rod Worth Measurements

Several rod worth measurements were made during the process of obtaining the reactivity data. These data are given in Table 11.2. The ten measurements on Actuators 4, 5, and 6 together average -1.7080 ± 0.0337%Δk. Single measurements on Actuators 3, and 6, 1 to 6 inclusive and 1 to 7 inclusive gave values of -1.3947%Δk, -3.619%Δk and -4.044%Δk, respectively.

11.3 Uranium Worth Measurements in the Reflector

The measurements using the special fuel plate and wand assembly included measurements of the wand and plate without fuel and the complete assembly with fuel so that it was possible to deduce the worth of uranium only. In all cases the amount of uranium in the measurement data was 8.54 gm of U^{235}. Because of the control rod guide tubes in the end reflector of the fixed tank, it was not possible to obtain measurements directly on the radial centerline. Most of the measurements were taken with the long dimension of the plate on a radial reactor and the center of the plate 21.8 cm from the radial centerline. The plate was placed parallel to the end of the cavity and the long dimension of the plate was in the vertical plane during all measurements in the end reflector. The measurements in the radial reflector were made with the fuel plate parallel to the cavity wall and the long dimension of the plate normal to the ends of the cavity. All distances were with respect to the same reference grid specified in Section 2.3.

The reactivity data obtained with the special fuel plate in several positions in both the radial and end reflectors are given in Table 11.3. Also included in this table are the data for some additional measurements with the MTR fuel plates.

The first measurements were taken in the radial reflector with the fuel plate 19.0 cm from the wet surface of the cavity wall or 111.4 cm from the center of the core. A traverse was made from the center of the reactor (151.1 cm from the axial reference point) towards the end of the reactor containing the control rods. The primary purpose of this measurement was to see if there was a peak in the region where the radial and end reflectors join. Figure 11.2 presents the reactivity profile extrapolated linearly to 1 kg of U^{235}. The end of the cavity and the region where the radial and end reflectors join is 90.1 cm from the axial reference point. It will be observed that there was no indication of peaking in this region but the reactivity effect continued to decrease from the center of the reactor.

Figure 11.3 shows the axial variation in reactivity per kg of U^{235} in the end reflector, centered at 21.8 cm from the radial center of the reactor. The fuel actually has distributed over radial distances 7.2 to

36.4 cm. The axial peak reactivity occurs about 20 cm from the cavity, which is the same location as the peak in the radial reflector (Figure 10.1). The peak change in reactivity was about 9.8%Δk/kg of U^{235}, where the radial reflector peak was 8.1%Δk/kg of U^{235}. This would indicate a possible small advantage by placing the fuel in the end reflector. However, the end reflector does not lend itself to ease of distribution of fuel over as large an area as does the radial reflector particularly with control rods and guide tubes in the end reflector. The movable end reflector region could have been used for this measurement but this reflector tank contains the exhaust nozzle hole through the center and thus would make installation difficult.

Some measurements were also made in the radial reflector to determine what would happen if two layers of MTR type fuel plates, separated radially by 7.6 cm, were placed in the radial reflector. It was hoped that a sizeable increase in reactivity would be realized with only a small chage in power generation. The results are in Table 11.3. A single layer of 22 fuel plates was placed at 61.0 cm from the wet surface of the cavity wall (153.3 cm from the center of the core) and the reactivity effect measured. Then 22 more plates were placed 7.6 cm behind and then 7.6 cm in front of the first set of fuel plates and the measurements repeated. Taking the average reactivity worth per kg of U^{235} in the D_2O for these two double plate arrangements and comparing with the result for the single layers at 153.3 cm from the core center, it is found that the double layer of fuel gives a 16% increase in reactivity per unit mass of fuel and a 9% increase in specific power (refer to Section 11.4). This implies less perturbation of the adjoint flux than of the direct flux. Although a slight advantage is gained in reactivity vs specific power by doubling up of the fuel plates at the 61 cm location, this location is far less desirable than the location around 20 cm from the cavity wall. In moving the fuel plates from about 61 to 19 cm from the cavity wall, there is a factor of 8 increase in reactivity worth of U^{235} where the specific power increases by a factor of 3.

11.4 Power Distribution Measurements

Power distribution measurements were taken using bare catcher foils on each of the measurement fuel plate positions described in the previous section. All of these data are given in Table 11.4. Detailed measurements were obtained within the active core on the measurement with the fuel plate in the end reflector at a radial position of 31.8 cm and an axial position of 81.2 cm. These data are shown graphically in Figures 11.4, 11.5, and 11.6. Detailed axial profiles were obtained from the core center towards the top of the reactor where the open sector in the MTR type fuel plates existed in the radial reflector and from the core center towards the bottom of the reactor 180 degrees away from the open sector in MTR type fuel plates. The radial profile shown in Figure 11.6 are the average of each of the axial profiles. The volume weighted average over the active core was 1.581 with respect to the core center. Catcher foils were also exposed on the measurement fuel plate and these data were normalized to the center of the core and averaged. Total power was then calculated for the active core and specific power for the measurement fuel plates. In each case, the fuel plate power was based on 1 kg of fuel.

Following this initial power map, a single catcher foil traverse was obtained at the center of the core for each fuel plate position and these data are given in Table 11.4. A plot of each of these axial profiles is not given, but curve averages were within 2% of each other. The data from the catcher foil exposed on the measurement fuel plate in the reflector are also given in Table 11.4. The specific power in the reflector is thus referenced to a fixed total power in the core. The power distribution in the core was assumed to be constant for each configuration. The power for 1 kg of U^{235} was based on the average count from the foils on the measurements fuel plate in the D_2O. In all cases these data were plotted to check for spurious data point, and where such occurred, smooth curve averages were used to calculate the specific power in the fuel plate.

The results of the power calculations and the fraction of total power generated in a 1 kg uranium fuel annulus in the reflector are given in Table 11.5 and Figures 11.7 and 11.8. The point at 81.2 cm in the end reflector was at a slightly different radial position than the remaining points but should be very close to the value for the same radial position as the other points.

Doubling up the MTR type fuel plates in the radial reflector caused, on the average, 9% increase in power. This is based on taking the average of the two cases where an additional fuel plate was placed 7.6 cm behind and then 7.6 cm in front of the fuel plates at 153.3 cm from the core center. This compares to a 16% increase in reactivity.

TABLE 11.1

Inverse Multiplication Data - 66 MTR Type Fuel Plates

19.0 cm from Cavity Wall

Increment	Number Elements	Channel No. 1 CR	Channel No. 1 CRo/CR	Channel No. 2 CR	Channel No. 2 CRo/CR	Channel No. 3 CR	Channel No. 3 CRo/CR	Average CRo/CR	Rod Positions
1	104	5183	0.167	3642	0.153	4074	0.166	0.162	In
1	104	7186	0.133	5082	0.124	5654	0.137	0.131	Out
2	132	8217	0.105	5767	0.096	6293	0.107	0.103	In
2	132	13267	0.072	9408	0.067	10212	0.076	0.072	Out
3	155	11622	0.074	8190	0.068	8932	0.076	0.073	In
3	155	22899	0.042	16068	0.039	17612	0.044	0.042	Out
4	182	20372	0.042	14145	0.039	15720	0.043	0.041	In
4	182	83466	0.011	58071	0.011	62218	0.012	0.011	Out
5	196	29592	0.029	20340	0.027	22837	0.030	0.029	In
5	196	Reactor was critical with about 0.26%Δk excess reactivity							

TABLE 11.2

Rod Worth Measurements

66 MTR Type Fuel Plates in Radial Reflector

19.0 cm From Cavity Wall

Run No.	Actuator Combinations and Worth (%Δk)			
	3 & 6 (6 rods)	4, 5, 6 (8 rods)	1 to 6 (17 rods)	1 to 7 (20 rods)
495	-1.3947			
497			-3.619	
498		-1.7119		
502		-1.6563		
503		-1.7170		
505		01.7110		
508		01.7085		
509		01.7423		
511		01.7273		
514		01.6409		
515				-4.044
516		-1.7440		
527		-1.7205		
	Avg	-1.7080 ± 0.0337		

TABLE 11.3

Fuel Worth and Power Factors in Reflector Regions

Position		Fuel	Worth of	Worth of	
Radial (cm)	Axial (cm)	Weight (gm) U^{235}	fuel and wand (%Δk)	wand (%Δk)	Worth/kg U^{235} - %Δk (2)
Small fuel plate on Al wand					
Radial Reflector					
111.4	43.1	8.54	0.0079	-0.0163	2.834
111.4	76.1	8.54	0.0205	-0.0197 (1)	4.707
111.4	109.2	8.54	0.0424	-0.0231	7.670
111.4	151.1	8.54	0.0539	-0.0157	8.150
End Reflector					
31.8	81.2	8.54	0.0323	-0.0342 (1)	7.787
21.8	81.2	8.54	0.0218	-0.0287	9.790
21.8	58.3	8.54	0.0555	-0.0220	9.075
21.8	27.8	8.54	0.0024	-0.0071	1.112
MTR Type fuel plate assemblies - Radial Reflector					
153.3	151.1	184.8	0.1557	-0.0271	0.989
153.3 160.9	151.1	369.6	0.2736	-0.0361	0.838
145.7 153.3	151.1	369.6	0.4790	-0.0570	1.450

(1) Assumed wand worth
(2) The estimated error in these values is about 0.8% Δk.

TABLE 11.4

Catcher Foil Data

66 MTR Type Fuel Plates in Radial Reflector

19 cm From Cavity Wall

Foil No.	Foil Type	Location Radial (cm)	Location Axial (cm)	Normalized Counts	Local to Foil (X)
1	Bare	91.4	90.8	118624	3.191
2	Bare	Bottom	102.8	101308	2.725
3	Bare	Bottom	118.0	123997	3.335
4	Bare	Bottom	148.5	105276	2.832
5	Bare	Bottom	179.0	101829	2.739
6	Bare	Bottom	194.2	105747	2.845
7	Bare	Bottom	206.9	107092	2.881
8	Bare	61.0	90.8	101616	2.733
9	Bare	Bottom	102.8	89834	2.417
10	Bare	Bottom	118.0	90986	2.448
11	Bare	Bottom	148.5	82928	2.231
12	Bare	Bottom	179.0	90331	2.430
13	Bare	Bottom	194.2	81729	2.199
14	Bare	Bottom	206.9	92880	2.498
15	Bare	45.7	90.8	71454	1.922
16	Bare	Bottom	102.8	61015	1.641
17	Bare	Bottom	118.0	53797	1.447
18	Bare	Bottom	148.5	59564	1.602
19	Bare	Bottom	179.0	56727	1.526
20	Bare	Bottom	194.2	59505	1.601
21	Bare	Bottom	206.9	74242	1.997
22	Bare	30.5	90.8	67253	1.809
23	Bare	Bottom	102.8	51938	1.397
24	Bare	Bottom	118.0	50253	1.352
25	Bare	Bottom	148.5	45998	1.237
26	Bare	Bottom	179.0	42757	1.150
27	Bare	Bottom	194.2	52253	1.406
28	Bare	Bottom	206.9	67524	1.816
29	Bare	0	90.8	64018	1.722
30	Bare	0	102.8	45396	1.221
31	Bare	0	118.0	40758	1.096
32	Bare	0	148.5	37178	1.000 (X)
33	Bare	0	179.0	42408	1.141
34	Bare	0	194.2	51410	1.383
35	Bare	0	206.9	76580	2.060
36	Bare	30.5	90.8	66162	1.780
37	Bare	Top	102.8	50318	1.354
38	Bare	Top	118.0	45652	1.228
39	Bare	Top	148.5	42919	1.155
40	Bare	Top	179.0	47107	1.267
41	Bare	Top	194.2	52377	1.409

TABLE 11.4
(Continued)

Foil No.	Type	Location Radial (cm)	Location Axial (cm)	Normalized Counts	Local to Foil (X)
Run 1122 (Cont'd)					
42	Bare	Top	206.9	67348	1.812
43	Bare	45.7	90.8	74711	2.010
44	Bare	Top	102.8	60196	1.619
45	Bare	Top	118.0	52411	1.410
46	Bare	Top	148.5	54292	1.460
47	Bare	45.7	179.0	57049	1.535
48	Bare	Top	194.2	61535	1.655
49	Bare	Top	206.9	82507	2.219
50	Bare	61.0	90.8	86690	2.332
51	Bare	Top	102.8	84682	2.278
52	Bare	Top	118.0	85566	2.302
53	Bare	Top	148.5	89354	2.404
54	Bare	Top	179.0	78668	2.116
55	Bare	Top	194.2	86846	2.336
56	Bare	Top	206.9	105392	2.835
57	Bare	91.4	90.8	133947	3.603
58	Bare	Top	102.8	116528	3.135
59	Bare	Top	118.0	112568	3.028
60	Bare	Top	148.5	98458	2.649
61	Bare	Top	179.0	104355	2.807
62	Bare	Top	194.2	102299	2.752
63	Bare	Top	206.9	106482	2.864
64	Bare	44.4	81.4	181694	4.888
65	Bare	44.4	81.6	177723	4.781
66	Bare	31.8	81.4	201841	5.430
67	Bare	31.8	81.6	187871	5.054
68	Bare	19.0	81.4	205159	5.519
69	Bare	19.0	81.6	221935	5.970

TABLE 11.4
(Continued)

Foil No.	Type	Location Radial (cm)	Location Axial (cm)	Normalized Counts	Local to Foil (X)
Run 1123 (Fuel plate in end reflector (radial-21.8 cm, axial = 81.2 cm)					
1	Bare	0	90.8	64792	1.711
2	Bare	0	102.8	52337	1.382
3	Bare	0	118.0	40353	1.066
4	Bare	0	148.5	37859	1.000 (X)
5	Bare	0	179.0	42086	1.111
6	Bare	0	194.2	52051	1.375
7	Bare	0	206.9	72738	1.921
8	Bare	34.4	73.8	242523	6.405
9	Bare	34.4	74.0	121345 (wet)	3.205
10	Bare	21.7	73.8	239540	6.326
11	Bare	21.7	74.0	236308	6.241
12	Bare	9.0	73.8	251468	6.641
13	Bare	9.0	74.0	241185	6.370
Run 1124 (Fuel plate in end reflector (radial = 21.8 cm, axial = 58.3 cm)					
1	Bare	0	90.8	59676	1.634
2	Bare	0	102.8	46789	1.281
3	Bare	0	118.0	35375	0.969
4	Bare	0	148.5	36520	1.000 (X)
5	Bare	0	179.0	37443	1.025
6	Bare	0	194.2	45821	1.255
7	Bare	0	206.9	69975	1.916
8	Bare	34.4	58.6	196723	5.386
9	Bare	34.4	58.8	192465	5.270
10	Bare	21.7	58.6	64901 (wet)	1.777
11	Bare	21.7	58.8	210202	5.755
12	Bare	9.0	58.6	213775	5.853
13	Bare	9.0	58.8	222701	6.098
Run 1125 Fuel plate in radial reflector (radial = 111.4 cm, axial = 109.2 cm)					
1	Bare	0	90.8	63304	1.713
2	Bare	0	102.8	47622	1.288
3	Bare	0	118.0	39506	1.069
4	Bare	0	148.5	36961	1.000 (X)
5	Bare	0	179.0	38975	1.054
6	Bare	0	194.2	26549	1.259
7	Bare	0	206.9	67186	1.818
8	Bare	111.7	121.8	222974	6.033
9	Bare	111.5	121.8	224054	6.062
10	Bare	111.7	109.1	199510	5.398
11	Bare	111.5	109.1	201908	5.463
12	Bare	111.7	96.4	187700	5.078
13	Bare	111.5	96.4	183919	4.976

TABLE 11.4

(Continued)

Foil No.	Type	Location Radial (cm)	Location Axial (cm)	Normalized Counts	Local to Foil (X)
Run 1126	Fuel plate in radial reflector (radial = 111.4 cm, axial = 76.1 cm)				
1	Bare	0	90.8	59246	1.577
2	Bare	0	102.8	46642	1.242
3	Bare	0	118.0	40663	1.082
4	Bare	0	148.5	37565	1.000 (X)
5	Bare	0	179.0	38562	1.027
6	Bare	0	194.2	50089	1.333
7	Bare	0	206.9	70935	1.888
8	Bare	0	89.4	81940	2.181
9	Bare	0	74.9	278901	7.425
10	Bare	0	59.6	256304	6.823
11	Bare	0	44.4	195566	5.206
12	Bare	0	29.1	122187	3.253
13	Bare	0	13.9	56385	1.501
14	Bare	0	0	8302	0.221
15	Bare	111.7	88.8	175273	4.666
16	Bare	111.5	88.8	175729	4.678
17	Bare	111.7	76.1	146161	3.891
18	Bare	111.5	76.1	145355	3.869
19	Bare	111.7	63.4	117378	3.125
20	Bare	111.5	63.4	123392	3.285
Run 1127	Fuel plate in radial reflector (radial = 111.4, axial = 151.1 cm)				
1	Bare	0	90.8	62655	1.770
2	Bare	0	102.8	46246	1.306
3	Bare	0	118.0	38611	1.091
4	Bare	0	148.5	35394	1.000 (X)
5	Bare	0	179.0	39410	1.113
6	Bare	0	194.2	47517	1.342
7	Bare	0	206.9	70984	2.005
8	Bare	111.5	138.4	231640	6.544
9	Bare	111.3	138.4	230284	6.506
10	Bare	111.5	151.1	212066	5.991
11	Bare	111.3	151.1	219455	6.200
12	Bare	111,5	163.8	218523	6.173
13	Bare	111.3	163.8	214674	6.065

TABLE 11.4

(Continued)

Foil No.	Type	Location Radial (cm)	Location Axial (cm)	Normalized Counts	Local to Foil (X)
Run 1128 Fuel plate in radial reflector (radial = 111.4, axial = 43.1 cm)					
1	Bare	0	90.8	63365	1.769
2	Bare	0	102.8	46750	1.305
3	Bare	0	118.0	38766	1.082
4	Bare	0	148.5	35815	1.000 (X)
5	Bare	0	179.0	39373	1.099
6	Bare	0	194.2	46370	1.295
7	Bare	0	206.9	71839	2.006
8	Bare	111.5	55.8	132986	3.713
9	Bare	111.3	55.8	135133	3.773
10	Bare	111.5	43.1	103640	2.894
11	Bare	111.3	43.1	98081	2.738
12	Bare	111.5	30.4	74210	2.072
13	Bare	111.3	30.4	75259	2.101
Run 1129 Fuel plate in end reflector (radial = 21.8 cm, axial = 27.8 cm)					
1	Bare	0	90.8	64164	1.718
2	Bare	0	102.8	47480	1.271
3	Bare	0	118.0	40289	1.079
4	Bare	0	148.5	37353	1.000 (X)
5	Bare	0	179.0	40156	1.075
6	Bare	0	194.2	47214	1.264
7	Bare	0	206.9	62921	1.685
8	Bare	34.4	28.2	89407	2.394
9	Bare	34.4	28.0	84030	2.250
10	Bare	21.7	28.2	97804	2.618
11	Bare	21.7	28.0	93221	2.496
12	Bare	9.0	28.2	99585	2.666
13	Bare	9.0	28.0	100782	2.698
Run 1130 22 MTR type fuel plate in radial reflector (radial = 153.3 cm, axial 151.1 cm)					
1	Bare	0	90.8	64949	1.788
2	Bare	0	102.8	47317	1.303
3	Bare	0	118.0	37836	1.042
4	Bare	0	148.5	36326	1.000 (X)
5	Bare	0	179.0	38738	1.066
6	Bare	0	194.2	46454	1.279
7	Bare	0	206.9	70573	1.943
8	Bare	153.6	128.3	80201	2.208
9	Bare	153.0	128.3	83015	2.285
10	Bare	153.6	151.1	80401	2.213
11	Bare	153.0	151.1	84636	2.330
12	Bare	153.6	173.9	77215	2.126
13	Bare	153.0	173.9	73264	2.017

TABLE 11.4

(Continued)

Foil No.	Type	Location Radial (cm)	Location Axial (cm)	Normalized Counts	Local to Foil (X)
Run 1131	Double layer of MTR type fuel plates in radial reflector (radial = 153.3 and 160.9 cm, axial = 151.1 cm)				
1	Bare	0	90.8	65721	1.797
2	Bare	0	102.8	47361	1.295
3	Bare	0	118.0	40142	1.098
4	Bare	0	148.5	36569	1.000 (X)
5	Bare	0	179.0	40648	1.112
6	Bare	0	194.2	45992	1.258
7	Bare	0	206.9	70114	1.917
8	Bare	161.2	123.8	63670	1.741
9	Bare	160.6	123.8	60748	1.661
10	Bare	161.2	151.1	58875	1.610
11	Bare	160.6	151.1	58907	1.611
12	Bare	161.2	173.9	52922	1.447
13	Bare	160.6	173.9	58584	1.602
14	Bare	153.6	123.8	82937	2.268
15	Bare	153.0	123.8	93382	2.554
16	Bare	153.6	151.1	88397	2.417
17	Bare	153.0	151.1	96129	2.629
18	Bare	153.6	173.9	79466	2.173
19	Bare	153.0	173.9	89024	2.434
Run 1132	Double layer of MTR type fuel plates in radial reflector (radial = 145.7 and 153.3 cm, axial = 151.1 cm)				
1	Bare	0	90.8	62572	1.610
2	Bare	0	102.8	45235	1.164
3	Bare	0	118.0	40084	1.031
4	Bare	0	148.5	38870	1.000 (X)
5	Bare	0	179.0	40304	1.037
6	Bare	0	194.2	49156	1.265
7	Bare	0	206.9	69802	1.796
8	Bare	153.6	128.3	108438	2.790
9	Bare	153.0	128.3	109121	2.807
10	Bare	153.6	151.1	108114	2.781
11	Bare	153.0	151.1	111455	2.867
12	Bare	153.6	173.9	102276	2.631
13	Bare	153.0	173.9	98582	2.536
14	Bare	153.6	128.3	100670	2.590
15	Bare	153.0	128.3	102834	2.590
16	Bare	153.6	151.1	95860	2,646
17	Bare	153.0	151.1	99079	2.549
18	Bare	153.6	173.9	89287	2.297

TABLE 11.4

(Continued)

Foil No.	Type	Location Radial (cm)	Location Axial (cm)	Normalized Counts	Local to Foil (X)
Run 1132 (Cont'd)					
19	Bare	153.0	173.9	99341	2.273
20	Bare	153.6	128.3	114638	2.949
21	Bare	153.0	128.3	110642	2.846
22	Bare	153.6	151.1	115310	2.967
23	Bare	153.0	151.1	104078	2.178
24	Bare	153.6	173.9	113178	2.912
25	Bare	153.0	173.9	111042	2.857
26	Bare	146.0	128.3	136224	3.505
27	Bare	145.4	128.3	144472	3.717
28	Bare	146.0	151.1	143730	3.698
29	Bare	145.4	151.1	152949	3.935
30	Bare	146.0	173.9	146933	3.780
31	Bare	145.4	173.9	149540	3.847
32	Bare	146.0	128.3	120350	3.096
33	Bare	145.4	128.3	125299	3.224
34	Bare	146.0	151.1	120665	3.104
35	Bare	145.4	151.1	122686	3.156
36	Bare	146.0	173.9	117035	3.011
37	Bare	145.4	173.9	119925	3.085
38	Bare	146.0	128.3	141055	3.629
39	Bare	145.4	128.3	143573	3,694
40	Bare	146.0	151.1	144681	3.722
41	Bare	145.4	151.1	147795	3.802
42	Bare	146.0	173.9	133398	3.432
43	Bare	145.4	173.9	132234	3.402

TABLE 11.5

Power Fraction in Uranium

Located in Reflector Regions

Location				
Radial (cm)	Axial (cm)	Core Power (watts)	Fuel Plate (1) Power in D_2O (watts)	Power Fraction in Fuel Plate in D_2O
Radial Reflector				
111.4	43.1	12.23	1.02	0.077
111.4	76.1	12.83	1.46	0.102
111.4	109.2	12.63	2.02	0.138
111.4	151.1	12.09	2.22	0.155
End Reflector				
31.8	81.2	12.70	1.44	0.102
21.8	73.6	12.93	1.77	0.120
21.8	58.3	12.48	1.53	0.109
21.8	27.8	12.76	0.95	0.069
MTR Type fuel plate in radial reflector				
153.3	151.1	12.41	0.81	0.061
153.3 160.9	151.1	12.49	0.75	0.057
145.7 153.3	151.1	13.28	1.09	0.076

(1) Based on 1 kg of U^{235} in reflector

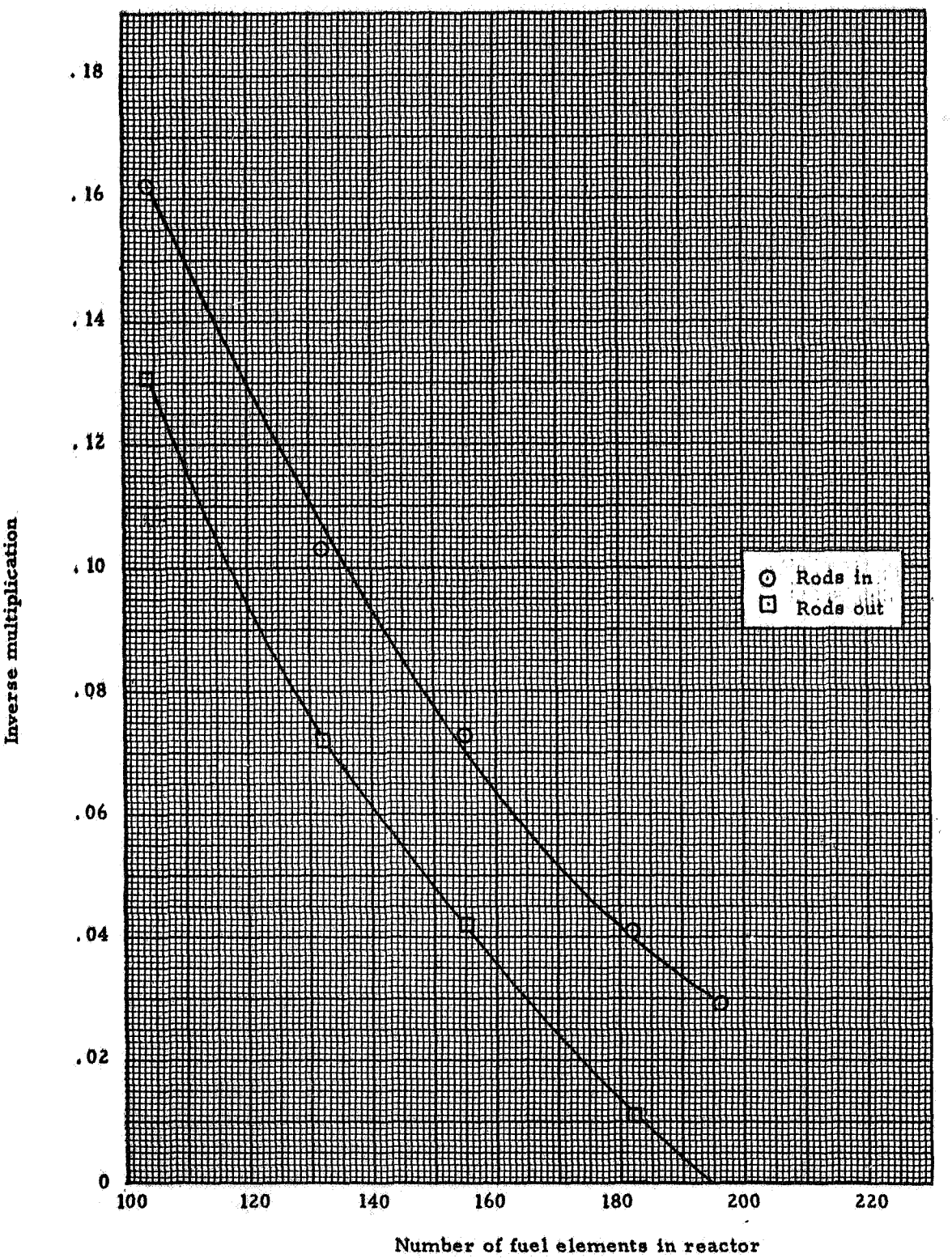

Fig. 11.1 Inverse multiplication curves, additional measurements with fuel in reflector

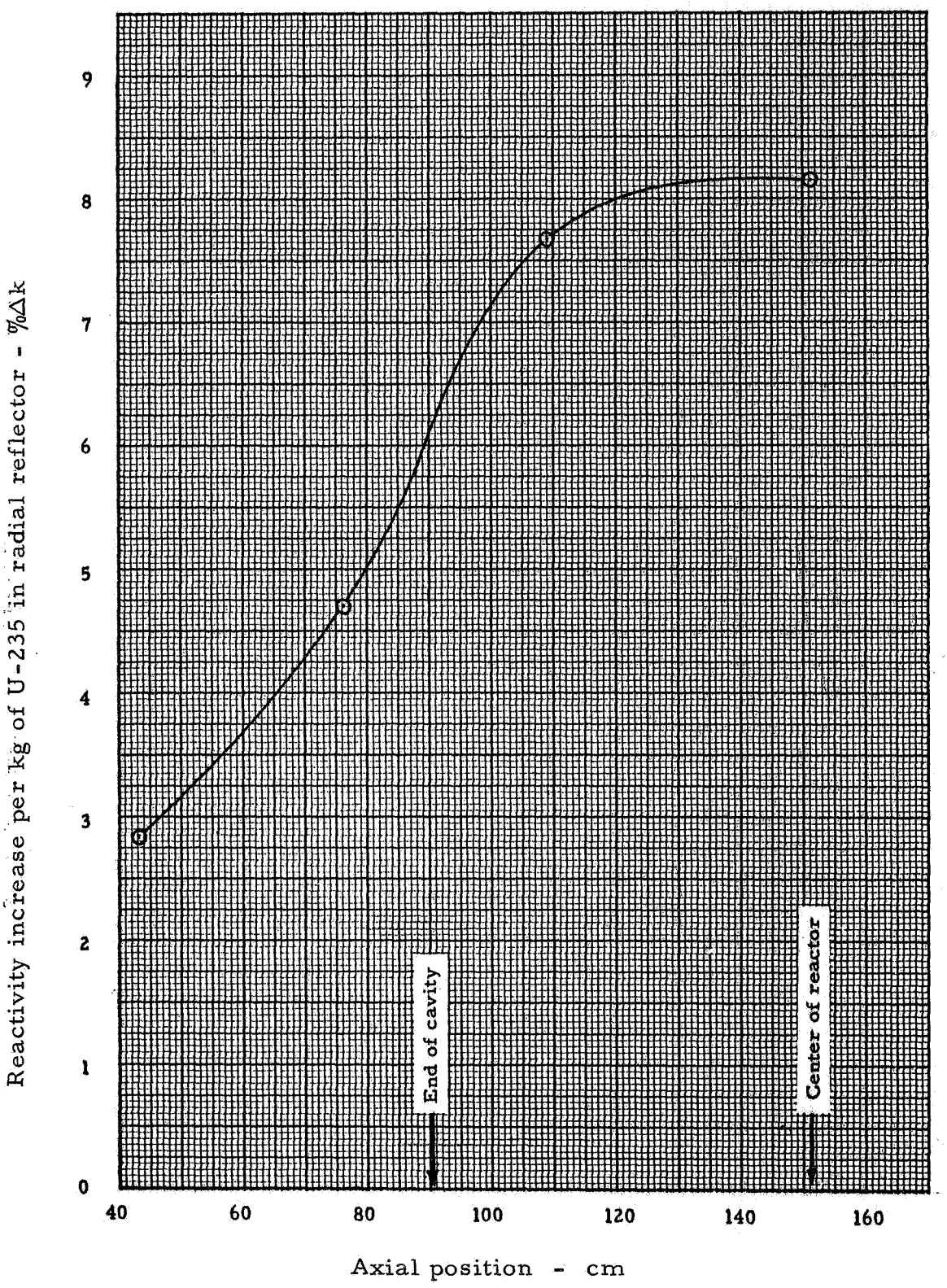

Fig. 11.2 Reactivity increase per kg of fuel in radial reflector

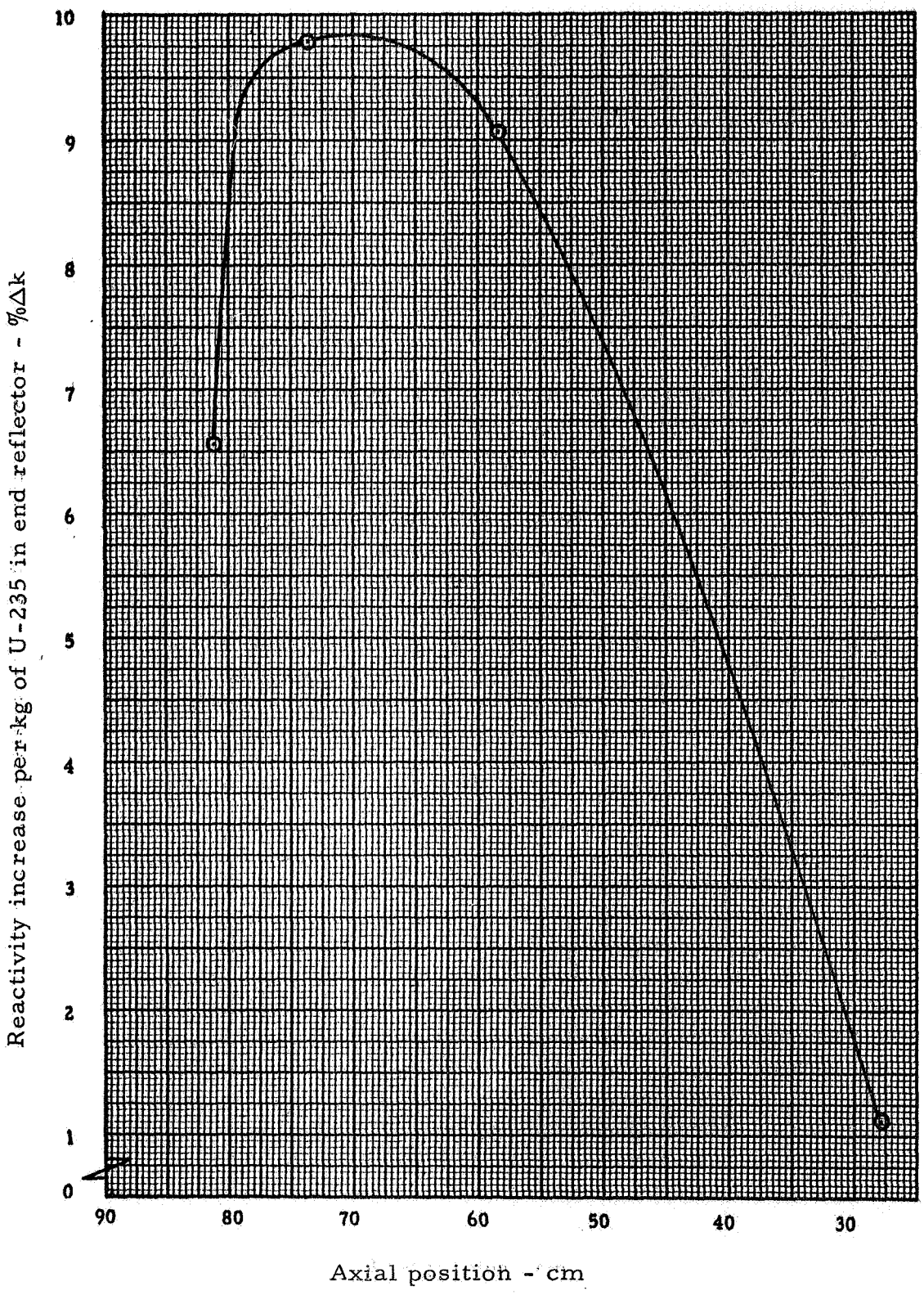

Fig. 11.3 Axial variation in reactivity per kg of fuel in end reflector

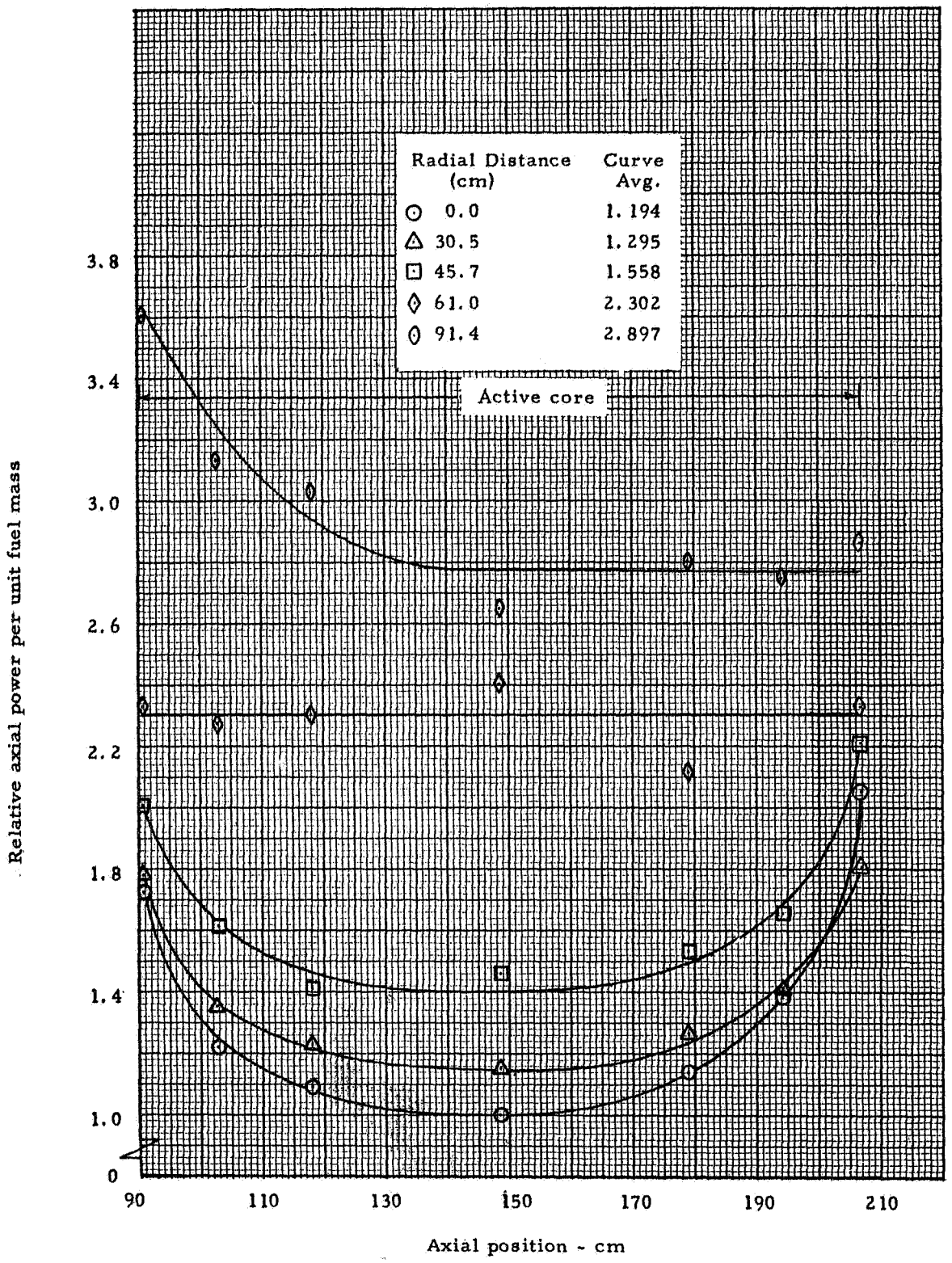

Fig. 11.4 Relative axial power profiles in cavity region adjacent to fuel sector, fuel sector 7.6 cm from cavity wall in reflector

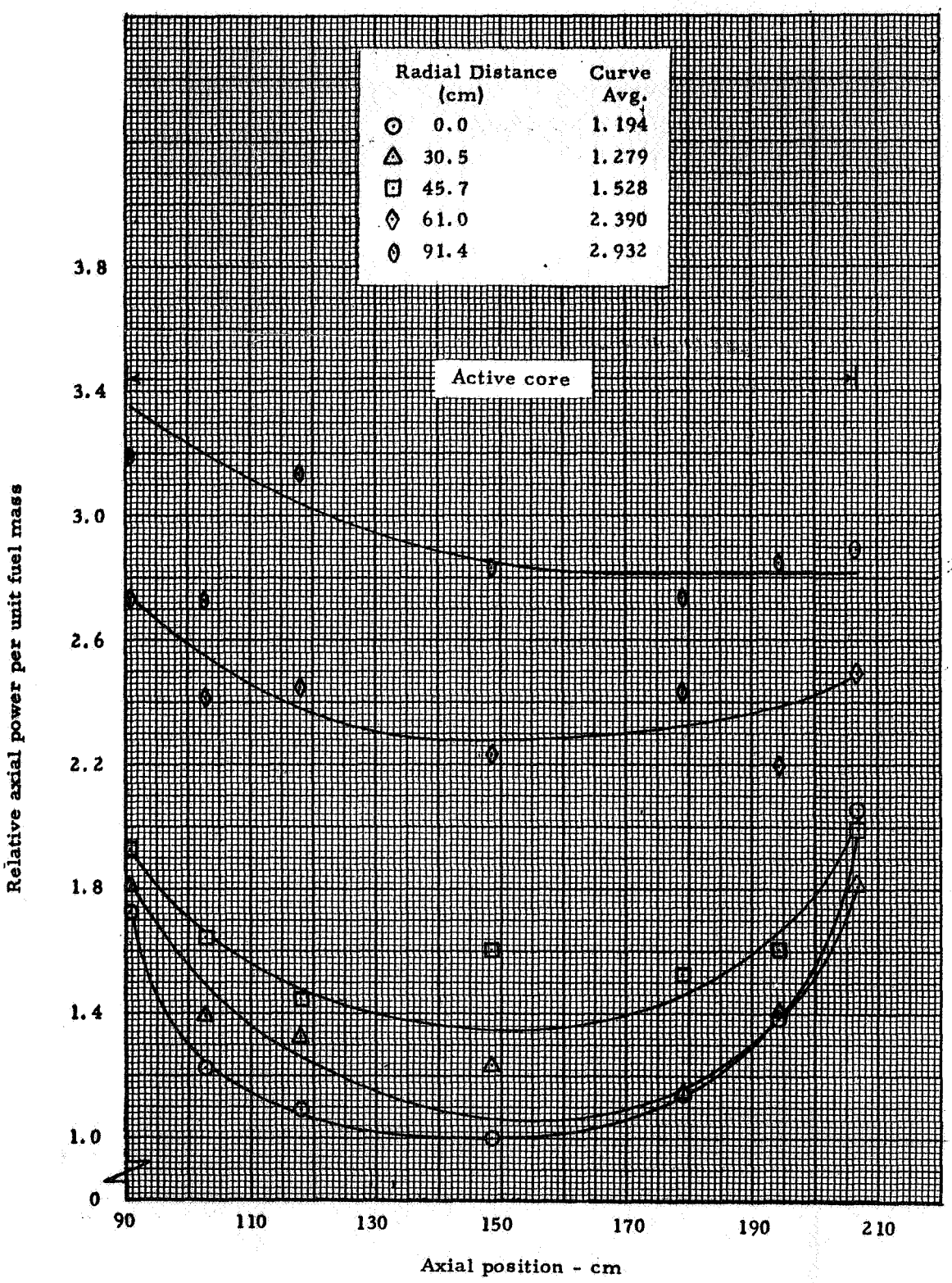

Fig. 11.5 Relative axial power profiles in cavity region, 180° from sector, fuel sector 7.6 cm from cavity wall in reflector

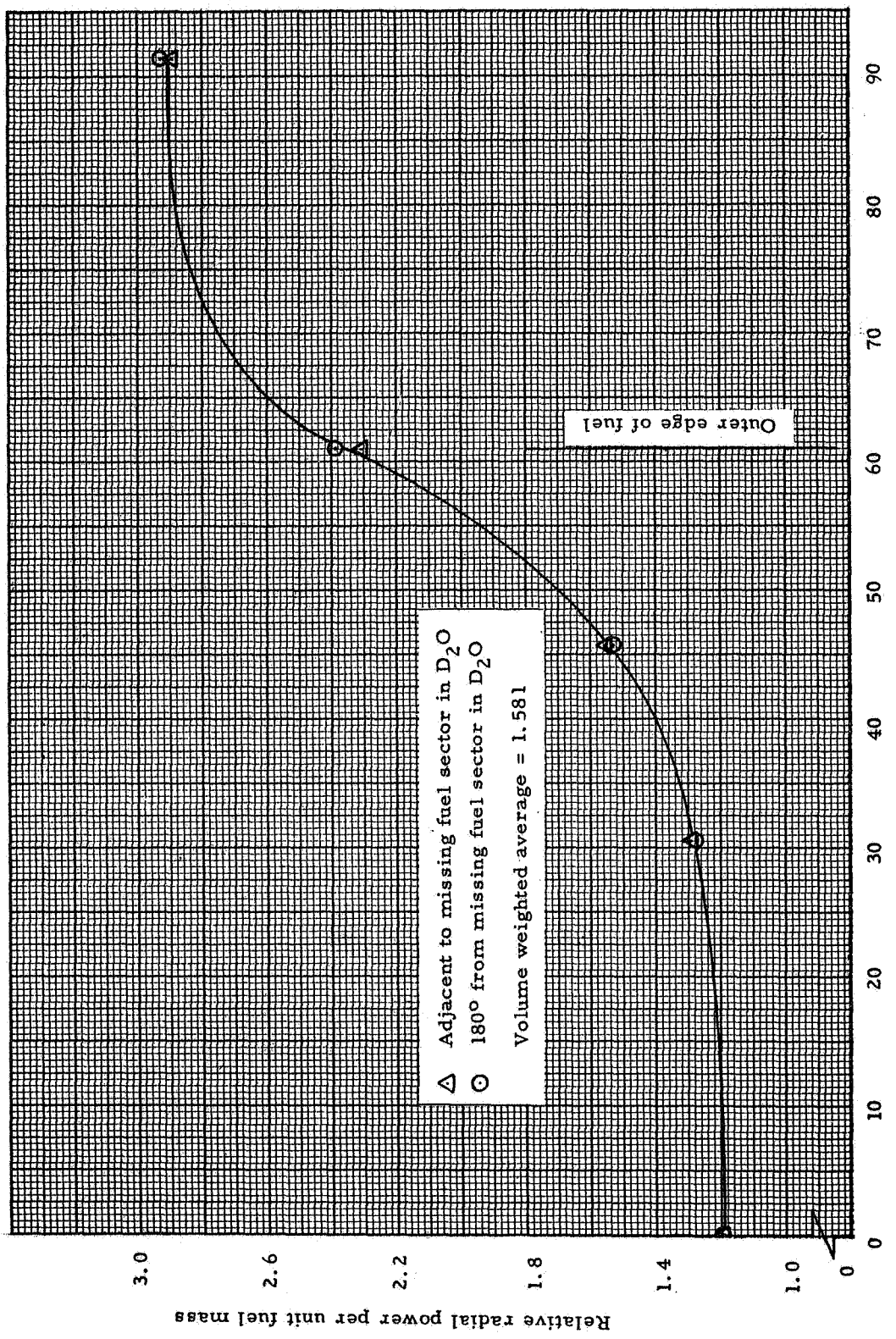

Fig. 11.6 Relative radial power profiles in cavity region, averages of axial profiles from Figures 11.4 and 11.5

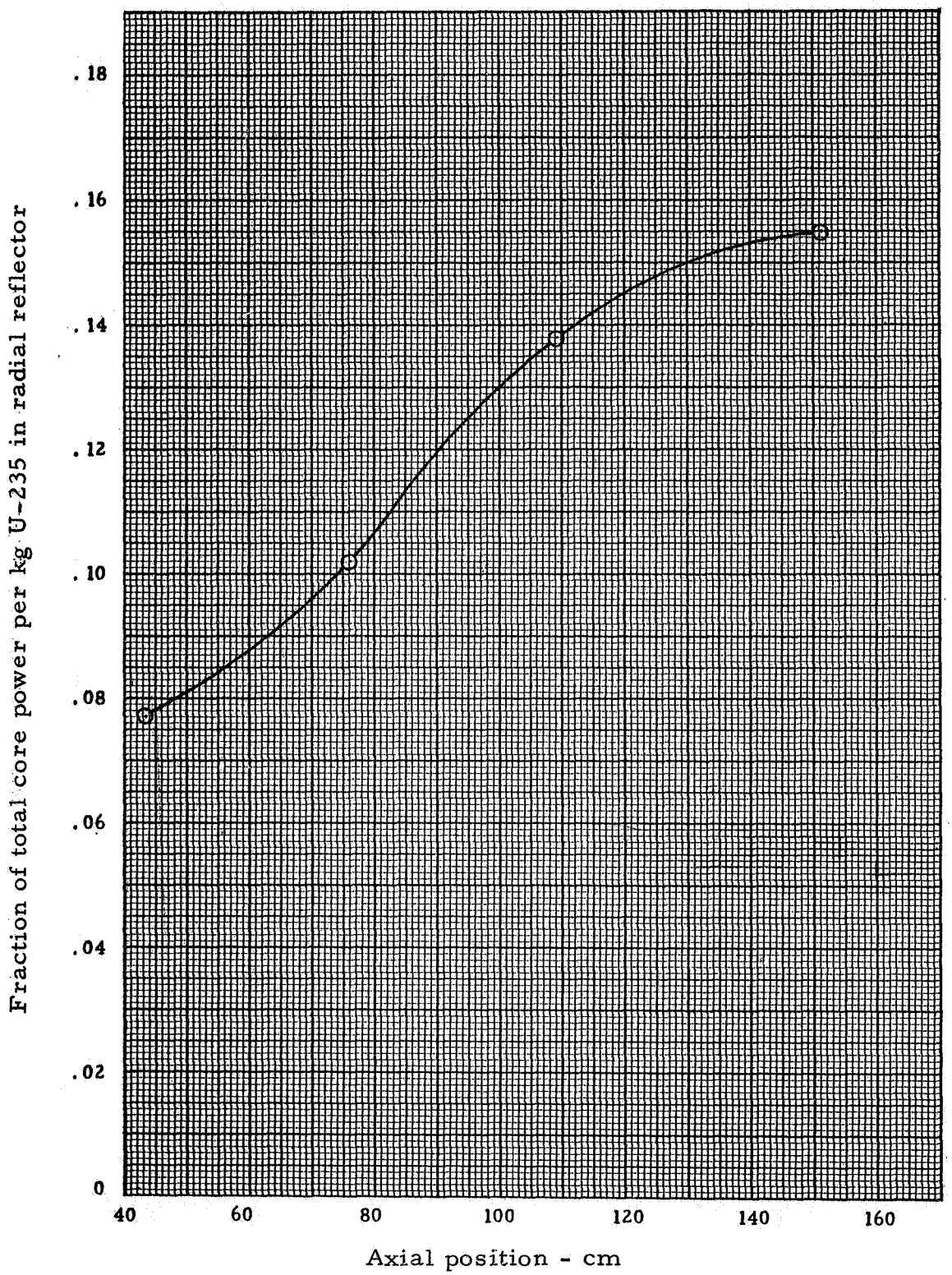

Fig. 11.7 Fraction of total power generated by fuel in radial reflector

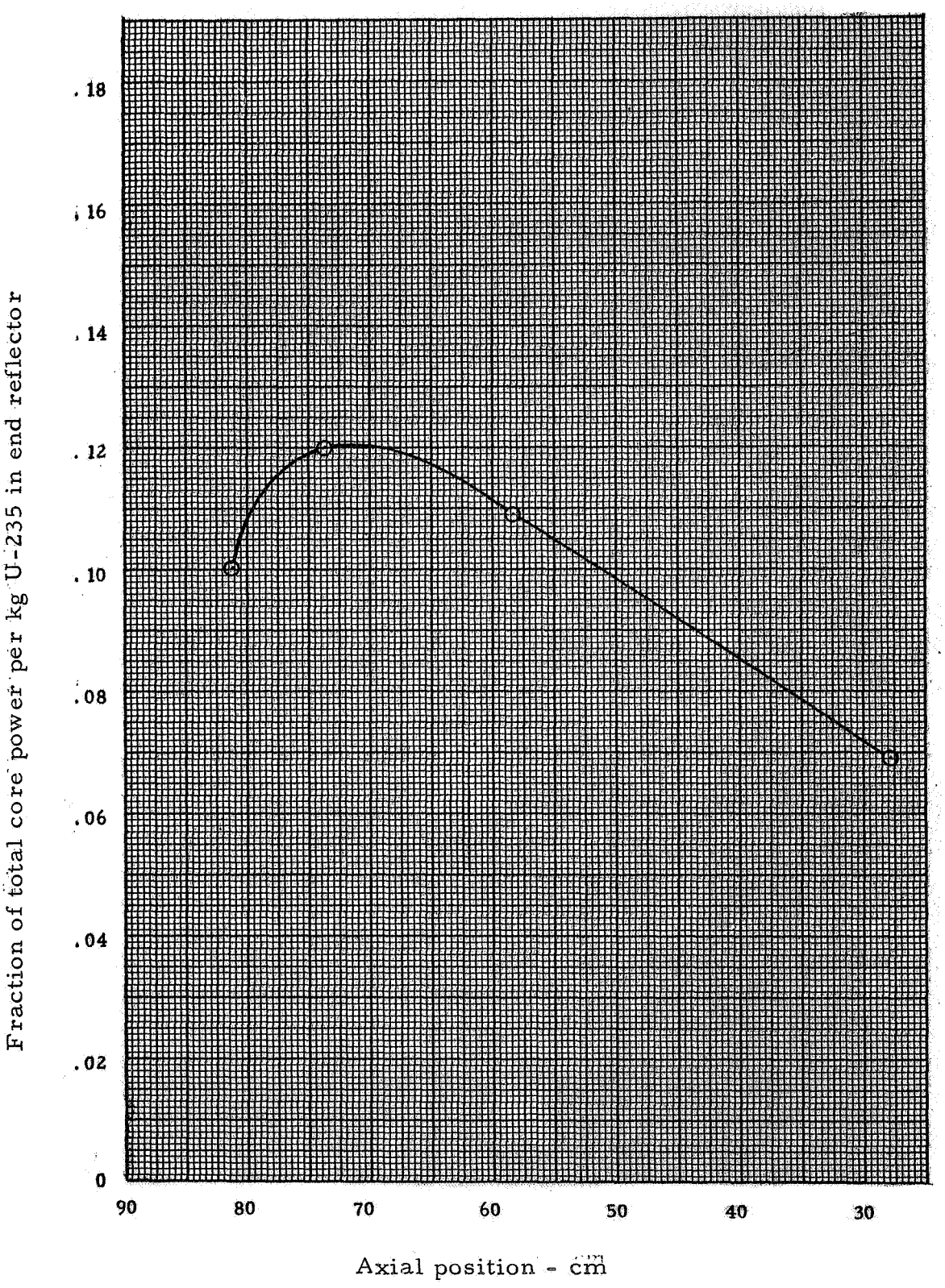

Fig. 11.8 Fraction of total power generated by fuel in end reflector

REFERENCES

1. Pincock G. D., and Kunze, J. F., "Cavity Reactor Critical Experiment," Volume I, NASA CR-72234, September 1967.

2. Pincock, G. D., and Kunze, J. F., "Cavity Reactir Critical Experiment," Volume II, NASA-CR-72415, May 1968.

3. Bekkurts, K. H., et. al., "Thermal Activation Cross Sections and Resonance Integrals of In-115," Nuc. Science and Engineering Volume 17, November 1963, p. 329.

4. Stephenson, T. E., and Pearlstein, S., " Parametric Fit of the Total Neutron Cross Section of Manganese from 0.01 ev to 50 Kev," Nuc. Science and Engineering, 32, (June 1968), p. 377

5. Wescott, C. H., et. al., "Effective Cross Sections and Cadmium Ratios," Proc. 1958 General Conf. 16, Paper 202, p. 70

6. Brown and Connally, "Cadmium Cut-Off Energies," Nuc. Science and Engineering, Volume 24, January 1966, p. 6

INDEX

INDEX
(Cont'd)

DISTRIBUTION

INTERNAL

Idaho

JF Kunze
JW Morfitt
RB O'Brien
GD Pincock

Library (2)

Evendale

WE Edwards
GF Hamby (3)
WB Henderson
MA Zipkin

Library (2)

EXTERNAL

AEC, CAO

CL Karl

AEC, ORO

WL Smalley

AEC, DTIE

NASA Scientific & Technical Information Facility
P. O. Box 33
College Park, Maryland

NASA-Lewis Research Center

TJ Flanagan
RE Hyland (3)
JC Liwosz (2)
NT Musial
RW Patch
RG Ragsdale
FE Rom
Report Control Office (1)
Nuclear Technology Office (1)

Library (2)

DISTRIBUTION

(Continued)

Mr. D. R. Bartz
Manager, Research & Advanced
Concepts Section
Propulsion Division
Jet Propulsion Laboratory
Pasadena, California 91103

Dr. Paul T. Bauer
Research Institute
University of Dayton
300 College Park
Dayton, Ohio 45409

Dr. J. R. Beyster
General Atomic
P. O. Box 608
San Diego, California 92115

Mr. Keith Boyer
N Division
Los Alamos Scientific Laboratory
Los Alamos, New Mexico 87544

Dr. Charles J. Bridgman
Associate Professor of Physics
Air Force Institute of Technology
Wright-Patterson Air Force Base
Ohio 45433

Dr. Wayne G. Burwell
United Aircraft Corporation
Research Laboratories
400 Main Street
East Hartford, Connecticut 06108

Dr. Robert W. Bussard
Electro-Optical Systems, Inc.
300 N. Halstead Street
Pasadena, California 91107

Mr. Richard W. Carkeek
The Boeing Company
P. O. Box 3868
Mail Stop 85-85
Seattle, Washington 98124

Mr. James Carton
Advanced Concepts
REON Division
Aerojet-General Corporation
Sacramento, California 95801

Dr. C. C. Chang
Head, Space Sciences & Applied Physics
Catholic University of America
Washington, D.C. 20017

Dr. Peter Chiarulli
Head, Mechanics Department
Illinois Institute of Technology
Chicago, Illinois 60616

Mr. James W. Clark
United Aircraft Corporation
Research Laboratories
400 Main Street
East Hartford, Connecticut 06108

Dr. Joseph Clement
Nuclear Engineering Department
Georgia Institute of Technology
Atlanta, Georgia 30332

Professor Terence Cool
Thermal Engineering Department
Cornell University
Ithaca, New York 14850

Dr. Ralph S. Cooper
Donald W. Couglas Laboratories
2955 George Washington Way
Richland, Washington 99352

Mr. J. S. Cory
Donald W. Douglas Laboratories
2955 George Washington Way
Richland, Washington 99352

Mr. Holmes F. Crouch
Lockheed Missiles & Space Co.
Space Systems Division
Department 62-90; Building 104
Sunnyvale, California 94408

Professor Ron Dalton
Department of Nuclear Engineering
University of Florida
Gainesville, Florida 32601

DISTRIBUTION

(Continued)

Mr. Jerry P. Davis
Building 122-3
Jet Propulsion Laboratory
4800 Oak Grove Drive
Pasadena, California 91103

Dr. Robert Dillaway
Nucleonic Department
Rocketdyne
6633 Canoga Avenue
Canoga Park, California 91303

Dr. D. W. Drawbaugh
Astronuclear Laboratory
Westinghouse Electric Corporation
Pittsburgh, Pennsylvania 15236

Mr. Frederick C. Durant, III
Assistant Director, Astonautics
National Air Museum
Smithsonian Institute
Washington, D.C. 20560

Dr. J. C. Evvard
Associate Director
Mail Stop 3-5
NASA-Lewis Research Center
21000 Brookpark Road
Cleveland, Ohio 44135

Dr. Andrew Fejer
Head, Mechanical & Aerospace
Engineering Department
Illinois Insitute of Technology
Chicago, Illinois 60616

Dr. William M. Foley
United Aircraft Corporation
Research Laboratories
400 Main Street
East Hartford, Connecticut 06108

Dr. Robert H. Fox
Institute for Defense Analysis
400 Army-Navy Drive
Arlington, Virginia 22202

Mr. A. P. Fraas
Oak Ridge National Laboratory
P. O. Box Y
Oak Ridge, Tennessee 37831

Mr. E. A. Franco-Ferreira
Metals & Ceramics Division
Oak Ridge National Laboratory
P. O. Box X
Oak Ridge, Tennessee 37831

Captain C. E. Franklin
AEC/NASA Space Nuclear Propulsion
Office
Division of Reactor Development
U. S. Atomic Energy Commission
Washington, D.C. 20545

Professor Chien Ho
Division of Nuclear Science
Room 287, Mudd Building
Columbia University
New York, New York 10027

Dr. Jerry Grey
Grey-Rad Corporation
61 Adams Street
Princeton, New Jersey 08540

Professor Robert A. Gross
School of Engineering & Applied Scienc
Columbia University
New York, New York 10027

Dr. A. V. Grosse
Research Institute of Temple
University
4150 Henry Avenue
Philadelphia, Pennsylvania 19144

Dr. George Grover (N-5)
Los Alamos Scientific Laboratory
P. O. Box 1663
Los Alamos, New Mexico 87544

Dr. S. V. Gunn
Rocketdyne
6633 Canoga Avenue
Canoga Park, California 91303

Professor Elias P. Gyftopoulos
Room 24-109
Massachusetts Insitute of Technology
Cambridge, Massachusetts 02139

DISTRIBUTION

(Continued)

Mr. L. P. Hatch
Brookhaven National Laboratory
Upton, Long Island, New York 11101

Dr. Clifford J. Heindl
Building 180-805
Jet Propulsion Laboratory
4800 Oak Grove Drive
Pasadena, California 91103

Dr. J. W. Hilborn
Reactor Physics Branch
Advanced Projects & Reactor
Physics Division
Atomic Energy of Canada Limited
Chalk River, Ontario, Canada

Dr. R. J. Holl
Missiles & Space Systems Division
Douglas Aircraft Company
Santa Monica, California 90405

Mr. William J. Houghton
Department 7040, Building 2019A2
Aerojet-General Corporation
P. O. Box 1947
Sacramento, California 95809

Mr. Maxwell Hunter
Department 50-01, Building 102
Lockheed Missiles & Space Company
P. O. Box 504
Sunnyvale, California 94408

Professor Abraham Hyatt
1700 E. Imperial Highway
El Segundo, California 90246

Dr. Kurt P. Johnson
Advanced Space Technology, A2-263
Douglas Missiles & Space Systems
Division
Santa Monica, California 90405

Mr. Carmen Jones
Rocketdyne
6633 Canoga Avenue
Canoga Park, California 91303

Dr. Larry Kaufman
Director of Research
Manlabs, Inc.
21 Erie Street
Cambridge, Massachusetts 02139

Lt. Col. M. R. Keller (ARN)
Aerospace Research Laboratories
Wright-Patterson Air Force Base
Ohio 45433

Professor J. L. Kerrebrock
Room 33-115
Massachusetts Institute of Technology
Cambridge, Massachusetts 02139

Dr. John J. Keyes, Jr.
Reactor Division
Oak Ridge National Laboratory
P. O. Box Y
Oak Ridge, Tennessee 37831

Dr. D. E. Knapp
Donald W. Douglas Laboratories
2955 George Washington Way
Richland, Washington 99352

Mr. Walter F. Krieve
Building S
TRW Systems
One Space Park
Redondo Beach, California 90278

Mr. George T. Lalos
U. S. Naval Ordnance Laboratory
White Oaks, Silver Springs,
Maryland 20900

Mr. Thomas Latham
United Aircraft Corporation
Research Laboratories
400 Main Street
East Hartford, Connecticut 06108

Dr. Zalman Lavan
Illinois Institute of Technology
M. A. E. Department
Technology Center
Chicago, Illinois 60616

Dr. W. S. Lewellen
Room 33-119
Massachusetts Institute of Technology
Cambridge, Massachusetts 02139

Mr. A. B. Longyear
New Technology - NRO
Aerojet-General Corporation
P. O. Box 15847
Sacramento, California 95813

DISTRIBUTION

(Continued)

Mr. David Mallon
Allison Division
General Motors Corporation
2355 S. Tibbs Avenue
Indianapolis, Indiana 46206

Professor Edward Mason
Room NW12
Massachusetts Institute of Technology
Cambridge, Massachusetts 02139

Mr. Goerge H. McLafferty
United Aircraft Corporation
Research Laboratories
400 Main Street
East Hartford, Connecticut 06108

Dr. Robert V. Meghreblian
Jet Propulsion Laboratory
4800 Oak Grove Avenue
Pasadena, California 91103

Dr. A. J. Miller
Oak Ridge National Laboratory
P. O. Box Y
Oak Ridge, Tennessee 37831

Dr. Franklin K. Moore, Head
Thermal Engineering Department
Cornell University
Ithaca, New York 14850

Dr. George Nelson
University of Arizona
Nuclear Engineering Department
Tucson, Arizona 85721

Mr. John D. Orndoff
N Division
Los Alamos Scientific Laboratory
Los Alamos, New Mexico 87544

Professor Clyde Orr, Jr.
Chemical Engineering Department
Georgia Institute of Technology
Atlanta, Georgia 30332

Mr. Frank S. Owen
United Aircraft Corporation
Research Laboratories
400 Main Street
East Hartford, Connecticut 06108

Mr. P. Patriarca
Oak Ridge National Laboratory
P. O. Box X
Oak Ridge, Tennessee 37831

Professor Rafael Perez
Nuclear Engineering Department
University of Florida
Gainesville, Florida 32601

Professor H. C. Perkins
Energy, Mass & Momentum Transfer Laboratory
Aerospace & Mechanical Engineering Department
University of Arizona
Tucson, Arizona 85721

Mr. Ben Pinkel
RAND Corporation
1700 Main Street
Santa Monica, California 90406

Mr. Jack Ravets
Westinghouse Astronuclear Laboratory
P. O. Box 10864
Pittsburgh, Pennsylvania 15236

Dr. Bruce A. Reese, Director
Jet Propulsion Center
Mechanical Engineering Department
Purdue University
Lafayette, Indiana 47907

Dr. Jacob B. Romero
Chemical Engineering Department
University of Idaho
Moscow, Idaho 83843

Dr. Richard Rosa
Avco Everett Research Laboratory
2385 Revere Beach Parkway
Everett, Massachusetts 02149

Dr. S. M. Scala
Manager, Theoretical Fluid Physics Section
General Electric Company
Space Sciences Laboratory
P. O. Box 8555
Philadelphia, Pennsylvania 19101

DISTRIBUTION

(Continued)

Professor Glen J. Schoessow
Department of Nuclear Engineering Sciences
202 Nuclear Sciences Building
University of Florida
Gainesville, Florida 32601

Mr. F. C. Schwenk
AEC/NASA Space Nuclear Propulsion Office
Division of Reactor Development
U. S. Atomic Energy Commission
Washington, D.C. 20545

Mr. W. L. Snapp
Aerojet-General Corporation
20545 Center Ridge Road
Cleveland, Ohio 44116

Mr. C. K. Soppet, Manager
Engine Test Operations
NERVA Test Operations
P. O. Box 2027
Jackass Flats, Nevada 89023

Dr. Henry Stumpf
Astronuclear Laboratories
Westinghouse Electric Corporation
Pittsburgh, Pennsylvania 15236

Dr. Theodore B. Taylor
Defense Atomic Support Agency
Pentagon
Washington, D.C. 20301

Mr. Merle Thorpe
TAFA Division
Humphreys Corporation
180 North Main Street
Concord, New Hampshire 03301

Dr. T. P. Torda
Illinois Institute of Technology
M.A.E. Department, Technology Center
Chicago, Illinois 60616

Dr. Robert Uhrig, Chairman
Department of Nuclear Engineering
University of Florida
Gainesville, Florida 32601

Dr. Hans von Ohain
Aerospace Research Laboratories (ARD-1)
Wright-Patterson Air Force Base
Ohio 45433

Dr. Herbert Weinstein
Chemical Engineering Department
Illinois Institute of Technology
Chicago, Illinois 60616

Professor E. P. Wigner
Department of Physics
Princeton University
Princeton, New Jersey 08540

Dr. J. Richard Williams
Nuclear Engineering Department
Georgia Institute of Technology
Atlanta, Georgia 30332

Mr. Jerrold M. Yos
Avco Corporation
Research & Advanced Development Division
Wilmington, Massachusetts 01887